UNIVERSITÉ DE STRASBOURG

ÉCOLE DOCTORALE des Sciences Chimiques

UMR 7006

THÈSE présentée par :

Viktoria WOLLRAB

soutenue le : **08 Septembre 2014**

pour obtenir le grade de : **Docteur de l'université de Strasbourg**

Discipline/ Spécialité : Physique

Active gels *in vivo*: Patterns and dynamics in cytokinetic rings and their functions in cell division

THÈSE dirigée par :

RIVELINE, Daniel	Directeur de recherche, Université de Strasbourg, Strasbourg
KRUSE, Karsten	Professeur, Universität des Saarlandes, Saarbrücken

RAPPORTEURS :

KOENDERINK, Gijsje	Professeur, AMOLF, Amsterdam
OTT, Albrecht	Professeur, Universität des Saarlandes, Saarbrücken

---

AUTRES MEMBRES DU JURY :

BLANCHOIN, Laurent	Directeur de recherche, CEA, Grenoble
FLEURY, Jean-Baptiste	Docteur, Universität des Saarlandes, Saarbrücken
KRUSE, Karsten	Professeur, Universität des Saarlandes, Saarbrücken
PROST, Jacques	Directeur de recherche, Institut Curie, Paris
RIVELINE, Daniel	Directeur de recherche, Université de Strasbourg, Strasbourg
VERMOT, Julien	Chargé de recherche, IGBMC, Strasbourg

Acknowledgments

Foremost, I would like to express my sincere gratitude to my supervisor Daniel Riveline for the great support and promotion throughout the years. Thank you for the fantastic encouragement, the lively discussions and all I could learn from you!

I also wish to thank with a big “danke schön” my co-supervisor Karsten Kruse for the wonderful collaboration, the inspiring discussions and all he taught me. I am also grateful that he accepted to be the referee of my thesis.

I thank Gijsje Koenderink and Albrecht Ott for accepting to be referee for the thesis and to be Jury member. I am also grateful to Jacques Prost, Laurent Blanchoin, Julien Vermot and Jean-Baptiste Fleury for accepting to be member of the jury and attending my defense. Dank u wel, vielen Dank and merci beaucoup.

I also want to thank François Nédélec and Eszter Lakatos for the stimulating collaboration, the intense discussions and all I could learn from them.

I also thank Anne Wald for the good collaboration and pleasant exchange.

I thank Ewa Paluch, Guillaume Charras and Tony Hyman for cell lines and plasmids, Michael Glotzer, Sadanori Watanabe and Sasha Bershadsky for plasmids and antibodies and William Trimble for advices concerning the septin antibody.

I thank the French-German University (UFA-DFH) for the support of the collaboration.

A very warm thanks goes to my fantastic colleagues! I thank David Caballero-Vila for showing me everything in the lab, sharing his knowledge, his helpful advices, his great patience, his constant good humor and dry-ice experiments. I thank Alicia Bornert for support with the microcontact printing. I am also grateful to Vishwajeet Mehandia for the many discussions. A grand merci belongs also to Antonin Hoël and Fanny Evenou for the support with the microcavities. I wish to thank Claire Menouna-Ekani for the logistic support and her help. I am also grateful to Jordi Comelles-Pujadas for the excellent discussions, his support, help with the statistical analysis and introduction in Catalan and Spanish culture and richness of language. I want to thank Amélie Godeau for amplifying plasmids, great fun and discussions and the excellent, lifesaving coffee and cake. I wish to thank Raghavan Thiagarajan for the good desk-neighborhood, the perfect collaboration and the mutual teasing. Thank you for the great time, encouragement and laughter!

I am grateful to Daniel Riveline, Karsten Kruse, Jordi Comelles-Pujadas, Amélie Godeau, Raghavan Thiagarajan and Eva Wollrab for proofreading and commenting on the manuscript.

I thank Naël Osmani for teaching me plasmid amplification and the advices about transfection. I thank Bertrand Benazeraf for the protocol to bind polyacrylamide gel to glass coverslips.

I thank the ISIS staff for the technical and logistic support and good atmosphere and the pleasant small talk. I am also grateful to the IGBMC image facility and in particular to Pascal Kessler, Marc Koch and Yves Lutz for their support. I also thank the IGMBC media facility. I am grateful to Christian Rick for the technical support.

I thank all my friends and family who encouraged me during my thesis and in particular during the writing. I would like to express a special “Merci!” to Sonia for her support, respect for my work and encouragement. A big thanks goes to my sister Eva for the important support, encouragement and great *fön*! I am very grateful to my parents who always support me!

Abstract – Resumé court – Kurzzusammenfassung

Abstract

Actomyosin structures are involved in many cell functions. Understanding their organization and collective behavior is still challenging. We study the cytokinetic ring in mammalian cells and in fission yeasts, by orienting cells in microcavities. This allows seeing the ring in a single plane of focus. With this setup, we reveal new structures and distinct dynamics for both cellular systems. In mammalian cells we find a pattern of regular clusters of myosin and formin. The characteristics of this pattern are stable throughout closure and its formation coincides with the onset of constriction. We propose that its characteristic is an inherent property of the actomyosin network and that its formation leads to an increase in stress generation. These hypotheses are supported by our theoretical mean field model. In contrast, fission yeast rings show rotating inhomogeneities (*speckles*), i.e. rotations of actin, myosin, cell wall building proteins (Bgs) and other proteins. Myosin speckles dynamic is unchanged, if wall growth is inhibited. However, the inhibition of speckle motion leads to stalled closure. We propose that the ring closure is driven by the rotation of actin and myosin, which pull Bgs thereby building the septum. This model is supported by our calculations and by simulations. We suggest that the transition between states of different orders and dynamics might be a way to regulate actomyosin systems *in vivo*.

Resumé court

Les structures d'acto-myosine sont impliquées dans de nombreuses fonctions cellulaires. Comprendre leur organisation et leur comportement collectif est toujours difficile. Nous avons étudié l'anneau cytokinétique dans les cellules de mammifères et dans les levures de fission, en orientant les cellules dans les microcavités, ce qui permet de voir l'anneau dans un seul plan focal. Avec cette configuration, nous révélons de nouvelles structures et des dynamiques distinctes pour les deux systèmes cellulaires. Dans les cellules de mammifères, nous trouvons des motifs réguliers de la myosine et la formine. Les caractéristiques de ces motifs sont stables tout au long de sa fermeture et leur apparition coïncide avec la constriction. Nous proposons que ce phénomène est une propriété inhérente du réseau d'actomyosine et que la formation de ces motifs entraîne une augmentation du stress. Ces hypothèses sont confirmées par notre modèle en champ moyen. Par contraste, l'anneau de levure de fission montre des inhomogénéités tournantes de l'actine, de la myosine, des protéines de la construction de la paroi (Bgs) et d'autres protéines. La dynamique des inhomogénéités de myosine est inchangée, si la croissance de la paroi est inhibée. Cependant, l'inhibition du mouvement des inhomogénéités conduit à l'arrêt de la fermeture. Nous proposons que la fermeture de l'anneau est entraînée par la rotation de l'actine et de la myosine qui tire des protéines de Bgs, lesquelles construisent ainsi le septum. Cette hypothèse est confirmée par nos calculs et des simulations. Nous suggérons que la transition entre les états de différents ordres et dynamiques pourrait être une façon de réguler in vivo les systèmes d'actomyosine.

Kurzzusammenfassung

Aktomyosinstrukturen sind involviert in viele Zellfunktionen. Ihre Organisation und kollektives Verhalten zu verstehen, ist immer noch eine Herausforderung. Wir studieren den zytokinetischen Ring in Säugetierzellen und Spalthefe, indem wir Zellen in Mikrovertiefungen orientieren, die es uns erlauben, den Ring in einer einzigen Ebene zu fokussieren. Damit zeigen wir neue Strukturen und Dynamiken in beiden Systemen. In Säugetierzellen finden wir ein Muster aus regelmäßigen Anhäufungen von Myosin und Formin. Die Charakteristiken des Musters sind stabil und die Entstehung des Musters fällt mit dem Begin der Teilung zusammen. Wir schlagen vor, dass die Charakteristiken des Musters inhärente Eigenschaften des Aktomyosinnetzwerkes sind und dass das Muster zu einer erhöhten Spannungserzeugung führt. Diese Hypothesen werden von unserer Molekularfeldheorie-Beschreibung unterstützt. Ringe der Hefe zeigen rotierende Inhomogenitäten in Aktin, Myosin, zellwandbildenden Proteinen (Bgs) und anderen Proteinen. Die Myosindynamik ist unverändert, wenn die Wandbildung inhibiert ist. Hemmung der Myosinrotation, führt jedoch zu einem Anhalten der Teilung. Wir schlagen vor, dass die Schließung des Ringes durch die Rotationen von Aktin und Myosin angetrieben wird, die wiederum Bgs ziehen. Unsere Berechnungen und Simulationen unterstützen dieses Modell. Wir schlagen vor, dass Übergänge von Zuständen von unterschiedlicher Struktur oder Dynamik ein Weg sein könnten, Aktomyosinsysteme zu regulieren.

Summary – Resumé – Zusammenfassung

Summary

Cell division is one of the most basic events for cells. Single cell organisms proliferate by dividing, and multicellular organisms grow and renew tissue by this mechanism. After the chromosomes are separated, a ring of actin, myosin and other proteins forms. Its closure leads to cell separation. This mechanism is conserved in fungi, amoebae and animal cells.

Dynamics of actin and myosin, or more generally filaments and motors are relevant for cell division, but also for cells in general, be it for their internal organization, be it for the sensing of the environment or auto-organization in tissues and embryogenesis. Networks of dynamic filaments and active motors are also termed *active gels*, since they are out-of-equilibrium system. Therefore they constitutes not only important structures in cell, but also a new kind of materials. Numerous theoretical and experimental studies have been carried out on this topic.

It is more challenging to study these gels *in vivo*, since many proteins and signaling are involved in their organization. Due to its circular geometry, the cytokinetic ring is a relatively simple active gel *in vivo*. Its components are well studied. However, it is still not clear how the ring constricts and how stress is generated in this system. By elucidating this question, we hope that we can also contribute to a better understanding of other active gel structures in cells.

Based on an existing setup for fission yeast, invented by Daniel Riveline, we developed

a setup and protocol to study cytokinesis in mammalian cells. More specifically, we investigate the cytokinetic ring by using an array of microcavities, which allowed us to orient cells and to see the ring in a single plane of focus. We visualize the ring with fluorescently labeled actin filaments, myosin and other proteins for two cellular systems: mammalian cells and fission yeast. This setup allowed us to reveal, characterize and compare patterns and dynamics in both cell types.

Interestingly we see a structure within the cytokinetic ring in mammalian cells: myosin and formin form a pattern of regular clusters. This pattern can exhibit global dynamics during closure, like collective rotations or local fusions and separations of single clusters. However, our characterization of the pattern reveals that its properties remain mainly constant throughout closure. This suggests that it is an inherent property of the ring. Interestingly, the pattern is not disturbed after laser cutting the ring. Furrow constriction is even continuing after cutting; this shows that contractility is a local property. We also find an inhomogeneous distribution of anillin and septin in the ring, but no systematic colocalization with myosin clusters. Furthermore we show that cytoskeletal drugs disturb the pattern. In particular they render the pattern less regular. Strikingly this pattern is forming as the ring begins to close. This suggests that the pattern is related to stress generation. Indeed, the model and calculations of Karsten Kruse and Anne Wald support this interpretation. Our model is built on simple assumptions about the ingredients in the ring. It shows that such patterns of regular motor, nucleator and filament clusters form due to a dynamic instability which occurs above a critical motor activity. This pattern leads to an increased stress generation due to the ordering of filaments. Therefore, we propose that the ring components organize in a regular pattern and that this pattern is the key to the stress generation in the cytokinetic ring.

In fission yeast cells, we find also inhomogeneities (*speckles*) of actin, myosin, the wall building machinery (Bgs) and other proteins. But in contrast to our findings in mammalian cells, these speckles are rotating on the ring. This rotation also occurs in the absence of ring closure, which suggests that it is a built-in property of the cytokinetic ring in fission yeast. Inhibition of the myosin speckle rotation leads also to an arrest of cell closure, suggesting a correlation between speckles rotations and ring closure. François

Nédélec and Eszter Lakatos proposed that the ring closes because the cytoskeleton components drive the rotation of the wall building machinery. Rotations allow to grow the wall against the turgor pressure. We implemented the ring with a minimal set of ingredients and we can reproduce speckle motion and ring closure *in silico*. Furthermore we propose that another function of rotation might be to render the ring more stable. Indeed our laser ablation experiments show that the ring can repair within seconds.

In both systems we discovered mesoscopic structures in the active gel. We characterized their patterns and dynamics and probed their changes under different conditions. Our observations and measurements led us to two models, explaining the stress generation and ring closure in the respective systems. However, it is surprising that two actomyosin rings exhibit different dynamics. Future experiments will aim at understanding, which system parameters lead to either still or rotating clusters. We suggest that the transition between states of different orders and dynamics might be one way to regulate actomyosin systems *in vivo*, in addition to traditional signaling.

Resumé

La division cellulaire est l'un des événements les plus fondamentaux en Biologie. Les organismes unicellulaires prolifèrent en se divisant, et les organismes multicellulaires se développent et renouvèlent leurs tissus par ce phénomène. Après que les chromosomes se sont séparés, un anneau d'actine, de myosine et d'autres protéines se forme. Sa fermeture conduit à la séparation des cellules. Ce mécanisme est conservé dans les cellules de champignons, chez les amibes et pour les cellules animales.

La dynamique de l'actine et de la myosine, ou plus généralement des filaments et des moteurs est essentielle pour la division cellulaire, mais aussi pour les cellules en général, que ce soit pour leur organisation interne, que ce soit pour la détection de l'environnement ou pour l'auto-organisation dans les tissus et pour l'embryogenèse. Le réseau de filaments dynamiques et moteurs est appelé *gels actifs*, car c'est un système hors d'équilibre. Par conséquent, il constitue non seulement une structure importante dans la cellule, mais aussi un nouveau type de matériaux. De nombreuses études théoriques et expérimentales ont été menées sur ce sujet.

Il est plus difficile d'étudier ces gels *in vivo*, car de nombreuses protéines et la signalisation cellulaire sont impliquées dans l'organisation de ces gels. Grâce à sa géométrie circulaire, l'anneau cytokinétique est un gel actif *in vivo* complet, relativement simple. Ses composants sont bien étudiés. Cependant, il n'est pas toujours clair comment l'anneau se contracte et comment le stress est généré dans ce système. En élucidant cette question, nous espérons que nous pouvons aussi contribuer à une meilleure compréhension des autres structures de gels actifs dans les cellules.

A partir d'un montage existant pour la levure à fission, inventé par Daniel Riveline, nous avons développé une configuration et un protocole pour étudier la cytokinèse dans les cellules de mammifères. Plus précisément, nous étudions l'anneau en utilisant un arrangement régulier de microcavités, ce qui nous a permis d'orienter les cellules et de voir l'anneau cytokinétique dans un seul plan focal. Nous avons étudié l'anneau en utilisant une configuration de microcavité qui permet de voir l'anneau dans un seul plan focal. Nous

visualisons l'anneau en marquant les filaments d'actine, la myosine et d'autres protéines avec des marqueurs fluorescents pour deux systèmes cellulaires : les cellules de mammifères et les levures à fission. Cette configuration nous a permis de révéler, caractériser et comparer des motifs et des dynamiques dans les deux types cellulaires.

Nous avons révélé une structure à l'intérieur de l'anneau de la cytokinèse dans les cellules de mammifères: la myosine et la formine forment un motif régulier. Ces motifs peuvent présenter une dynamique globale pendant la constriction, comme les rotations collectives ou des fusions et séparations locales de motifs. Cependant, notre caractérisation du motif révèle que ses propriétés restent principalement constantes tout au long de la fermeture. Cela suggère qu'il s'agit d'une propriété inhérente de l'anneau. Curieusement, le motif n'est pas perturbé après la découpe au laser de l'anneau. La constriction de sillon se poursuit, même après le découpage. Cela montre que la contractilité est une propriété locale. Nous constatons également une distribution inhomogène de l'anilline et de la septine dans l'anneau, mais pas une co-localisation systématique avec des motifs de myosine. En outre, nous montrons que les inhibiteurs de cytosquelette perturbent des motifs. En particulier, ils les rendent moins réguliers. Il est frappant que ce motif se forme, quand l'anneau se ferme. Cela suggère que le motif est lié à la génération de tension. En effet, le modèle et les calculs de Karsten Kruse et Anne Wald supportent cette interprétation. Notre modèle est construit avec des hypothèses simples sur les ingrédients dans l'anneau. Il montre que ce motif régulier de moteurs, de nucléateurs et des filaments se forme en raison d'une instabilité dynamique qui se produit au-dessus d'une activité critique des moteurs. Ce modèle conduit à une génération de stress accru en raison de l'ordre des filaments. Par conséquent, nous proposons que les ingrédients d'anneau s'organisent selon un motif régulier et que ce mécanisme est la clé de la génération de tension dans l'anneau de cytokinèse.

Dans les cellules de levure à fission, nous avons aussi révélé des inhomogénéités de l'actine, de myosine, des protéines de la construction de la paroi (Bgs) et d'autres protéines. Mais contrairement à nos résultats dans les cellules de mammifères, ces inhomogénéités tournent sur l'anneau. Cette rotation se produit également en l'absence de fermeture de l'anneau, ce qui suggère qu'elle est une propriété inhérente de l'anneau de

la cytokinèse de la levure à fission. L'inhibition de la rotation de la myosine conduit également à un arrêt de la fermeture de la cellule, indiquant une connexion entre les rotations et la fermeture de l'anneau. François Nédélec et Eszter Lakatos proposent que l'anneau se ferme parce que les composants du cytosquelette font tourner la machine de construction de la paroi de la levure. Les rotations permettent de soulever le mur contre la pression de turgescence. Nous avons simulé numériquement l'anneau avec un ensemble minimal d'ingrédients et de règles d'interaction, et nous avons reproduit le mouvement de la granularité et la fermeture de l'anneau *in silico*. En outre, nous proposons qu'une autre fonction des rotations pourrait être de rendre l'anneau plus stable. En effet, nos expériences d'ablation laser montrent que l'anneau peut se réparer en quelques secondes.

Dans les deux systèmes, nous avons découvert des structures mésoscopiques dans le gel actif. Nous avons caractérisé ses structures et ses dynamiques et nous avons sondé leurs changements dans des conditions différentes. Nos observations et nos mesures nous conduisent à deux modèles, expliquant la génération de tension et la fermeture de l'anneau dans les systèmes respectifs. Cependant, il est surprenant que les deux anneaux d'actomyosine présentent des dynamiques différentes. Les expériences futures viseront à comprendre, quels paramètres des systèmes conduisent à des inhomogénéités fixes ou tournantes. Nous suggérons que la transition entre les états de différents ordres et dynamiques pourrait être une façon de réguler *in vivo* les systèmes d'actomyosine, en plus de la signalisation traditionnelle.

Zusammenfassung

Die Zellteilung ist eines der grundlegendsten Ereignisse für eine Zelle. Einzeller vermehren sich durch Zellteilung und multizellulare Organismen wachsen und erneuern sich durch diesen Mechanismus. Nachdem die Chromosomen getrennt sind, bildet sich ein Ring aus Aktin, Myosin und anderen Proteinen, der zur Zellteilung führt. Bemerkenswerterweise ist dieser Mechanismus zwischen Fungi, Amöben und Tierzellen erhalten.

Strukturen aus Aktin und Myosin, oder, allgemein gesagt, Filamenten und Motoren, sind nicht nur relevant in der Zellteilung, sondern auch für Zellen im Allgemeinen, sei es für die interne Organisation, sei es für das "Ertasten" ihrer Umgebung, sei es für das kollektive Verhalten in Gewebe und in der Embryogenese. Netzwerke aus dynamischen Filamenten und aktiven Motoren werden auch als *aktive Gele* bezeichnet, da es sich um ein System außerhalb des Gleichgewichts handelt. Daher ist es nicht nur eine wichtige Zellstrukture, sondern auch eine neue Art von Material. Eine Vielzahl an theoretischen und experimentellen Arbeiten wurde auf diesem Feld durchgeführt.

Es ist eine Herausforderung, diese Gele in *in vivo* zu studieren, da viele Proteine und Signale in die Organisation dieser Gele involviert sind. Aufgrund seiner ringförmigen Geometrie ist der zytokinetische Ring ein relativ übersichtliches aktives Gel *in vivo*. Zudem sind seine Komponenten gut beschrieben. Es ist jedoch immer noch nicht klar, warum sich der Ring zusammenzieht und wie Spannung in diesem System erzeugt wird. Durch das Aufhellen dieser Fragen hoffen wir, generell zum Verständnis von aktiven Gel-Strukturen beitragen zu können.

Basierend auf einer existierenden Methode, erfunden von Daniel Riveline, haben wir eine Konfiguration und ein Protokoll entwickelt, um die Zytokinese in Säugetierzellen zu untersuchen. Genauer gesagt haben wir den Zytokinetischenring mit der Hilfe eines Aufbaus aus einer regelmäßigen Anordnung mit Mikrovertiefungen untersucht, die es erlauben, die Zellen zu orientieren und den Ring in einer einzigen Ebene zu fokussieren. Wir haben den Ring durch das Markieren von Aktinfilamenten, Myosin und anderer Proteinen mit Fluoreszenzmarkern visualisiert. Wir arbeiten mit zwei Zelltypen: Säugetierzellen

und Spalthefen. Unser experimenteller Aufbau erlaubt es uns Muster und Dynamiken in beiden Systemen zu visualisieren, charakterisieren und zu vergleichen.

Interessanterweise sehen wir in Säugetierzellen Strukturen im zytokinetischen Ring: Myosin und Formin bilden ein Muster aus regelmäßigen Häufungen. Diese Muster zeigen globale Dynamiken, wie kollektive Rotationen oder lokale wie Fusion und Teilung von einzelnen Anhäufungen. Jedoch zeigt unsere Charakterisierung des Musters, dass seine Eigenschaften im Wesentlichen konstant während der Teilung bleiben. Das deutet darauf hin, dass es sich um inhärente Eigenschaften des Rings handelt. Interessanterweise ist das Muster nicht gestört nach der Laserablation des Ringes. Die Teilungsfurche zieht sich auch weiterhin zusammen. Das zeigt, dass die Kontraktilität eine lokale Eigenschaft ist. Wir beobachten ebenfalls eine inhomogene Verteilung von Anillin und Septin im Ring, jedoch keine systematische Kolokalisierung mit Myosinanhäufungen. Weiterhin können wir zeigen, dass Substanzen, die das Zytoskelett inhibieren das Muster zerstören. Insbesondere sehen wir, dass das Muster unregelmäßiger wird. Bemerkenswerterweise bildet sich dieses Muster aus, wenn der Ring anfängt sich, zu schließen. Das deutet darauf hin, dass die Musterentstehung mit der Spannungserzeugung in Verbindung steht. Das Modell und die Berechnungen von Karsten Kruse und Anne Wald unterstützen diese Interpretation. Unser Modell beruht auf einfachen Annahmen bezüglich der Zusammensetzung des Rings. Es zeigt, dass sich ein solches Muster aus regelmäßig angeordneten Motoren, Filament und Nukleatoren formt, wenn die Motoraktivität einen Schwellenwert überschreitet. Wir demonstrieren weiterhin, dass dieses Muster zu einer erhöhten Spannung führt, die der Anordnung der Filamente geschuldet ist. Wir schlagen daher vor, dass die Ringbestandteile sich zu einem regelmäßigen Muster anordnen und dass diese Musterbildung ein Schlüssel zur Spannungserzeugung im zytokinetischen Ring ist.

In Hefezellen finden wir ebenfalls Inhomogenitäten in der Verteilung von Aktin, Myosin, zellwandbildenden Proteinen (Bgs) und weitere Proteinen. Aber im Gegensatz zu unseren Ergebnissen zu Säugetierzellen rotieren diese Inhomogenitäten im Ring. Diese Rotation tritt auch dann auf, wenn die Zellwand nicht gebildet wird und sich der Ring nicht schließt. Das weist darauf hin, dass es sich bei der Rotation um eine inhärente Eigenschaft des Rings handelt. Die Inhibition der Rotation von Myosininhomogenitäten führt

zum Anhalten der Zellteilung, was auf eine Verbindung zwischen den Rotationen und der Ringschließung hindeutet. François Nédélec und Eszter Lakatos haben vorgeschlagen, dass der Ring sich schließt, weil Zytoskelettbestandteile die Rotation der zellwandbildenden Maschinerie antreiben. Rotationen erlauben es, die Wand gegen den Turgordruck aufzubauen. Wir implementieren den Ring mit einem minimalen Satz an Bestandteilen und können damit die Rotationen und die Schließung des Rings *in silico* reproduzieren. Weiterhin schlagen wir vor, dass eine zusätzliche Funktion der Rotationen sein könnte, dass sie den Ring stabiler machen. Tatsächlich zeigen unsere Laserablationsexperimente, dass der Ring sich innerhalb von wenigen Sekunden nach der Ablation repariert.

In beiden Systemen haben wir mesoskopische Strukturen im aktiven Gel gefunden. Wir charakterisierten die Muster und Dynamiken und maßen wie sie sich unter verschiedenen Bedingungen ändern. Unsere Beobachtungen und Messungen führten uns zu zwei Modellen, die die Spannungserzeugung und die Ringschließung in den jeweiligen Systemen erklären. Es ist überraschend, dass zwei Aktomyosin Ringe unterschiedliche Dynamiken aufweisen können. Zukünftige Experimente werden darauf abzielen zu verstehen, welche Systemparameter entweder zu ruhenden oder rotierenden Inhomogenitäten führen. Wir schlagen vor, dass der Übergang von Zuständen von unterschiedlicher Struktur oder Dynamik ein Weg sein könnten, Aktomyosin-Systeme *in vivo* zu regulieren, zusätzlich zu traditionellen Signalwegen.

Contents

1 Preface

It is fascinating to watch a flock of birds on a day in autumn. As they "*swooped and circled high up in the air. Some raced in the furrows of the wind and turned and sliced through them as if they were one body cut into a thousand shreds*" [177]. It is spellbinding for the observer that individuals seem to perfectly work together, as if they were one.

Similar process take place in every moment in cells. The fine-tuned interactions of proteins, lipids and polynucleotides give rise to cells, tissues and organisms and they can also be described as one, as *living matter*.

The mechanical properties of cells and tissues are largely influenced by the cytoskeleton, a dynamic network of filaments and crosslinkers. In contrast to conventional gels, these filaments can change their length and even move by coordinated shrinkage on the one end and growth on the other. Additionally, motor proteins induce sliding and stress on filaments. Both processes, motor activity and polymerization, dissipate energy. These networks are therefore referred to as *active gels*.

In cells these structures are involved in a variety of events related to dynamics in cells or movement of cells and tissues, shape transformations and cell division. Cells can also sense the flows and elasticity of their environment with their "skeleton" and thereby translate mechanical cues into gene expression. Therefore the relevance of the cytoskeleton extends into many aspects of biology such as embryogenesis, cancer research, immunology, wound healing and synaptic remodeling.

It is fascinating that proteins of the size of nanometer can build structures which are 10^3 to 10^4 larger than themselves and exert forces much larger than the forces of individual motors. But how is that possible? What are the interaction rules guiding the formation of large, structured networks? How do they organize to generate stress to divide a cell or to constrict a tissue in embryogenesis?

Theoretical and experimental *in vitro* studies revealed that filament-motor systems can exhibit different spatial and temporal patterns, such as bidirectional motion and oscillations [131, 120], swirls [141, 156], traveling waves [32, 41, 85], asters [12, 156] and contractile rings [139, 125]. The beauty of *in vitro* systems is that parameters, geometries and proteins composition can be varied. However, in cells the parameter set is regulated by signaling and gene expression levels. The activity of active gel networks is often associated to a function and the network structure and dynamics have to be robustly reproduced in sensitive processes such as in cytokinesis or dorsal closure. Explaining the origin and dynamic of these structures is challenging. There is a variety of nucleators, crosslinkers and attachment proteins which build asymmetric 2D and 3D structures. This multitude of different proteins in addition to activity gradients is difficult to realize in *in vitro* systems, but is crucial to understand the complexity of active gels *in vivo*.

The cytokinetic ring is a relatively simple active gel *in vivo* due to its ring geometry. In animal and fission yeast cells it is composed of actin and myosin, amongst other proteins. After the cell has separated its chromosomes, an actomyosin ring forms and its constriction divides the cell into two. In this step actin filaments are aligned circumferentially to build a ring [142, 62]. But it is not clear how stress is generated in this system. Due to the alignment of actin filaments, a filament sliding mechanism as in muscles suggests itself. However, no sarcomeric structure was found in electron microscopy studies. It was also proposed that enhanced myosin activity and cortical flows lead to a higher contractility in the furrow [166]. Carvahlo *et al.* [20] proposed that the ring is composed of contractile units of actomyosin and membrane anchoring proteins. In any case, the mesoscopic mechanisms of stress generation and ring closure remain unclear.

We study the actomyosin ring in mammalian cells and in fission yeasts. Fission yeast is a fungus with a wall and under pressure, which influences its cell shape [128]. The molecular partners at cytokinesis are very well characterized. Mammalian cells do not have a wall, but an actomyosin cortex. They are about five times larger than fission yeast cells, but divide about six times faster. The difference in mechanical constraints and closure dynamics might be due to different closure mechanisms. Additionally both systems offer different technical options, e.g. mammalian cells are easy to stain and sensitive to cytoskeleton drugs, whereas the genetic toolbox for fission yeast is larger.

Cells on flat coverslips divide perpendicularly to the plane of observation. Z-reconstructions with conventional microscopy methods are poor in spatial and temporal resolutions. Observation of the rings in one plane of focus is possible in some stages of *C. elegans* development [20, 185], but this is a particular system and inconvenient to handle compared to stable cell lines. However, to reveal pattern or dynamics as predicted by active gel theory, one has to visualize the entire cytokinetic ring.

Daniel Riveline developed in his sabbatical stay in Paul Nurse Lab. at the Rockefeller University a setup to orient and observe fission yeast cells in microcavities ("*egg cups*") [130]. He found rotation of myosin and other protein speckles. We adapted this setup for mammalian cells. This allowed us to observe for the first time the cytokinetic ring in both systems in a single plane of focus. Our main findings are motifs in the distribution of cytoskeleton components in both rings. Intriguingly they reveal different dynamics. In fission yeast actin and myosin are rotating along the perimeter. In mammalian cells myosin and formin clusters move mainly radially during closure.

Together with our collaboration partners Karsten Kruse and Anne Wald from Saarland University and François Nédélec and Eszter Lakatos from EMBL, Heidelberg, we developed models for both systems to understand these patterns and dynamics. We were also able to associate a function to both structures. The order in mammalian rings leads to an overshoot in stress generation which allows an efficient closure. However, since fission yeast cells have to overcome the pressure difference between the cytoplasm and the medium, only ring contractility would not be sufficient for closure. Instead we propose that actomyosin is rotating the wall building machinery, which is then able to build the septum.

In the following I will first give an **introduction** into the topic. I will present active gel theory, molecular aspects of the cytoskeleton and their function in cells. Here I will focus on the actomyosin ring in mammalian cells and in fission yeast. I will then describe in detail the used **materials and methods** to give the reader the opportunity to retrace all technical aspects of our results. In the then following chapter, I will present our results. I will first present our findings regarding the **cytokinetic ring in mammalian cells** together with our analytic description of the ring. I will also mention alternative setups to observe actomyosin rings. Subsequently, the results about the **cytokinetic ring in fission yeast** are presented and the corresponding model. I will end the presentation of my PhD work with a **discussion** of the results and an outlook on future questions and experiments.

2 Introduction

Every life starts from one single cell. In the following, the cell divides giving rise to two new lives in the case of single cell organisms or it describes the onset of embryogenesis. In all steps the proper sequence of events is crucial.

Studying cell division means addressing fundamental questions for the understanding of cell biology. We aim at understanding this process under a physics perspective. At the onset of cytokinesis the cell changes dramatically its shape, rounds up and in its equatorial plane a ring gets formed. The constriction of the ring leads to the physical separation of the cell into two. Remembering the experience of squeezing a balloon, it is intuitive, that such a deformation needs force. Even though the molecular players in this process are known and well studied, it is not yet possible to explain how force is generated, so ultimately why the ring is closing.

This leads to a fascinating aspect of this event. Let us consider single proteins, they span dimensions of nanometers and are able to apply forces in the order of pN. However, in cytokinesis they organize into a ring structure that is much larger than themselves, tens of micrometers, and exert forces much larger than the highest force of individual proteins. Motor protein and filament are the key players of force development. They are also essential in muscle contraction. However, in contrast to muscle cells, there is often no evidence that filaments and motors are ordered in a specific manner in the cytokinetic ring or in other organelles built from these proteins. That is why it is still an open question how stress is generated in such networks.

Formally the network properties of motors proteins and filaments can be described as a gel, but an *active gel*. Both, filaments and motors, can transform chemical energy into mechanical work. Active gel theory aims at giving a generic description of these networks. A general theory accounts for any filament or motor type. However, in the introduction I will focus on myosin II motor proteins and actin filaments.

In this introduction I want to lay the foundation for the understanding and the motivation of our work. I will start with introducing the active gel theory, so the physical framework for the description of actin and myosin, but also other *active* networks. I will then present the molecular details of actin and myosin in particular, but also mention other cytoskeleton structures. After this, I will present *in vitro* and *in vivo* systems of filaments and motors, to give finally an introduction in the state of knowledge of the cytokinetic ring.

2.1 Active gel theory

Many phenomena in biology involve the cytoskeleton. The cytoskeleton can exhibit a variety of shapes and is involved in different cell functions. During cytokinesis (reviewed in e.g. [122]) and wound healing [91, 16] cytoskeleton rings form, in cell motility the leading edge is expanded to probe and the cell is then pulled in the direction of motion (reviewed in [9]). The cytoskeleton can also exhibit oscillatory behaviors on all levels of organization (reviewed in [78] and [77]). Although these phenomena might appear quite different, the underlying structure is the same: A network of biopolymers crosslinked by passive crosslinkers and motors – an *active gel*. Their interaction rules and activation schemes lead to different shapes, patterns and dynamics.

Active gel theory aims at giving a generic, quantitative description for these networks and to provide a conceptual framework for understanding the manifold cellular and supracellular process associated to active gels.

Since the cytoskeleton is essentially composed of crosslinked filaments, it can be described as a gel. However, in contrast to simple polymer gels, its components are *active*, that is, they can transform chemical energy into mechanical work. They undergo shape transformations by dissipating energy. Actin filaments dynamically change their length due to polymerization and depolymerization/disassembly and myosin motors induce filament sliding and stress generation. Other proteins regulate these processes e.g. Rho activation can locally increase myosin activity (see Section 2.2.1). These processes are driven by the hydrolysis of nucleotides, in particular ATP. Cytoskeleton networks are therefore out-of-equilibrium systems.

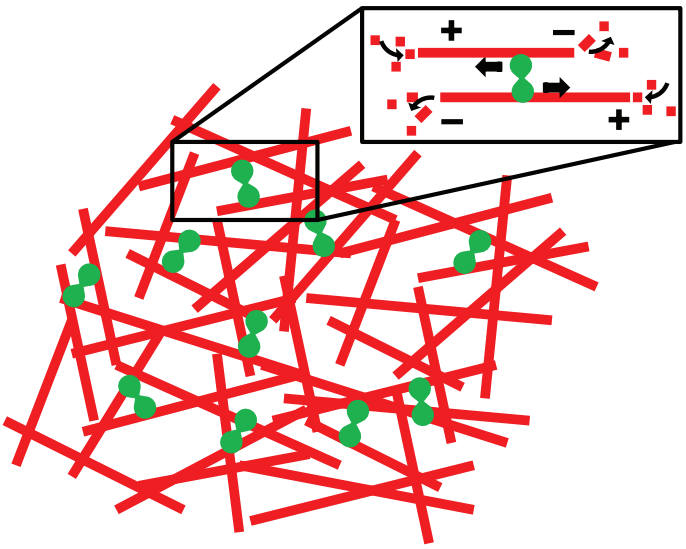

FIGURE 2.1: Schematic representation of a polar active gel. Filaments (here actin-like, red) and motors (here myosin II-like, green) form a network. Motors induce filament movement and the filaments grow and shrink.

The cytoskeleton can display macroscopic polar order, which is another important characteristic. Ultimately, the macroscopic polarity has its origin in a structural polarity of the cytoskeletal filaments. Filaments are asymmetric, they have two distinct ends: the (+)- and (–)-end. Molecular motors are sensitive to the polarity. For example myosin II motors move towards the (+)-end. Other motors are (–)-end-directed (Fig. 2.1). The

same is true for microtubules and associated motors (see Section 2.2.2).

Active gels can be described in two prominent ways [60]: (i) starting from a hydrodynamic approach. The hydrodynamics of active (polar) gels captures the behavior on large length and time scales similar to the hydrodynamics of Newtonian fluids. The gel is essentially viewed as viscoelastic fluid and characterized by phenomenological parameters that are analogous to the viscosity of a Newtonian fluid. This description is largely independent of the molecular details of the gel components. This allows to apply this framework to a variety of systems. (ii) Another way of capturing active gels is to build their description on the characterization of the molecular players and to define interaction rules. This approach requires detailed knowledge of the biological system but allows to describe the system on shorter length- and timescales and to identify molecular mechanisms of stress generation.

Both approaches are complementary. In the following, both will be presented.

Hydrodynamic theory Generally one distinguishes between chemical and physical gels. In the former, the filaments are crosslinked by covalent bonds, in the latter polymers are connected via physical bond, such as polar interactions. Physical gels can be remodeled upon stress application. Depending on the lifetime of the bonds, they will show a viscous or elastic response within certain time windows.

In general active gels are thus viscoelastic. Often they show an elastic response on short and a viscous response on long timescales. The Maxwell relation gives a characteristic time (*relaxation time* or *Maxwell time*) for this transition as $\tau = \frac{\eta}{\mathrm{E}}$, where η denotes the viscosity coefficient and E the elastic modulus.

Kruse *et al.* [74] presented a hydrodynamic theory of active polar gels. They found three constitutive equations, relating momentum flux, polarization changes and the rate of ATP hydrolysis with velocity gradients, the molecular field h and the activity $\zeta\Delta\mu$.

In a simplified, linear hydrodynamic theory, one can write for the stress in an active gel [58]:

$$\sigma = 2\eta u - \zeta\Delta\mu \tag{2.1}$$

where σ denoted the stress, η the viscosity, u the velocity gradient, which is in general a tensorial quantity. This is neglected in this one dimensional approach. ζ is a material property describing the active processes of (de-)polymerization and myosin activity and $\Delta\mu$ the free energy linked to the hydrolysis of ATP ($\Delta\mu = \mu_{ATP} - \mu_{ADP} - \mu_{P_i}$). For polar gels other terms need to be added, which couple the orientational field to the stress.

Application of the hydrodynamic theory will be presented in the Section 2.5.1.2 “Theoretical description of cytokinesis”.

Microscopic approach In the mentioned above hydrodynamic approach, the activity is often assumed to lead to a contractile stress. However, the molecular mechanisms for stress generation are not specified within this approach. The microscopic approach is defining interactions between filaments and motors and captures the dynamic of the sin-

gle elements. The dynamic of an actomyosin system, e.g. a bundle of polar filaments, can then be described in a mean-field description. Finally the material parameters can be linked to the molecular interactions.

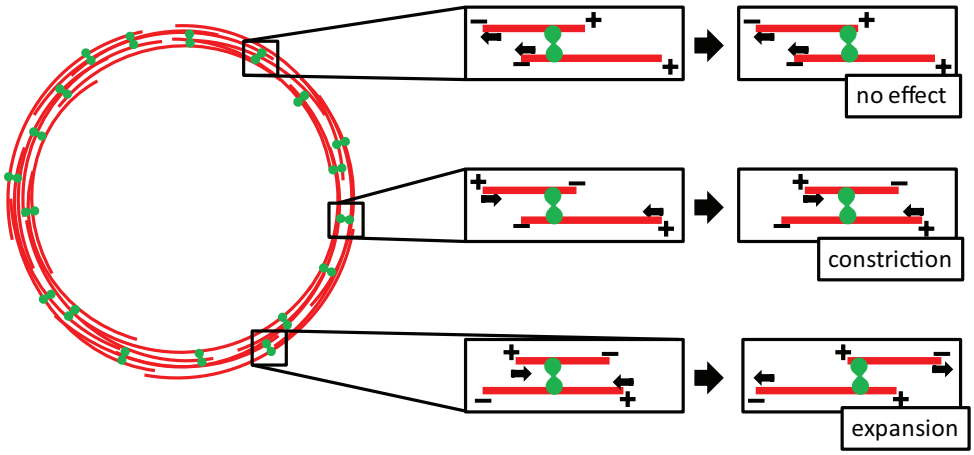

FIGURE 2.2: Schematic representation of a simple description of the interaction of two actin filaments via myosin motors. If actin filaments are parallel, myosin moves them in the same direction. This does not lead to constriction. Antiparallel filaments get first constricted but then pushed apart. So both mechanisms do not lead to constriction.

It is not obvious how a system of filaments and motors would be contractile. As represented in Figure 2.2, in the simplest picture of actomyosin interaction, myosin can constrict and expand a two-filament system.

Kruse and Jülicher [75, 76] introduced a model to describe an active contractile bundle. In these 1D systems, they differentiate essentially between filaments pointing with the (+)-end in the one or the other direction. Their concentrations are referred to as c^+ and c^-. Motors induce filament currents. They mediate interactions between overlapping filaments. The model is a coarse-grained description of the system, that is to say, that not single filaments are considered but their concentration distributions. Only two-filament interactions are considered.

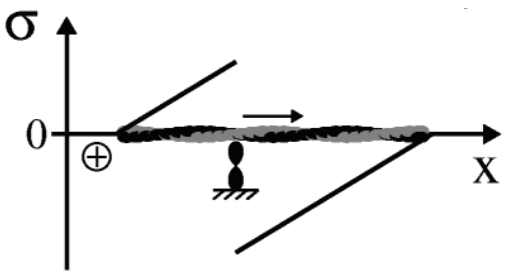

FIGURE 2.3: Displacement of filaments due to motors leads to the depicted tension σ profile. Filaments are considered as rigid rods being moved through a viscous medium. (Figure from [75].)

Kruse and Jülicher showed that these filament bundles shorten. This is due to interactions of parallel filaments. Interaction of antiparallel filaments leads to filament sorting [159].

Motors pulling on filaments lead to a tension profile as depicted in Figure 2.3. Filaments are considered as rigid rods being dragged through a viscous fluid. The tension on the rod is highest at the point, where the motor binds and decreases linearly along its length. It is zero at its end. The tension is negative in the part in front of the motor

and positive behind the motor, where the filament is tensed due to friction with the fluid. Interactions between other filaments are neglected. To derive the tension of a bundle, the tension of individual filaments is summed up. For a stable, homogeneous bundle with periodic boundary conditions – a ring – the tension is positive and the ring contractile.

Another way of describing active gels on a molecular level is to implement the gel ingredients and their interactions in a numerical simulation [156]. With this approach one can easily simulate also complex, 3 dimensional systems, with several kinds of interaction partners with complex behaviors [86, 87]. Single protein behavior as well as the dynamics of the entire systems can be calculated. Also small systems might be well captured by this approach, whereas a mean-field description might be problematic due to the small amount of interaction partner and the importance of molecular noise [45]. However, such simulations require good knowledge about all kinds of parameters describing different aspects of the involved proteins. These parameters are generally either not known or not known in physiological conditions or measured, but for different organisms, than the organism under study. The large number of free parameters introduces potentially large errors. Apart from that, the entire parameter space has to be probed, that is to say simulated, to derive a general description of the system, e.g. to predict dependencies of the system from a specific parameter.

2.2 The cytoskeleton

So far we have seen how to describe a network of active filaments and active crosslinkers. But what is the molecular basis for this description? What are the physical and biochemical properties of these building blocks? I will now present the experimental description of such systems by first introducing the molecular aspects of the gel components and then describing their collective behavior *in vitro* and *in vivo*.

The cytoskeleton is a generic expression for these filaments, whose organization and dynamic results in shapes and shape transformations of cells. The three main types of filaments are *actin filaments*, *microtubules* and *intermediate filaments*. I will focus in the following sections on actin filaments and microtubules, since these structures are relevant to follow the reasoning of this work.

2.2.1 Actomyosin and associated proteins

In the following section, I will describe the actin and myosin and associated proteins from a single molecule perspective to establish a basis to understand collective effects and regulatory mechanisms in the following chapters.

2.2.1.1 Actin and related proteins

Actin is a 45 kDa protein [55]. These monomers are able to polymerize to filamentous structures (F-actin). The monomers are held together by weak noncovalent interactions which allow fast remodeling [8]. Actin filaments are built of two *protofilaments* which organize into a helix (Fig. 2.4). Since the monomers and the filaments are asymmetric,

one distinguishes between the (+)-end or *barbed end* and (–)-end or *pointed end*.

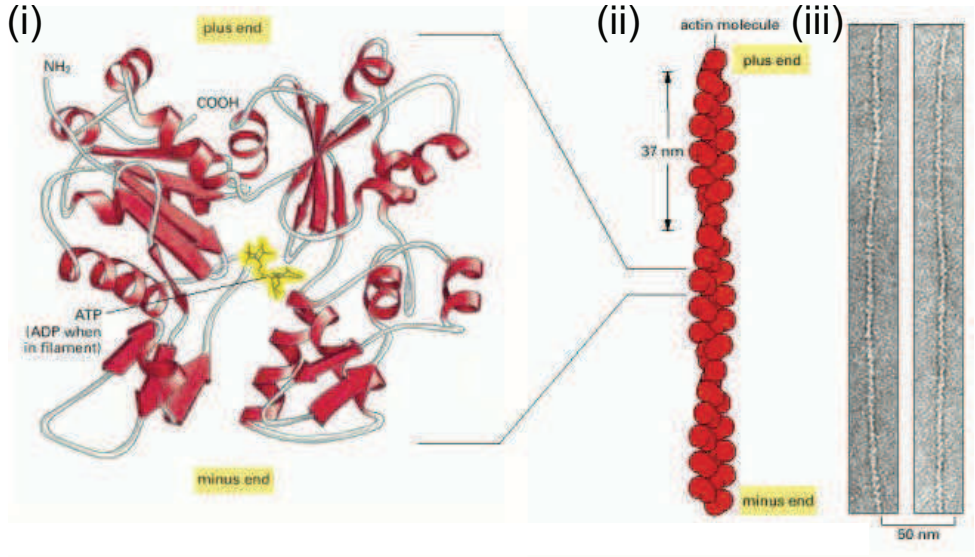

FIGURE 2.4: (A) Actin monomer have a binding site for ATP and ADP. They are asymmetric, and the filament ends are denoted (+)-end or barbed end and (–)-end or pointed end. (B) Monomers organize to helical filaments. Their helical pitch is 37 nm. (C) Electron microscopy images of actin filaments. (Figure from [8]).

After the assembly of monomers, ATP is hydrolyzed to ADP, which reduces the binding affinity of the monomers [8]. Therefore the polymerization and depolymerization are dependent on the form of the nucleotide bound to the subunit.

However, the polymerization kinetics depends also on the filament end to which a subunit is added or removed, since the monomers are asymmetric. The (+)-end is considered to be the fast growing end and the (–)-end is slowly growing or shrinking. Absolute values depend on the salt, actin and ATP/ADP concentrations.

Depending on the (de-)polymerization rates, filaments can undergo a net shrinkage or net growth. If filaments are essentially added to the (+)-end and removed from the (–)-end, the filament moves in the direction to which the (+)-end is pointing. This dynamic is called *treadmilling*.

These rates vary depending on the salt, ATP/ADP and monomer concentrations. In cells polymerization is favorable, since the actin-ATP concentration is above the critical value for polymerization [55].

The mechanical properties are described by the Young's modulus of actin filaments, which lays at around 2GPa [55]. Their persistent length is 15 µm and diameter at around 7 nm [55].

Nucleators Formins are members of a protein family, having in common a formin homology 2 (FH2) domain. Mammals have 15 genes associated to this domain [14]. It is probably this domain, which is responsible for accelerated nucleation and polymerization

on the barbed end [52]. Formin is a leaky cap nucleator, that is to say, that it is attached to the (+)-end while the filament is still growing on this end [184] (Fig. 2.5 (B)). It is also protecting the (+)-end from other capping protein [184]. Together with profilin, formins are accelerating polymerization. Formins of the mDia subfamily are shown to bind also to microtubules [14].

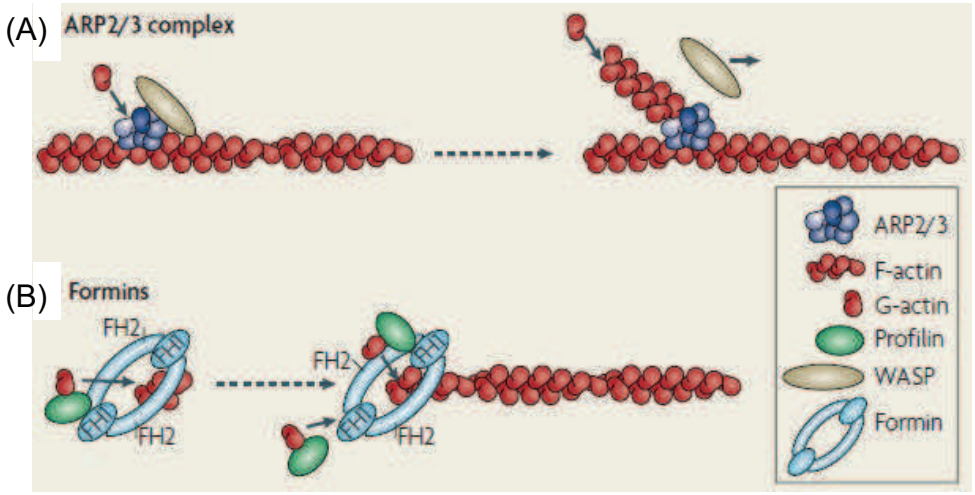

FIGURE 2.5: (A) Arp2/3 binds to existing filaments and nucleates new filaments. Arp2/3 is bound to the (–)-end of the newly formed filament. WASP is activating Arp2/3 and unbinds after the new filament is nucleated. (B) Formin consists of FH1 and FH2 domains. The FH2 domain is bound to the (+)-end of the filament and stays on this end, although the filament is growing. FH1 is recruiting profilin, which is accelerating polymerization. (Figure from [93]).

The Arp2/3 (actin-related protein) complex is thought to generate branched actin networks [8]. It binds to preexisting actin filaments and nucleates new actin filaments. These filaments will grow at fixed angle to the old filament (Fig. 2.5 (A)). Arp2/3 is involved in numerous cell functions, such as lamellipodia growth, endo- and exocytosis and vesicle and organelle motility [49].

Crosslinker A variety of different actin crosslinkers exists, such as fimbrin, α-actinin and filamin. Crosslinkers have strong influence on the mechanics of actin gels, e.g. permanent crosslinking renders the gel stiffer, whereas crosslinkers with a lower affinity render the gel rather viscous [171, 170, 154].

There are two kinds of crosslinkers: crosslinkers which build bundles and crosslinkers which allow large angles between filaments, building 3D gels. Fimbrin and α-actinin are bundling actin filaments. A loose packing, as induced by α-actinin, allows myosin entering the bundle, whereas too tight packing, as induced by fimbrin, excludes myosin [8]. These tightly packed actin networks of parallel filaments can be found in microvilli for example. α-actinin was reported to be involved in cytokinesis in fission yeasts and mammalian cells [103, 82].

Filamin on the other hand crosslinks filaments in an angle of about 90°. It is involved

in lamellipodia formation for example [8].

Actin monomers build polar filaments, which can dynamically grow and shrink. Actin networks are regulated by crosslinkers. Affinity and crosslinking geometry define the mechanical properties and the network architecture. One other important class of proteins interacting with actin are motor proteins, which will be presented in the following.

2.2.1.2 Myosin

Myosin is an actin related motor protein. The superfamily of myosins knows 14 myosin types. The subfamily of myosin II consists of skeletal, cardiac and smooth muscle myosins, as well as non-muscle myosin [26]. I will focus on non-muscle myosin II in the following, since this type is relevant for cytokinesis.

Figure 2.6 shows a schematic representation of myosin II molecules (i) and their organization in filaments (ii). Myosin consists of two heavy chains and four light chains. It has two motor heads. Myosins form bipolar filaments, which are also called mini-filaments due to their appearance in electron-microscopy imaging [8].

Myosin activity is regulated by phosphorylation of the heavy and light chain [8]. The light chain is phosphorylated by myosin light chain kinase (MLCK), which is a downstream target of Rho. Phosphorylation of myosin light chain also favors the organization in mini-filaments [8].

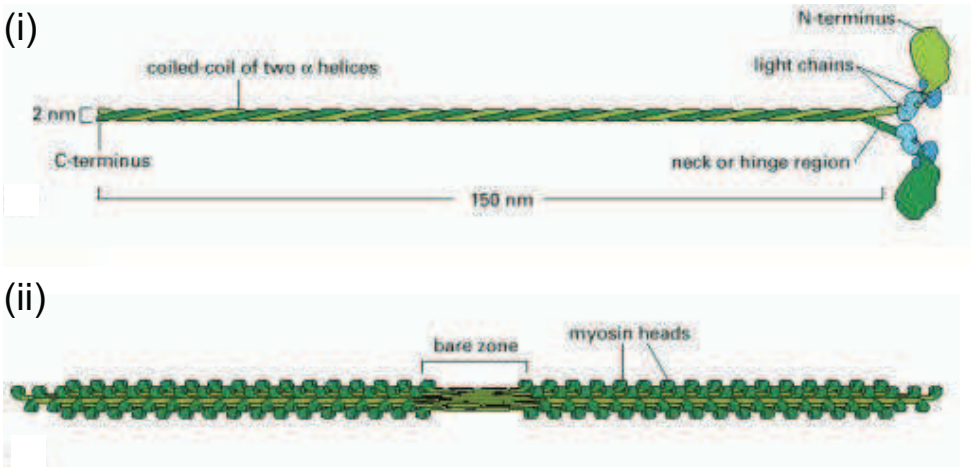

FIGURE 2.6: (i) Myosin consists of two heavy chains and four light chains. The two heavy chains are coiled and the light chains are located in the neck regions. (ii) Myosins can organize in filaments. (Figure from [8]).

Myosin heads can undergo conformational changes while being attached to actin filaments. This cycle of conformational changes is schematically presented in Figure 2.7. While binding ATP, myosin is not attached to actin. After the hydrolysis of ATP to ADP + P_i the head undergoes a conformational change and myosin binds to actin. Phosphate release results in a movement of the head (*power stroke*). The cycle restarts after the release of ADP, the dissociation of myosin from actin and the binding to ATP [8]. Myosin

is only strongly bound to actin in the conformations colored in red. During this cycle it is only about 3 % to 5 % of the time in this state [55, 8, 150]. So, the so-called *duty ratio* of myosin is low.

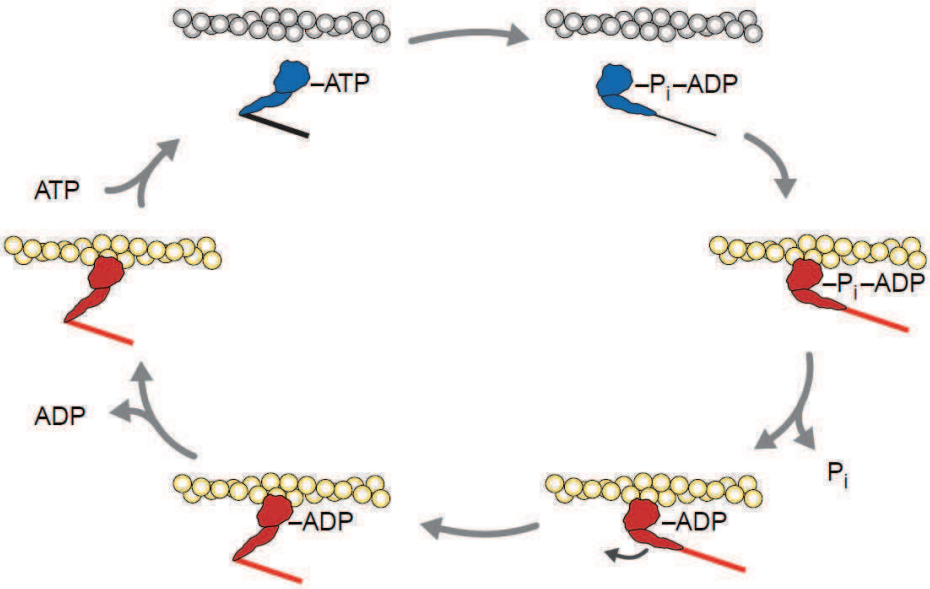

FIGURE 2.7: Schematic representation of the cycle of myosin conformational changes. After hydrolysis of ATP, myosin binds to actin. The release of phosphate leads to a conformational change, the *power stroke*. Binding to ATP leads to detachment of myosin from actin. (Figure from [104]).

Due to the polarity of actin filaments, myosin II moves with respect to actin always in the same direction, towards the (+)-end. Myosin II is not a processive motor, that is to say, it is not attached to actin in between ATP hydrolysis cycles. However, myosin filaments are effectively processive, since some heads will always be bound to actin, if the filament is long enough.

Finer *et al.* [40] measured the step size of myosin to be 11 nm and its force to be between 3 pN and 4 pN. In sliding filament assays, myosin is attached to a surface and actin filaments *slide*, so move on the surface driven by myosin in the presence of ATP. Actin speed is then dependent on the myosin density and on ATP concentrations, among other parameters. Depending on the myosin type, velocities between 0.2 µm/s and 60 µm/s were found [8].

Actin and myosin are involved in different cellular processes, which will be discussed in the following. But before I want to introduce another cytoskeleton structure: Microtubules.

2.2.2 Microtubule

Microtubules are another important cytoskeleton structure. They are also involved in cytokinesis, since microtubule structures (spindle) are separating chromosomes (in mammalian cells) or position the nucleus (in fission yeast). I will therefore give a brief introduction.

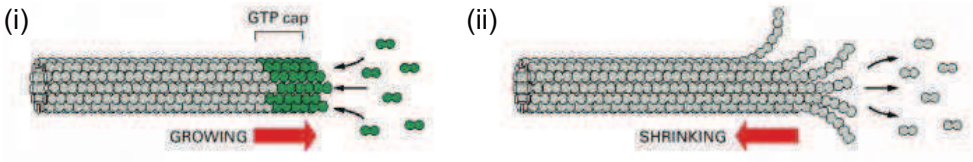

FIGURE 2.8: (i) Microtubule polymerize by adding tubulin dimers with GTP. GTP in β-tubulin is hydrolyzed after the dimer is bound to the filament. However, if polymerization is fast, a *cap* of GTP-bound dimers forms. (ii) If the polymerization is not fast enough, GTP is hydrolyzed to GDP. Then the depolymerization is faster and the filament is shrinking rapidly (*catastrophe*). Figure from [8].

As actin, microtubules are filamentous structures composed of dimers of α- and β-tubulin. The dimers can form protofilaments. Microtubules are built of 13 parallel protofilaments, which form a hollow cylinder (Fig. 2.8 (i)). Also they have a much larger persistent length than actin filaments i.e. 5 mm [47]. They are polar filaments: α-tubulin point to the (–)-end, the β-tubulin to the (+)-end. [8]

Both, α- and β-tubulin bind GTP. However, only in β-tubulin it gets hydrolyzed after the dimer is bound to the filament. If the rate of polymerization is larger than the hydrolysis rate, a cap of tubulins bound to GTP is generated (*GTP cap*). Depolymerization is about 100 times faster on a GDP-end than on a GTP-end. If the polymerization speed slows down, e.g. because dimer concentration is low, a filament might lose its GTP cap. As a consequence the filament turns into a rapidly depolymerizing state. This event is called *catastrophe* (Fig. 2.8 (ii)). Rapid change between shrinking (*catastrophe*) and growing (*rescue*) is called *dynamic instability*. Microtubule can be stabilized or destabilized by proteins. [8]

There are two types of microtubule related motors: dynein and kinesin, which are superfamilies of motor proteins. Dyneins move towards the (–)-end of the microtubule. They are involved in vesicle transport in the cell. Kinesin is a (+)-end-directed motor. Similar to myosin, kinesin can form two-headed motors and crosslink filaments. They are involved in mitotic and meiotic spindle. [8]

We have now discussed the properties of individual filaments and motors. In the next section I will discuss how networks of filaments and motors behave *in vitro* and *in vivo* and how they are associated to cell functions.

2.3 *In vitro* actomyosin systems

In the previous section, I introduced the proteins forming filaments and motors. This knowledge is helpful to describe the interaction between single filaments and motors. However, one cannot deduce in an obvious manner the collective behavior rising from their activities. *In vitro* experiments are an ideal assays to control the protein composition and their concentrations. I will now discuss some selected examples of *in vitro* experiments. Please note that *in vitro* experiments, which concern the cytokinetic ring are presented later, in section 2.5.3.

By controlling the protein composition, Loisel *et al.* [84] were able to reconstitute minimal requirements for actin-based movement. They were able to reconstitute the actin-based motility of the bacterium *Listeria monocytogenes* using a minimal set of purified proteins (actin, Arp2/3, ADF(cofilin), capping protein). Indeed, *Listeria monocytogenes* moves by controlled actin polymerization, which illustrates that actin polymerization can build forces [162] (Fig. 2.9 (A)). Cameron *et al.* [19] were able to reconstitute this motion *in vitro* with polystyrene beads (Fig. 2.9 (B)).

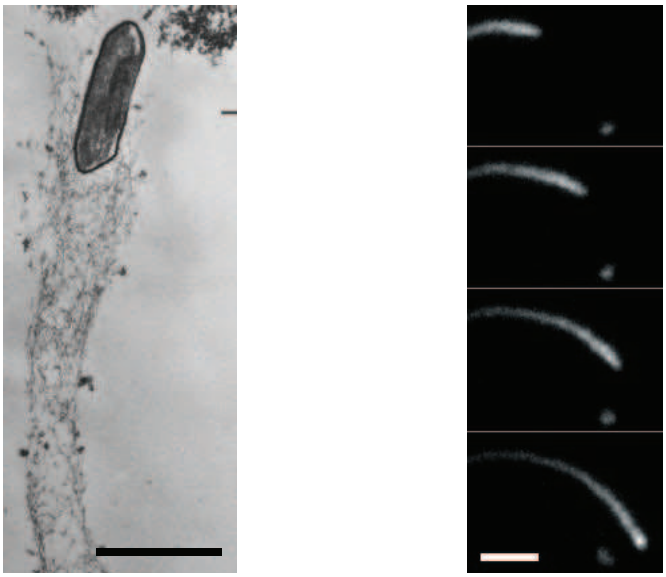

(A) (B)

FIGURE 2.9: (A) Motion of *Listeria monocytogenes* by actin polymerization. The trajectory can be retraced by the actin tail. Scale bar = 1 µm. Figure from [162]. (B) *In vitro* reconstitution of actin-driven motion. Beads are coated with ActA-His, which is allowing actin polymerization. Scale bar = 5 µm. Figure from [19].

Kron and Spudich [72] presented in 1986 a motility assay, where myosin is bound on a surface, but still able to move actin filaments. This approach is also working for microtubule and associated motors [56]. Since then, many experiments have been performed in this type of assay. Actin motion depends on the type of motor and the motor density. Additionally, the filament motion can be manipulated by applying external forces such as optical tweezer [66] and microneedles [66]. In an electric field actin filaments can show a

coexistence of two velocity regimes [131]. This is probably a consequent of the collective effect of several motors interacting with one filament as predicted by Jülicher and Prost [61]. At high filament densities, the interaction of filaments leads to the formation of different kinds of patterns, such as waves and swirls [141].

In bulk experiments, motors are not bound to the surface, but can crosslink filaments and apply stress. Surrey *et al.* [156] showed that (+)-end-motors and microtubule organize into structures like vortices and asters. These assays are also used to measure the mechanical properties of actomyosin gels as a function of the composition [170, 57, 152]. Myosin activity gives these networks unusual material properties [67].

In vitro assays allow to control the composition and geometry of active gels. This allows to reconstitute cell phenomena with a minimal set of proteins. The collective behavior leads to regular patterns and dynamics. Networks of filaments, crosslinkers and motors exhibit unusual material properties and constitute a new class of materials. To learn about these networks it is critically important to understand associated cell phenomena. In the following I will first discuss briefly the organization and function of actomyosin networks *in vivo* in general, to continue with a more detailed illustration of the knowledge of the cytokinetic ring in mammalian cells and in fission yeasts.

2.4 *In vivo* actomyosin systems

Actomyosin networks are involved in many cell structures. I will present some of these structures in the following pages.

2.4.1 Muscle cells

The muscle cell is an excellent example of how the action in concert of actin and myosin leads to efficient stress generation. This is due to the optimized order between actin filaments and (muscle) myosin II motors.

Figure 2.10 (i) shows muscle fibers, which are built of fused myoblasts and which are the contractile units of muscles. The mechanism of muscle contraction is schematized in Figure 2.10 (ii). Actin (red) and myosin II (green) filaments are aligned between Z-disks. This unit is called *sarcomere*. Upon muscle activation, myosin pulls the Z-disks together. Because the filaments seem to slide on each other, this model is called *sliding filament* model. The sarcomere organization is depicted in Figure 2.10 (iii). Myosin and actin filaments are parallel. Their structure is given by their attachment to the Z-disks, where the actin filament (+)-ends are bound. Since myosin II filaments "walk" towards the (+)-end, they bring the two Z-disk closer. Because this event is highly coordinated in the muscle, the entire muscle contracts.

The muscle cell is an example for a clear organization of actin and myosin. The mechanism for stress generation is evident in these cells. In the following, I will present examples of actomyosin networks in other cells, which do not show that apparent order.

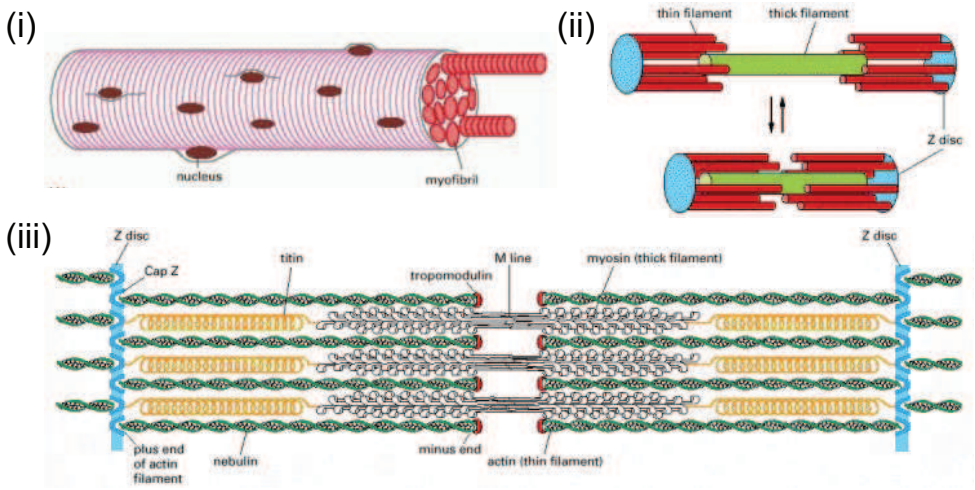

FIGURE 2.10: (i) Muscle cell precursor, myoblasts, fuse and give rise to muscle fibers, with several nuclei. (ii) Schematic representation of the sliding filament mechanism. Myosin filaments are green, actin filaments are red. Due to their alignment, they contract efficiently. (iii) Sarcomere organization. Actin and myosin filaments are aligned in between so-called *Z-disks*. In this configuration myosin can contract the sarcomere efficiently. Myosin is held by titin. (Figures from [8].)

2.4.2 Cell cortex

The cortex is a thin actomyosin layer directly underneath the plasma membrane of animal cells. Electron microscopy studies reveal that filaments form a isotropic mesh of filaments which are mainly parallel to the membrane (Fig. 2.11). The mesh size ranges from 20 nm to 250 nm and the cortex thickness is about 50 nm to 100 nm [100, 24].

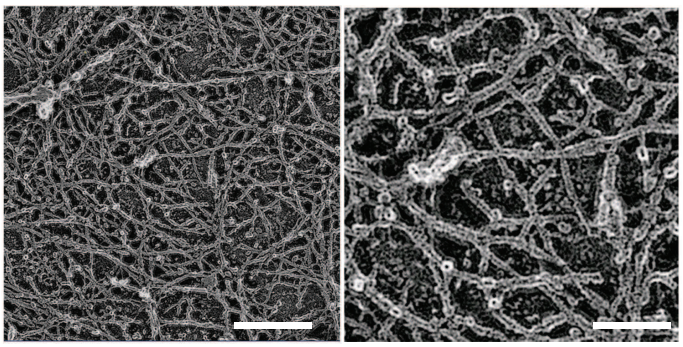

FIGURE 2.11: Electron microscopy image of the cortex in normal rat kidney fibroblast. Right: Magnification of left image. Scale bar 300 nm (left) and 100 nm (right). (Figure from [100].)

Apart from actin and myosin, crosslinkers like α-actinin, fimbrin and filamin are in the cortex, as well as membrane attachment proteins from the ERM-family (Ezrin-Radixin-Moesin) [24, 37]. Formins nucleate actin in the cortex [34].

The cortex is a viscoelastic structure. On timescales shorter than its turnover time it is elastic. Turnover relaxes the system. The elastic modulus was estimated to be in the order of 10^3 Pa [163]. On longer timescales than the turnover time, the cortex behaves like a fluid. The turnover half time was estimated to be between 15 s and 45 s for actin and faster for other components (see review [138]).

Another interesting parameter of the cortex is the tension. Prior to cytokinesis the cell rounds up and increases its volume by osmotic pressure [151]. Lancaster *et al.* [80] show that confined cells show defects in cell division. Increase in cortex tension and the associated rounding seem thus to be crucial for successful cell division. This is for example relevant in tissues, where cells are confined by neighboring cells. The values for cortical tension vary by two orders of magnitude and lay between $10\,\mathrm{pN/\mu m}$ and $10^3\,\mathrm{pN/\mu m}$, depending on the cell type. For fibroblast they lay in the order of $10^2\,\mathrm{pN/\mu m}$ (see review [138]). Collective increase in cortex tension is relevant in different processes in embryogenesis, such as mesoderm invagination in Drosophila or neural tube closure in vertebrates. This topic would exceed the scope of this introduction, but an overview is given in the review of Martin [90]. However, the paragraph demonstrates, that the cortical actomyosin gels are involved in many processes. And understanding them requires knowledge of actomyosin networks and associated proteins. In the following, I will present another cellular phenomena, which shows how polarized actomyosin organization and activity can lead to cell migration.

2.4.3 Cell migration

Some cells move by swimming using cilia or flagella. Although these are also interesting cytoskeleton structures, I will focus here on the movement of cells on substrate, on cell crawling, driven by actomyosin networks.

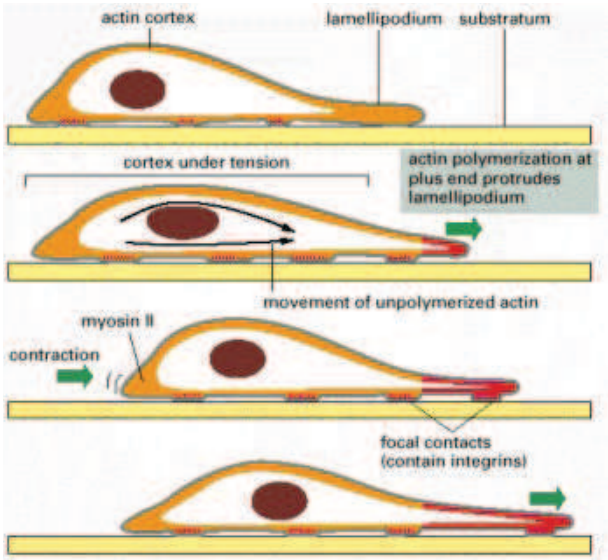

FIGURE 2.12: Schematic of cell motility. The cell is attached to the surface by focal contacts. As it is moving, it expands protrusions (lamellipodia) and builds new attachment sites (focal contacts) with the surface. The rear of the cell is contracting to allow the cell to move forward. (Figure from [8].)

The process of cell migration can be roughly divided in a cycle of three steps (Fig. 2.12). (i) The cell is elongating its front. These protrusions are laminar (lamellipodia) or filamentous (filopodia) [148, 93]. (ii) The cell attaches to the surface, building focal contacts or other forms of attachment sites. (iii) The rear of the cell is retracted.

In the beginning of the 1970th Abercrombie, Heaysman and Pegrum [1, 2, 3, 4, 5] published a series of papers describing lamellipodia morphology and dynamics. They described them as flat cell protrusions of a thickness of about $0.2\,\mu\mathrm{m}$. They also found dense patches in electron microscopy (EM) images, which they identified as adhesion sites.

Importantly they pushed forward the idea that a cell is migrating by extending itself to form protrusions over the substrate.

Today one knows that lamellipodia grow by actin polymerization. Actin filaments are organized in a dense network, with filaments mainly oriented with their (+)-ends towards the direction of motion. Thus filaments assembly takes mainly place at the leading edge, which is pushed by polymerization. Figure 2.13 (A) shows images from the lamellipodia of keratocytes, which are cells from fish epidermis with large lamellipodia and strong polarization. Svitkina and Borisy [157] showed that Arp2/3 localizes in these cells in the leading edge. EM pictures reveal branched actin networks in this region. They also showed that cofilin localizes in the lamellipodia, but not in its very edge. These findings lead to the scheme of lamellipodia growth as depicted in Figure 2.13 (B). Actin and Arp2/3 build a branched network. Cofilin is severing actin. Since it binds preferentially to "old" filaments (actin-ADP), it is not locate in the very leading edge. The actin assembly pushed the front of the lamellipodia.

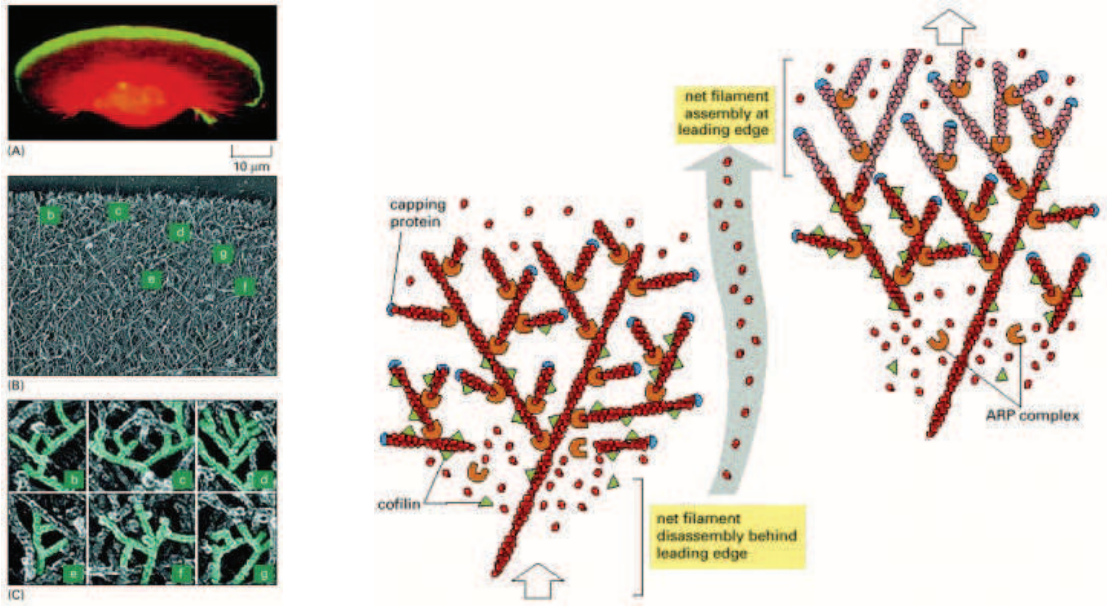

(A) (B)

FIGURE 2.13: (A) Top: Migrating keratocyte. Actin is labeled in red, Arp2/3 in green. Middle and bottom: Electron microscopy images of the leading edge of a keratocyte, revealing the branched actin network. (B) Model of actin-driven protrusions. Actin is organized in a network branched by Arp2/3 nucleation. Cofilin is destabilizing the network in the back of the lamellipodia. (Both panels from [8], (A) originally published in [157].)

Contractile stress during motion is built by stress fibers. These actomyosin bundles contain actin and myosin. In some types of stress fibers periodic accumulations of myosin, α-actinin and other proteins are found (reviewed in [105]). Laser ablation of stress fiber led to retraction [69] and cell shape remodeling [79]. Stress fibers are attached to the substrate via focal contacts, which are protein complexes connecting the extracellular matrix (ECM) with the cytoskeleton.

But stress fibers do not only allow cell movement, they are also important sensors of the mechanical properties of the environment. Riveline *et al.* showed that focal contacts grow upon force application, emphasizing the ability to sense forces and the active regulation of these units [133] by signaling. Later Plotnikov *et al.* [121] demonstrated, that focal contacts can measure ECM rigidity in some range fluctuating forces applied by stress fibers and they identified this as a mechanism for durotaxis. The ability to measure rigidity, forces and flows is crucial for some steps in embryogenesis: for example stem cell differentiation is influenced by the elasticity of the substrate [35] and cardiac morphogenesis is dependent on blood flow [54].

We have seen that the actomyosin networks in cells are involved in many basic cell functions and therefore also in multicellular dynamics such as in embryogenesis. They do not only allow to apply force to the environment, but also enable the cell to sense the mechanical properties of their surrounding. In my PhD project we studied a particular actomyosin structure: the cytokinetic ring. In the following I will give an introduction into cytokinesis and the current understanding of the cytokinetic ring derived from studies *in vivo* and *in vitro* together with theoretical works.

2.5 Cytokinesis

Cytokinesis is the event where the cell divides in two. This is fundamental for single cell organism for proliferation, such as bacteria and yeast. But it is also the mechanism which leads to growth in developing organisms. And also in adult animals and humans, this process takes constantly place to renew tissues.

Yeast and mammalian cells divide by forming an actomyosin ring. Bacteria have a similar but different system. They form so-called Z-rings of FtsZ, a tubulin homologue (reviewed in e.g. [6]). Plants divide by the formation of a *cell plate*, which is growing from the inside of the cytoplasm to the wall (review in e.g. [53]).

I will focus on the cell division in mammalian and fission yeast cells and in particular on the role of the actomyosin ring.

2.5.1 Cytokinesis in mammalian cells

During the cell cycle, i.e. the time between two divisions, the cell prepares for the next cell division. All organelles are replicated and the entire DNA is duplicated. Figure 2.14 shows a scheme of the cell division [123]. Prior to cytokinesis, the cell rounds up and DNA aligns at the center of the cell, it is departed and each identical part of the chromosome is pulled by microtubules (spindle) to one of the two poles of the cell. Then the physical separation of the cell begins. A contractile ring of actin filaments and myosin II motors is formed and able to exert a force which is contracting the cell in its middle plane and leading to a physical division of one cell into two.

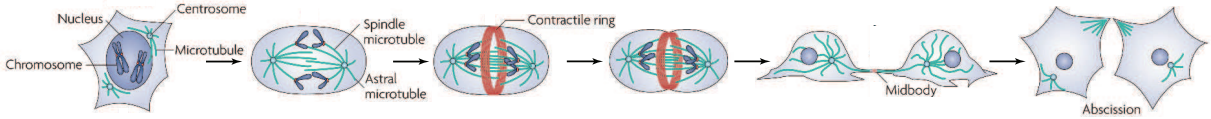

FIGURE 2.14: At the onset of cytokinesis, the cell rounds up. The nucleus disassembles and the chromosoms get aligned in the equatorial plane of the cell. Microtubules and associated proteins help to separate the chromosomes. A contractile ring is cleaving the cell into two. A midbody, still containing microtubules stays stable for some time before cell division is completed by abscission. (Figure with slight modifications from [123].)

2.5.1.1 Cytokinesis in mammalian cells – Experiments

The position of the division plane is given by the cell geometry and its attachment points [98, 161]. Théry *et al.* [161] proposed that the position of the chromosomes, and thereby of the division side, is depending on the cytoskeleton, i.e. microtubules. They argued that microtubules, which are attached at anchoring points to the cell membrane and the nucleus exert forces, which position the chromosomes during cell division. In their model the equilibrium position, when microtubule forces are balanced, depends on the geometry of attachment sides. They supported this idea experimentally on mammalian cells by imposing different geometries by microcontact printing of fibronectin motifs. A similar model was presented some years later by Minc *et al.* [98]. They squeezed sea urchin cells in microchambers of different shapes. They emphasized that the position of the nucleus depends on the geometry of the cell in a similar manner as in the model of Théry *et al.*.

The biological characterization of the cytokinetic ring and its formation were reviewed by Glotzer [48]. Studies on different organisms suggest that – as for other parts of the cytoskeleton – the assembly of the ring depends on the regulatory proteins of the Rho pathway [33, 65, 109]. When the chromosomes are separated and pulled towards the poles of the cell, a high microtubule concentration occurs in the division plane of the cell, where microtubules overlap. There are indications, that microtubules are involved in the activation of Rho A [180, 15, 155]. Ect2 seems to be essential in this process. It interacts with microtubule related proteins (Centralspindlin) and activates Rho A [181, 107]. Also the astral microtubules seem to help to restrict the Rho activity to the mid-zone [169, 44, 15].

The Rho pathway activates actin assembly and myosin, and thereby the assembly of the cytokinetic ring (Fig. 2.15): On the one hand Rho activates ROCK, which phosphorilates the regulatory light chain, which leads to myosin assembly and activation (see Section 2.2.1.2). Rho also activates formins [7], which together with profilin increase actin nucleation and polymerization (see Section 2.2.1.1).

The architecture of the ring was visualized by electron microscopy (EM) studies from the 70s and 80s on mammalian cells (Fig. 2.16). They revealed that the ring is composed of bundles composed of actin filaments and myosin [143, 140, 94]. Schroeder [143] described the ring in HeLa cells as a band of 0.25 µm to 0.5 µm width and a thickness of about 0.1 µm. Decoration of actin filaments with heavy meromyosin allows to determine their

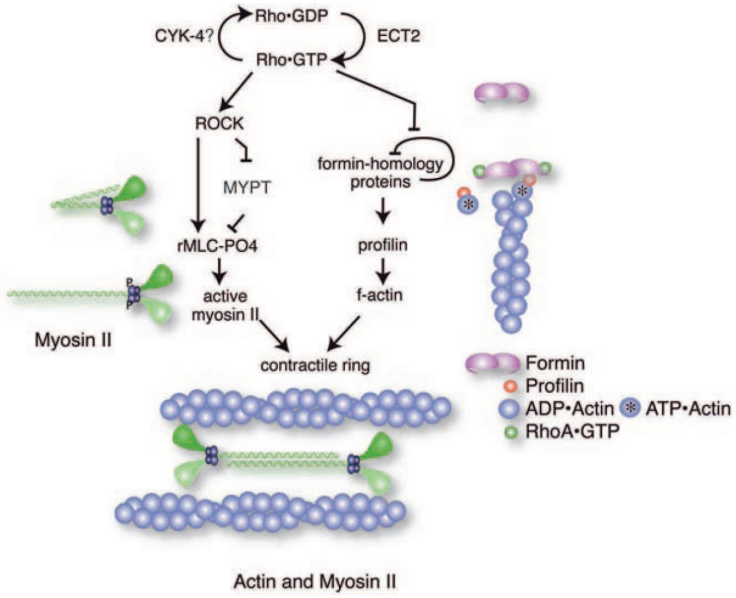

FIGURE 2.15: Ect2 activates Rho. Rho is on the one hand leading to the activating myosin and myosin assembly via activation of ROCK and the phosphorylation of the regulatory light chain. Also other kinases are involved in its phosphorylation, such as citron kinase. On the other hand Rho is stopping the auto-inhibition of formin. Together with profilin, formin is nucleating actin filaments. According to the scheme, the activation of Rho in the division plane leads to the formation of the cytokinetic ring. (Figure from [48].)

orientation in EM images. Actin filaments are found in both orientations within the ring [140], i.e. the filaments point with the (+)-end clockwise as well as counterclockwise. Maupin and Pollard reported [94] electron-dense sites from which actin filaments are radiating out. They speculated that these could correspond to membrane attachment sites.

The orientation of filaments parallel to the ring was later confirmed by fluorescence detected linear dichroism microscopy [42], which reveals the orientation of actin filaments by using polarized light. The study also showed, that actin filaments are not aligned during metaphase but they orient at the onset of cytokinesis.

But how is the ring attached to the membrane? Septin and anillin seem to play an important role here. Septin is a family of proteins – humans have more than 10 septin genes – that assemble to filaments [38, 63, 136]. Septin is an interesting candidate to attach the cytokinetic ring to the membrane. On the one hand, it interacts with lipid membranes [182, 17]. On the other hand, septins are shown to interact with myosin [59] as well as with actin via anillin or directly [110, 64, 39, 95]. Septin bundles and bends actin filaments [64, 95]. Anillin was reported to be important for recruitment of septin and furrow localization [39]. Apart from this, it interacts with main proteins involved in cytokinesis (amongst others, ect2, actin, myosin, septin, rho) and has potentially many roles in this event [119].

Why is the ring contractile? Carvalho *et al.* [20] proposed a closure mechanism based on their observation in *C. elegans* embryos – a system different from mammalian cells in its organization and its mechanical rules, yet relevant for its cytokinetic ring. In their

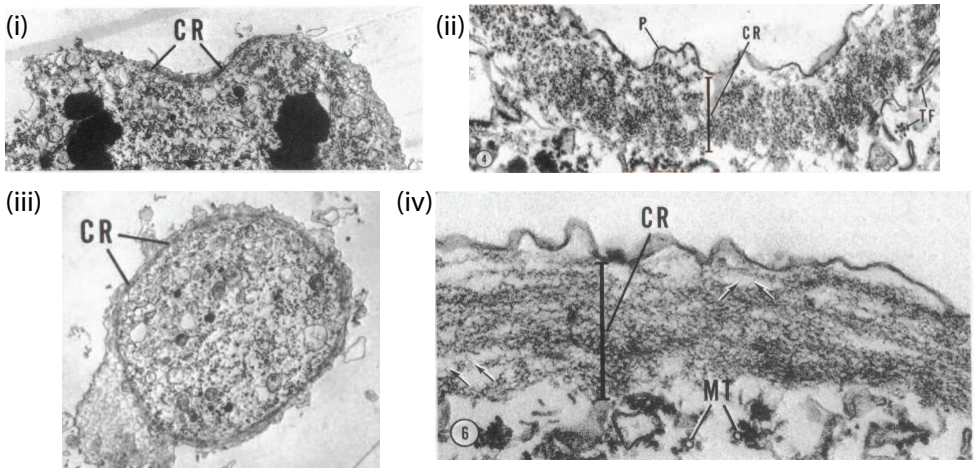

FIGURE 2.16: Electron microscope images of the cytokinetic ring in HeLa cells. (i) and (ii) show a cut perpendicular to the plane of the ring, whereas the cut in (iii) and (iv) goes parallel through the plane. The ring is a band of actin filaments. The filaments are aligned and curved. Arrows point at fibers which are thought to correspond to myosin filaments. (CR: cytokinetic ring, P: plasma membrane, MT: microtubule) (Images from [143].)

study, they were analyzing the closure with respect to the initial size of the cell and accordingly the initial perimeter of the ring. The closure rate was linearly dependent on the initial size of the cell and was constant in duration in the first phase of cell division. They investigated the behavior of myosin, anillin and septin in the ring and find that their concentrations stay constant during closure. They present a model, describing the cytokinetic ring as built by *contractile units* comprising myosin, actin, anillin and septin (Fig. 2.17). They propose that the length of the units is constant and thus that their number scales with the perimeter. Hence, larger rings would contain more units than smaller ones. If units contract with a constant speed, larger rings would close faster. They furthermore suggest that the contractile units shorten during constriction, which leads to a constant concentration of the involved proteins. The observation that the closure speed is proportional to the perimeter is indeed intriguing. Also the fact that the concentration of myosin, septin and anillin are constant together with the low turnover, suggest that they might form stable units or protein complexes. However, the model does not make clear how the contractile units are organized or why they are contractile. Additionally, there are no evidences for separated mesoscopic units.

At the onset of cytokinesis an actomyosin ring forms in the equatorial plane. Actin filaments align circumferentially in the division plane. Actin and myosin built a circular bundle. However, it is not clear how this leads to constriction. Carvalho *et al.* [20] propose that the ring is organized in contractile units, but there is no experimental support for an ordered organization in the ring. In the following section, I will present theoretical studies which aim at explaining aspects of cytokinesis and stress generation.

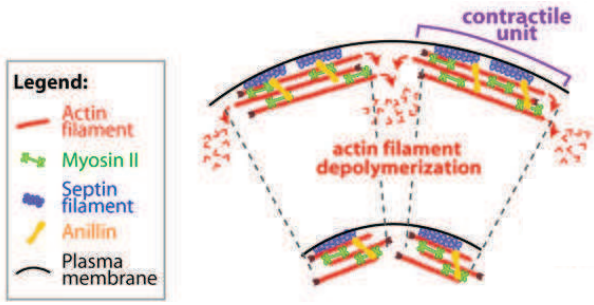

FIGURE 2.17: Schematic of the contractile unit model, proposed by Carvalho *et al.* [20]. In the model, the ring is composed of units of actin, myosin, septin and anillin. Septin and anillin attach the ring to the plasma membrane. They propose that contractile units shorten due to actin depolymerization. The shortening is therefore independent of the size of the units. The number of units scales with the ring diameters. Therefore the closure speed is proportional to the initial perimeter. (Figure from [20].)

2.5.1.2 Theoretical description of cytokinesis

In the following section, I will present models explaining the formation and closure of the cytokinetic ring. They represent hydrodynamic and microscopic approaches to active gels.

Upon increase of Rho activity in the mid-zone, the ring formation begins: myosin is activated and filaments align in one plane.

2005, Zumdieck *et al.* [186] presented a general continuum theory, which demonstrates how rings can form in the cortex. They show that different patterns can form in a two-dimensional cortex due to dynamic instabilities associated to active processes of filaments and motors. In particular they show filament alignment to rings. These rings can be stationary and oscillatory, as it was reported in [18, 112].

The formation of the ring was also reconstituted by a model of Salbreux *et al.* [139]. They modeled the cortex as polar active gel in a hydrodynamic framework, as introduced in section 2.1, describing its activity with $\zeta\Delta\mu$ and the order with a nematic order parameter Q. They can show that an increase in myosin activity in the furrow, induces cortical flows, which compress the cortex in the furrow and stretch it outside (Fig. 2.18). Additionally these flows lead to an alignment of filaments in the furrow as it was observed in different studies [143, 140, 94, 42].

Turlier *et al.* [166] reproduced the full furrow ingression dynamics. The cortex is again modeled as a viscous fluid, since the release of elastic stress is fast due to rapid turnover. Myosin activity is not immediately increased, but implemented by a time-dependent spatial profile, similar to profiles measured from fluorescently labeled RhoA [15]. The increase in activity in the furrow leads to cortical flows and accumulation of cortex in the furrow, which goes along with an increased thickness in the furrow. The model reproduces the dynamic of furrow ingression and the cell shape. According to the model, furrow activity needs to overcome a threshold value to complete ingression. The model also predicts that

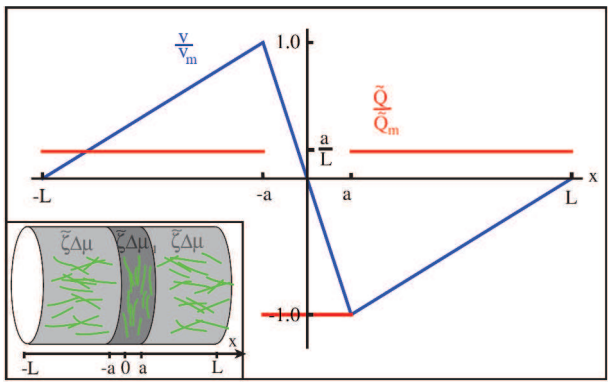

FIGURE 2.18: Result of the hydrodynamic model of the cortex by Salbreux *et al.* [139]. L indicates the length of the system and a the width of the zone of myosin activation. Increase of activity in the furrow $\tilde{\zeta}\Delta\mu_1$ leads to cortical flows (blue: normalized cortical flows $\frac{v}{v_m}$) and filament alignment (red: normalized order parameter $\frac{\tilde{Q}}{\tilde{Q}_m}$). (Figure from [139].)

actin turnover plays a critical role in division. With a too high turnover, the effect of cortical flows would be eliminated and thereby the accumulation of matter in the furrow. But the latter is crucial for tension. Interestingly, the model gives a time for closure, which is independent of the cell size, as observed by Carvalho *et al.* [20].

Another approach of describing ring closure consists in the microscopic description of actomyosin interaction. As described in Section 2.1, Kruse and Jülicher [75, 76] studied the mechanical properties of active bundles. The bundle can be reduced to a one dimensional system, due to symmetry arguments. With periodic boundary conditions, it corresponds to a ring and its contraction to a ring closure.

2007, Zumdieck *et al.* [185] built on this model and combined it with a mesoscopic description of cytokinesis. The latter consisted in expressing the mechanical work, which has to be done during ring constriction. In their picture, the generated stress has to elastically deform the ring and work against the viscous forces associated to the cell constriction.

The expression of the generated stress is derived from microscopic considerations: The study presents mechanisms of stress generation due to motors and to filament treadmilling. Motor activity can generate stress in a two-filament system, if the motor stays attached to the (+)-end. Parallel filaments become then aligned. However, they show also that stress is generated more efficiently by treadmilling of filaments connected with passive, end-tracking crosslinkers. This mechanism is more efficient, since interaction of parallel and antiparallel filaments contribute to stress generation. The total stress in the bundle is roughly proportional to the square of the filament concentrations. The proportionality constant is a material constant which includes the number of bundles and their length but also the interaction activities of filaments in the presented stress generation processes. Zumdieck *et al.* were able to reproduce quantitatively the closure dynamics of *C.elegans* embryos.

I introduced experimental and theoretical studies and hypotheses about the formation and closure of the cytokinetic ring. Increased contractility due to myosin can explain ring formation and furrow ingression. However, it is not clear if and how myosin and actin are organizing in the ring and experimental data are missing to explain how stress is

generated. These results will be compared to our findings and discussed in the following chapters. But before that, I will present the state of knowledge about the cytokinetic ring in fission yeast.

2.5.2 Cytokinesis in fission yeast

Fission yeast or *Schizosaccharomyces pombe* is a fungus. It is a single cell organisms surrounded by a rigid sugar cell wall. Despite these differences to animal and human cells, these organisms have in common, that they divide by the formation of an actomyosin ring. In fact, amoebae, fungi and animals share most of the genes used for cytokinesis [123]. This makes it an interesting model organism for the understanding of cytokinesis.

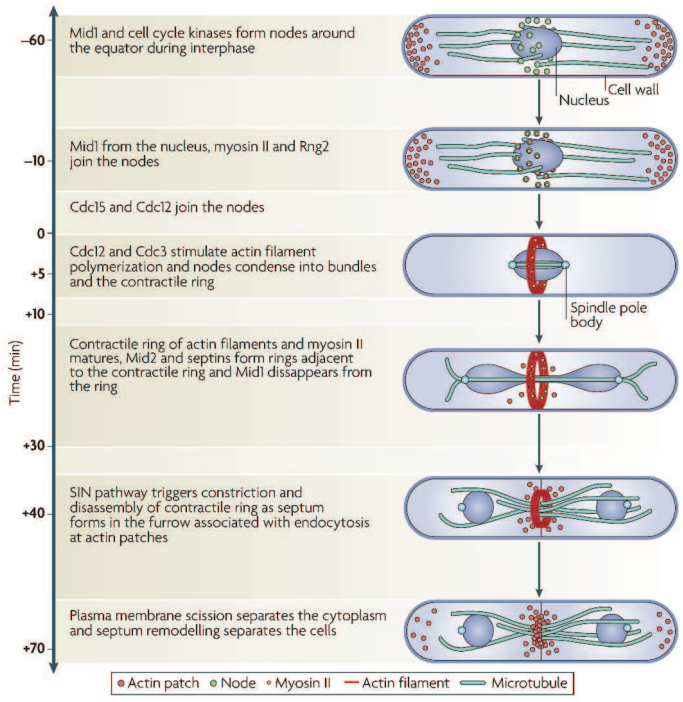

FIGURE 2.19: About one hour before the spindle pole bodies separate, node form around the nucleus. They contain at this stage anillin-like Mid1 and other proteins. Nodes mature and myosin II, Rng2 Cdc15 (F-BAR) and Cdc12 (formin) join the nodes. Together with Cdc3 (profilin) nodes nucleate actin filaments. Nodes and filaments condense to a ring. Septin and Mid1 form adjacent rings. While the ring closes, the septum forms and actin patches appear around the cleavage furrow. The DNA is separated in the nucleus. Finally the plasma membrane is separated and the septum completed. (Figure from [123].)

The formation of the ring is well understood in fission yeast, although some questions remain open [123]. Prior to cell division, nodes (protein complexes) form around the nucleus. They form at this location due to a local signaling from the nucleus [114]. As the cell grows, the concentration of this inhibitor is lowered in the mid-zone and the accumulation of node protein takes place [101, 92]. About 10 min before the separation of spindle poles begins, other proteins are added to the nodes. In particular about 25 myosin II and about two formin Cdc12 join the nodes [178]. Cdc12 nucleates actin filaments together with Cdc3 (profilin) [71, 23]. Actin filaments assemble and the ring starts closing [25]. As the ring closes, cell wall is building continuously in the equatorial plane, the *septum*.

The cell wall is composed of two main polysaccharides of (1,3)β-glucan and (1,3)α-glucan [117]. It is mainly built by a family of proteins, the glucan synthases α-glucan-synthase (Ags) and β-glucan-synthase (Bgs). They localize at the poles during growth and at the septum during cell division. Amongst other factors, this might be mediated

by the membrane tension [128]. Ags1, Bgs1 and Bgs4 are shown to be essential for the growth of the septum [28, 27, 29]. Muñoz *et al.* propose that Bgs4-derived (1,3)β-glucan is required for correct and stable actomyosin ring positioning [102]. Interestingly Rho is involved in the activation of Bgs [11].

Organization of F-actin polarities in the fission yeast ring is controversial. Electron microscopy studies on fission yeast cells indicated that the ring formation emanates from one point near the plasma membrane. Filaments grow around the cytoplasm and start to overlap on the opposite side of the cell, after 180° [62]. Such a mechanism for formation of the ring would – at least at the beginning of closure – lead to a very efficient stress generation, since the ring architecture would be comparable to the highly ordered structure of actin and myosin in muscles (*sarcomeric structure*). However other studies reported that the ring is forming in a less ordered manner [167]: Nodes contain on average two formins and can therefore nucleate two filaments. Vavylonis *et al.* [167] suggest a *search and capture* mechanism (Fig. 2.20). Nodes are distributed in a band around the nucleus. When actin polymerization begins, nodes can interact via actin filaments. Since nodes contain myosin, they pull on the filaments of neighboring nodes. This leads to the condensation of the band of nodes and to the formation of the ring. Such a mechanism would result in an unordered mesh of actin and myosin and is therefore difficult to reconcile with the electron microscopy presented above.

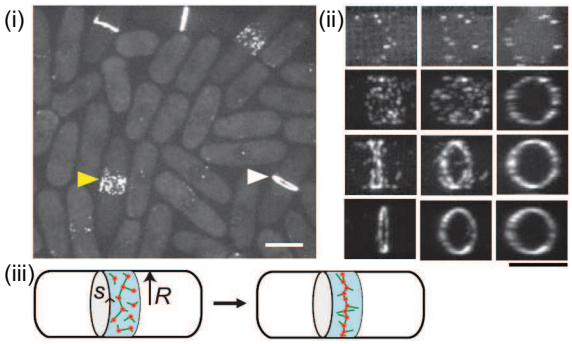

FIGURE 2.20: (i) A fission yeast culture expressing the labeled node protein Rlc1p-3GFP. Before division, nodes are distributed in a band (yellow arrow head). The cytokinetic ring is condensed (white arrow head). (ii) 3D reconstruction of cells at different stages of ring formation. Nodes are distributed in a band before they condense to a ring. (iii) Schematic representation of the search and capture model (nodes: red, actin: green). When a node "finds" the filament of a neighboring node, it pulls the other node: the ring condenses. Scale bars 5 µm. (Figure from [167].)

Regarding the mechanical aspects of cyokinesis, one has to know that fission yeast cell stand under a high turgor pressure of about 1 MPa [97]. The cell shape is maintained by a rigid cell wall [128]. The requirements for cytokinesis are in so far different as the cell has to work against the pressure to close the ring and build a septum. Force generation is potentially due to actin dynamics and myosin activity. Wu and Pollard [178] gave absolute numbers and concentration for the 28 cytoskeleton and signaling proteins during cytokinesis. They found that myosin concentration increases during closure, while the concentration of actin-binding proteins remains constant. It is not clear if stress generation is only due to myosin activity. It is proposed that actin activity can contribute to stress

generation [115]. Mendes-Pinto *et al.* [96] observed that actin depolymerization plays a major role for constriction in budding yeast cytokinesis. A recent study are also suggested that at least part of the stress generated to close the ring is not generated by actin and myosin, but by parts of the protein machinery which is building the wall [124]. One main argument for this claim is, that myosin is not applying enough force to overcome the turgor pressure of cells.

It is clear that despite a large amount of data on this topic, many questions remain open for explaining cell division. *In vitro* experiments can help to improve the understanding of contractile actomyosin rings and cytokinesis. Amongst others, there is a debate how stress is generated by the cytokinetic ring and how it can constrict against the high turgor pressure.

2.5.3 Contractile rings *in vitro*

In mammalian cells and fission yeasts a large number of proteins is involved in the formation and closure of the cytokinetic ring. But what is the exact role of these proteins? Are they all required for contractility? *In vitro* systems allow potentially finding a minimal system of proteins to allow ring contraction, as it was demonstrated by Loisel *et al.* [84] for actin-based motility (see section 2.3).

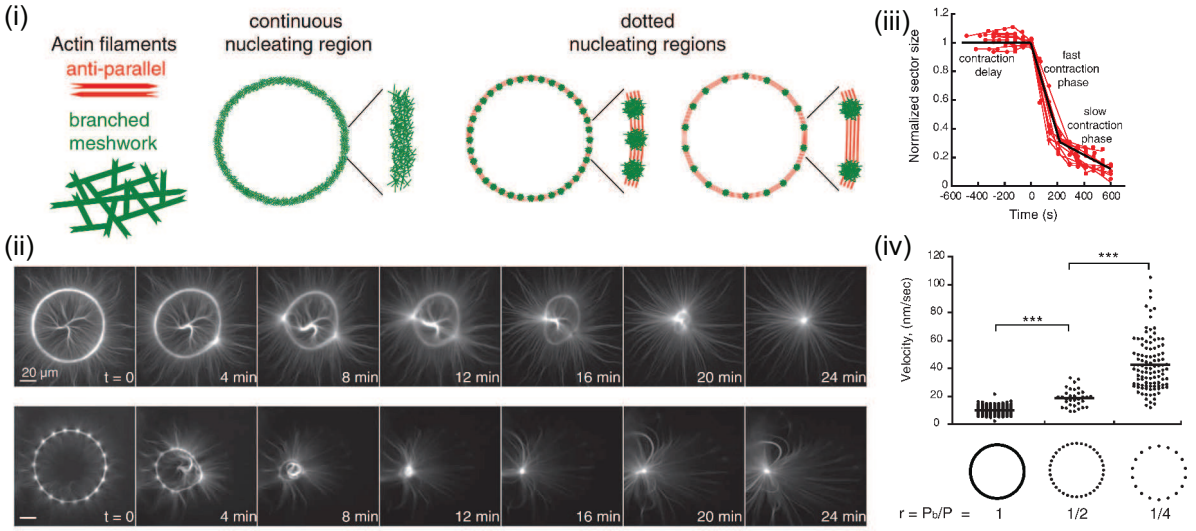

FIGURE 2.21: Reymann *et al.* patterned a surface with actin nucleation sites. (i) Schematic representation of the configuration of actin filaments depending on the pattern of nucleators. In regions with nucleation sites, the filaments are branched, in between they are antiparallel. (ii) Examples of closing actin rings. The ring on the top is built of a branched network; the ring on the bottom is built of an only partially branched network. The latter is closing faster. (iii) Ring diameter as a function of time. The closure can be divided in three phases: a contraction delay, a fast and a slow contraction phase. (iv) Comparison of branched and less branched networks. Rings with a higher proportion of antiparallel filaments close faster. (Figures from [125].)

Reymann *et al.* [126] presented an *in vitro* assay to control the nucleation sites of actin, which allowed them to master the geometry of actin networks. The polymerization was

induced by patterning a surface with Wiskott-Aldrich syndrome protein pWA domain and Arp2/3, profilin and actin monomers. In their assay, they used different motors, but mainly myosin VI, a processive (–)-end-directed motor, which can bind to two filaments without forming mini-filaments. They used this setup to generate contractile ring structures [125] (Fig. 2.21). A continuous pattern of nucleation sites leads to a branched actin network. Dotted ring patterns give rise to regions where filaments align antiparallel. The size of these regions depends on the density of dots (Fig. 2.21 (i)). These rings are contractile and close on minute-timescales (Fig. 2.21 (ii)). The closure behavior describes a S-shape (Fig. 2.21 (iii)). Interestingly the closure speed is dependent on the pattern: rings with a higher ratio of antiparallel filaments close faster (Fig. 2.21 (iv)). They also report that networks crosslinked with α-actinin do not undergo closure. Instead myosin accumulations rotate on the ring and disassemble the actin mesh.

This study show that branched and ordered circular actomyosin networks contract. It is interesting to note that they used a (–)-end-directed motor. However the filaments are also attached with the (–)-end to the substrate. In the cytokinetic ring the situation might be inverted: Actin is nucleated by formin, which binds to the (+)-end. But myosin II is also a (+)-end-directed motor. This assay is therefore a very interesting model for the cytokinetic ring, and shows that a system of nucleator, filaments and motors leads to ring contraction. The closure is on similar timescales as the ring closure in mammalian cells.

Mishra *et al.* [99] reported a setup to study the cytokinetic ring *in vitro*, which is based on deriving the ring from fission yeast cells. They removed the cell wall of fission yeast cells and obtained so-called *spheroplasts*. After ring formation in spheroplasts, they permeabilized these cells and obtained "*cell ghosts*", *i.e.* cells with a cytokinetic ring surrounded by a plasma membrane full of holes. This setup allows them to manipulate the ring with cytoskeleton drugs and mutation of fission yeast proteins.

They report that proteins necessary for ring formation and closure stayed in the ring, whereas cytoplasmic proteins were drastically diluted. Upon addition of ATP the ring constricts. Membrane attachment seems to be largely disrupted, since they observe no membrane invagination. The ring closes much faster than in fission yeasts with cell wall: in about 1 min, which corresponds to a speed of about 100 nm/s. These values depend on ATP concentration, but lay in the same order of magnitude as the closure speed for mammalian cells and the *in vitro* rings of Reymann *et al.* [125].

They show that the ring closure is driven by myosin, whereas actin seems not to be actively involved in the closure. Myosin inhibitor Blebbistatin treatment stalled closure and rings with myosin mutants, which show a decreased ATPase activity, slowed down the closure speed. Filamentous actin even nearly completely disappears from the ring. Stabilization with Jasplakinolide and phalloidin did not affect the closure rate and decreased polymerization with Latrunculin A or Cytochalasin D did not have an important effect on the closure speed either. As suggested by other studies [82], they also find that a proper balance of crosslinking is essential for contraction. They conclude that the minimal requirements of the cytokinetic ring consist in myosin activity, filamentous actin and appropriate actin crosslinking. Actin polymerization and disassembly are not required.

Mishra *et al.* present a setup which allows them to study freestanding actomyosin rings and to manipulate them with drugs and mutations. They identify main proteins for cytokinesis and show that myosin is required for ring closure, but not actin polymerization or disassembly. Myosin is in both systems – the ring from Reymann *et al.* and from Mishra *et al.* – crucial for contractility. Both rings close on similar timescales, though no obvious order is observable. However, Reymann *et al.* show that closure speed is increased when imposing a regular pattern of dots, which leads to a higher fraction of antiparallel aligned filaments. Mishra *et al.* point out the importance of appropriate crosslinking. The contractile ring of Reymann *et al.* closes without other crosslinker than myosin.

So the two presented experiments show a proper crosslinking, motors and filaments are needed for closure. The closure is driven by myosin, which might also play a role in crosslinking. Patterns with a higher ratio of antiparallel filament close faster.

3 Materials and Methods

3.1 Microfabrication

In the following section different techniques are presented to obtain shapes and patterns of the size of micrometers. First, I introduce photolithography, which is used to form microstructures in a photoresist layer. These structures are then replicated to PDMS by replica molding. The PDMS piece can then serve as stamp for microcontact printing or as mold for microcavities (*egg cups*). Afterwards I detail the preparation of microcavities. Finally it is explained how to obtain micropatterns of proteins by microcontact printing. Detailed product and equipment information can be found in Table A.2 and Table A.3.

3.1.1 Photolithography

Photolithography is a widely used technique. The following protocol is schematically depicted in Figure 3.1. A silicon wafer is heated at 200 °C for at least 15 min. This will improve the attachment of the photoresist to the wafer. After the wafer has cooled down, photoresist is spin-coated for 30 s. The spinning speed as well as the following parameters vary depending on the desired thickness and on the photoresist. An overview of the parameters is given in Table 3.1. After spin-coating the wafer is heated for a given time on 65 °C and 95 °C (*prebake*). In the mask aligner a photolithography mask is pressed on the photoresist layer: During the exposure with UV light, it protects some areas from light. We used negative photoresist, which means that the parts which are exposed to light will not be solvable anymore, whereas the other part stay solvable and will be removed in the development step. Next the wafer is heated first at 65 °C then at 95 °C (*postbake*). Then the photoresist layer is incubated with the corresponding developer for 2 min and then spin-coated for 30 s at 1500 rpm. This step is repeated twice. A small volume of isopropanol is poured on the photoresist layer. If this is revealing white streaks, this means that not all photoresist was removed yet and the developing step is repeated. Finally the wafer is kept for at least 10 min on 200 °C (*hard bake*). This improves the stability of the photoresist layer.

3.1.2 Replica molding

PDMS and the curing agent are mixed in a ratio of 10:1 (v/v). After centrifuging the mixture at 800 g to remove air bubbles, it is poured on the photoresist layer, which was patterned by means of photolithography. To remove air inclusions, the wafer is exposed to vacuum in a desiccator until all bubbles disappear. This makes sure, that PDMS fills all the mircostructures. The PDMS is cured at 65 °C for at least 2 h. The part of interest

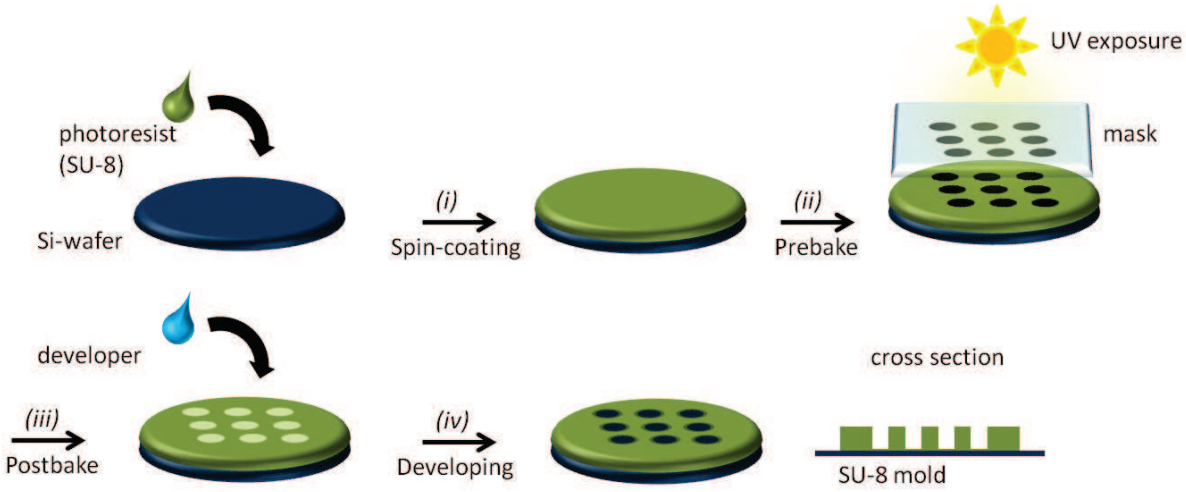

FIGURE 3.1: (i) Photoresist is spin-coated on a silicon wafer. (ii) After the preback, the photoresist layer is exposed to UV light through a photolithography mask. (iii) After the postbake, only the exposed parts are solvable and (iv) can be removed with developer, to obtain an SU-8 mold.

is carefully cut out with a scalpel and can then easily be removed from the photoresist. The same wafer can be used over and over again to obtain new replicas.

For fission yeast a master with conical pillars was used. It was produced by means of reactive ion etching by Antonin Hoël, engineer in the Riveline Lab, at Femto (Besancon). The replica of the master contained conical wells. To derive a mold with pillars, a replica of the replica was produced: The first PDMS replica (primary) was plasma activated (30 s, O_2, flow 5,5, power 2,5) and silanized, by incubating the master for 7 min with chlorotrimethylsilane (TMCS) vapor. The silanizied replica was covered with freshly mixed, and therefore liquid, PDMS. After curing, the part of interest was carefully cut with a scalpel and could then easily be removed from the other primary PDMS replica. The primary replica can be used several times to obtain new replicas.

3.1.3 Microcavity preparation

This section presents how to produce coverslips with a thin layer of PDMS containing microcavities at the upper surface. Two techniques are used and presented in the following.

Technique 1 was developed by Daniel Riveline at the Rockefeller University in a sabbatical stay [130, 129]. Technique 2 is a modification of technique 1 and was developed by Fanny Evenou, postdoc in the Riveline Lab, and Christian Rick (IBMC, Strasbourg). Both protocols have in common that cavities are derived from a mold. The molds are produced as explained above with photolithography and replica molding. The used photolithography mask contained black disks of 15 µm to 27 µm, depending of the cell type and purpose. Such a mask produces holes of the same size in the photoresist layer and posts in the replica. The thickness of the photoresist layer was chosen to be 30 µm to 50 µm and determines the depth of the future microcavities.

Table 3.1: Parameters for different photoresists and thicknesses

Photoresist	desired thickness [µm]	spin-coating speed [rpm]	prebake time at 65 °C / 95 °C [min]	exposure time [s]	postbake time at 65 °C / 95 °C [min]
SU-8 2007	7	3000	1 / 2	20	1 / 2
SU-8 2007	10	1400	1 / 2	23.5	1 / 2
SU-8 2007	12.5	1000	1 / 2	24	1 / 2
SU-8 2015	15	3000	1 / 2	25	1 / 2
SU-8 2015	20	2200	1 / 3	31	1 / 2
SU-8 2015	30	1500	1.5 / 4	41.5	1 / 3
SU-8 2025	30	2800	1 / 3	41.5	1 / 3
SU-8 2025	40	2100	2 / 5	52.5	1 / 3
SU-8 2025	50	1700	2.5 / 7	62.5	1 / 4
SU-8 2025	75	1000	3 / 9	79	1 / 7

Technique 1 The PDMS molds are activated with a plasma cleaner (30 s, O_2, flow 5,5, power 2,5). Right after activation, they are silanized with chlorotrimethylsilane (TMCS). To do this the molds are stored for 7 min in a Petri dish (14.5 cm) together with a 15 ml tube cap filled with 0.5 ml of TMCS. The PDMS pre-polymer and the curing agent are mixed in a ratio of 10:1 (v/v). This mixture will be referred to as *liquid PDMS*. Coverslips (#0) are plasma activated with the same parameters as above. The liquid PDMS is poured on the coverslips. To obtain a thin and homogeneous layer, the coverslips are spin-coated at 1500 rpm for 30 s. The silanized patterned surface of the molds is carefully pressed into the liquid PDMS layer. This "sandwich" is kept at room temperature for at least 1 h to remove air bubbles and then put at 65 °C for at least 2 h. After curing, the mold can be very carefully removed from the coverslip and the cavities are revealed. A schematic description can be found in Figure 3.2 (A).

Technique 2 The PDMS molds are activated with a plasma cleaner and silanized with TMCS as described above. Liquid PDMS is spin-coated on the molds at 1500 rpm for 30 s. The PDMS is cured for at least 2 h at 65 °C. For plasma binding of the cured PDMS layer to a coverslip (#0), both – the PDMS stamp and the coverslip – are plasma activated as above. The thin PDMS layer is then pressed on the coverslip. After being sure that no air bubbles are at the interface the pressure is maintained for several seconds. After about 30 min the PDMS mold can be unpeeled. The thin PDMS layer is plasma bound to the coverslip. A schematic description of this protocol can be found in Figure 3.2 (B).

It is very useful to glue a "handle" to the coverslip. A small (mm-size) piece of PDMS can be attached with liquid PDMS to the coverslip. This will facilitates the further handling of the coverslip.

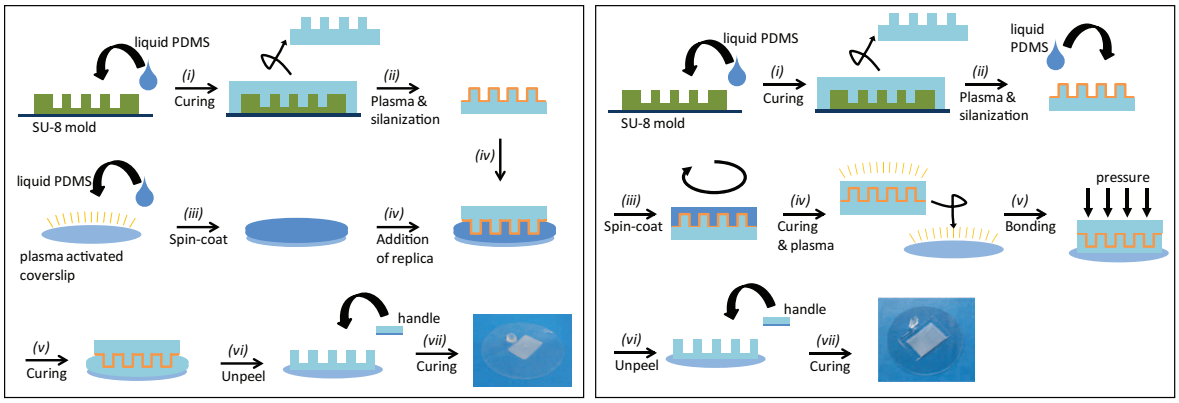

(A) Technique 1 (B) Technique 2

FIGURE 3.2: (A) Technique 1: Liquid PDMS is poured on a SU-8 mold. After curing (i), the replica can be removed. The replica is plasma activated and silanized (ii). In parallel, liquid PDMS is poured on a plasma activated coverslip. The PDMS is spin-coated (iii) and the silanized replica gently pressed in the PDMS layer (iv). After curing (v), the replica is removed (vi) and a "handle" added (vii). (B) Technique 2: Liquid PDMS is poured on a mold. After curing (i), the replica is removed. The replica is plasma activated and silanized (ii). Liquid PDMS is poured on the replica and spin-coated (iii). After curing (iv), the thin PDMS layer on the replica is plasma bound to a coverslip (v). The replica can be unpeeled (vi) after bonding and a "handle" attached (vii).

3.1.4 Micro-contact printing

Micro-contact printing is a common technique to transfer protein patterns on glass coverslips or other surfaces. Fibronectin is an adhesion protein, which allows cells to attach to surfaces. Fibronectin patterns can therefore be used to impose shapes on cells and thereby to influence their division axis [161]. The following protocol presents how a fibronectin micropattern was transferred to a glass coverslip (Fig. 3.3).

Coverslip silanization

i) All glassware used in the protocol is cleaned with soap, then rinsed with acetone and dried with nitrogen flow.

ii) Coverslips are rinsed with ethanol (70 %), carefully dried in nitrogen flow and put into a glass Petri dish.

iii) To hydrolyse the surface of the glass coverslips, *pyranha*[1] solution is added. *Pyranha* is handled with great care.

iv) After 5 to 10 min in *pyranha* the coverslips are first rinsed with ultra-pure water, then sonicated in a glass beaker with ultra-pure water for 10 min.

[1] *Pyranha* is composed of 3 parts if hydrogen peroxide (35 wt %) and 7 parts of concentrated sulfuric acid.

v) Coverslips are dried thoroughly and put in a oven heated on 65 °C for about 10 min.

vi) Coverslips are put together with a separate beaker containing about 100 µl of silane (3-(Mercapto)propyltrimethoxysilane) in a desiccator. The desiccator is evacuated.

vii) After 1 h in vacuum, the coverslips are put in an oven at 65 °C for 1 h.

Stamp preparation

i) The stamp is cleaned with water and ethanol, if necessary.

ii) The stamp is hydrophilized with a plasma cleaner (30 s, O_2, flow 5,5, power 2,5).

iii) A drop (about 100 µl) of fluorescent fibronectin solution (10 µg/ml in PBS) is put on the stamp and incubated for 1 h. The stamp is protected from light and evaporation during this time, by covering it with a lid, whose inside contains wet paper.

Stamping and Passivation

i) Fibronectin solution is removed with a micropipette and the stamp let to dry for about 5 min.

ii) The stamp is carefully posed on the coverslip. Care is taken not to move it laterally.

iii) The stamp is gently pressed on the coverslip with tweezers.

iv) A weight (e.g. a small glass jar filled with about 5 ml of water) is put on the stamp. It is kept there for 5 min.

v) The coverslip is incubated for 1 h in PLL-g-PEG solution (0.1 mg/ml) to passivate the surface for unspecific protein adhesion.

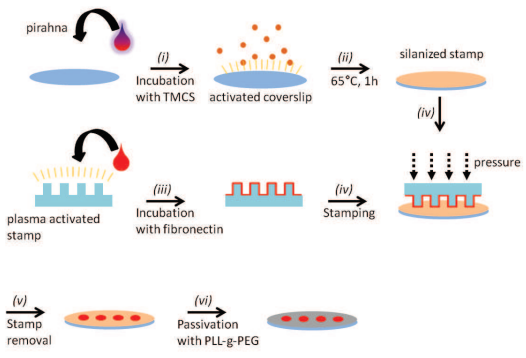

FIGURE 3.3: Schematic representation of microcontact printing protocol. The cleaned coverslip is incubated with *pirahna*. After rinsing, the activated coverslip is incubated in TMCS vapor (i). The coverslip is kept for 1 h at 65 °C (ii). In parallel, the plasma activated stamp is incubated with fibronectin solution (iii). Fibronectin in stamped on the silanized coverslip (iv), then the surface is passivated with PLL-g-PEG (vi).

It is also possible to pattern polystyrene sheets. The sheets were washed with ethanol and ultra-pure water. They were then plasma activated (30 s, O_2, flow 5,5, power 2,5). The stamp preparation and stamping itself was performed as described before. In the few experiments with polystyrene sheets, no passivation was done.

3.2 Mammalian cells: Experimental procedures and setups

3.2.1 Cell culture maintenance

3.2.1.1 Culturing cells

Mammalian cells are maintained at 37 °C and in a 5 % CO_2 in an incubator. Cells are cultured in DMEM with antibiotics (penicillin-streptomycin) and serum (see Table 3.2). When reaching 70 % to 90 % confluence, cells are replated using trypsin and 0.25 % EDTA. Antibiotics are added to the medium of permanently transfected cells after replating (see Table 3.3).

Detailed product description and references can be found in A.4.

Table 3.2: Medium composition.

Cell line	Serum	Other supplements
NIH3T3	10 % BCS	–
REF52	10 % FBS	–
HeLa	10 % FBS	2mM L-Glutamine
U2OS	10 % FBS	–

Table 3.3: Cell lines and selection antibiotics.

Cell line	Fluorescent markers	Antibiotic	Source
HeLa actin-GFP	Actin-GFP	Geneticin (0.5 mg/ml)	Tony Hyman Lab
HeLa myosin-GFP	MYH10-GFP	Geneticin (0.5 mg/ml)	Tony Hyman Lab
HeLa myosin-GFP LifeAct-mCherry	MYH10-GFP and Lifeact-mCherry	Geneticin (0.5 mg/ml) and puromycin (1µl/ml)	Tony Hyman Lab
U2OS actin-YFP	Actin-YFP	Geneticin (0.5 mg/ml)	MarinPharm

3.2.1.2 Thawing and freezing

For gentle thawing, cells are transferred from the -80 °C refriderator or liquid nitrogen container to ice for 30 min and then kept at room temperature for another 10 min. Cells are centrifuged for 5 min at 200 g. The pellet is resuspended in 5 ml of culture medium and cells are plated in a 60 mm Petri dish.

Prior to freezing, cells are trypsinized and resuspended in 1 ml to 1.5 ml of freezing medium (culture medium containing additional 10 % of serum and 10 % DMSO) per Petri dish. The freezing vials are stored at -80 °C. After two days they can be transferred to the liquid nitrogen container for longer storage.

3.2.2 DNA amplification and transfection

Different plasmids were used to transfect cells. An overview can be found in Table 3.4. To have a sufficient amount of DNA, they were amplified and purified. Both protocols will be detailed in the following paragraph. Information about the products can be found in A.7.

3.2.2.1 DNA amplification and purification

DNA amplification in bacteria

i) If the DNA was received dried on a paper, the corresponding area is cut in small pieces with a scalpel. The pieces are put in an Eppendorf and rinsed with endotoxin free TE buffer. The Eppendorf is centrifuged. The DNA is now in the buffer.

ii) Competent bacteria are kept on ice for 10 min.

iii) 50 µl of competent bacteria are mixed with 1 µg of DNA (or 1 µl of DNA if concentration is unknown).

iv) The mixture is kept on ice for 30 min.

v) The mixture is put for exactly 1.5 min on 42 °C and then back on ice.

vi) 500 µl of LB medium is poured on the bacteria-DNA mix and then shaken for 30 min at 250 rpm and at 37 °C.

vii) 250 µl of the bacteria solution is poured on a LB Agar plate and then distributed evenly. The agar plate should contain the antibiotics for which the plasmid contains a resistance.

viii) The agar plate is kept upside down and for overnight at 37 °C. The storage upside down prevents, that condensation water accumulates in the plate.

ix) A colony is picked from the agar plate with a sterile tooth pick and the tooth pick is put in a tube with LB medium and the corresponding antibiotics.

x) The tube with the tooth pick is shaken (about 250 rpm) for about 8h at 37 °C .

xi) 0.3 ml glycerol is mixed with 0.7 ml cell culture and frozen at -80 °C. The frozen cells can be used as a starting point for new amplifications of the same plasmid.

xii) About 24 h after step (ix), 1 ml of bacteria solution is diluted in 4 ml of LB medium with antibiotics. Alternatively frozen cells can be used at this step.

xiii) The tube is shaken (about 250 rpm) for about 8h at 37 °C .

xiv) 2 ml of bacteria culture is added to 100 ml of LB medium with antibiotics.

xv) It is shaken (about 250 rpm) overnight at 37 °C.

Table 3.4: Plasmids used for transfection.

Plasmid	Antibiotics	Source and Reference
DAAM1-PATag-RFP	Kanamycin / Geneticin	Alexander D. Bershadsky [88]
DAAM1-GFP	Kanamycin / Geneticin	Ed Manser [10]
mDia2-mCherry	Kanamycin / Geneticin	Sadanori Watanabe, unpublished
mDia2-GFP	Kanamycin / Geneticin	Sadanori Watanabe [173]
RFP	Kanamycin / Geneticin	Riveline Lab

DNA purification with Maxi Kit At this step the protocol from the Quiagen Endofree® Plasmid Purification Handbook is followed (Figure A.1). A short summary:

i) Bacteria are harvested by centrifugation.

ii) Cells are lysed.

iii) Lysate is cleared by filtration from proteins and genomic DNA.

iv) Plasmid are bound to QIAGEN Anion-Exchange Resin and RNA, proteins, dyes, and low-molecular weight impurities are removed by washing with medium-salt buffer.

v) Plasmids are eluted with high-salt buffer.

vi) Plasmids are washed and concentrated by isopropanol precipitation.

vii) They are washed with ethanol 70 %, dried and then re-dissolved in endo-toxin free buffer.

To quantify the purity and amount of plasmid, the solution is analyzed with an absorption measurement in a spectrometer (*NanoDrop*). The absorption at the wavelengths 230 nm, 260 nm and 280 nm are measured where ethanol, proteins and DNA respectively absorb strongly.

3.2.2.2 Transfection

The transfection is done by liposome transfection with transfection reagent Lipofectamin 2000 (Invitrogen). The protocol suggested by Invitrogen was followed. Details about used masses and volumes can be found in Table 3.5.

i) One (or two) days before the transfection, cells are replated. At the day of transfection the cells should be at least 70 % confluent.

ii) Cell medium is changed to serum-free medium.

iii) DNA is diluted in Opti-MEM.

iv) Lipofectamine is diluted in Opti-MEM.

v) The diluted DNA is added to the lipofectamine vial.

vi) After 5 min the DNA-lipofectamine mixture is added to the cells.

vii) After 2 h to 6 h cell medium is changed to standard culture medium.

Table 3.5: Transfection details

Cell culture vessel	Volume of growth medium	Opti-MEM + DNA	Opti-MEM + Lipofectamine 2000
6-well plate	2 ml	150 µl Opti-MEM + 6 µg DNA	150 µl Opti-MEM + 12 µl Lipofectamine
60 mm Petri dish	5 ml	250 µl Opti-MEM + 10 µg DNA	250 µl Opti-MEM + 25 µl Lipofectamine
T75 flask	10 ml	750 µl Opti-MEM + 35 µg DNA	750 µl Opti-MEM + 80 µl Lipofectamine

3.2.3 Drug experiments

Different drugs were used to act on key proteins in the cytokinetic ring. The compounds, their targets and the used doses can be found in Table 3.6. The drugs are added by either adding directly the corresponding volume of dissolved compounds to the cells. Alternatively, cells are cultured in 0.5 ml of medium. 0.5 ml of pre-warmed medium with twice the drug concentration than the desired concentration is added. This allows immediate optimal mixing of the drug in the medium and is therefore particularly useful in experiments where the drug was added while observing a closing cytokinetic ring. Further information about the used are listed in A.5.

3.2.4 Synchronization

To observe efficiently cytokinesis, cells were synchronized to have a high amount of dividing cells in each experiment. Different protocols were used to synchronize cells. For the *double thymidine block* and the *mitotic block* chemical compounds are added to arrest cells in different phases of the cell cycle. Cells are synchronized within a certain time window. The *mitotic shake-off* uses the fact that cells are loosely attached before and during cell division. Cells get detached by mechanically agitating the culture flask. Associated drugs are listed in A.5.

Double thymidine block Cells are incubated for 16 h in medium containing 2.5 mM thymidine. They are are cultured in normal medium for 8 h and again incubated with 2.5 mM of thymidine. Cells are observed 9 h to 14 h after release. We used the protocol as published by Tang *et al.* [160].

Mitotic block Cells are treated for 18 h with 2 mM thymidine. They are released for 3 h and then incubated for 12 h in 100 ng/ml nocodazole. Cells are observed 2 h after release. This protocol was published by Whitfield *et al.* [175].

Table 3.6: Cytoskeleton drugs, effects and used concentrations

Compound	Effect	Stock solution concentration [µM]	Added volume for 1 ml [µl]	Concentrations in experiment [µM]
Blebbistatin	Myosin [70, 153]	10 mM in DMSO	1, 2, 3, 4, 5, 10	10, 20, 30, 40, 50, 100
ML-7	Myosin regulatory light chain kinase [137]	10 µM in DMSO	5	50
Latrunculine A	Sequesters monomeric actin [149]	1 mM in DMSO	1.5	1.5
Cytochalasin D	Caps actin (+)-end, inhibits actin polymerization [43]	1 mM in DMSO	1	1
Jasplakinolide	Stabilizes actin [30]	1 mM	1	1
SMIFH2	Formin inhibitor [134]	10 mM in DMSO	4	40
CK666	Arp2/3 inhibitor [108]	10 µM in DMSO	10	100

Mitotic shake-off We adapted the protocol presented by Robbins *et al.* [135]. Culture cells in one to four 75 cm^2 flasks for one or two days before the experiment. At the moment of the experiment, cell confluence should be around 50 %. If too much dead cells float in the flask (e.g. due to culturing with antibiotics) the medium should be changed. In this case, it is recommended waited for at least 30 min. To harvest the mitotic cells the flasks are knocked on a table up to 30 times. Cells, which are floating after this treatment, are used for further experiments.

3.2.5 Fixation and staining

For some experiments it was useful to make measurements on fixed cells instead of live cells. The corresponding protocol is described here. To visualize certain proteins, cells are stained for specific proteins by using antibodies or fluorescent dyes. The most used staining procedure is explained below and other protocols can be found in the Appendix (Section A.2.2.1). Finally a protocol is presented which allows to visualize DNA in live cells. Detailed products information can be found in Table A.8.

Fixation and staining The following staining protocol was applied for most staining. Only for staining with the mDia2 antibody and the corresponding control experiments,

different protocols were used, which can be found in section A.2.2.1.

i) To fix cells, they are incubated with pre-warmed PFA (3 %) for 17 min. Fixed cells can be washed and stored in PBS.

ii) Cells are incubated with 0.5 % triton for 3 min to permeabilize the membrane.

iii) Cells are washed three times with PBS.

iv) Fixed cells are incubated with the primary antibody for 45 min (details see Table 3.7).

v) Cells are washed three times in PBS.

vi) Cells are incubated with the secondary antibody or dye for 45 min (details see Table 3.8).

vii) Cells are washed three times with PBS. The protocol can be stopped here and cells can be stored at 4 °C in PBS.

viii) A 12 µl drop of 1:1 PBS:Glycerol (v:v) is added on a glass slide.

ix) The coverslip (25 mm) with cells is mounted upside down on the slide. This is done carefully to prevent bubbles at the interface.

x) The sample is prevented from drying by sealing the edges with nail polish.

Table 3.7: List of primary antibodies

Antibody	Mono- or polyclonal	Concentration	Stock solution concentration
Anti-anillin	polyclonal	1:500	conc. unknown, we followed the instruction of the source lab.
Anti-mDia2	polyclonal	1:200	conc. unknown, we followed the instruction of the source lab.
Anti-paxilin	monoclonal	1:200	250 µg/ml
Anti-phospho-tyrosine	monoclonal	1:200	1 mg/ml
Anti-septin7	polyclonal	1:500	260 µg/ml

Live cell experiments with Hoechst staining To visualize DNA in living cells, Hoechst was used. Hoechst (33342) is diluted in PBS to final concentrations of 50 ng/ml to 150 ng/ml. Cell medium is removed and cells are incubated for 20 min at 37 °C in the Hoechst dilution. Afterwards cells are washed once with PBS and then they are ready for observation or fixing (inspired from [51]).

Table 3.8: List of secondary antibodies and other dyes

Antibody	mono- or poly-clonal	concentration	Stock solution concentration
AlexaFluro 350	polyclonal	1:500	2 mg/ml
AlexaFluro 488	polyclonal	1:500	2 mg/ml
AlexaFluro 647	polyclonal	1:200	2 mg/ml
Cy3-Anti-mouse	monoclonal	1:2000	1.3 mg/ml
Other dyes			
Name	target	concentration	Stock solution concentration
DAPI	DNA	1.75:100	2 mg/ml
Phalloidin 488	F-actin	1:200	6.6 µM
Phalloidin 546	F-actin	1:200	6.6 µM

3.2.6 Giant cells

To obtain very large cells, two protocols were used. One based on the inhibition of cell division (Cytochalasin D-protocol), one based on fusing cells (PEG-protocol).

Cytochalasin D-protocol Cells are replated and diluted by about 1:40. After cells adhere to the surface, they are incubated for 3 to 5 days with 0.2 µg/ml of Cytochalasin D [21, 89]. The concentration was varied by factor 0.75 to 0.1 to improve cell viability. Cytochalasin D is inhibiting the division but not the multiplication of organelles and multinucleated cells are generated.

PEG-protocol Cells are incubated for 2 min with 200 µl PEG in 2 ml of culture medium. Additional 2 ml of serum-free medium are added and cells are kept for 30 min at room temperature. Finally the medium is removed and cells are washed twice with serum-free medium, before L-15 is added and cells are observed under the microscope. L-15 is a medium suited to maintain cells under atmospheric CO_2 conditions. This protocol was published by Yang *et al.* [179].

3.2.7 Experimental setups to orient the cytokinetic ring

The project aims at studying the cytokinetic ring. In standard observation techniques, such as visualizing cells on flat surfaces, the ring cannot be seen entirely, but only a slice.

To overcome these limitations, two different techniques were developed to orient the cytokinetic ring in one plane of focus. In the *vertical setup* coverslips with cells are turned to see cells from the side. In the *microcavities*, cells are confined in small wells and divide perpendicularly to the plane of focus. Product information can be found in A.6.

3.2.7.1 Vertical setup

To visualize cells from the side, cells were plated on glass coverslips. The coverslips were oriented vertically with different techniques. To impose an orientation to the cells, the coverslip was mirco-patterned.

Preparation of cells Coverslips were not treated for preliminary experiments. However, to orient cells on coverslips, fibronectin was stamped on the coverslip as described in section 3.1.4. The patterns consisted of lines. The stamping was usually best, in the center of the stamped area. To make sure that the pattern was in a good quality also on the bottom edge of the coverslip, two rectangular coverslips were laid edge to edge. The coverslips were stamped at this interface. The orientation of the lines was perpendicular to the edge.

Preparation of cells Cells were trypsinized and plated on a coverslip. For experiments aiming at observing the cytokinetic ring, synchronized cells (3.2.4) were used. Cells were plated on the coverslips at least 1 h before the experiment to allow them to spread. Experiments were performed in L-15 medium with 10 % serum.

Orienting the coverslip Different methods were useful to orient stably a coverslip in a perpendicular manner. In overview is given in Figure 3.4. The coverslip can be held by two clips. The clips can easily be positioned to hold vertically the coverslip. The drawback in the setup is that coverslips might break, when being hold by clips (Fig. 3.4a). Another easy way to orient the coverslip is to insert it in an O-ring. This is convenient since this setup can be used with the usual metal holder. Additionally the coverslip can still be adjusted in this configuration which allows to place it very close to the bottom coverslip and to objectives with low working distance. However it is less stable. Moving to different xy-positions during acquisition, might lead to defocusing (Fig. 3.4b).

A more demanding but most stable setup is presented in Figure (Fig. 3.4c). Liquid PDMS is cured in the metal holder together with coverslips. The coverslips must be stabilized in a vertical position at the beginning of curing. After curing the coverslips are removed, and thin slots remain. Additionally a hole is cut into the PDMS piece which serves as reservoir for medium. The coverslips with cells can be introduced in the slot and carefully pressed on the bottom of the holder. This setup is very stable, small and the coverslips can be easily introduced with some training. In all configurations, evaporation of medium is prevented by adding enough mineral oil to cover the surface completely.

3.2.7.2 Microcavities

Preparation of the microcavities The coverslip with the microcavities is plasma activated (30 s, O_2, flow 5,5, power 2,5) and then incubated with fibronectin (20 µg/ml) for at least 1 h or overnight at 4 °C. The coated microcavities are used directly or stored at 4 °C.

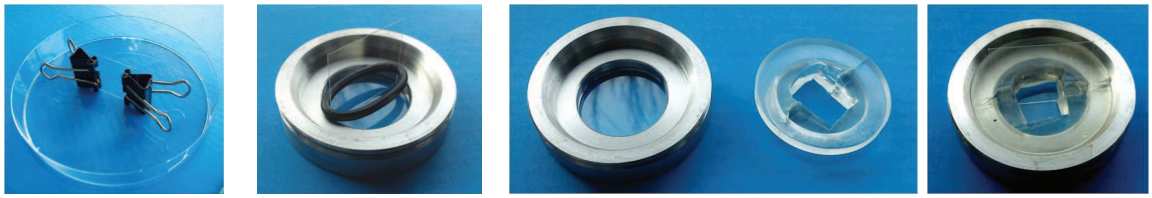

(A) (B) (C)

FIGURE 3.4: Different ways of orienting a coverslip vertically: (A) the coverslip is held by two binder clips. (B) The coverslip is stabilized in the metallic holder with an O-ring. (C) A PDMS piece which fits the holder is prepared. It contains a slot for the coverslip (left). The PDMS piece holds very stably the coverslip (right). 18x18 mm coverslips are convenient for this setup.

FIGURE 3.5: The cylinder is introduced in a 50 ml tube held coverslips in a vertical position.

Filling of the microcavities The supporting cylinder (Fig. 3.5) is inserted in a 50 ml tube. Sufficient culture medium is added to cover the cylinder. The coverslip with the microcavity surface is carefully placed on top of the cylinder the the opening of the microcavities up. Then the cell suspension is added. For experiments aiming at observing the cell division, synchronized cells are used. The tube with the cell suspension is centrifuged at 3000 g one to three times. The total time of centrifugation is 5 min to 15 min. Different centrifugation cycles are used to obtain a higher filling percentage. After centrifugation the coverslip is carefully removed by holding it with its handle and placed in the metal holder. If a high number of cells is on top of the surface, the coverslip is rinsed with medium. Experiments were performed in L-15 medium with 10 % serum. This protocol was developed and patented by Riveline et al. [130]. Another patent is published [132].

3.2.7.3 Cells on soft surfaces

To culture cells in very soft environments, acrylamide gels were used. They can be produced with different stiffnesses. Fluorescent beads were incorporated in these gels to visualize their deformation and estimate the force applied by cells. Detailed product information can be found in A.10.

Coverslip preparation To bind the acrylamide gel to glass coverslips, they were incubated for 25 min with a mix of 1:1:14 (v/v/v) of acetic acid:3-(trimethoxysilyl)propylmethacrylate:ethanol. Afterwards there were washed twice with ethanol for 5 min.

Polyacrylamide gel preparation To make polyacrylamide gels, acrylamide and bis-acrylamide (Bis) are mixed and their cross-linking is catalyzed by ammonium persulfate (APS) and tetramethylethylenediamine (TEMED). The stiffness of the gel depends on the acrylamide:bis-acrylamide ratio [165]. Additionally fluorescent beads (1 %) are added to improve cell adhesion and to visualize gel deformation. The bead suspension is briefly

sonicated before addition to prevent accumulations. To bind fibronectin to the gel, N-hydroxysuccinimide ester (NHS) is added. The exact recipe can be found in Tabel 3.9.

100 µl of non-reticulated gel are pipetted on the prepared coverslips (25 mm). To obtain a flat surface, small coverslips (12 mm) are laid on top during reticulation. The small coverslips are wiped to render the surface hydrophobic. After about 30 min the gel is reticulated and the small coverslip can be carefully removed. The surface is incubated with fibronectin (1 mg/ml) solution to allow cell spreading. Experiments were performed in L-15 medium with 10 % serum.

To obtain a structured gel, the non-reticulated gel is added on a SU-8 mold (see section 3.1.1). The mold contains the negative motive of the desired motive. The prepared coverslip in laid on top. After about 30 min the gel is reticulated. To remove the coverslip with the gel, the gel is incubated with PBS for about 2 h. The coverslip can then be lifted very carefully.

Table 3.9: Acrylamid gel recipes for different stiffnesses (as published in [165]). The beads are added in PBS. To reticulate the gel 6.67 µl APS, 0.67 µl TEMED and 1 µl of NHS are added.

Stiffness [kPa]	Acrylamid [µl]	Bisacrylamid [µl]	PBS [µl]
1.37	75	75	850
4.47	125	75	800
10.61	250	50	700

3.2.7.4 Cells between two surfaces

Different methods were used to confine cells between two surfaces. Cells were brought in suspension by trypsinizing them and optionally densified by centrifugation. Two slides or coverslips were pressed together with binder clips and a drop of cell suspension in between. The pressure depends on the size of the binder clips. Additionally spacers can be installed at the interface (aluminium foil (13 µm)). Cells were incubated vertically and horizontally. Experiments were performed in L-15 medium with 10 % serum.

3.3 Fission yeast: Experimental procedures and setups

3.3.1 Cell culture maintenance

3.3.1.1 Culture

A so-called *starter* is made from a YE5S-agar plate: a yeast colony is transferred with an inoculation loop in 5 ml YE5S medium. The starter is grown at room temperature. After three to four days the starter is diluted in culture medium and kept at culture temperature on a shaker overnight up to 24 h. When cells are in the exponential growing phase (optical density (OD) between 0.2 and 0.8), they can be diluted again in the culture

or experiment media. Culture procedures were followed as described in the Fission Yeast Handbook of the Paul Nurse Lab..

Prior to experiments the strains are grown at the temperature of the experiment in the medium of the experiment. The strains and their specifications are listed in Table 3.10. JW1348 and JW1349 are grown in EMM5S medium for 18 h to 23 h at the temperature of the experiment. EMM5S allows the expression of CHD-GFP in these cell lines. The experiment should take place in the time window of 18 h to 24 h of cells in EMM5S. This allows an expression level of CHD-GFP, which high enough to obtain a good signal and low enough to not influence the actin dynamics. PN4461 is a temperature sensitive mutant of cps1. It is cultured at 27°C and at the restrictive temperature of 36°C for 1.5 h before the experiment. Information about the used products can be found in (A.12).

Table 3.10: Fission yeast strains and their specifications.

Strain	Fluorescent markers and mutations	Culture condition	Experiment condition
DR2	Rlc1-mCherry	EMM5S, 32°C	EMM5S
JW1348	Rlc1-mCherry and CHD-GFP	YE5S, 32°C	EMM5S (between 18 h to 24 h in EMM5S)
JW1349	Rlc1-tdTomato and CHD-GFP	YE5S, 32°C	EMM5S (between 18 h to 24 h in EMM5S)
PN4461	Rlc1-mCherry, mutation in cps1 (restrictive temperature 36°C)	EMM5S, 27°C	EMM5S, 36°C
519	Bgs1-GFP	EMM5S, 32°C	EMM5S
561	Bgs4-GFP	EMM5S, 32°C	EMM5S

3.3.1.2 Thawing and freezing

For thawing cells, a vial frozen at -80 °C is removed from the freezer, but maintained in a special holder, to prevent thawing of the whole vial. Frozen cells are scratched from the vial with an inoculation loop and spread in a line on a YE5S-agar plate. After about 2 min to 3 min perpendicular lines are drawn from the first one to dilute cells further.

Prior to freezing, cells are plated densely on a YE5S-agar plate. After 2 to 3 days cells are ready for freezing. For this a freezing mix is prepared containing 30 % glycerol in YE5S medium. With an inoculation loop yeast cells are taken from the plate and mixed in about 1 ml of freezing mix and transferred to -80 °C.

3.3.2 Filling in microcavities

The supporting cylinder is inserted in a 50 ml tube. Sufficient culture medium is added to cover the cylinder. The coverslip with the microcavity surface is carefully placed on top of the cylinder with the cavities up. Some milliliter of fission yeast culture in the exponential growing phase are briefly sonicated to separate cells and then added in the tube. The

tube with the cell suspension is centrifuged at 800 g for one to three times. The total time of centrifugation is at least 5 min and maximally 15 min. Different centrifugation cycles are used to obtain a higher filling percentage. For experiments with temperature sensitive mutants, the centrifuge was preheated to the temperature of the experiment. After centrifugation the coverslip is carefully removed by holding it with its handle and placed in the metal holder. If a high number of cells is on top of the microfabricated PDMS surface, the coverslip is rinsed with medium.

3.4 Optical setups

3.4.1 Microscopes

We used different optical setups. If not stated differently, we used the Leica SP5 for the observation of the cytokinetic ring in mammalian cells and the Leica spinning disk microscope for the observation of fission yeast cells. Images were processed with ImageJ.

Epifluorescence setups Nikon Eclipse Ti inverted microscope equipped with a charge-coupled device (CCD) camera coolSNAP HQ^2 (Photometrics), a Lambda DG-4 lamp (Sutter Instrument Company) and a temperature control system from Life Imaging Services. The objective was a Plan Apo 60x objective (oil, 1.40 NA, DIC, Nikon). Occasionally other objectives were used (10x, 40x, 20x). Images were captured and processed with the NIS Elements software (v3.10, SP3, Nikon). Additionally a CKX41 inverted phase-contrast microscope (Olympus) was used. For acquisition, the ImageJ plugin Micro-manager and a cooled CCD camera (Hamamatsu) were used. The system is equipped with 10x, 20x and 40x phase contrast air objectives.

Confocal Setups Leica TCS SP5-MP or SP8-MP based on a Leica DM6000 CFS upright microscope were used, equipped with a Leica Application Suite Advanced Fluorescence LAS AF 2.6.3.8173/LAS AF 3.1.2.8785 acquisition system with photomultiplier tube (PMT) and hybrid detectors (HyD). We used a 25X or 63X HCX IR APO L water objective (0.95 NA, Leica). Alternatively a spinning disk based on a Leica DMI6000 inverted microscope was used, equipped with a Yokogawa CSU22 spinning disk unit and Andor iQ 1.9.1 acquisition system. A 63x or 100X HCX PL APO CS oil objective (1.4 NA, Leica) was used.

3.4.2 FRAP setup

For FRAP experiments we used the Leica TCS SP2 AOBS MP based on a Leica DMIRE2 microscope, equipped with a PMT detector and a 63x HCX PL APO oil (1.4 NA, Leica) objective and the Leica Confocal Software LCS 2.61.1537.

3.4.3 Laser Ablation setup

For laser ablation a Leica TCS SP5-MP or SP8-MP based on a Leica DM6000 CFS upright microscope was used, equipped with a Leica Application Suite Advanced Fluo-

rescence LAS AF 2.6.3.8173/LAS AF 3.1.2.8785 acquisition system with photomultiplier tube (PMT) and hybrid detectors (HyD). A 25X or 63X HCX IR APO L water objective (0.95 NA, Leica). For laser ablation we used infrared femtosecond pulsed lasers (SP-5: Coherent Ultra, SP-8: Coherent Vision II with precompensation). Laser ablation experiments on mammalian cells were performed with the SP-5, on fission yeast with the SP-8.

4 The cytokinetic ring in mammalian cells – Results

4.1 Establishment of setups and protocols

4.1.1 Setups to visualize the cytokinetic ring.

We probed three different setups to orient the cytokinetic ring during closure. According to Théry *et al.* [161] the geometry of the attachment sides of the cell defines the orientation of the division axis. This brought us to two ideas. On the one hand, we probed if cells being attached to two parallel surfaces would divide with a division plane perpendicular to these surfaces (*"sandwich" setup*). On the other hand, we oriented cells by simply turning the coverslip to which they are attached. The division axis was imposed by a fibronectin pattern (*vertical setup*).

A third setup was inspired from the work of Riveline *et al.* [130] on fission yeast. They demonstrate how to orient fission yeast cells in an array of microcavities. The setup was adapted for mammalian cells (*microcavity setup*).

4.1.1.1 "Sandwich" setup

Cells are confined between two glass coverslips. We hypothesized that cells attached to two opposing surfaces would divide in a plane in between as depicted in the scheme in Figure 4.1. The coverslips are held together by binder clips. Figure 4.2 shows a 3D reconstruction of an U2OS cell in this setup. The cell is attached to both sides but is slightly tilted. We observe also that cells tend to spread on surface even though they were originally adhering to both sides (Fig. A.2).

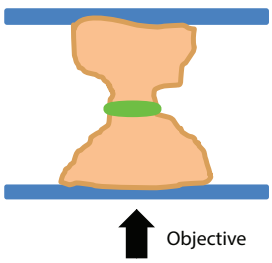

FIGURE 4.1: Scheme of the vertical setup. Cells on a pattern are oriented vertically. The cytokinetic ring can then be visualized in a single plane of focus.

Finally we never saw a cell division in the desired plane of focus. We speculated, that cells need to elongate to divide, which is not possible in this setup [80].

4.1.1.2 Vertical setup

Cells plated on coverslip were oriented vertically. This allowed to see cells from the side. In Figure 4.3 (A) a moving cell is shown. The probing activity at the front is well visible.

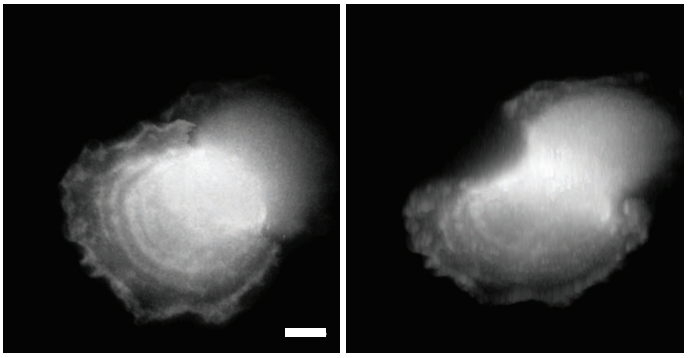

FIGURE 4.2: An U2OS cell between to parallel surfaces. LEFT: projection of 8 z-planes (distance 2.5 µm). Scale bar 5 µm. RIGHT: 3D reconstruction of cell. The perspective is tilted by 59° with respect to the projection on the left.

While moving the nucleus is compressed. The probing of the lamellipodia is shown in Figure 4.3 (B). The front is repeatedly elongated and then retracted.

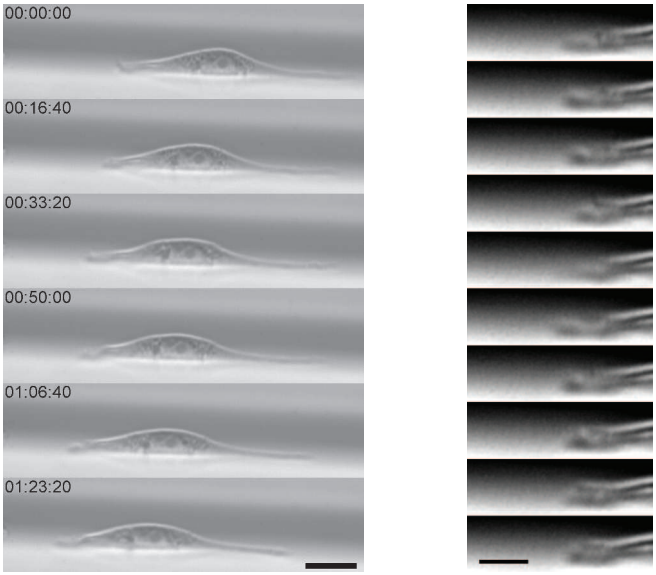

(A) (B)

FIGURE 4.3: NIH3T3 cell on a glass coverslip visualized from the side.(A) The cell is moving from the right to the left. Time in hh:mm:ss, scale bar 20 µm.(B) A zoom of the probing activity at the front of the cell. Time between images 80 s, scale bar 20 µm.

To orient cells and cell division of cells on the coverslips, the coverslips were micropatterned with fibronectin. As it was reported in different studies [161, 98], the shape of the cell affects the division axis orientation. Roughly, the division axis is perpendicular to the long axis of the cell. We designed different elongated patterns to impose different shapes to cells (Fig. 4.4). In preliminary experiments, cells were observed on these patterns on flat coverslip or polystyrene foil. Fluorescent fibronectin was used to visualize the pattern. We confirmed that these patterns are suited to impose an axis of division (Fig. 4.5).

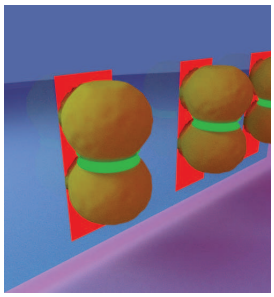

FIGURE 4.6: Scheme of the vertical setup. Cells on a pattern are oriented vertically. The cytokinetic ring can then be visualized in a single plane of focus.

In a third step, we combined these two setups, that is to say, we oriented micropatterned coverslips perpendicularly to the plane of focus (Fig. 4.6). Additionally cells were synchronized with a double thymidine block (Section 3.2.4). This allowed to see a division from the

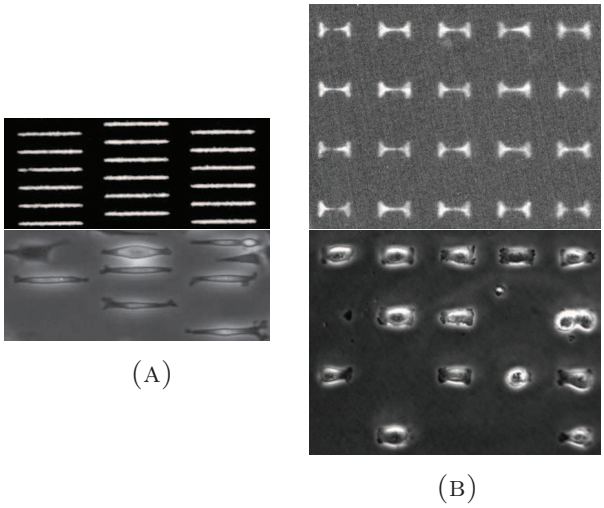

(A) (B)

FIGURE 4.4: (A) Top: Pattern of labeled fibronectin lines (length 100 µm) on a glass coverslip. Bottom: U2OS cells spread along the lines. (B) Top: Dumbbell pattern (40 µmx25 µm) of fibronectin on polystyrene foil. Bottom: HeLa cells spread on the pattern.

FIGURE 4.5: U2OS cell on fibronectin pattern (red). The cell is elongating and dividing along the lines. Time between images 20 min, length of the lines 100 µm.

side (Fig. 4.7). We compared the division time in this configuration with the division time of cells on normal coverslips (see Fig. 4.12). The closure dynamics was the same in both setups.

We tried furthermore to increase the number of observed cells by stacking layers of polystyrene foil. However, the imaging quality was not sufficiently good to pursue this path (Fig. A.3).

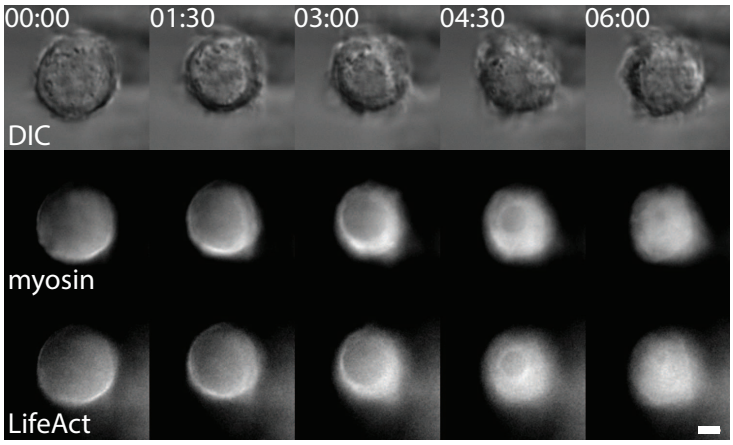

FIGURE 4.7: Cytokinetic ring of HeLa cell closing in vertical setup. The ring is visualized by differential interference contrast (DIC) microscopy, and the fluorescence of myosin (GFP) and actin (LifeAct-mCherry). Time in mm:ss, scale bar 5 µm.

4.1.1.3 Microcavity setup

Cells are introduced in microcavities. Due to their confinement, they orient during division along the long axis of the cavities (Fig. 4.8). We checked different parameters to optimize the protocol.

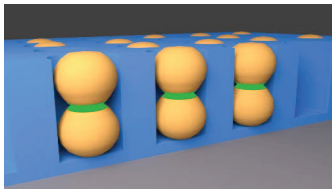

FIGURE 4.8: Scheme of the microcavity setup. Cells are oriented vertically. The cytokinetic ring can then be visualized in a single plane of focus.

To optimize the filling of the microcavities and thereby potentially the number of dividing cells per experiment, we checked the influence of different parameters on the filling percentage (Fig. 4.9). We changed the centrifugation speed and time. While time seemed not to have an influence on the filling percentage, increasing the centrifugation speed from 200 g to 3200 g increased the filling. We found that neither the fibronectin concentration of the coating, nor the cavity depth had an effect on the filling percentage. We therefore fixed the centrifugation speed to 3200 g and kept a fibronectin concentration of 20 µg/ml. It is obvious that the number of cells is a crucial parameter. We tried to keep this value high. Furthermore Fanny Evenou (postdoc in Riveline Lab.) demonstrated that it is advantageous for the filling percentage to increase the number of centrifugation cycles. We used preferentially three cycles.

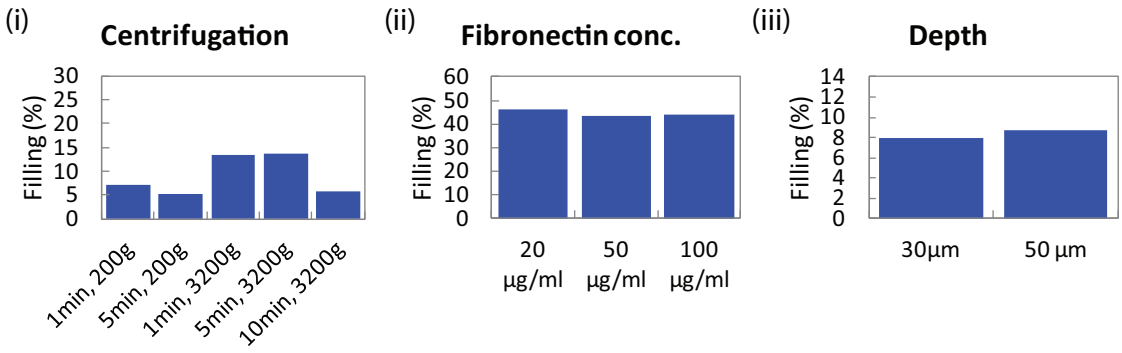

FIGURE 4.9: To optimize the filling percentage in microcavities different parameters were tested. (i) Filling percentage for different centrifugation speeds and times (fibronectin concentration 20 µg/ml, depth 40 µm). (ii) Filling percentage for different fibronectin concentrations (centrifugation 5 min, 200 g, depth 40 µm). (iii) Filling percentage for different cavity depths (fibronectin concentration 20 µg/ml, centrifugation 5 min, 200 g). We find that the centrifugation speed can improve the filling percentage. Please note that total filling percentage in the three experiments cannot be compared, since different cell concentrations were used.

The cavity sizes were optimized for HeLa cells. Figure 4.10 illustrates what happens if the diameter of the well is not adapted. Cells round up and increase their volume before division and, thus, might get ejected by the associated pressure [151] from too small cavities (Fig. 4.10 (A)). However, if the cavity is too large, the cell does not get oriented but divides in a very tilted plane (Fig. 4.10 (B)).

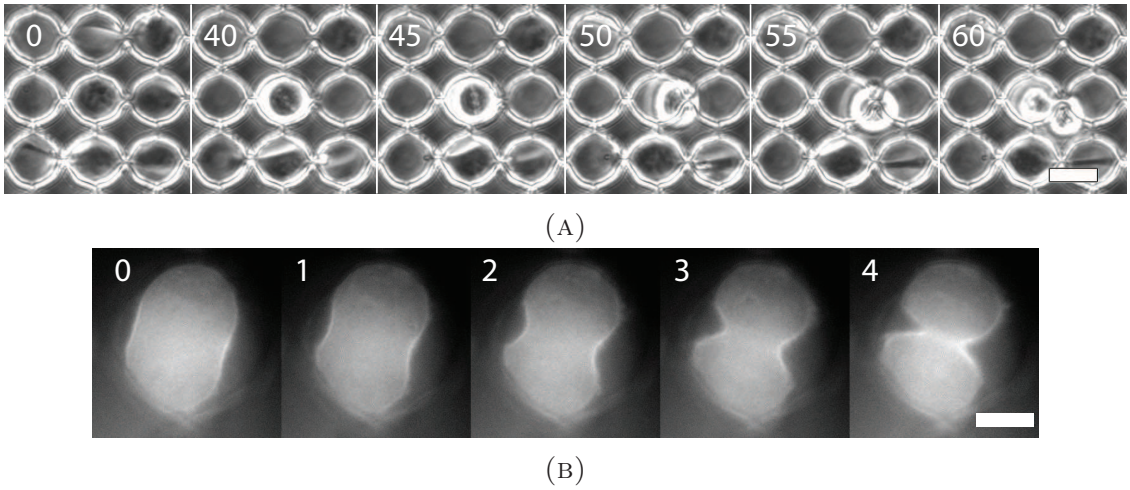

FIGURE 4.10: (A) U2OS cell in a cavity of 20 µm in diameter. Prior to division the cell rounds up, leaves the cavity and divides outside of the array. (B) HeLa cell in a 27 µm cavity. The cavity is too large to orient the cell and the cytokinetic ring is visualized from the side. Time in min, scale bar 5 µm in both panels.

We choose a cavity diameter of 25 µm for the subsequent experiments. Figure 4.11 shows a 3D reconstruction of a HeLa cell in these cavities. The cytokinetic ring is nearly perfectly parallel to the plane of observation.

We patented this method [132].

FIGURE 4.11: 3D reconstruction of a HeLa cell, fixed in a microcavity. The cytokinetic ring is visible by myosin fluorescence (GFP). The distance between z-planes is 0.3 µm and the diameter of the cavity is 25 µm. The dashed line indicates the cavity.

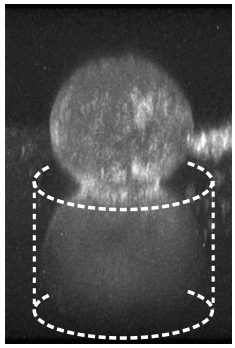

4.1.1.4 Comparison of setups

We developed two setups which allowed to observe cell division in a single plane of focus. We compared the change in diameter as a function of time in all setups and compared it with the division time of cells on simple coverslips (Fig. 4.12). The cells divide with the same dynamics in all configurations.

The microcavity setup allows observing several cells at the same time. A whole surface of about 10^3 to 10^4 microcavities can be used for the experiments. In addition the protocol is easy and quick, once the microcavities are fabricated. For these reasons, we continued to approach our scientific questions with the microcavity setup.

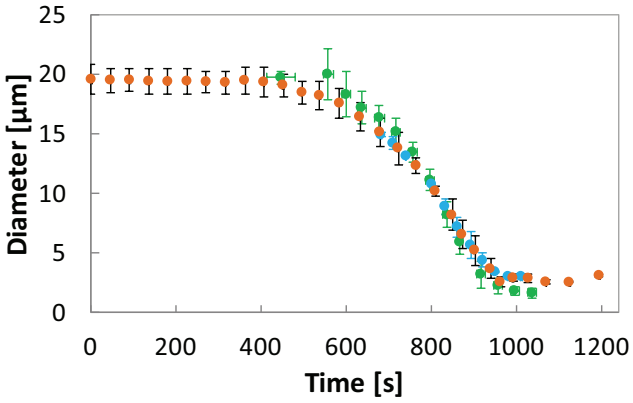

FIGURE 4.12: Closure behavior of HeLa cells on coverslips (green), in the vertical setup (blue) and in microcavities (orange). Error bars indicate the standard deviation, coverslips: N = 12, vertical setup: N = 6, microcavities: N = 18.

4.1.2 Cell types

Cell division is very well conserved in different cell types. To my knowledge, all mammalian cells divide by the constriction of an actomyosin ring. We therefore considered that the cell type itself would not play an important role to study cell division. Our aim was mainly to work with a cell line stably transfected with one or both of these proteins.

Transfection and selection of cells, which are stably transfected, that is to say, that integrated the transfected plasmid in their genome, are well known procedures and can easily be carried out in any Laboratory equipped with cell culture facilities. However, we obtained a HeLa cell line from the Lab. of Tony Hyman, which was already stably transfected with either only with MYH9-GFP (myosin heavy chain) or with MYH9-GFP and LifeAct-mCherry, which is marker for filamentous actin [127].

Figure 4.13 show a HeLa cell stably transfected with MYH9-GFP and LifeAct-mCherry. The labeling reveals that actin and myosin localize in the cleavage furrow. The expression level is high enough to obtain good images without exposing the cells too much. To prevent loss of the plasmids, cells were cultured in the presence of the selection antibiotics, kanamycin and geneticin.

If not stated otherwise, all following experiments are done with these two cell lines.

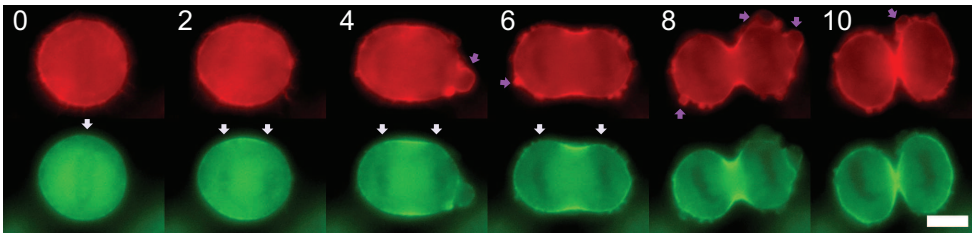

FIGURE 4.13: Dividing HeLa cell, stably transfected with myosin-GFP and LifeAct-mCherry. At the onset of cell division, the cell is rounding up. The chromosomes (visible as dark region, indicated by arrows) are getting aligned in the middle of the cell. The cell is then elongating and the chromosomes get separated. The cytokinetic ring is forming as actin and myosin accumulate in the cleavage furrow. The constriction of the furrow leads to cell division. Cell blebbing is visible during division (lavender arrows). Time in min, scale bar 10 µm.

4.1.3 Synchronization protocols

The cell cycle of HeLa cells is approximately 20 h. However the time of cell division is only 5 min. To increase the likelihood of observing a cell division event, we increased the number of cells dividing in a certain time window by synchronizing their cell cycles. We used two kinds of protocols: we arrested cells in different phases of the cell cycle with chemicals (mitotic block [175] and double thymidine block [160]). Another protocol, the mitotic shake-off, consists in detaching loosely attached cells, such as mitotic cells, by mechanical agitation [135].

We compared the two protocols which biochemically synchronize cells: the mitotic block and the thymidine block. We synchronized cells according to these protocols and fixed them after 2 h (mitotic block) and 10 h (thymidine block). The thymidine block gave a better synchronization result and we continued with this protocol.

For the final experimental protocol, we aimed at plating synchronized cells on fibronectin patterns. So we wondered if trypsinization could alter the synchronization efficiency or timing. Hence, we compared the amount of dividing cells, which were replated after the release of the drugs to cells, which were not replated (Fig. 4.14). Cells were treated according to the protocol (described in 3.2.4). One part of the cells was replated after the last drug was washed out. Cells were fixed 8.5 h to 13 h after the release from the block and the DNA was stained with DAPI (Fig. A.4). Afterwards mitotic cells were counted.

We find that the total amount of synchronized cells in the time window of 9 h to 13 h after the release from the block is not changed. Thus, trypsinization does not decrease the efficiency of the protocol. However the maximum of the respective distribution is shifted from 11 h to 11.5 h.

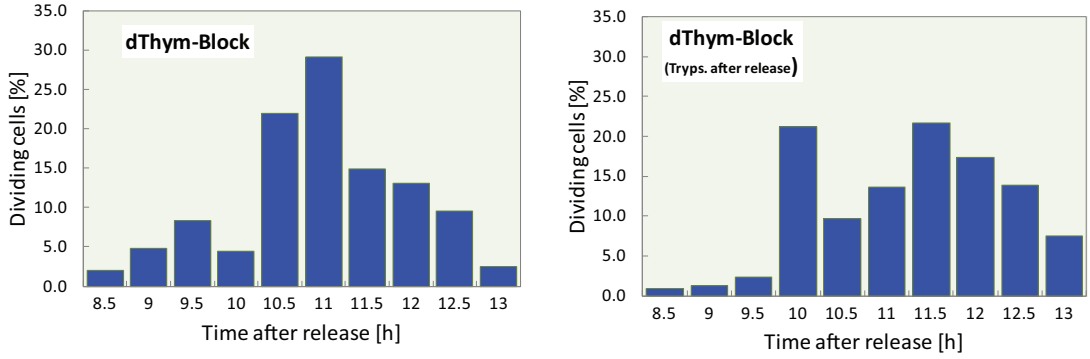

FIGURE 4.14: Comparison of the synchronization efficiency of cells which were not replated and replated after the release from the block. The amount of dividing cells is the same in the time window of 9 h to 13 h, but the maximum of the distributions is shifted from 11 h to 11.5 h for the replated cells. Without trypsin: n = 4273, with trypsin: n = 2272.

The mitotic shake-off protocol takes advantage of the fact that cells round up before division and are loosely attached at this stage. By mechanically agitating the culture flask, they can be brought in suspension. We wanted to know in which time window the cells divide after filling. We find that most rings close after filling the cavities (Fig. A.5).

However even after about 1.5 h cell divisions can be observed.

Comparing all protocols, we decided to proceed with the mitotic shake-off. The mitotic shake-off is particularly suitable for the microcavity protocol, since filling the cavities needs suspended cells. Moreover, the shake-off protocol does not require the addition of drugs, which might potentially change the cell behavior. Additionally the protocol is much shorter than the chemical synchronization protocols. On the other hand, it is not well suited for the vertical setup, since cells sediment and will probably not attach to a vertically oriented pattern. Additionally, for the mitotic shake-off protocol large culture surfaces are needed to obtain a high amount of mitotic cells which can be harvested. The working window of the double thymidine block (about 4 h) is larger than the one of the mitotic shake-off (about 1 h to 1.5 h).

Weighting the advantages and disadvantages of each protocol, we decided to use the mitotic shake-off in the following experiments. The protocol is easy and experiments are not submitted to a strict timing. Drawbacks are overcome by using up to four 75 cm^2 flasks to have a high amount of cells. To have a longer window for experiments, samples were prepared every 1 h to 1.5 h.

4.1.4 Giant Cells

Carvalho *et al.* [20] showed in *C. elegans* embryos that the closure time is independent of the cell size. They propose that the cytokinetic ring is composed of contractile units. If the number of these units would scale with the length of the perimeter, the closure speed would increase accordingly. We wanted to test this hypothesis for HeLa cells. To vary the cell size, we produced multinucleated cells, *i.e.* giant cells.

We produced giant cells in two ways: we inhibited cell division with Cytochalasin D [21, 89] and we fused cells with PEG [179]. Even several days of Cytochalasin D treatment produced only cells with mainly two or three nuclei. PEG was much more efficient. We were able to fuse large parts of a cell colony. However, too large cells died quickly. Figure A.6 shows cells on a coverslip, fused with PEG. Many multinucleated cells can be found.

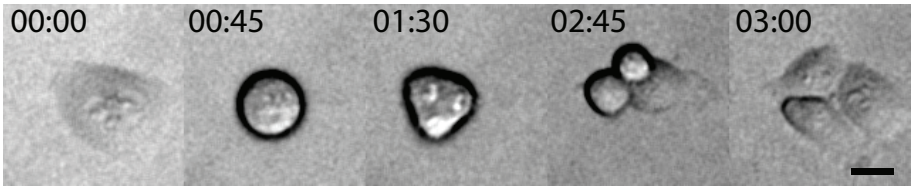

FIGURE 4.15: Division of a giant cell. During division it develops three division axes and divides in three daughter cells. Time in hh:mm, scale bar 20 µm.

We observed the cell colonies for several days. Cells with more than one nucleus, which were undergoing division, formed more than one division axis (Fig. 4.15). The larger the cells, the more likely they died before undergoing division.

We were able to produce cells of different sizes. However, when they divided, they formed several division axes. This kind of division is difficult to compare to the division

if only one ring is forming. We therefore did not pursue this experimental line.

4.2 The cytokinetic ring in mammalian cells

In the microcavities cells orient during division in a way that the cytokinetic ring is in the plane of focus. The ring has an initial diameter of about 20 µm. The constriction rate increases quickly until it reaches the maximum of around 60 µm/s at a diameter of around 7 µm (Fig. 4.16) . The closure takes place in about 5 min.

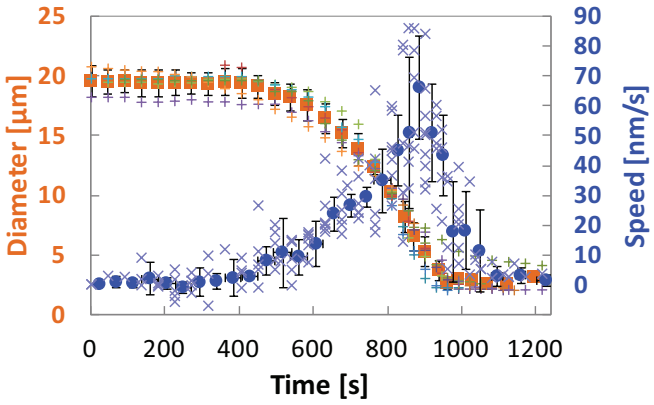

FIGURE 4.16: Closure behavior of HeLa cells in microcavities. The diameter as a function of time describes a S-shape (mean values (orange) and individual curves (various colors). The diameter reduction accelerates. At about 7 µm the change in diameter slows down. Correspondingly the velocity increases at the beginning until it reaches a maximum of about 60 nm/s (mean in blue, individual values in light blue). It then decreases quickly to zero. Error bars indicate the standard deviation, N = 14.

We visualized the ring with the fluorescence from filamentous actin (LifeAct-mCherry) and myosin (GFP) (Fig. 4.17). Parts of the cell cortex are also visible around the ring. The myosin signal is clearly contrasted with the cortex. A "patchy structure" is visible which will be described in the next section. The actin distribution along the ring is smoother. Actin concentration in the cortex and the ring do not differ as clearly as for myosin. In general, the center of the ring is moving during closure and at the end it is rarely found exactly in the center of the initial ring.

We quantified the changes in concentration of actin and myosin during closure. We measured the intensity of closing rings in both channels and normalized them by the respective intensity values at a diameter of 10 µm. We chose 10 µm for technical reasons, since for all measured cells, we had values for this diameter. Considering the high similarity between closure events and the high temporal precision, we assume that intensity changes between cells can be compared. For these measurements we imaged cells with a low frame rate and exposure time and intensity to minimize photobleaching. Figure 4.18 shows the change in mean and total intensity during closure. Both, actin and myosin mean intensity increase at the beginning until about 12 µm. Then actin intensity is decreasing again, whereas myosin intensity stays about constant until the very end, where it decreases quickly. Overall, the respective intensities vary around about 80 % and 110 %

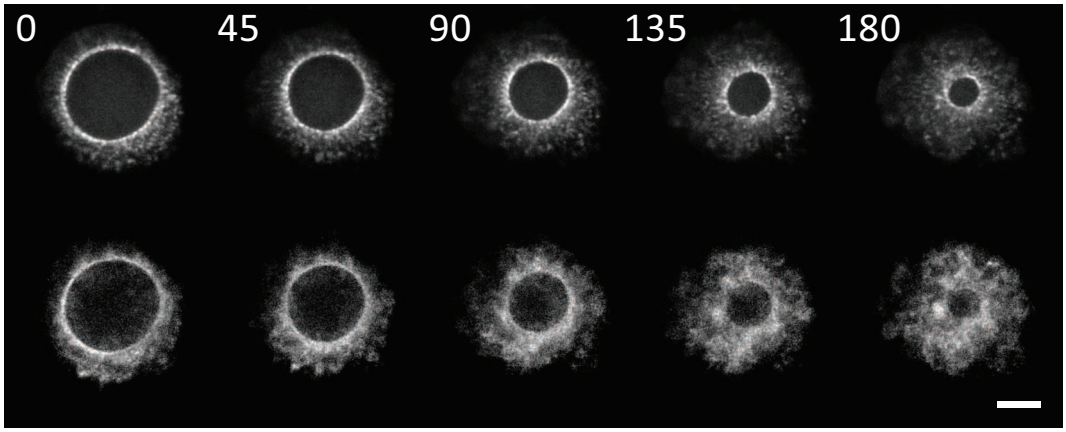

FIGURE 4.17: Timelapse of a closing cytokinetic ring visualized in myosin (top) and actin (bottom). The image is the superimposition of 5 z-planes and smoothed with ImageJ. Time in s, scale bar 5 µm.

of the reference value. Correspondingly the total intensity is decreasing linearly with the diameter. Matter gets lost during closure. The measurement of myosin shows a higher standard deviation than the actin measurements, indicating a higher biological variability.

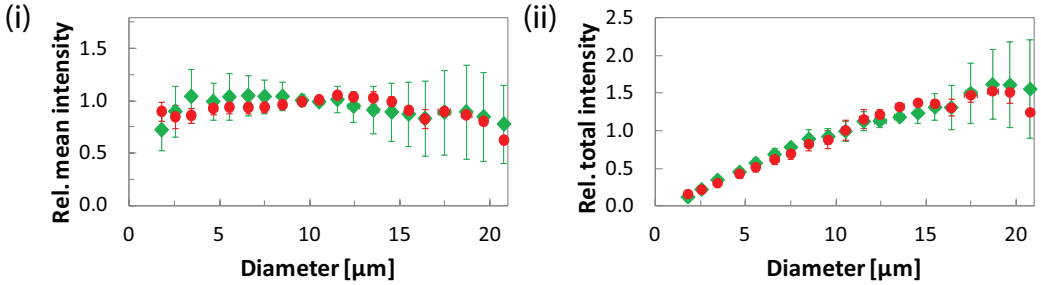

FIGURE 4.18: Relative mean (i) and total (ii) intensity of actin and myosin during closure. The intensities were normalized at diameter 10 µm. (i) The mean intensity is varying between about 80 % and 110 % of the reference value. Actin intensity is first increasing and then decreasing. Myosin intensity is also first increasing and stays then about constant until the ring has reached a small diameter. (ii) The total intensity is about constant for large rings and is then linearly decreasing. Error bars indicate the standard deviation, N = 10 for myosin, N = 6 for actin.

Interestingly the closure speed and the actin and myosin concentrations show a very different behavior. This points in the direction that stress generation might not only be explained with actomyosin concentrations. We take a close look at the density distribution in the ring in the next section.

4.2.1 Pattern in the cytokinetic ring

4.2.1.1 Myosin exhibits a pattern of regular motifs

Myosin density distribution shows a prominent pattern of regular clusters (motifs) spanning the ring. The actin ring shows also some small accumulations, but they are much less pronounced than the myosin ones (Fig. 4.17). Figure 4.19 presents an overlay of subsequent time frames. It reveals that these motifs move mainly radially as the ring is closing. This pattern was in our hands only visible with an upright microscope. In other setups the patterns were not resolved (Fig. A.7). We presume that this is due to the structured PDMS layer at the bottom of our device.

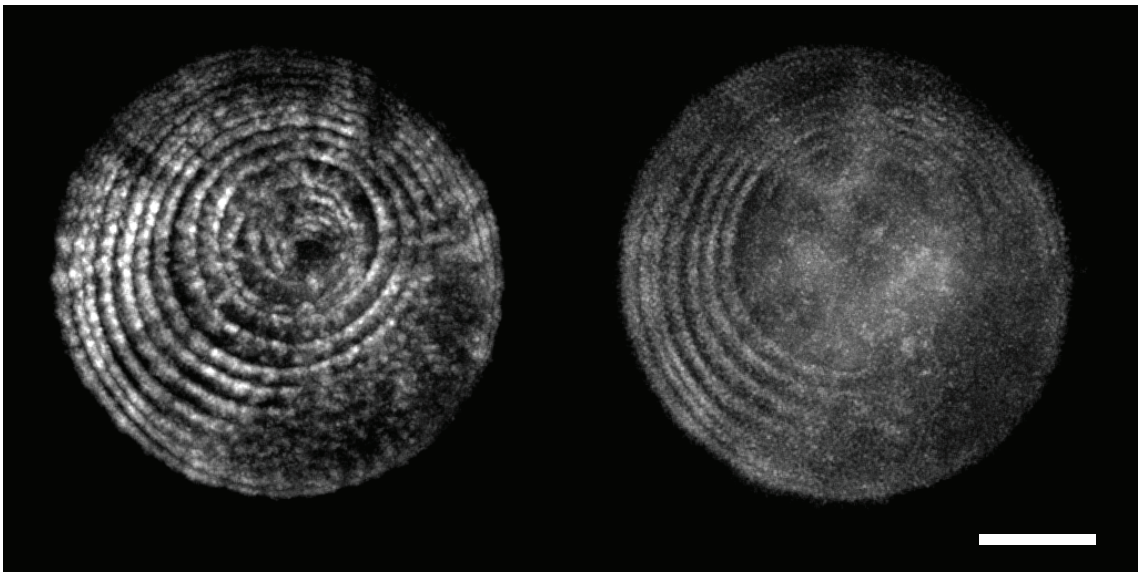

FIGURE 4.19: Overlay of 26 subsequent frames of a closing ring visualized by the fluorescence labeling of myosin (left) and actin (right). Myosin shows clusters which move mainly radially as the ring closes. Actin clusters are much less pronounced. The corresponding timelapse sequence is depicted in Figure 4.17. Images are smoothed with ImageJ. Time between images 45 s, scale bar 5 µm.

Another example is depicted in Figure 4.20. It shows regular myosin clusters on the cytokinetic ring (left) and their radial movement (right). The motifs span the entire perimeter. They seem remarkably regular in terms of intensity, size and interdistance. The close up (see inset) reveals irregularities of these parameters. The right side of Figure 4.20 presents the corresponding maximal projection of the image on the left and the 24 subsequent time frames. The clusters move basically radially (see inset). On the lower part of the ring little tangential movements can be recognized for larger diameter by slightly curved trajectories. Neighboring clusters move nearly in the same manner, or, stated differently, the angle between the myosin accumulation measured from the center of the ring stays about constant.

Further features are depicted in Figure 4.21. Again myosin accumulations move essentially to the center of the ring. However, occasionally separation and fusion events can be observed. The inset magnifies a region where two clusters split. The separated parts

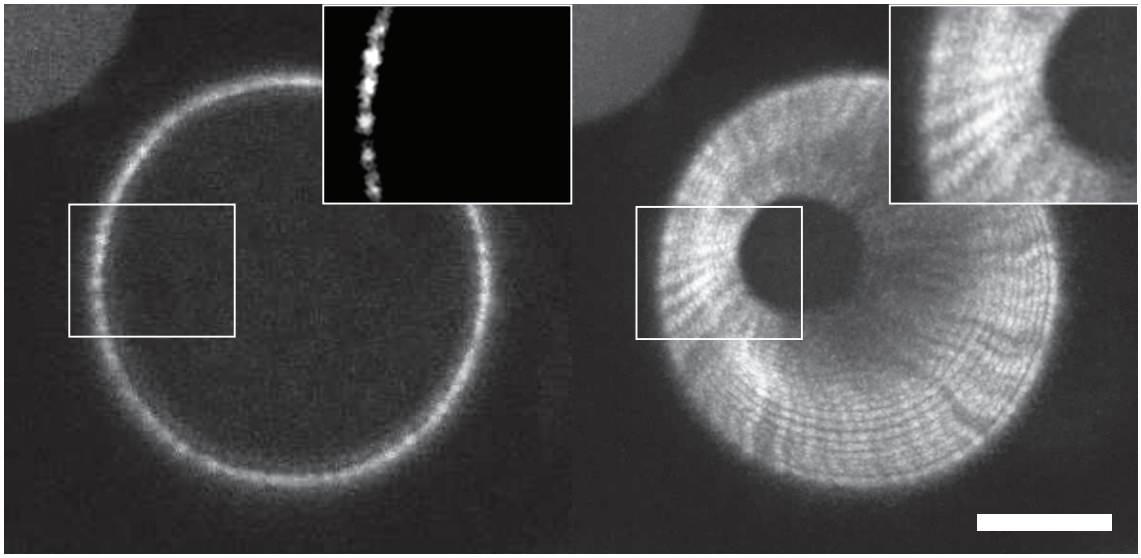

FIGURE 4.20: Left: Snapshot of the cytokinetic ring visualized by myosin labeling. Myosin is distributed in regular clusters around the perimeter. The inset shows a magnification of the marked region. Right: Overlay of 25 frames, starting from the frame shown on the left. The clusters move basically radially, though little and collective rotations are visible for larger diameter. The inset magnifies a region where the clusters move remarkably straight. Images are smoothed with ImageJ. Time between images 10 s, scale bar 5 μm.

fuse then with other myosin accumulations. Fusion and separation are common events.

Another feature, which we observe, is rotations of clusters. Figure 4.22 shows a ring, which is rotating while closing. This is further emphasized in the overlay, which reveals curved trajectories of myosin motifs. The clusters turn in the same direction. Though neighboring clusters describe similar motion, that is to say, they move about the same lateral distance, the extent of rotation is not equally pronounced along the entire ring. Clusters on the right undergo a stronger rotation than on the left. Interestingly the right side of the ring shows also a region of low intensity. This is not due to focusing, since the intensity in actin is not decreased in this area. We speculate that the rotation might be induced by a force miss-balance, associated to unequal myosin distribution.

Curved trajectories are also visible for high density spots in actin. However, these spots are rather located next to the ring, in the cortex. This is indicating that not only the ring, but also the cortex in the cleavage furrow undergoes rotation.

Rotations are a feature which can be seen in nearly all rings. These very pronounced rotations as presented in 4.22 are less common. Further example can be found in the appendix A.8.

4.2.1.2 Formin colocalizes with myosin

It is reported that formin plays an important role in different aspects of the cytokinetic ring [71, 22, 173]. It was shown for fission yeast that the ring is assembling from protein complexes (nodes) which organize in the vicinity of the nucleus [168]. Among other proteins, these nodes contain myosin and the formin cdc12 [178]. Cdc12 is nucleating

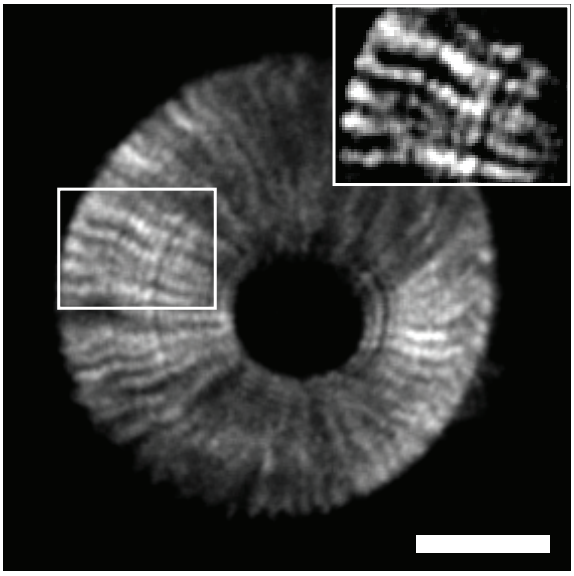

FIGURE 4.21: Overlay of 25 frames of a myosin ring. The inset shows a region of the ring, where myosin clusters split and fuse. Images are smoothed with ImageJ. Time between images 20 s, scale bar 5 µm.

actin [71], which makes it crucial for ring formation. Watanabe *et al.* [173] show that the cdc12 homolog mDia2 is involved in the cytokinetic ring in mammalian cells in positioning and building the actin scaffold.

We transfected HeLa cells with mDia2-mCherry [173] and visualized the cytokinetic ring in myosin and mDia2 (Fig. 4.23). Figure 4.23 (B) shows an overlay of the subsequent time frames. mDia clusters move mainly radially. Their trajectories colocalize with the ones of myosin. The mDia2 signal is not very strong. We believe that for this reason, we cannot resolve the entire pattern. However, we expect that we would see otherwise even stronger similarities between myosin and mDia patterns.

We tried to stain for mDia2 with the antibodies presented in [173] and [174]. Though we tried different staining protocols (see section 3.2.5 and A.2.2.1), but in our hands, mDia2 did not accumulate in the cleavage furrow (Fig. A.9). Possibly the antibody was not working due to damage during transport e.g. thawing.

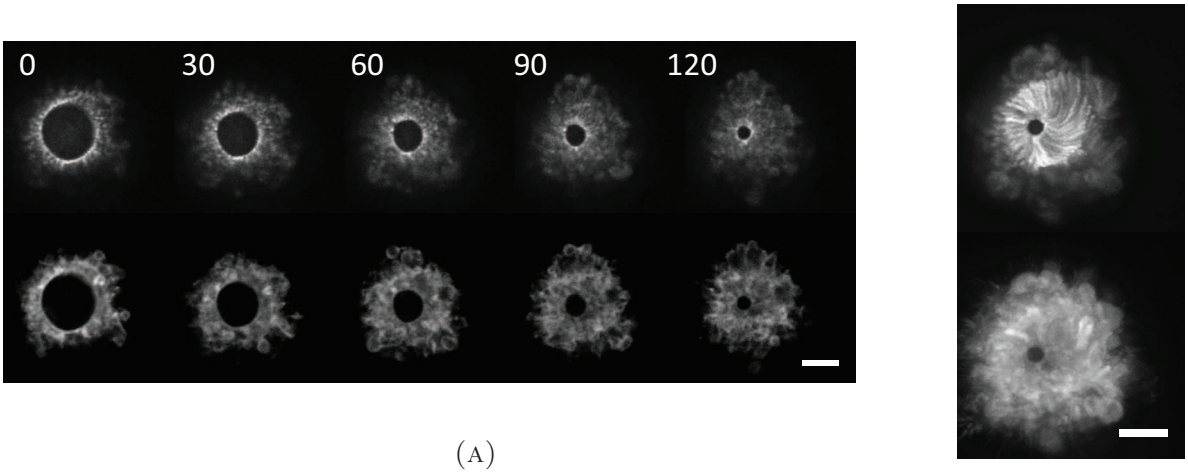

(A)

(B)

FIGURE 4.22: (A) A closing cytokinetic ring visualized by myosin (top) and actin (bottom) labeling. The ring is rotating while closing. This is also clearly visible in the maximal projection of subsequent frames. Time in s, scale bar 5 µm. (B). The trajectories describe curved lines. Overlay of 45 frames of a myosin ring. Time between images 3 s, scale bar 5 µm.

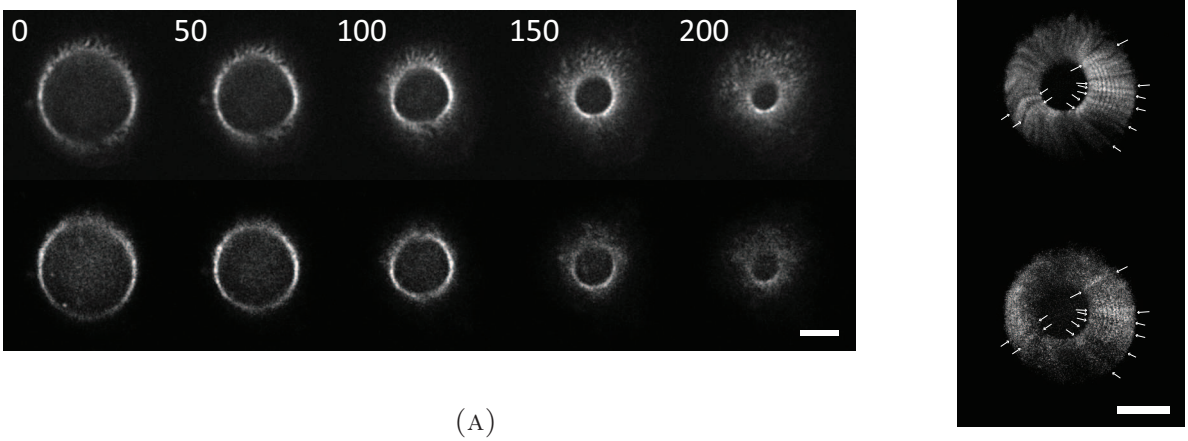

(A)

(B)

FIGURE 4.23: (A) Timelapse of a closing ring labeled in myosin (top) and mDia2 (bottom). Time in s, scale bar 5 µm. (B) Overlay of 17 subsequent time frames (top: myosin, bottom: mDia2). mDia clusters move mainly radially. The comparison with the corresponding myosin pattern, show that formin colocalizes with myosin. Time between images 10 s, scale bar 5 µm.

4.2.1.3 Distribution of anillin and septin

We see motifs of myosin and formin in the cytokinetic ring. Formin is an actin nucleator, but at the same time it might indirectly be involved in the attachment of the ring to the cortex. Carvalho *et al.* [20] observed in *C. elegans* embryos that myosin, anillin and septin behave essentially the same way during closure. Their total amount decrease proportionally with the ring perimeter. This and other observations brought them to the model that the ring is built of contractile units, composed of myosin, anillin and septin. As reviewed in [50] and [119], septin is an interesting candidate to attach the ring to the membrane, since it interacts with lipid membranes [182, 17] as well as with myosin [59] and actin via anillin [110, 64, 39] or directly [95]. We wondered if we could see a pattern for both proteins in the cytokinetic ring.

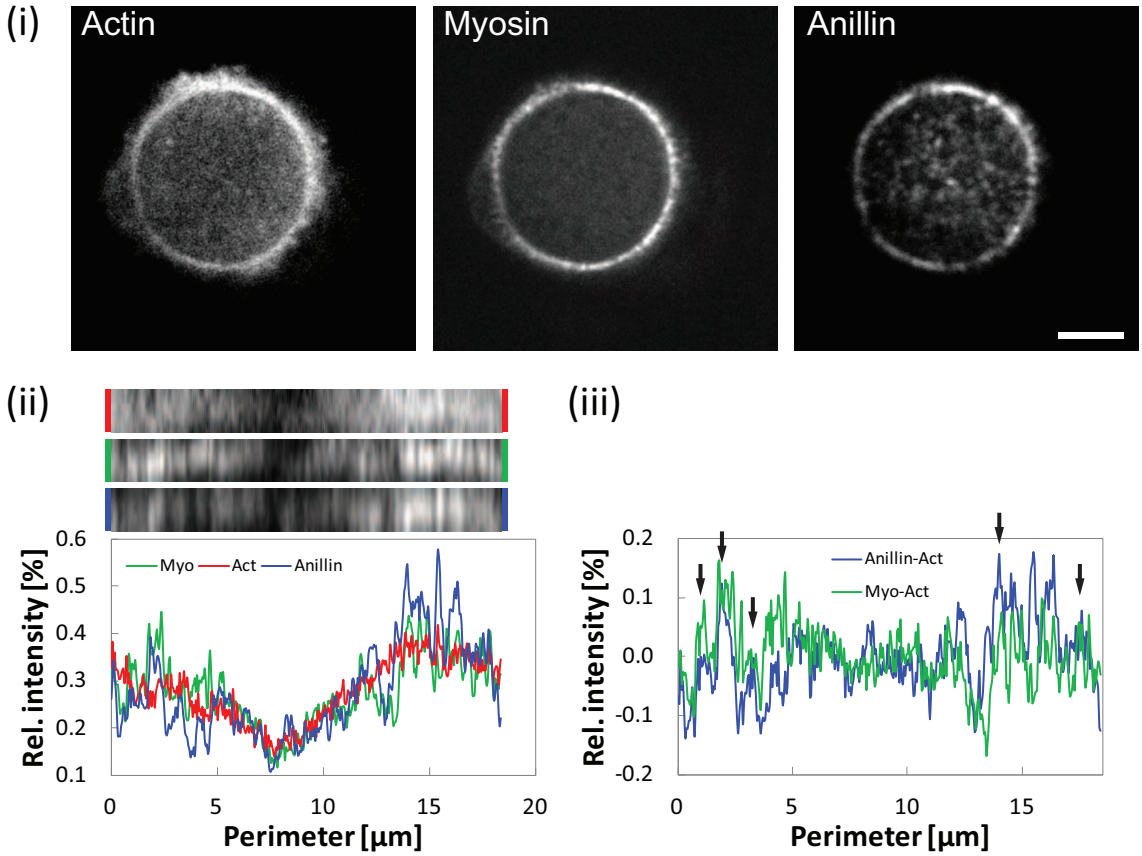

FIGURE 4.24: (i) HeLa cells expressing LifeAct-mCherry and myosin-GFP stained for anillin. As myosin, anillin shows a "patchy" distribution. Smoothed with ImageJ, scale bar 5 µm. (ii) Polar transformation of the rings and the corresponding intensity spectra. The intensities are normalized by their total intensity. Anillin and myosin show strong peaks whereas the actin spectrum is rather flat. Large scale variations are due to slight differences in focus. (iii) Anillin and myosin spectra are subtracted by the actin signal, to flatten the profiles. Anillin and myosin show colocalization in some parts (arrows).

We stained LifeAct and myosin-GFP expressing HeLa cells in microcavities for anillin and septin (Sept7, [36]). Figure 4.24 shows a cytokinetic ring stained for anillin. Anillin

shows a "patchy" pattern of accumulations similar to myosin. Other examples for anillin staining can be found in the appendix (Fig. A.10). Figure 4.24 (ii) shows the polar transformation of the rings and the corresponding intensity spectra. They reveal pronounced maxima and minima for anillin and myosin, but not for actin. To obtain profiles corrected for large scale intensity variation, we subtracted the actin profile (Fig. 4.24 (iii)). In some parts of the ring we see colocalization of anillin and myosin clusters, but not systematically.

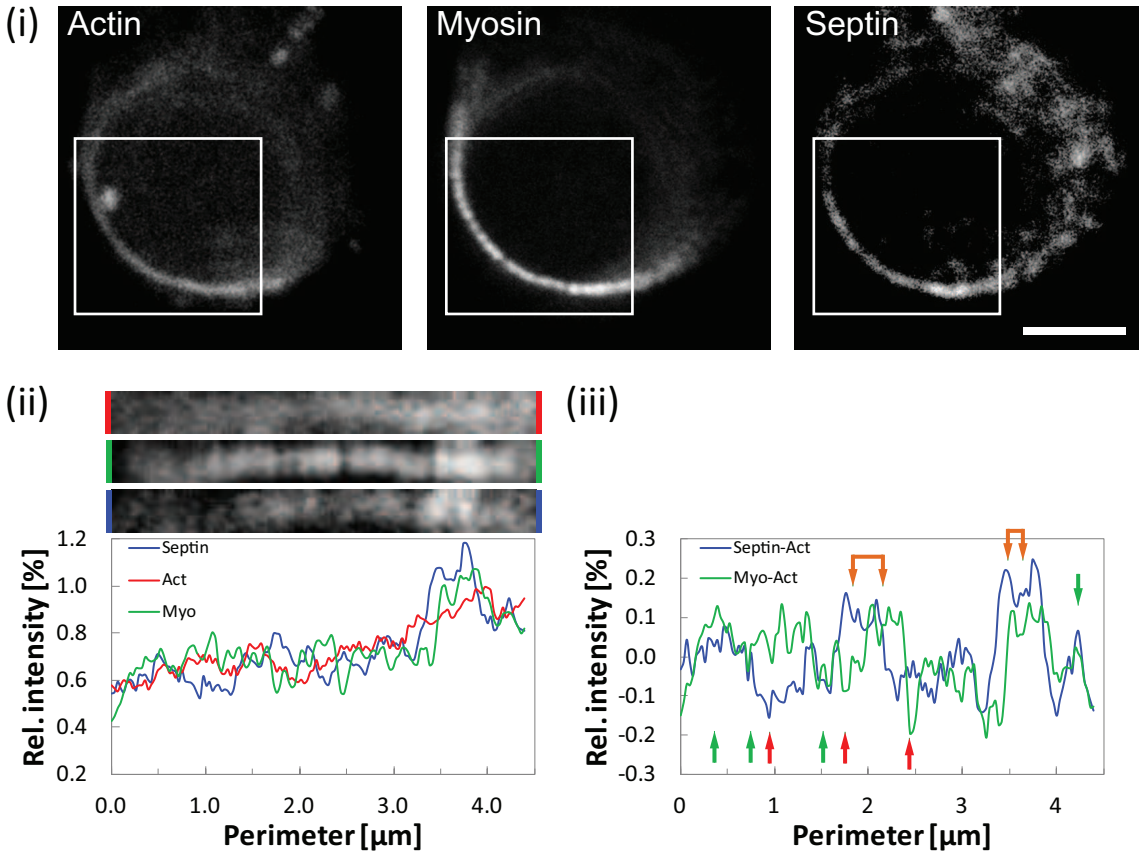

FIGURE 4.25: (i) HeLa cells expressing LifeAct-mCherry and myosin-GFP stained for septin7. Septin reveals a "patchy" distribution. Smoothed with ImageJ, scale bar 5 µm. (ii) Polar transformation of the indicated part of the rings and the corresponding intensity spectra. The intensities are normalized by their total intensity. Septin and myosin show strong peaks whereas the actin spectrum is rather flat. (iii) Septin and myosin spectra subtracted by the actin signal. Arrows indicate where the profiles seem to show colocalization (green), anti-correlation (red) and a shift (orange).

Figure 4.25 presents a cytokinetic ring stained for septin 7. The septin distribution reveals also a "patchy" structure. However, the size of the clusters seems to be larger than for myosin. Further examples for septin staining of cytokinetic rings can be found in the appendix (Fig. A.11). Figure 4.25 (ii) shows the polar transformation of the indicated regions in the rings and the corresponding intensity profiles. In (iii) the myosin and septin profiles corrected for the baseline (actin profile) are depicted. In some areas septin and myosin clusters seem to colocalize (green arrows), in others they seem to be

anti-correlated (red arrows) and in some regions they seem to be shifted (orange arrows). Overall it is difficult to conclude for a connection between the respective distributions.

4.2.1.4 Pattern characterization

The pattern consists of myosin clusters of different sizes, intensities and interdistances. We characterized these myosin clusters by measuring these quantities as a function of the diameter.

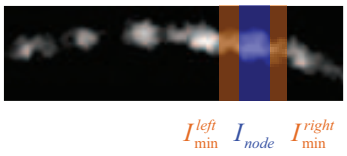

$$PC = \frac{I_{node}}{\frac{1}{2}(I^{left}_{\min} + I^{right}_{\min})}$$

FIGURE 4.26: Schematic explanation of the definition of the pattern coefficient (PC). The PC is the ratio between the intensities of the myosin motifs and the neighbouring low intensity regions.

We measured the intensity of clusters and the segments in between. To evaluate the *pattern coefficient*, we took the ratio of the respective mean intensities of the clusters and their neighboring low density regions (Fig. 4.26). The intensity values were corrected by subtracting the background. The result is depicted in Figure 4.27. As the cytokinetic ring is closing, the pattern coefficient is first slightly increasing and from a diameter of 15 µm onward decreasing. At the end it stays about constant. The cluster density is increasing during closure. This is expected, since the ring perimeter is decreasing. The dashed line in Figure 4.27 (ii) indicates the densification for the case that the number of clusters would remain constant. The measured increase in density stays below this curve, which means that the absolute number of clusters is decreasing. This can happen by fusion events and loss of single clusters. Potentially this might also be due to active remodeling of the pattern. Interestingly densification cannot be observed for rings smaller than 10 µm. However, for small rings it is sometimes difficult to distinguish clusters. In these cases parts of the rings were not analyzed. This is potentially screening out clusters, which are close together. The analysis for rings smaller than 10 µm might be therefore biased towards smaller densities. The cluster size is slightly decreasing during closure.

Though the perimeter is strongly decreasing, the pattern characteristic stays astonishingly constant. In particular one would expect a much stronger densification of clusters. This is not observed. These measurements suggest that an active regulation of the pattern might be involved.

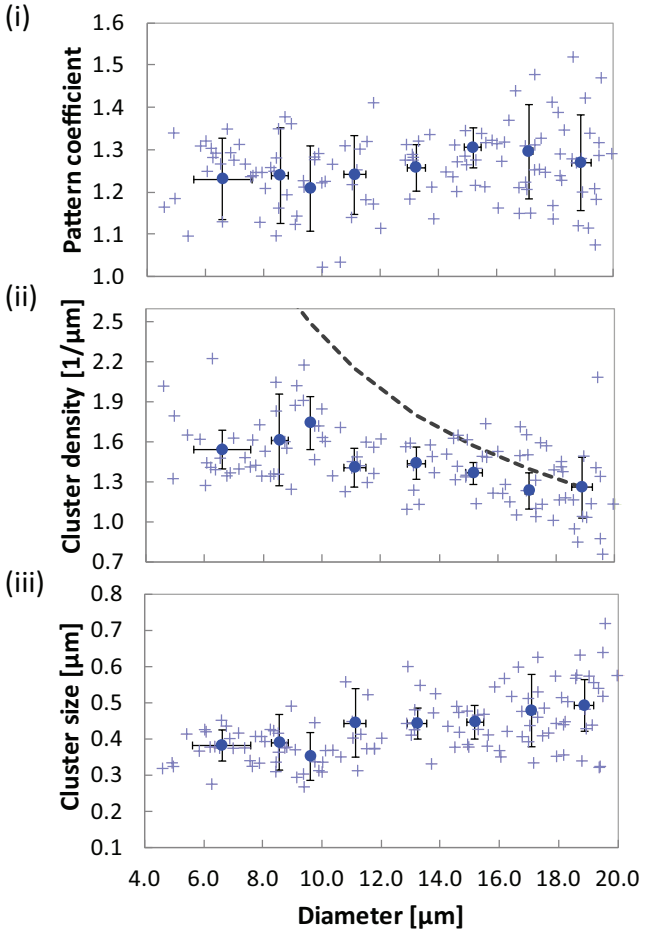

FIGURE 4.27: Characterization of the myosin pattern. (i) Pattern coefficient as a function of the diameter. The pattern coefficient is first increasing and for diameter smaller than 15 µm decreasing. At the end it stays about constant. (ii) cluster density as a function of the diameter. The density is increasing while the ring is closing. However, if the number of clusters would stay constant during closure, the densification would be much stronger, as indicated by the dashed line. (iii) The cluster size has a decreasing density as the ring closes. Each cross corresponds to the mean values of one ring, the error bars indicate the standard deviation, timelapses of 11 closing rings were analyzed.

4.2.2 Probing mechanical properties

In order to probe the mechanical properties of the cytokinetic ring, we performed laser ablation experiments, where we cut the ring locally. If the ring would be stabilized by the cortex, it would probably not deform after cutting. A strong deformation would suggest that the ring is under tension, similar to a rubber band, which is tensed and gets then cut.

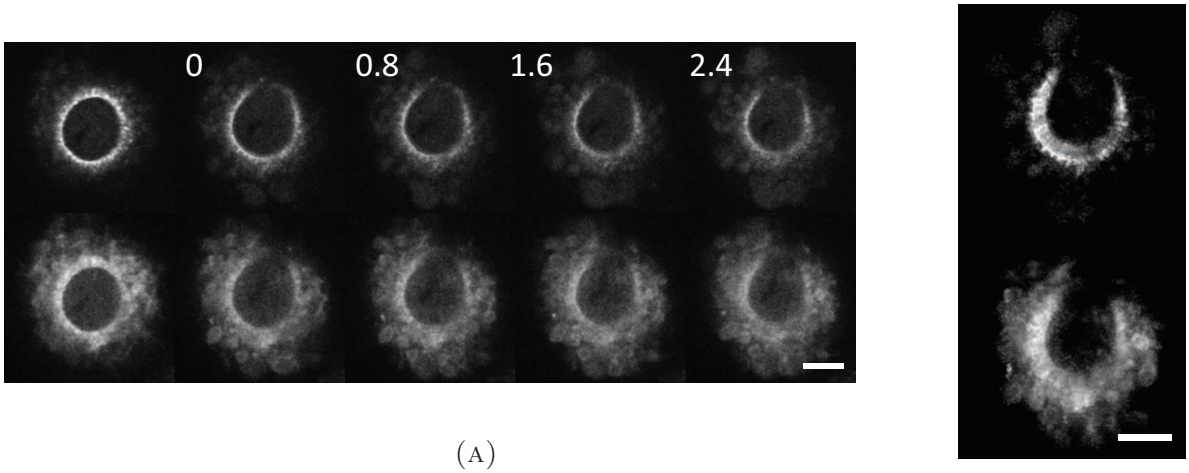

(A) (B)

FIGURE 4.28: Ablation of closing ring visualized in myosin (top) and actin (bottom): (A) Timelapse of a cytokinetic ring. The ablation took place between the first and the second frame. Time in s, scale bar 5 µm. (B) Maximal projection of 9 frames. Radial movement of myosin motifs is still visible. Stack histogram normalized and smoothed with ImageJ. Time between images 0.8 s, scale bar 5 µm.

Figure 4.28 (A) shows a timelapse of such an experiment. The ring was cut and it opens subsequently. We conclude from that, that the ring is under tension. Additionally the free ends are straight. This is expected if the ring is bent. We observed this behavior in all ablation experiments.

Interestingly the ring continues to close. Thus the circular geometry seems not to be required for stress generation. Astonishingly, the closure speed is faster than in control cells (Fig. 4.29).

We observe that the myosin clusters still move mainly radially. This speaks against the hypothesis that force unbalance would lead to a rotation of myosin clusters. However, we were not able to trace the ring sufficiently long to come to a conclusive statement about the rotation. The ring losses very quickly its fluorescence after ablation.

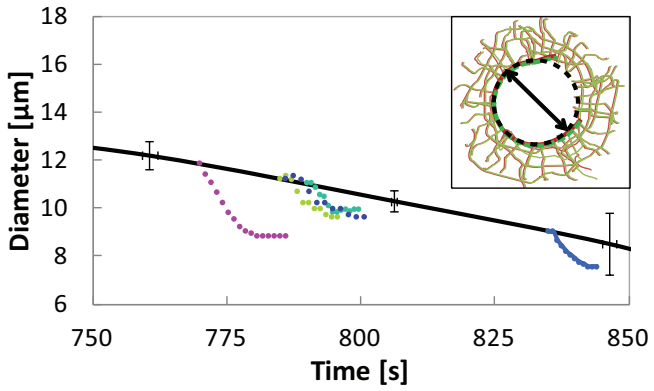

FIGURE 4.29: Closure behaviors after ablation of the ring. The cut rings were fitted with a circle and their diameter measured as a function of time. The individual curves were aligned to the closure curve of intact rings (data from Figure 4.16). The cut rings close faster than control rings.

4.2.3 Theoretical description of the cytokinetic ring

We observed in the cytokinetic ring that myosin is organized in a pattern of regular clusters. Formin clusters colocalize with myosin. We wanted to better understand why our circular active gel is exhibiting these structures and if there could be a function associated to it. In order to get a better sense of our observations and measurements, we collaborated with Karsten Kruse and Anne Wald (Saarland University).

In the following section I will present briefly our model [172].

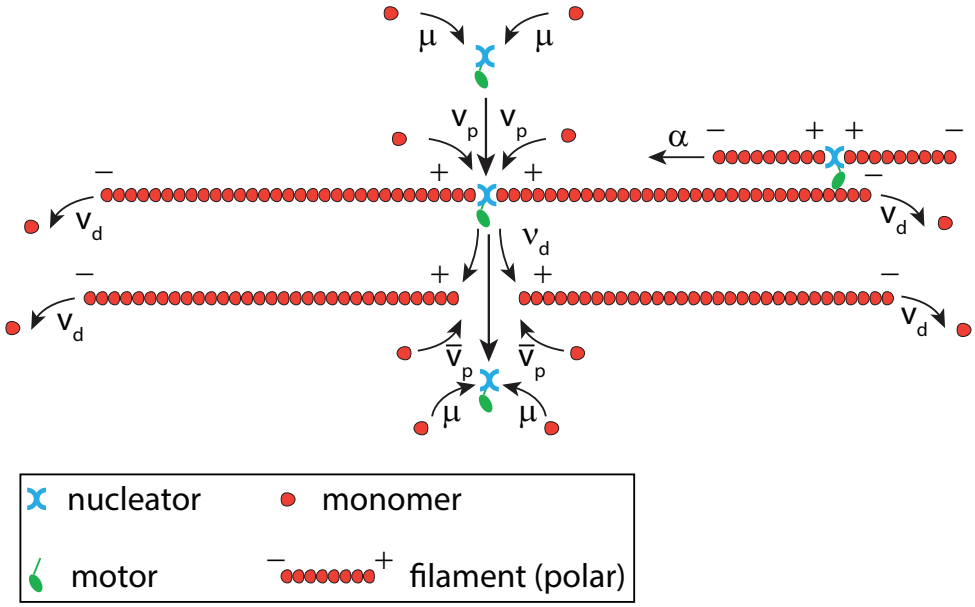

FIGURE 4.30: Schematic representation of the model. Nucleator nucleate two filaments with a rate μ, giving rise to a bipolar filament. The filaments are attached with their (+)-ends to the nucleator and grow on this end with a speed v_p. They depolymerize at the (–)-end with a speed v_d. Bipolar filaments detach from the nucleator with a rate of ν_d. Their polymerization speed at the (+)-end is then lowered to $\bar{v}_p$. Myosin is attached to formin. It moves towards the (+)-end of filaments. Its activity is denoted as α. The figure was prepared by Karsten Kruse and is shown with slight modifications.

Figure 4.30 represents schematically the model. Its three basic ingredients are motors, filaments and nucleators, which represent myosin, actin filaments and formin respectively. Actin filaments are treated as rigid rods. Myosin and formin are attached to each other (*nodes*). Formin can nucleate two filaments. This is motivated by our observation that myosin and formin colocalize (section 4.2.1.2). We do not describe here how these structures form, but have different reasons to implement motors and nucleators like this. The two proteins might build a complex similar to fission yeast, where nodes contain, beyond other proteins, myosin and on average two formins [178]. Additionally formin (DAAM1, disheveled-associated activator of morphogenesis) nodes associated to myosin near the plasma membrane were reported in mammalian cells [88]. On the other hand, myosin does not have to be bound to formin, since formin is binding to the (+)-end, free myosin would accumulate on this end.

The ring is considered as 1D system with periodic boundary conditions. We reduce

cytokinesis to the closure of the actomyosin ring and neglect the cortex. The works of Mishra *et al.* [99] and Reymann *et al.* [126] show that a circular, minimal system can contract (see also section 2.5.3). Additionally, their rings close with a speed of the same order of magnitude as the cytokinetic ring. We are therefore focusing only on a ring structure for the time being, and not on the entire cell.

The nucleator is nucleating filaments with a rate of μ, giving rise to bipolar filaments. These filaments polymerize at the (+)-end with a speed of v_p and depolymerize with a speed of v_d at the (–)-end. v_p is chosen to be larger than v_d, which leads to a net growth with a speed of v_p–v_d. Bipolar filaments can have different lengths, but in our model they are always symmetric, that is to say, that their two filaments have the same length.

Bipolar filaments can detach with a rate ν_d from the nucleator. Their polymerization speed is then smaller and denoted as $\bar{v}_p$. Monopolar filaments undergo a net shrinkage with a speed of $\bar{v}_p$–v_d, since v_d is choosen to be larger than $\bar{v}_p$.

The total amount of filaments is given by the (de-)polymerization speeds, rate of dissociation from the nucleator and the nucleator density n_0. In the stationary state the lengths have an exponential distribution.

$$c_0^{bp}(l) = \frac{n_0}{v_p - v_d} e^{-l/\lambda} \tag{4.1}$$

$$c_0^{+}(l) = c_0^{-}(l) = -\frac{n_0}{\bar{v}_p - v_d} e^{-l/\lambda} \tag{4.2}$$

with

$$\lambda = \frac{v_p - v_d}{\nu_d} \tag{4.3}$$

c_0^{bp}, c_0^{+} and c_0^{-} denote the concentrations of bipolar filaments and monopolar filaments in the stationary state. The indices + and – indicate filaments pointing with the (+)-end right or the left direction of the system.

The motors mediate the interaction between bipolar filaments and polar and bipolar filaments. They are attached to the center of bipolar filaments and will move interacting filaments with respect to each other. Their activity is described by α, which has the unit of a velocity.

Additionally, filaments can move due to diffusion with a diffusion constant D. The diffusion should not only be understood as a term, which accounts for a pure Brownian motion. It also captures random motion due to e.g. length fluctuations of filaments.

Taking all these mechanisms together, one can express the dynamics of such a system in a continuum mean field description in three differential equations:

$$\begin{aligned}\partial_t c^{bp}(x,l,t) =& D\partial_x^2 c^{bp}(x,l,t) - \partial_x j^{bp}(x,l,t) - \nu_d c^{bp}(x,l,t) \\ &- (v_p - v_d)\partial_l c^{bp}(x,l,t)\end{aligned} \tag{4.4}$$

$$\begin{aligned}\partial_t c^{+}(x,l,t) =& 2D\partial_x^2 c^{+}(x,l,t) - \partial_x j^{+}(x,l,t) + \nu_d c^{bp}(x,l,t) \\ &- (\bar{v}_p - v_d)\partial_l c^{+}(x,l,t) - \bar{v}_p \partial_x c^{+}(x,l,t)\end{aligned} \tag{4.5}$$

$$\begin{aligned}\partial_t c^-(x,l,t) =& 2D\partial_x^2 c^-(x,l,t) - \partial_x j^-(x,l,t) + \nu_d c^{bp}(x,l,t) \\ & - (\bar{v}_p - v_d)\partial_l c^-(x,l,t) + \bar{v}_p \partial_x c^-(x,l,t)\end{aligned} \tag{4.6}$$

with $\partial_t = \frac{\partial}{\partial t}$, $\partial_x = \frac{\partial}{\partial x}$, $\partial_l = \frac{\partial}{\partial l}$

The first term on the right side of the equations describes the change of the density distribution due to diffusion. The diffusion is two times larger for monopolar filaments compared to bipolar filaments, because they are on average two times shorter. j^{bp}, j^+ and j^- stand for density currents induced by the motor activity. Bipolar filaments interact via motors with other bipolar filaments or (+)- and (−)-filaments, if the center of these bipolar filaments is overlapping with these other filaments. The exact expressions for the currents can be found in the appendix section A.3.2.2. The third term, which is proportional to $\pm\nu_d$, describes the decrease of bipolar filaments and the increase of monopolar filaments due to dissociation from the nucleator. The last terms express the density changes due to polymerization and depolymerization. This captures also nucleation events, since the nucleation is formally the polymerization of a filament of the length 0. This gives the boundary condition that $(v_p - v_d)c^{bp}(x, l = 0, t) = \mu n(x, t)$, with n the nucleator density. The exact expressions for the nucleator density can be found in the appendix section A.3.2.2. The differential equations for $c^{\pm}$ have an extra term which is proportional to $\mp\bar{v}_p$. It captures the treadmilling activity of monopolar filaments. The sign gives the direction in which the filaments move in this manner.

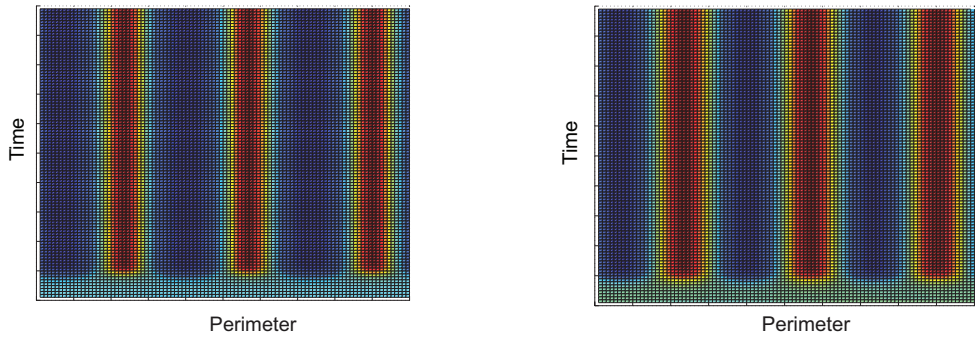

(A) (B)

FIGURE 4.31: Solution of the set of differential equations describing the density changes. The concentrations are color coded and presented as kymographs, as a function of the position on the ring and the time. (A) shows the distribution of filaments in the ring and (B) the distribution of motors. For a critical myosin activity, in both cases a periodic pattern forms from an initially homogeneous distribution of material. The peaks of both distributions are centered around the same values.

Figure 4.31 shows the numerical solution of these equations. At the beginning the nodes are distributed evenly. Filaments have not yet formed. As time goes on filaments form according to the length distribution described in equation 4.1 and 4.2. Strikingly both distributions reveal a pattern of periodic high and low density zones. The center of these

zones coincides in both cases. The pattern is stable over time.

This pattern only appears above a critical myosin activity α_{critical}. Below this threshold value, no structure is observed. This can be understood qualitatively: Myosin tends to bring all the (+)-ends together. It is building clusters. Diffusion on the other hand, is homogenizing the system. Only if myosin activity is exceeding a threshold value, the system turns into an ordered state.

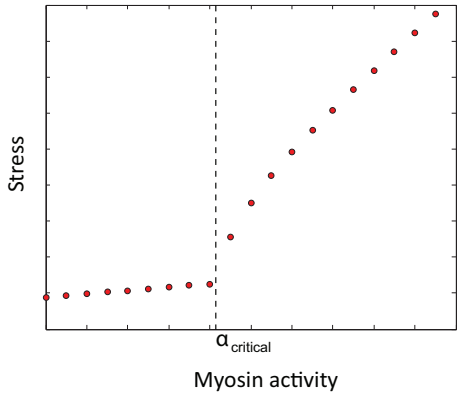

FIGURE 4.32: Stress as a function of myosin activity. The stress is initially increasing linearly with myosin activity. At a threshold value α_{critical}, the stress is over linearly increasing with myosin activity. [172]

The stress is a function of the myosin activity. It is evaluated by considering the overlap between interacting filaments as it was described in e.g. Kruse *et al.* [75]. Figure 4.32 shows the stress as a function of myosin activity. The stress is first linearly increasing with increasing myosin activity. Above a critical value α_{critical} the stress increase is over linear. α_{critical} is also the activity at which the pattern formation occurs. This demonstrates that stress generation is not only dependent on the motor activity, or the amount of motors, but also on the order in the network. Indeed, the ordering of filaments leads to a very efficient stress generation which would otherwise only be attained with much higher motor activity. In the example in Figure 4.32, an increase in 10% of myosin activity around α_{critical} leads to a more than threefold increase in stress. The linear tendency would increase the stress only by 10%.

In the version of the model presented in this section, we do not aim yet at making a quantitative comparison to the experiments. That is why we show the graphs without scale. These will be implemented in future versions. We will also include the reduction of the perimeter.

The mesoscopic model is gathering the essential ingredients of the cytokinetic ring and defines basic rules for their dynamics. With this description, it is able to show how a periodic pattern of myosin, formin and filaments can form. Beyond this, it is demonstrating that such an order can lead to a very efficient stress generation for low motor activities.

The model likewise shows that this pattern forms from a homogeneous myosin distribution, if a critical activity is reached. We were therefore wondering how the pattern is formed in mammalian cells. We also wanted to investigate how polymerization and myosin activity would influence the closure behavior and the myosin pattern.

4.2.4 Pattern formation

The theoretical model shows that myosin and nodes organize in a periodic pattern, similar to the one which we observe in experiments. In the model this pattern forms from an originally homogeneous distribution of the respective components. It only forms if the myosin activity is above a critical value.

We were therefore wondering if we could see a pattern formation in cells prior to closure. In preliminary experiments, we fixed cells on simple glass coverslips. We acquired cells in different stages of cytokinesis. Figure 4.33 shows 3D reconstructions of mitotic cells on flat coverslips. Round, but not yet elongated cells show no distinct region of myosin accumulation. As the cell elongates, myosin accumulates in the equatorial plane. Small, irregular patches are visible in Figure 4.33 (ii) and (iii). As the ring is closing, the myosin is mainly accumulated in the cleavage furrow to aligned strips (Figure 4.33 (iv)).

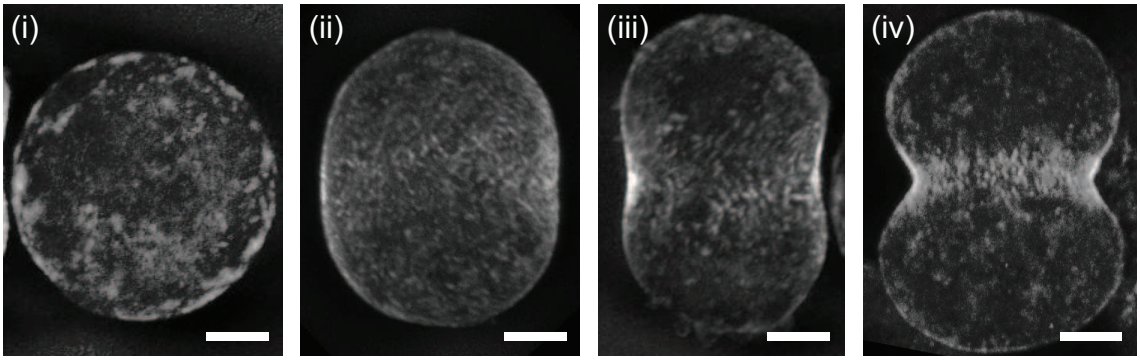

FIGURE 4.33: 3D reconstruction of fixed cells in different stages of cell division. Myosin is accumulating in the cleavage furrow (ii-iv). Only in later stages a pattern of parallel myosin stripes is visible (iv). Scale bars 5 µm.

This transition can be also observed in live cells. Figure 4.34 shows a timelapse of a forming ring. At the beginning the chromosomes (black areas in myosin channel in the first frame) are still aligned in the equatorial plane. Actin and myosin are accumulating in the furrow. Clusters are visible in the third frame. The diameter is already slightly reduced compared to the time-point before. We conclude that the constriction starts, when the pattern has formed.

The pattern formation is further illustrated in the close up in Figure 4.35. At the beginning, large scale inhomogeneities are visible but no pattern of clusters in a range smaller than 1 µm. Myosin is accumulating in the ring. Regular myosin motifs are only clearly visible in the fifth frame that is when the ring slowly starts to constrict.

We quantified the pattern formation by different means (Figure 4.36). Figure 4.36 (i) and (ii) show the myosin signal and the corresponding intensity profiles of myosin in

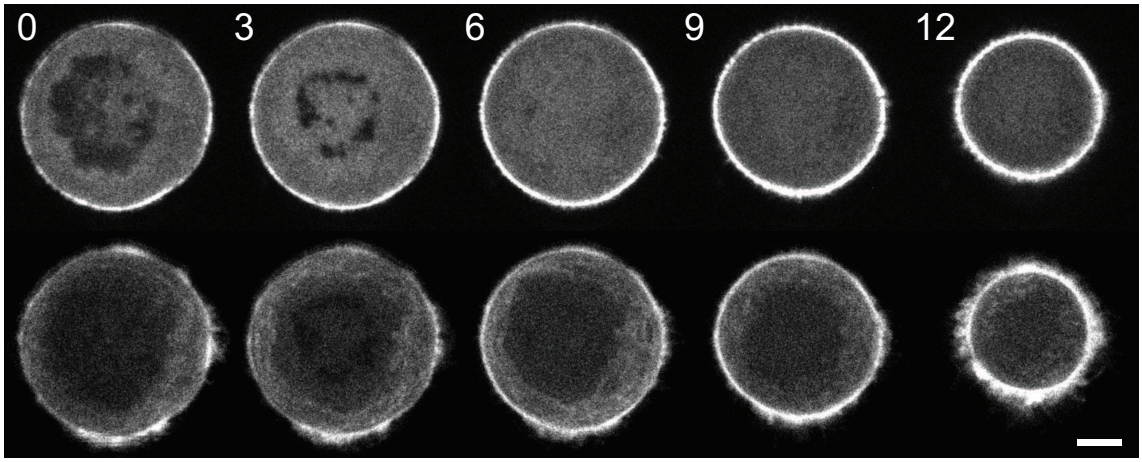

FIGURE 4.34: Formation of the cytokinetic ring visualized for myosin (top) and actin (bottom). The images were smoothed with ImageJ. Time in min, scale bar 5 µm.

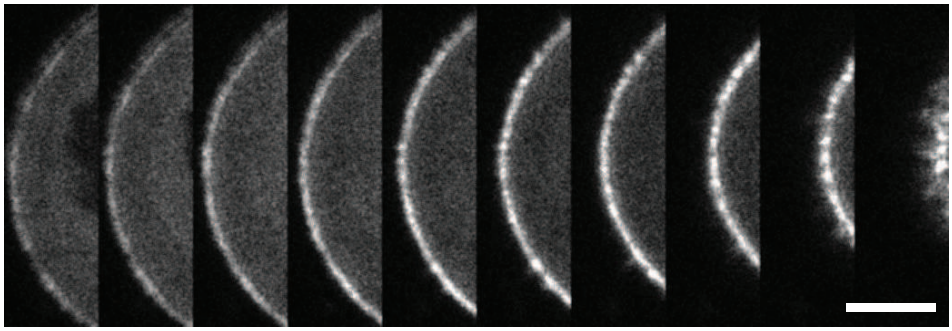

FIGURE 4.35: Close-up of one region of a forming ring. The images were smoothed with ImageJ. Time between images 90 s, scale bar 5 µm.

the plane of the ring before, during and after ring formation (Please note that subsequent intensity profiles are shifted by 100 a.u. for representation purposes.). Pronounced minima and maxima are visible for the last three profiles. This is when the ring starts to close, as indicated by the shortening of the profile. Figure 4.36 (iii) presents the autocorrelation signal for the respective intensity profiles. The curves are again shifted for representation purposes. They are normalized to have the value 1 at zero displacement. Again for the last three profiles a minimum is forming at a distance about 0.75 µm, the first maximum forms at 1.4 µm. "Distance" signifies the shift of a profile with respect to itself. This is indicating that a pattern forms with a cluster size of about 0.75 µm and a period of about 1.4 µm. This is in agreement with our measurements presented in Section 4.2.1.4 and Figure 4.27.

The pattern formation is also captured in a Fourier transformation of the profiles of all time frames (Fig. 4.36 (iv)). Low frequency features are present for all time-points and reveal large scale inhomogeneities. At about 1800 s a signal at frequencies between 0.4 μm^{-1} and 0.8 μm^{-1} appears abruptly. This points at a pattern period of about 1.25 µm. The broadness of the frequency range is partially due to real variations. It is also due to the fact that the Fourier transformation shows also a signal at multiples of the highest

period of the system.

We wanted to know how the pattern would behave after its formation and at the onset of closure. We therefore carried out the same kind of analysis for forming rings as it was presented above in Section 4.2.1.4. Figure 4.37 presents the corresponding results. The time 0 s indicates the onset of closure. Before this time-point, we only saw the characteristic motifs in one cell.

The pattern coefficient stays about constant at the onset of ring formation. That is to say, that the ratio between the intensities of minima and maxima did not change during ring formation. Also the cluster density stays roughly constant. It varies between 1.1 μm^{-1} to 1.4 μm^{-1}. This matches the results of the autocorrelation and Fourier transformation in Figure 4.36. The mean cluster size lays at around 0.5 µm. This corresponds roughly the result of the autocorrelation which gave a cluster size of 0.75 µm. The difference might rise from the different ways of analyzing. The autocorrelation is averaging over all clusters. Additionally the position of the value is also influenced by the intensity of neighboring motifs.

We show that a pattern is forming from a flat myosin distribution. This is visible in the microscopic pictures and the corresponding profiles as well as in the Fourier transformation and the autocorrelation. The formation of the pattern coincides with the beginning of closure. This is in agreement with the theoretical model, which predicts on the one hand that a pattern can form even from a perfectly homogeneous myosin distribution. On the other hand, it correlates the pattern formation with an increase in stress generation by the ring. This can explain why the ring only starts to close when the pattern has formed.

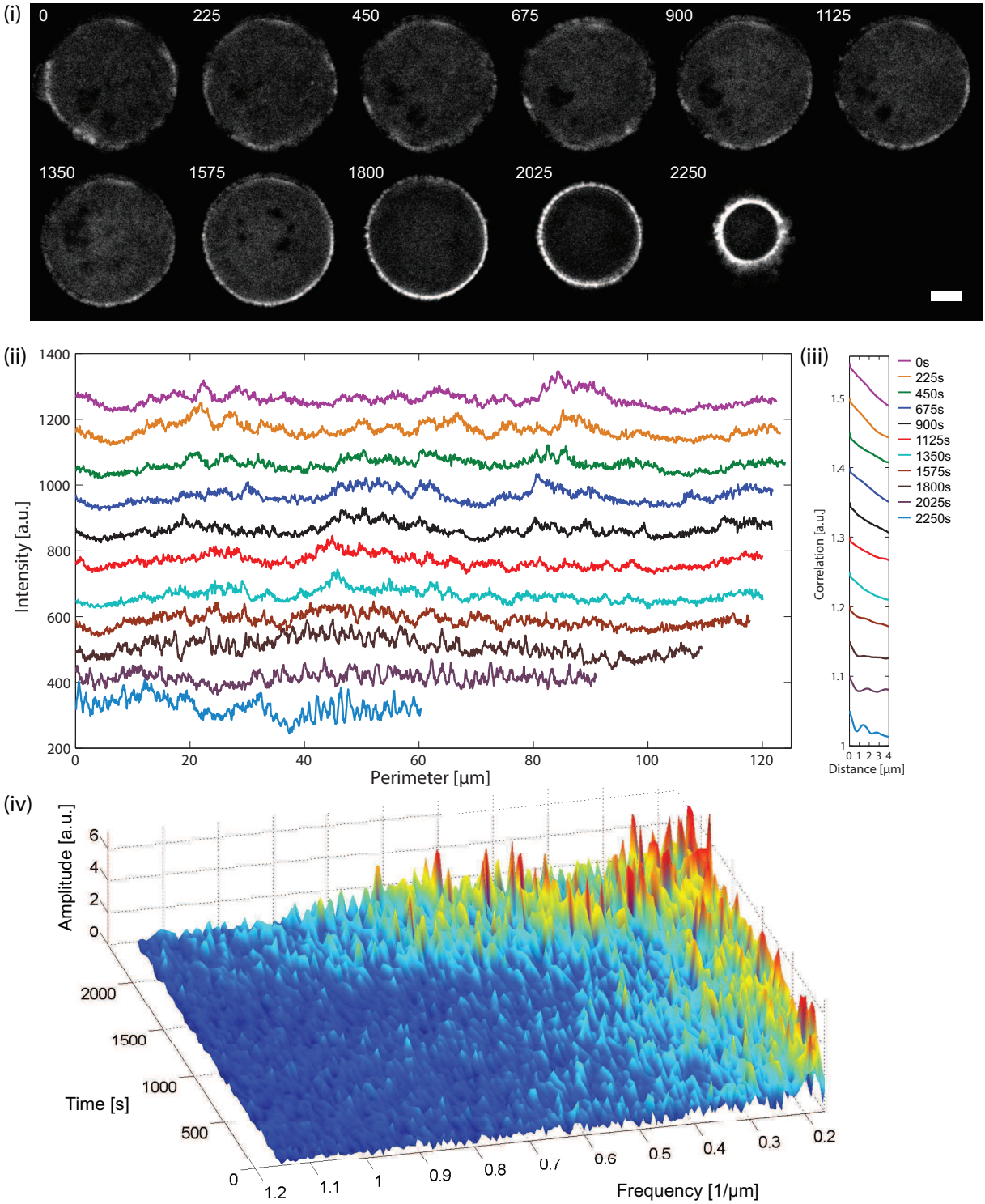
(i)
0
225
450
675
900
1125
1350
1575
1800
2025
2250
(ii)
Intensity [a.u.]
Perimeter [µm]
(iii)
Correlation [a.u.]
Distance [µm]
0s
225s
450s
675s
900s
1125s
1350s
1575s
1800s
2025s
2250s
(iv)
Amplitude [a.u.]
Time [s]
Frequency [1/µm]

FIGURE 4.36 *(previous page)*: (i) Timelapse of a cell before, during and after formation of the cytokinetic ring visualized for myosin. (ii) The corresponding intensity profiles for myosin. Please note, that subsequent profiles are shifted by 100 a.u. for representation purposes only. Strong peaks are visible as the ring starts to close. (iii) Autocorrelation of the profiles. A minimum appears at about 0,75 µm and a maximum at about 1,4 µm. This indicates the formation of a pattern with a mean period of 1,4 µm. The respective autocorrelation curves were normalized by their value at distance = 0. Subsequent curves are shifted by 0.5 a.u. for representation purposes. (iv) Fourier spectra of the intensity profiles for all time-points (dt = 45 s). Long range inhomogeneities are revealed by a signal at below 0.3 μm^{-1}. At about 1800 s higher frequency structures appear in the range of 0.4 μm^{-1} to 0.8 μm^{-1}. Time in s, scale bar 5 µm.

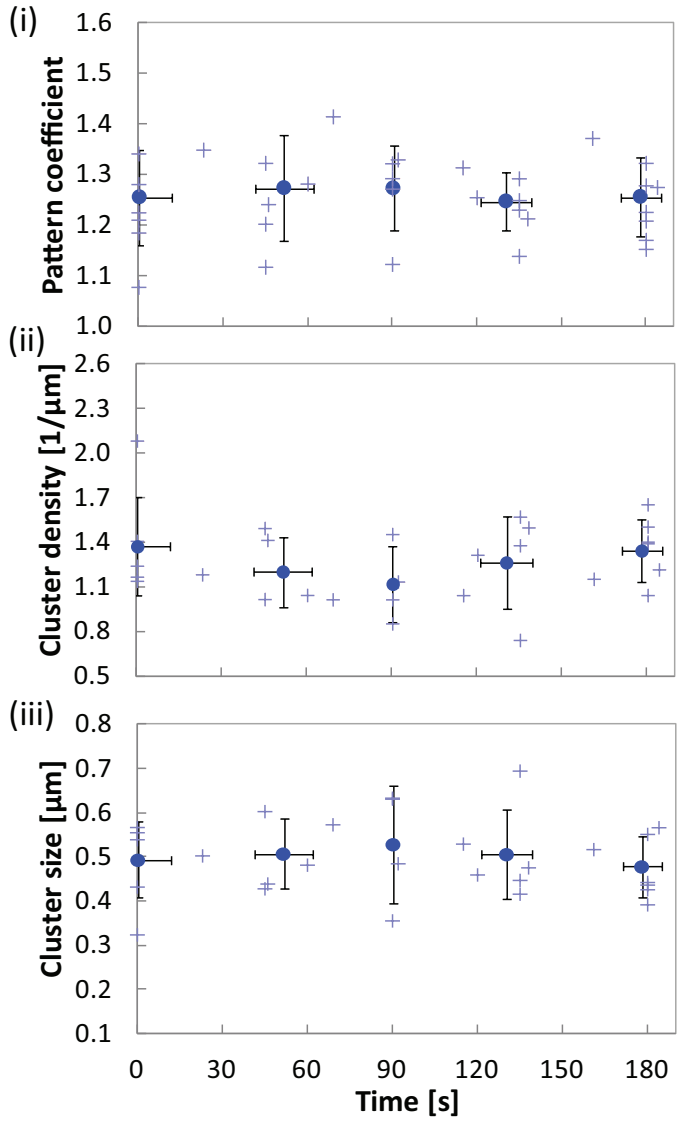

FIGURE 4.37: Characterization of a forming myosin pattern. The time-point 0 s indicates the onset of closure. (i) The pattern coefficient as a function of time. The value stays about constant at a mean value of 1.25. (ii) The cluster density is on average varying between 1 cluster per 1.1 µm to 1.4 µm. (iii) The cluster size remains constant during formation at about 0.5 µm. (N = 7, error bars = StDev.)

4.2.5 Probing material parameters

We wanted to probe the influence of the different parameters on the ring closure and the pattern. We were mainly focusing on changing myosin activity and actin polymerization, because these are the process which can generate stress in the ring. These are also the main parameters in the analytic description of the cytokinetic ring.

4.2.5.1 Myosin inhibition

Myosin is a motor protein. In our model, its activity is leading to stress generation in the cytokinetic ring. Additionally our model predicts, that the pattern formation is myosin dependent. However, other studies show experimentally in budding yeast [96] and theoretically [185] that actomyosin rings can close without myosin.

To test the influence of myosin activity on the closure and the ring pattern, we used the myosin inhibitor blebbistatin [153] and the myosin light chain kinase inhibitor ML-7 [137].

We added blebbistatin (100 µM) to closing cytokinetic rings. We followed the ring closure by acquiring the LifeAct-Cherry signal. Observing the cell in the GFP channel is not possible, since blebbistatin becomes toxic and probably inactive upon exposure to blue light [68]. Figure 4.38 shows an actin ring after addition of blebbistatin. The closure is immediately slowed down and the ring stalled eventually (Fig. 4.39). On minutes timescale we see actin bundles around the ring, suggesting that the ring might disassemble. However, the actin intensity remains constant after addition of the drug (Fig. 4.40).

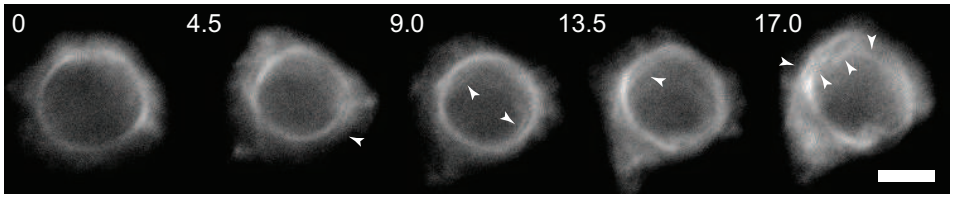

FIGURE 4.38: Actin ring after addition of blebbistatin (100 µM). The closure stalls. Only after some minutes the diameter increases slightly. Actin bundles are visible (arrow heads). The timelapse was acquired with an inverted epifluorescence microscope. Time in min, scale bar 5 µm.

Addition of ML-7 also stops the closure. In contrast to the effect of blebbistatin, the ring is not stalled, but opens after the addition of the drug (Fig. A.12).

These results confirm that the closure of the cytokinetic ring is myosin dependent. The ring gets either stalled or opens upon myosin inhibition. The model predicts a direct relationship between myosin activity and stress generation. We wondered if we could tune the closure speed varying the inhibition of myosin. We therefore scanned different concentrations of blebbistatin and measured the closure speed. Figure 4.41 shows the closure speed as a function of the blebbistatin concentration. Indeed, for small doses of blebbistatin the ring continues to close. The closure speed decreases with increasing blebbistatin concentrations. We do not find a linear relationship as predicted by the

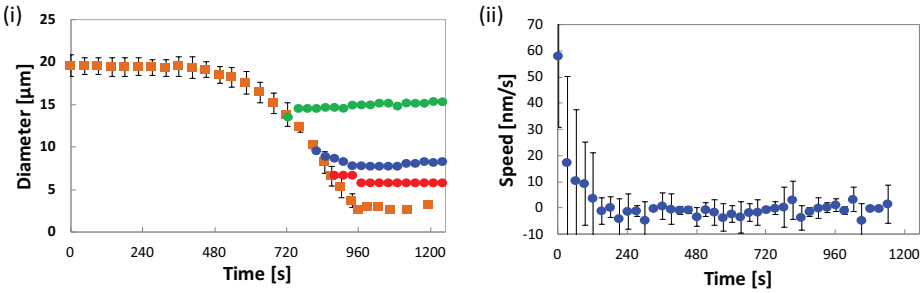

FIGURE 4.39: (i) The diameter as a function of time for control cells (orange) and after addition of blebbistatin (100 µM) (various colors). (ii) The closure speed decreases directly after addition of blebbistatin and stays at zero for several minutes. N = 10, error bars = StDev.

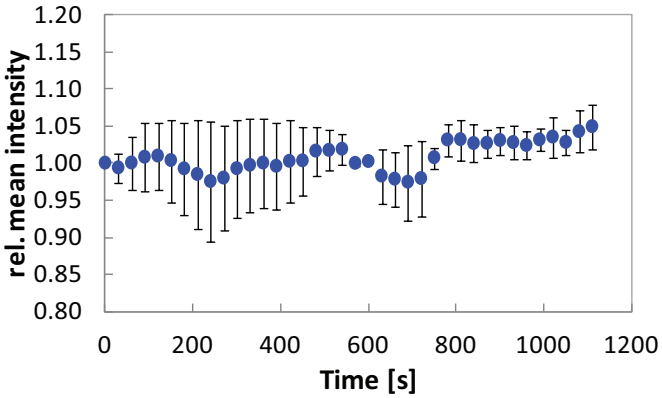

FIGURE 4.40: The relative mean intensity of actin as a function of time after addition of blebbistatin (100 µM). The intensity stays about constant. N = 6, error bars = StDev.

model. However, it is not clear if (i) closure speed depends linearly on the stress generated by the ring and (ii) how myosin activity depends on blebbistatin concentration. Both relationships are probably not linear. Since they are unknown, we cannot probe the model further. Nevertheless, we can confirm that the closure is myosin dependent and that the closure speed depends on myosin activity.

4.2.5.2 Inhibition of actin polymerization and actin related proteins

Actin filaments align parallel in the ring [143, 94, 42]. They might be attached to the membrane by anillin and septin and / or formin, as reviewed in [119] and [50]. In a naive picture, they would be ropes on which myosin is pulling to constrict the ring. However, in budding yeast is was shown that actin polymerization is driving the cytokinetic ring closure, and theoretical studies show how stress can be generated due to polymerization [185, 96].

In our model actomyosin dynamics set essentially the length scale of the pattern, that is to say, the interdistance between peaks.

We wanted to probe the effect of actin dynamics on the closure behavior and the pattern. We used different cytoskeleton drugs to either inhibit actin polymerization directly or inhibit actin related proteins such as Arp2/3 and formin.

To reduce the actin polymerization speed we used Latrunculin A and Cytochalasin D. Latrunculin A [149] is sequestering monomeric actin whereas Cytochalasin D is capping

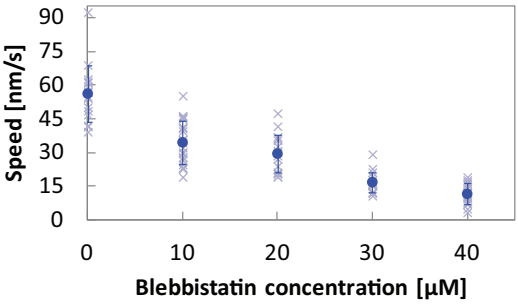

FIGURE 4.41: Closure speed as a function of blebbistatin concentration. At a concentration of 0 µM, 1 % DMSO was added. This corresponds to the amount of DMSO added when using blebbistatin at a concentration of 100 µM. The closure speed decreases with increasing blebbistatin concentration. The speed was determined by a linear fit of closure curves between a diameter of 3.5 µm to 17.5 µm. n $\geq$ 16 for each condition and at least two biological repeats, error bars = StDev.

the barbed end [43]. Both drugs lead to effective shrinkage of filaments.

Figure 4.42 shows a timelapse of a closing ring, after the addition of 1,5 µM Latrunculin A. The ring continues first to close, but is then opening. When the ring is opening, it is composed of clusters in myosin (see Fig. 4.42, top). In actin the ring is barely distinguishable from the cortex. Figure 4.43 (i) presents representative closure curve for cells treated with Latrunculin A. The closure is first accelerated before the ring is opening. We do not see an opening for all cells. We speculated that very small rings might somehow get stabilized. However, if a ring opens after addition, does not seem to depend on the diameter at which Latrunculin A was added.

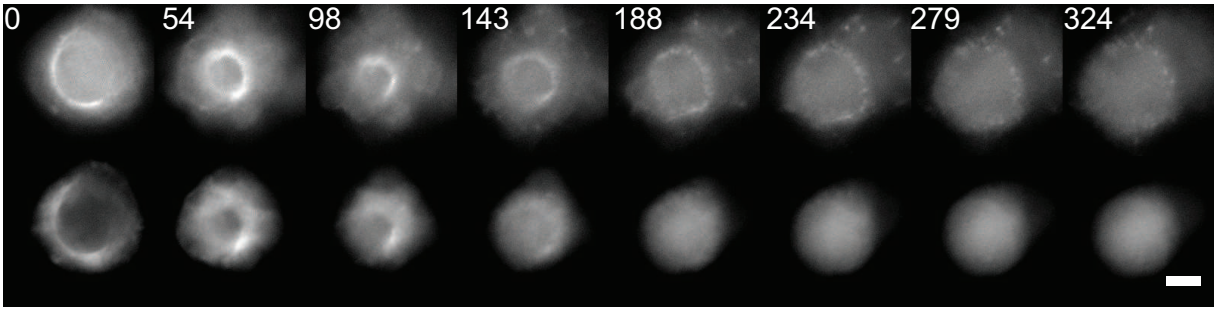

FIGURE 4.42: Timelapse of a ring after addition of Latrunculin A (top: myosin, bottom: actin). The ring continues to close and opens after about 1.5 min. Myosin reveals patches around the ring. The timelapse was acquired with an inverted epifluorescence microscope. Time in s, scale bar 5 µm.

We see for all rings treated with Latrunculin A an acceleration in closure speed (Figure 4.43 (ii)).

We measured the change in intensity for actin and myosin after the addition of the drug (Fig. 4.44). We find a slight increase in intensity. This is astonishing, since we expected actin filaments to become shorter. If their number would stay constant, the intensity should decrease. We speculate that also material from the cortex is dragged in the ring.

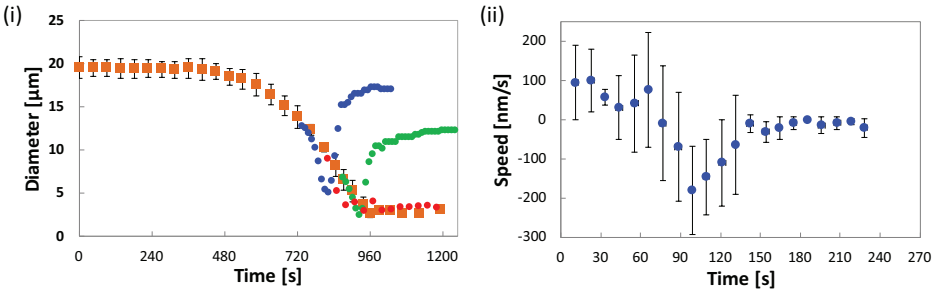

FIGURE 4.43: (i) The diameter as a function of time for control cells (orange) and after addition of Latrunculin A (various colors). Rings might open after addition of the drug or continue to close. (ii) After Latrunculin A addition, the closure speed is higher than the maximal speed in control cells (Fig. 4.16). The speed becomes then negative, which indicates that the ring opens. For this plot, only cells which open after addition were considered. N = 4, error bars = StDev.

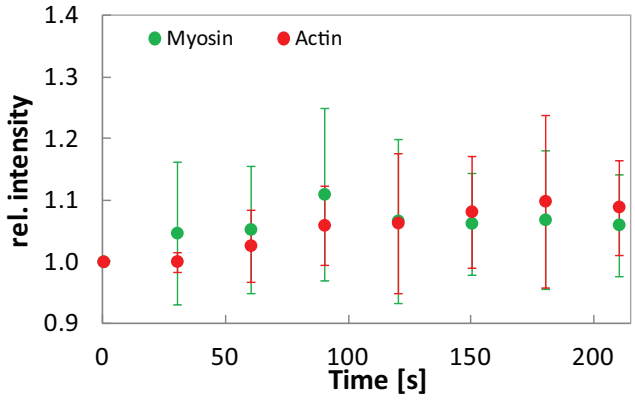

FIGURE 4.44: Relative mean intensity of actin and myosin after addition of Latrunculin A. Both intensities increase slightly but not more than 10 %. N = 6, error bars = StDev.

We performed the same experiments and analysis with Cytochalasin D (1 µM) and obtained the similar results as with Latrunculin A (Fig. A.13). The closure speed is accelerated and in several cases the ring is opening immediately. However, we see stronger actin and myosin clusters than with addition of Latrunculin A (Fig. 4.46) and also the increase in actin and myosin intensities is more pronounced (Fig. 4.45).

Latrunculin A and Cytochalasin D have different targets and their concentrations are not comparable. It is therefore difficult so say if these clusters rise from a principle, qualitative different between the effect of the two drugs, or if it should be rather seen as a qualitative different, rising from the differences in concentration or e.g. efficiency of the drug to enter the cell. To check latter hypothesis, we could probe the effect of different concentration of Latrunculin A and Cytochalasin D. However, this would exceed the scope of this work.

We believe that the opening of the ring is due to shortening of the filaments, which leads eventually to rupture of the ring. However, it is intriguing, that filament shrinkage is accelerating closure consistently. It seems to ease closure. There are two possible explanations. Either the stress generation is higher as filaments shorten or the opposing force are decreasing. Filaments are cross-linked by myosin but also by other cross-linkers

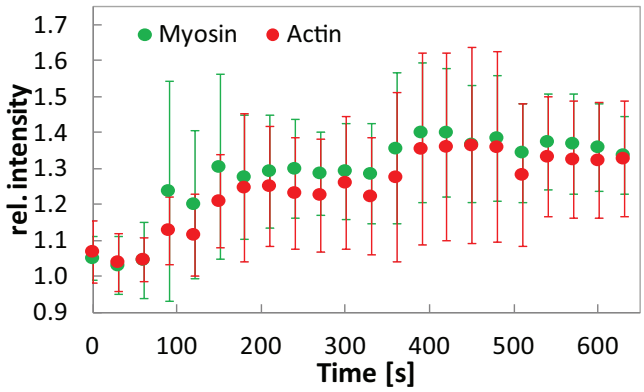

FIGURE 4.45: Relative mean intensity of actin and myosin after addition of Cytochalasin D. Both intensities increase by about 30 %. N = 7, error bars = StDev.

FIGURE 4.46: Ring diameter as a function of time for control cells (orange) and after addition of Cytochalasin D (various colors). Rings open after addition of the drug. In some cases, they continue to close and open after some seconds, similar to Latrunculin A. Error bars = StDev.

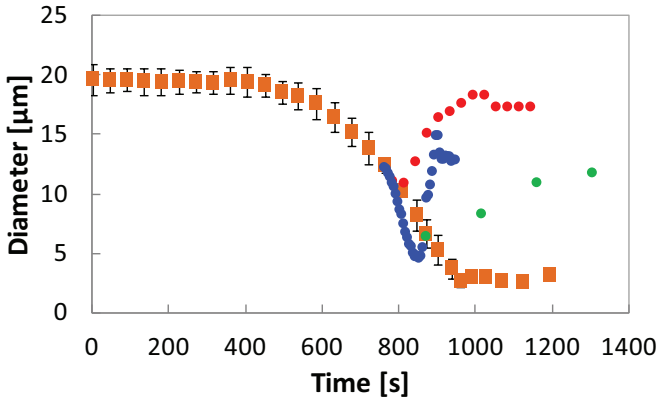

such as α-actinin [103]. The cross-linking, and therefore the effective friction is roughly proportional to the filament length. We speculate that shorter filaments could decrease internal friction and thereby facilitate closure. On the other hand, the ring is deforming the viscoelastic cortex. Shorter filaments might render the cortex more flexible, and facilitate closure on this way.

The presented drugs reduce polymerization speed. We wanted to test, what would happen if filaments would be stabilized instead. We therefore used Jasplakinolide, which is stabilizing actin [30]. We added 1 µM of Jasplakinolide to dividing cells and measured their closure behavior directly after addition up to 50 min after the addition. We did not observe a change in closure behavior (Fig. A.14).

Formin was reported to be important for the formation and the positioning of the ring [173]. SMIFH2 is a formin inhibitor [134]. We incubated dividing cells with 40 µM of SMIFH2. However, we did not notice a change in closure behavior (Fig. A.15). Additionally, we did not see any new cell division occurring after incubation with SMIFH2. This is consistent with what was reported about the role of formin for ring formation. We did not investigate the inhibition of ring formation systematically.

We cannot convincingly conclude that formin inhibition during closure would not alter the closure dynamics. SMIFH2 might need a higher incubation time than some minutes to enter the cell and act on formin. However, to probe formin further with SMIFH2 would

be difficult since no new rings formed in our experiments. Although it might be possible, but challenging, to observe a potential effect on formin inhibition during closure, with a well chosen concentration and timing.

Arp2/3 is branching actin filaments [113]. It is found in the cytokinetic ring in fission yeast [178] and seems dispensable for cytokinesis in *C. elegans* [146]. CK-666 is a Arp2/3 inhibitor [108]. We incubated cells in 100 µM and followed their closure behavior up to 4 h after addition. We did not see a difference in closure behavior compared to control cells.

We used different drugs which act on actin or actin associated proteins. Inhibiting polymerization showed a strong effect. Interestingly, closure is accelerated after addition of Cytochalasin D and Latrunculin A. We presume that this is either connected to a higher stress generation or a reduction of opposing forces. Actin filament stabilization did not change the closure dynamics. However, some rings opened about 1.5 min after drug addition. Actin and myosin were distributed in patches in the ring. The shortening of filaments leads probably to rupture of the ring. Formin inhibition during closure did not have a direct effect on the closure dynamic, but on the formation of new rings. We did not find an effect of Arp2/3 inhibition.

4.2.5.3 Influence of cytoskeleton drugs on myosin pattern

In the model the pattern is dependent on myosin activity and length of actin filaments. We wanted to see if we could indeed influence the actin and myosin distribution with cytoskeleton drugs. We fixed HeLa cells 1.5 min and 15 min after the addition of 1.5 µM Latrunculin A and 100 µM Blebbistatin, respectively. Figure 4.47 shows two examples of the cytokinetic ring after the drug treatment (further examples in Figure A.16). In both cases the myosin pattern is clearly disturbed. The motifs appear larger and less regular. Some actin rings show clusters after blebbistatin treatment.

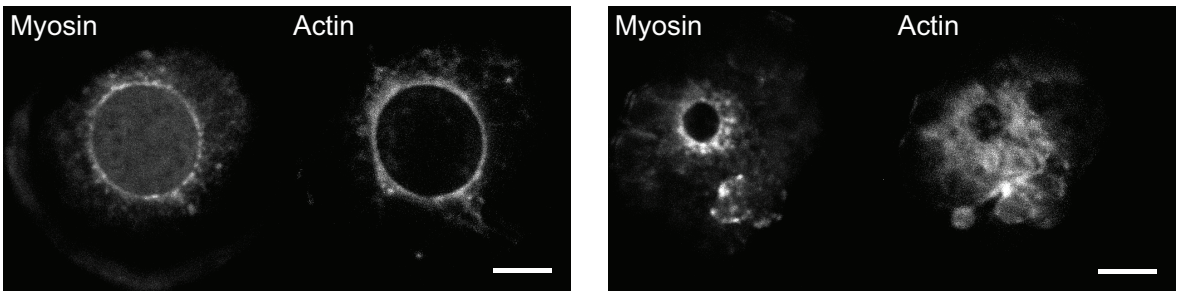

(A) Blebbistatin (B) Latrunculin A

FIGURE 4.47: (A) Ring in myosin and actin 15 min after the addition of 100 µM Blebbistatin. Overlay of 16 z-planes (dz = 0.3 µm). (B) Ring in myosin and actin 1.5 min after the addition of 1.5 µM Latrunculin A. Overlay of 11 z-planes (dz = 0.3 µm). Scale bars 5 µm.

We quantified the pattern as before in Section 4.2.1.4 and Section 4.2.4. Figure 4.48 (i) shows the pattern coefficient as a function of the diameter. The rings treated with

Latrunculin A and Blebbistatin reveal a less pronounced contrast between minima and maxima in their intensity profiles. However the values of the treated cells lay in the cloud of values for control cells. The cluster density is mainly below the average density in control cells. Most values are outside the spread of variation measured in untreated cells. Correspondingly the cluster size of the treated cells is above the average in control conditions. This corresponds to the visual impression one gets from the microscopy images.

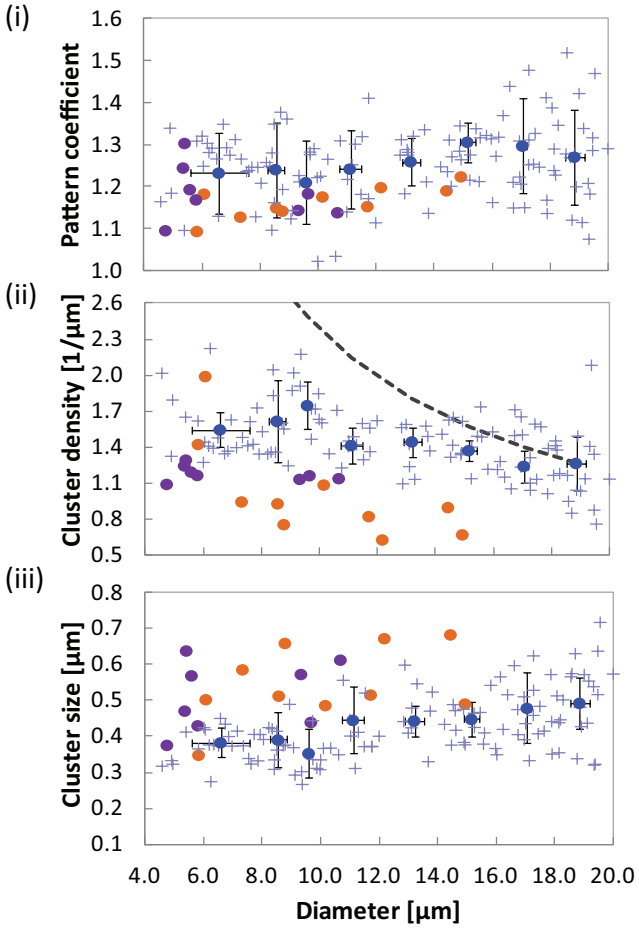

FIGURE 4.48: Characterization of the myosin pattern for control cells (data from Fig. 4.27) and cells treated with Blebbistatin (orange) and Latrunculin A (purple). Each orange or purple point corresponds to the averaged value of one ring. (i) Pattern coefficient as a function of the diameter. All values for rings treated with Blebbistatin and most of the values for Latrunculin A lay below the mean values for the control cells. (ii) cluster density as a function of the diameter. Again the cluster density of cells treated with the two cytoskeleton drugs is below the average of control cells. (iii) The average cluster sizes for rings treated with Latrunculin A and Blebbistatin are above the average cluster size in control cells. Error bars indicate the standard deviation

The visual impression and the pattern characterization suggest that the cluster size and density is altered by the drugs. Additionally the pattern seems to be less regular. Figure 4.49 shows in (i) the distribution of cluster sizes and in (iii) the corresponding mean values. The distributions of drug treated cells are broader and the mean values are larger. Both mean value and variance differ significantly from the untreated cells ($p < 0.001$ for comparison of control to Blebbistatin and Latrunculin A for mean and variance in t-test, ANOVA and f-test). The interdistance between clusters reveals a similar picture (4.49 (ii), (iv)). Both, variance and mean values are significantly different between rings treated with the cytoskeleton drugs and control cells ($p < 0.001$ for comparison of control to Blebbistatin and Latrunculin A for mean and variance in t-test, ANOVA and f-test).

The statistical analysis confirms the visual impression. The pattern is less regular and the clusters are broader and less frequent. We can show that myosin activity and actin

polymerization have an effect on the myosin pattern.

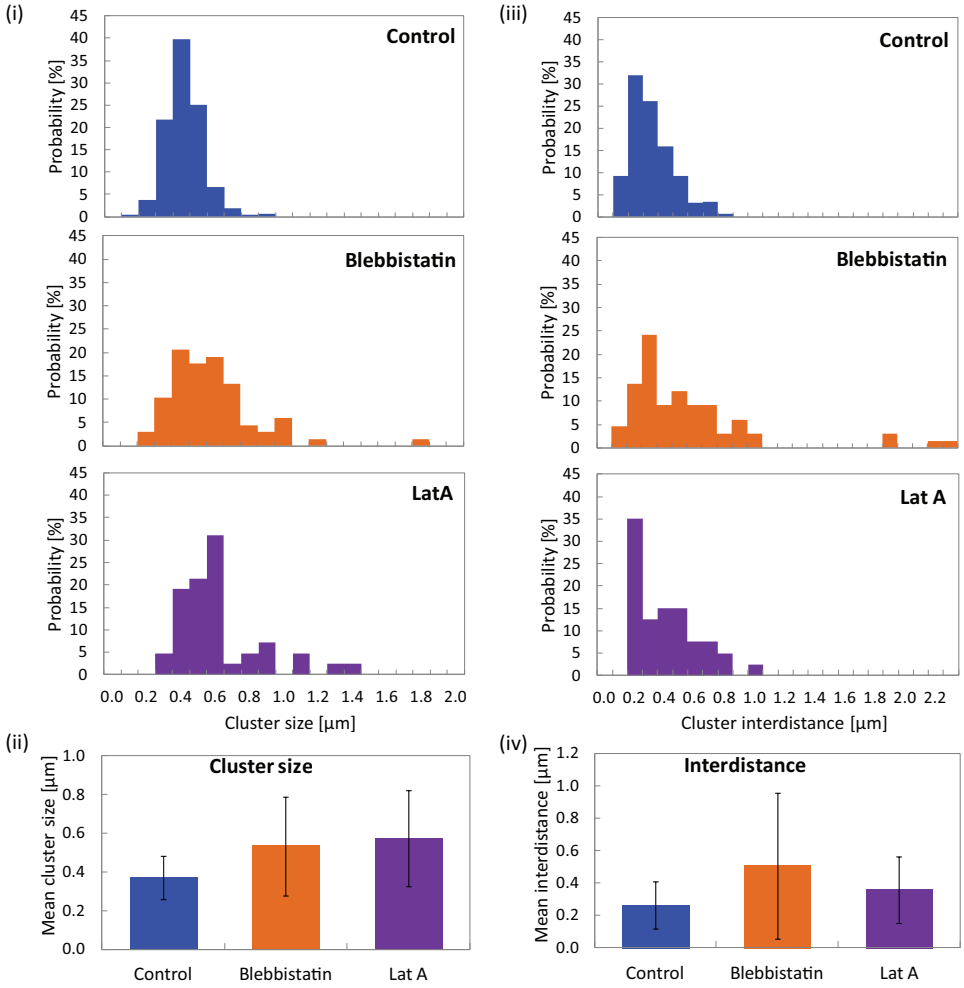

FIGURE 4.49: Distribution of (i) cluster size and (ii) distance between clusters for rings in the diameter range of 7 µm and 11 µm. (iii) and (iv) show the corresponding mean values and standard deviations. The mean values and distributions of treated cells are significantly different from untreated cells. $p < 0.001$ for comparison of control to Blebbistatin and Latrunculin A for mean and variance of the distributions in t-test, ANOVA and f-test. cluster size: $N_{control} = 22$, $n_{control} = 272$, $N_{Blebb} = 4$, $n_{Blebb} = 68$, $N_{LatA} = 3$, $n_{LatA} = 42$, interdistance: $N_{control} = 22$, $n_{control} = 259$, $N_{Blebb} = 4$, $n_{Blebb} = 66$, $N_{LatA} = 3$, $n_{LatA} = 40$. (N= number of rings, n = number of clusters/interdistances

4.2.5.4 Myosin mobility and turnover

We wanted to test mobility of myosin in the ring in fluorescence recovery after photobleaching (FRAP) experiments. Recovery of fluorescence might rise from lateral movement of myosin on the ring and from exchange with the cytoplasm. To distinguish between the two possibilities, we used different bleaching patterns (Fig. 4.50): (i) we bleached the entire ring, (ii) we bleached everything but a small part and (iii) we bleached one part of the ring.

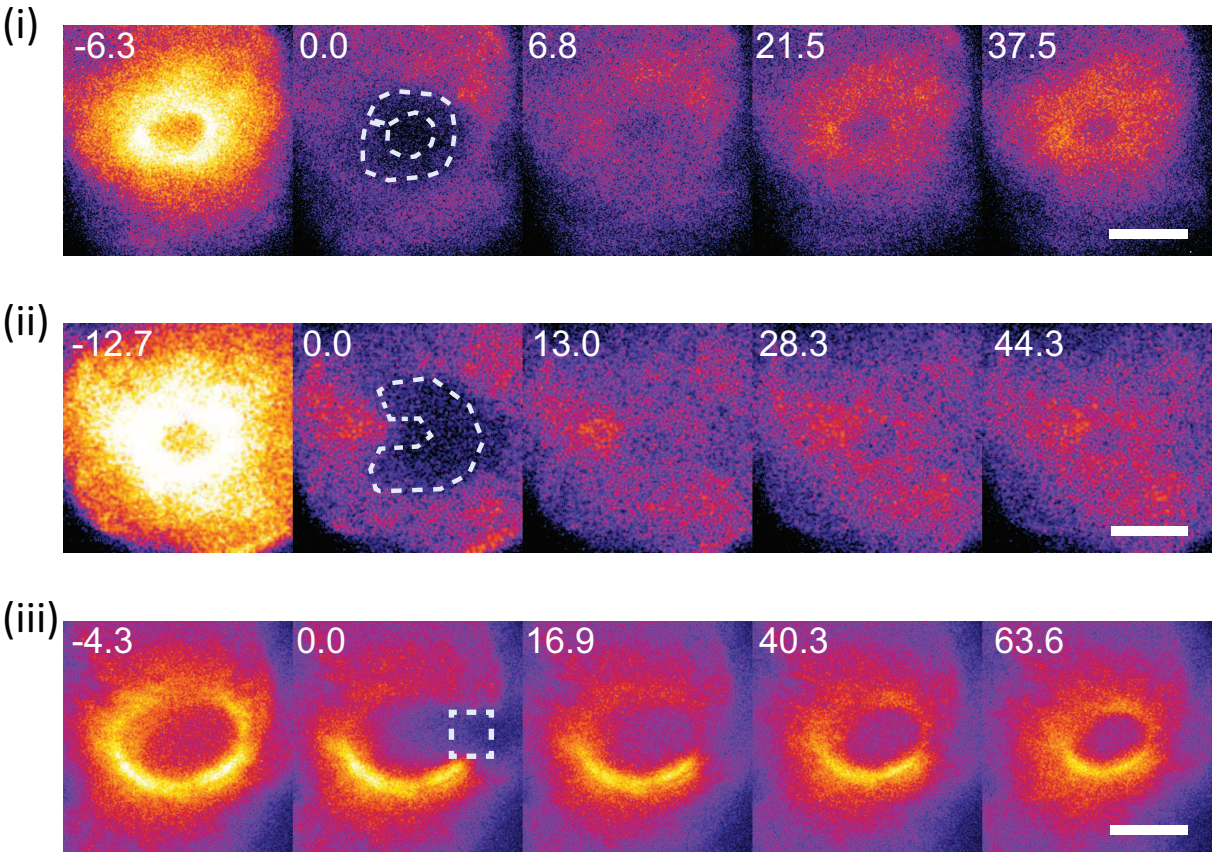

FIGURE 4.50: FRAP experiments with different bleaching patterns on myosin rings: (i) entire ring bleached, (ii) everything but a small region bleached and (iii) only one region bleached. The images were acquired with an inverted confocal microscope. Images were smoothed with ImageJ. Time in s, scale bars 5 µm.

When we bleach the entire ring, we find, that it never recovers its entire fluorescence. In fact, we find, that the recovery half-time is 23 s, so it takes than 60 s before the myosin fluorescence reaches a plateau (Fig. 4.51).

With this experiment we eliminated recovery from the ring itself. But what happens, if we bleach everything apart from a small region or only a small region? Such bleaching patterns would potentially reveal flows on the ring. In Figure 4.50 (ii) the entire ring was bleached apart from a small region on the left. We do not see an enlargement of the fluorescent region. Probably no big flows are present.

Finally we bleached only a small region in the ring (Fig. 4.50 (iii)). The region seems

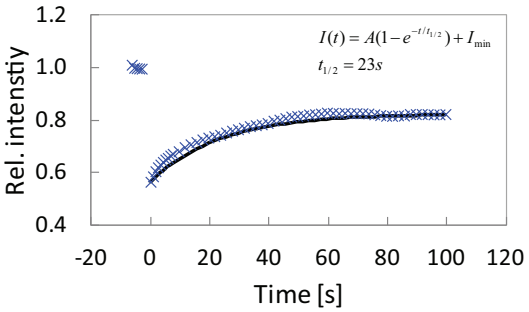

FIGURE 4.51: Recovery of the fluorescence of the entirely bleached ring. The half-time of recovery is 23 s.

to recover rather homogeneously and not by flows from the neighboring areas (Fig. A.17). However, the bleached spot becomes smaller as the ring reduces its perimeter.

The data is too preliminary to come to strong statements. Additionally the experiments were performed on a setup which did not allow resolving the myosin patterns. However, we do not see flows of myosin along the ring. We also find a relatively long recovery time which is rather in the order of tens of seconds, than seconds.

4.3 Rings on surfaces

To observe the cytokinetic ring, we need to have dividing cells and therefore to synchronize the cell culture. It would be more convenient, if 100 % of the cells would show a ring. Additionally the event of cell division is very short, only about 5 min. This does not give much time to manipulate cells. One parameter, which is difficult to access experimentally is the stress generation of the ring. I will present in the following, an observation that we made in microcavities, and how this might potentially be useful to study actomyosin rings in cells.

Observing cells in microcavities, we made an interesting observation. On the bottom of the wells, cells formed circular or nearly circular rings of actin and myosin (Fig. 4.52). These rings were closing in some cases as illustrated in Figure 4.52 (B).

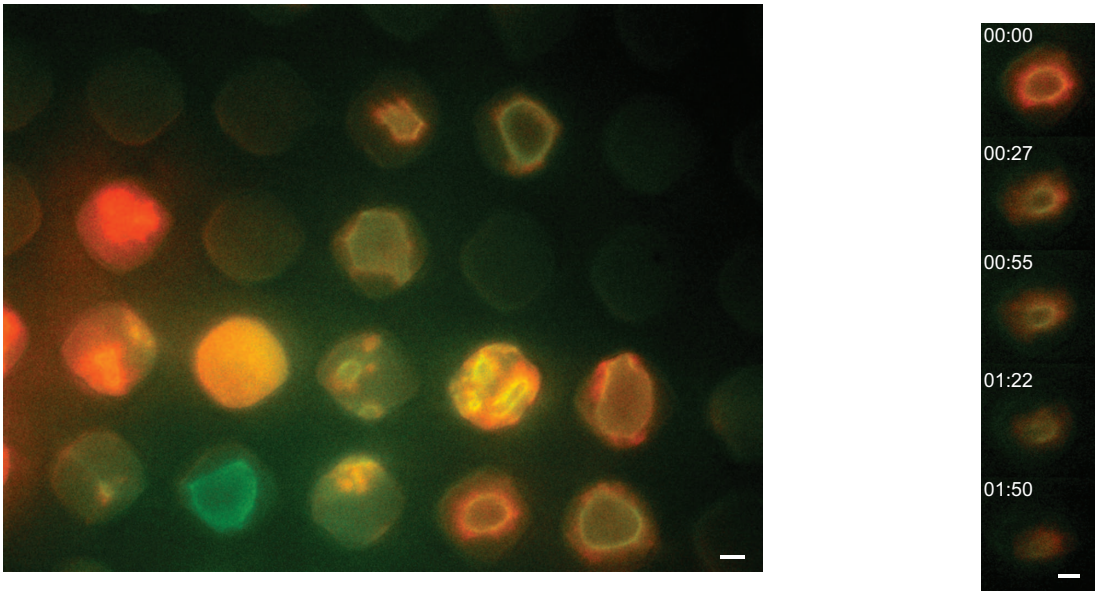

(A) (B)

FIGURE 4.52: Cells exhibit ring-like structures of actin (red) and myosin (green) on the bottom of microcavities. (A) Overview of HeLa cells in cavities. Several cells build nearly circular structures of actin and myosin on the bottom of the well. (B) Example of an actomyosin ring which is closing at the bottom of the cavity. Time in hh:mm, scale bars 5 µm.

These rings represent, as the cytokinetic ring, circular active gels *in vivo*. They are also closing, but on timescales about one or two orders of magnitude larger than the cytokinetic ring. This might be related to the attachment of the cell to the surface on the bottom of the well.

One important parameter, which was inaccessible for us experimentally, is the oposing force to the closure. We cannot measure what stress the cytokinetic ring applies. We wondered, if we could not access this information with these rings on surfaces.

Figure 4.53 shows a setup which would allow the force measurement of the ring while

it is closing. Cells would be inserted in very flexible cavities, which contain fluorescent beads. As the cells closes, the beads would be displaced. Knowing the Young's modulus of the flexible cavities, we could then calculate the force of the cell on the surface (e.g. [13, 164]).

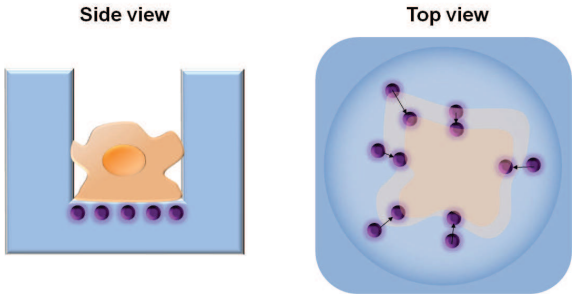

FIGURE 4.53: Schematic representation of the desired setup. Mircocavities are built of a flexible material containing fluorescent beads. As ring on the bottom closes, the beads would get pulled by the cell and the force on the surface could be determined.

The challenge for such a setup is to find a way of generating microcavities of a still very flexible material. We decided to use polyacrylamides gels. These gels allow a wide range of elasticities (between 0.2 kPa and 35 kPa in [165]) and the force measurement with fluorescent beads is well documented e.g. in [116] and [31].

HeLa cells are rather weak cells. At least on flat surfaces they are less spread and have less prominent stress fibers. We therefore decided to work with REF52 cells. Figure 4.54 shows a REF52 cell on a flat polyacrylamide gel of an elastic modulus of 10 kPa with fluorescent beads. The cell is moving to the bottom right. While moving it is deforming the surface and displacing the beads as emphazised in the inset.

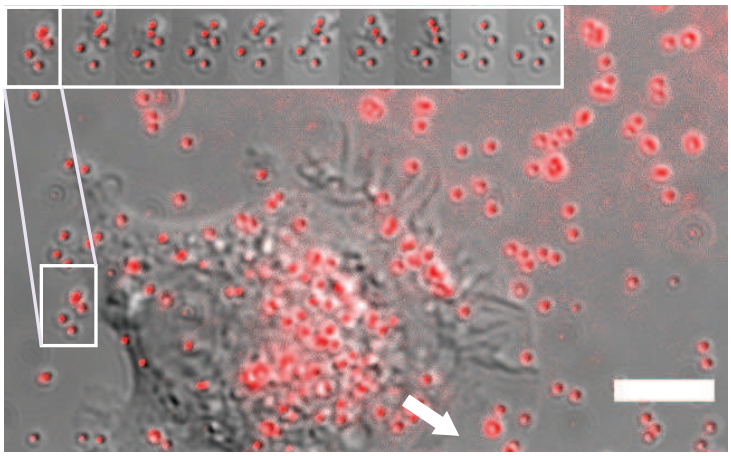

FIGURE 4.54: REF52 cell on a flat polyacrylamide gel of 10 kPa with red fluorescent beads. The cell deformes the surface and displaces the beads (inset) as it is moving to the bottom right (arrow). The inset illustrates the bead displacements. dt = 15 min, scale bar 5 µm.

We tried to insert REF52 cells in microcavities to see if they would build ring structures at the bottom. We transfected the cells with actin-GFP to be able to visualize the rings. Using cavities of the 20 µm in diameter, we were not able to see the same structures as in HeLa cells (Fig. 4.55). However, REF52 cells are larger than HeLa cells. Probably they would exhibit similar structures as HeLa cells in larger cavities.

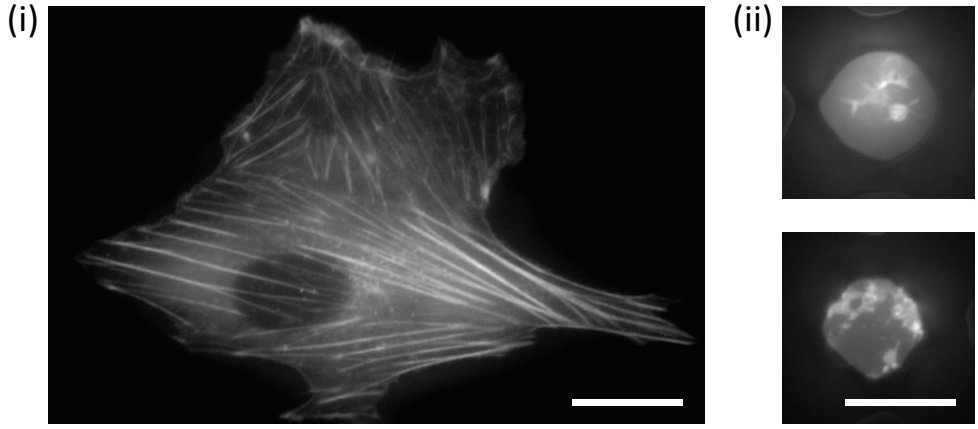

FIGURE 4.55: (i) REF52 transfected with actin-GFP on top of PDMS cavities. The pronounced stress fibers are clearly visible. (ii) Cells do not enter in 20 µm cavities and do not reveal rings structures on the bottom. Scale bars 20 µm.

At the same time we tried to build a surface with microcavities of elastic polyacrylamide gel. For soft gels we faced the difficulty, that the structures are not formed or deformed. Figure 4.56 shows a surface of an 10 kPa polyacrylammide gel with beads and HeLa cells on top. Some cavity walls have formed, but most of them are nearly not formed at all.

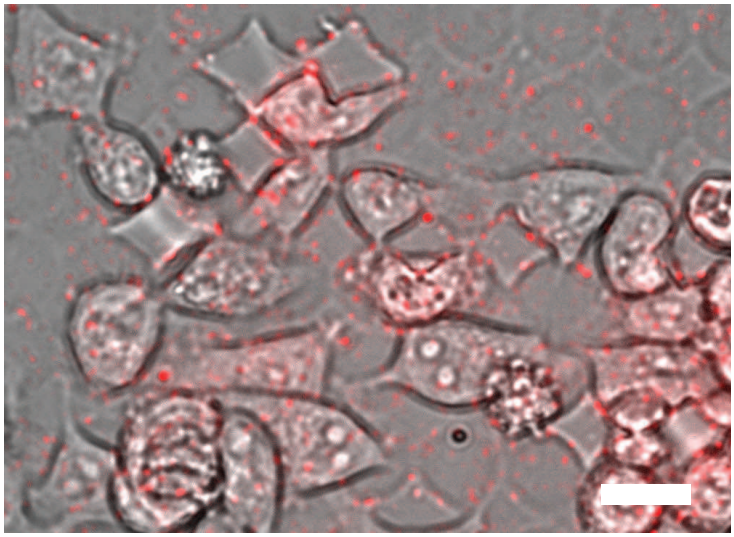

FIGURE 4.56: HeLa cells on a polyacrylamide gel structured with microcavities. Most of the cavities are not formed. Only few well walls are visible. Scale bar 20 µm.

We started to work on a promising setup, which would potentially allow to measure forces exerted by an actomyosin ring. REF52 cells are able to deform elastic surfaces. We can track the deformation with beads. However, the dimensions of the cavities have to be adapted. Additionally the protocol to make microcavities has to be refined to be able to produce cavities, which are elastic enough to be deformed by cells.

5 The cytokinetic ring in fission yeast – Results

Preface

In this chapter I will present our findings about cytokinesis in fission yeast. The data were generated in a team work. In his sabbatical at the Rockefeller University in Paul Nurse Lab., Daniel Riveline developed a setup to vertically orient fission yeast cells and observed rotation of speckles of many proteins (Myo2, Rlc1, Bgs1 Pxl1) [130] and setup the measurement and analysis. Together with Daniel Riveline and Raghavan Thiagarajan (PhD student in the lab.), I continued the research on this project. I acquired movies to measure the closure speed and the speckle rotations, but most of the following data were acquired by Daniel Riveline and Raghavan Thiagarajan. The laser ablation experiments were performed together by Raghavan Thiagarajan and me. I carried out most of the analysis of experimental and simulated data, if not stated otherwise. François Nédélec and Ester Lakatos (former Bachelor student in the Nédélec Lab.) developed the model and simulation.

5.1 The cytokinetic ring

We oriented fission yeast cells in a vertical fashion in microcavities (Fig. 5.1), this allowed us to observe the entire ring in a single plane of focus. Figure 5.2 shows the timelapse of a closing cytokinetic ring. The ring is visualized by the labeling of myosin by Rlc1-mCherry and of actin by CHD-GFP. CHD (calponin homology domain) is binding domain in an actin binding protein. Different features, such as inhomogeneities and emerging structures can be observed.

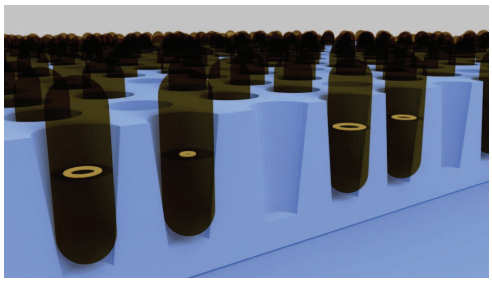

FIGURE 5.1: Schematic representation of fission yeast cells oriented in microcavities.

To characterize the closure dynamics, we measured the diameter of closing cytokinetic rings as a function of time. The corresponding individual and averaged curves are shown in Figure 5.3. To determine the average curve, individual curves were aligned between 1 µm and 2.5 µm. Cells divide in around 40 min at 27°C. The mean velocity is therefore roughly 75 nm/min. The ring closes nearly linearly at the beginning. The closure speed then increases.

We see in actin as well as in myosin features appearing around the ring. In actin we see patches

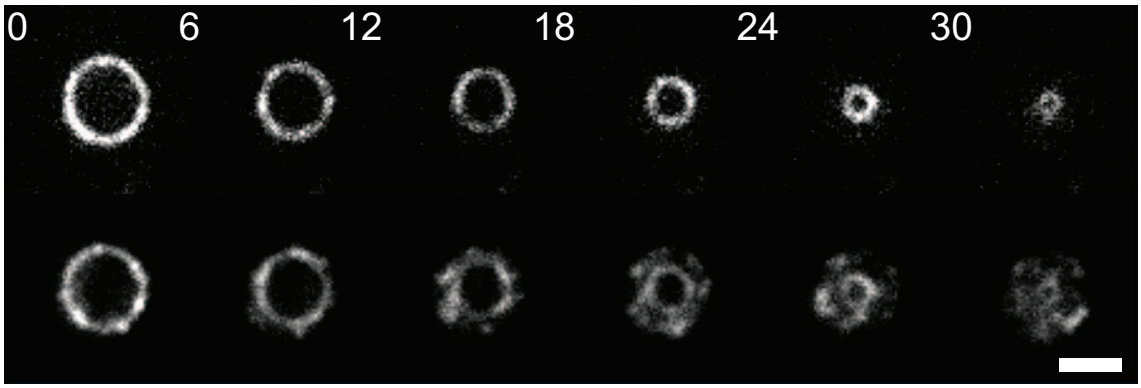

FIGURE 5.2: Timelapse of a closing cytokinetic ring visualized in myosin (Rlc1-mCherry) (top) and actin (CHD-GFP) (bottom) at 27 °C. Time in min, scale bar 2 µm.

in the vicinity of the ring. These patches might by associated to endocytosis [46, 147]. We see one to four emerging structures in myosin, *arms* (Fig. 5.4) around rings, which reached about 50 % of their original diameter and less. These arms are linked to the ring, mostly at bright spots on the ring. The arms grow and buckle when getting into contact with the cell periphery (Fig. 5.4 (ii)). Figure 5.4 (iii) shows that arms also rotate clockwise and counterclockwise.

We measured the total and mean intensity of actin (CHD) and myosin (Rlc1) during closure, by taking snapshots of individual rings with constant imaging parameters e.g. exposure time. The total intensity divided by the measured ring area correspond to the mean intensity. Figure 5.5 (i) and (ii) show the total and mean intensity of actin and myosin as a function of the diameter. The total intensity of actin is linearly decreasing. Its mean intensity is staying constant and is only decreasing for small radii. Myosin total intensity shows two regimes: For radii larger than 1.8 µm the total intensity of myosin is about constant. For smaller rings it is decreasing linearly. The mean intensity of myosin is increasing throughout closure. The curves are normalized by the intensity value at the beginning of the closure. Tendencies are indicated by guides for the eyes. The straight lines in the total intensity plot correspond to curved lines in the mean intensity plot, since the area is inversely linear to the diameter. The corresponding calculations can be found in the Appendix section A.4.1.

Interestingly actin and myosin do not show the same behavior. As indicated by the total intensity, the total amount of both proteins is decreasing. The decrease in myosin number is compensated by the closure of the ring, which leads to a densification of myosin. Loss of actin proteins and reduction in ring diameter are balanced, which leads to a constant concentration of actin until small diameters.

We propose that the loss of material is due to features that we see around the ring. For actin we find patches around the ring during the entire closure. We do not see that entire patches are leaving the ring. However, actin monomers might be used as they detach from the ring to help the actin driven endocytosis [46, 147]. According to the electron microscopy study of Kamasaki *et al.* [62] filaments become shorter during division.

Myosin arms, on the other hand, are not visible during the entire closure. We measured their appearance as a function of the ring diameter. Visible arms appear for rings smaller

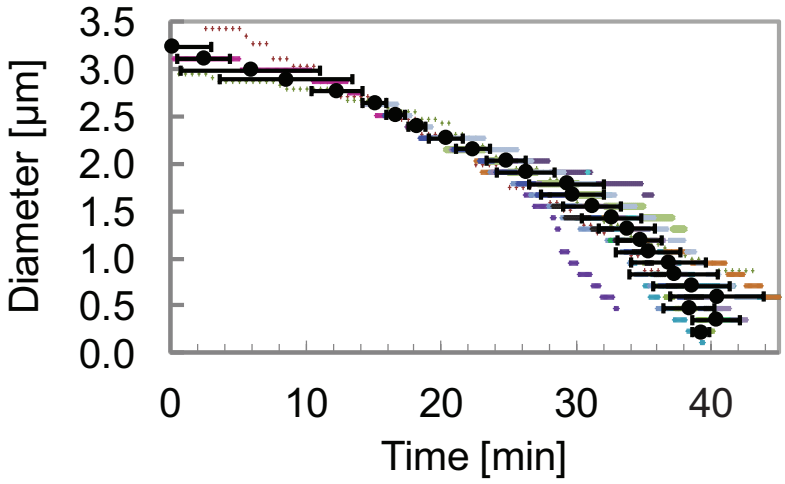

FIGURE 5.3: The diameter of a closing cytokinetic ring as a function of time. 18 individual curves are represented in different colors. The mean curve is black and the error bars indicate the standard deviation. Individual curves were aligned at their beginning with a master curve (the longest curve). Therefore the standard deviation is smaller at around 18 min.

than 1.6 µm (Figure 5.5 (iii)). This coincides with the decrease of total intensity of myosin. We therefore believe myosin arms to be one source, maybe the main source, of loss of myosin. For more quantitative analysis it would be needed to evaluate the absolute amount of myosin in arms and compare it with the loss of myosin in the ring. This is challenging since the arms are not very intense and not always entirely in the same plane of focus as the ring.

Since arms are very fine structures and actin patches form around the ring, we cannot convincingly prove that myosin arms contain actin. However we believe that myosin alone does not form these long filamentous structures. It appears therefore plausible that the arms also contain actin and that they contribute to the loss of actin material. The actin associated paxillin homologue Pxl1 is indeed present in the arms (data D.Riveline).

5.2 Rotating speckles in actin and myosin

The distributions of Rlc1-mCherry and CHD-GFP around the ring were inhomogeneous, and we could observe rotating speckles in the fluorescence intensity with both markers. The speckles associated with actin filaments and myosin were distinct and appeared uncorrelated. Figure 5.6 shows two examples of rotating speckles for actin and myosin. We performed a polar transformation of the ring and represented the speckle dynamics in a kymograph. Taking into account the measured diameter of the ring, we could derive the velocity at which speckles rotate around the rings (Fig. 5.7) as well as their lifetime (Fig. 5.8) and the rotation distance (Fig. 5.9). These velocities were in the range of µm/min. The velocity observed with CHD-GFP decreased as the ring closed, while for Rlc1-mCherry it remained nearly constant (Fig. 5.7). Velocities of CHD-GFP were on average larger than velocities of Rlc1-mCherry for all diameters. We speculate that CHD

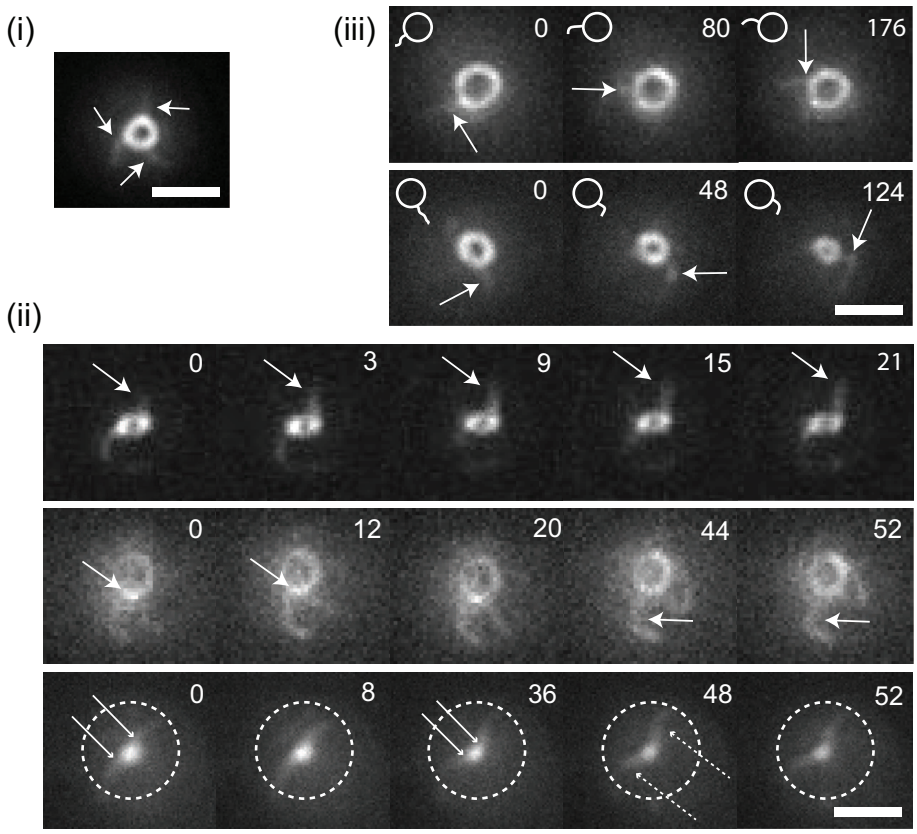

FIGURE 5.4: (i) Myosin arms radiate from the ring. Different behaviors can be observed. (ii) Different characteristics of arms (arrows). Top: Arms elongate over time. T = 27°C. Middle: Bright speckles are associated with arms. T = 36°C. Bottom: Growth of arms leads to buckling (dashed arrows), when they encounter the cell wall (outlined by a white circle). T = 27°C. The decrease in the ring diameter is indicated by continuous arrows. (iii) Rotation of arms. Rows show arm rotations for clockwise and counterclockwise directions respectively. Arrows indicate the arm position at different time points. T = 18°Cand 27°C(second row). Time in s, scale bars 2 µm. The figure was prepared by Daniel Riveline and Raghavan Thiagarajan, PhD student in the Riveline Lab.

speckle move faster, since actin filaments move due to polymerization and myosin activity. However, in general it is not expected that actin and myosin speckle rotate with the same velocity – even without polymerization. In an extreme case, myosin could move actin without moving itself. Speckles rotated equally far to the right and to the left (Fig. 5.9). Interestingly, the average distances traveled by both types of speckles were comparable, because the shorter lifetime of CHD speckles (Fig. 5.8) was compensated by their higher speeds (Fig. 5.7).

We wondered what could be the role of these rotations and turned to modeling to gain a better understanding of the closure mechanism in fission yeast.

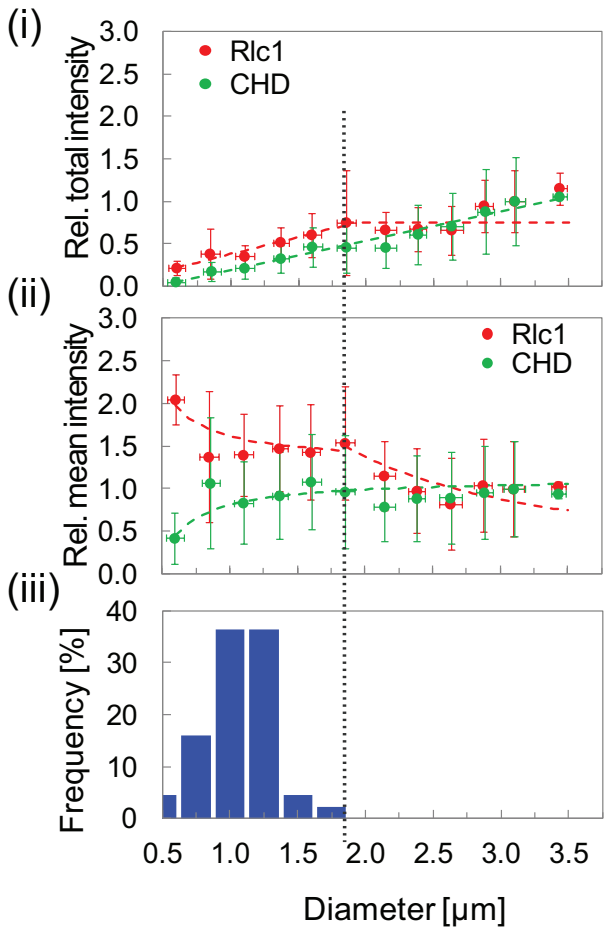

FIGURE 5.5: (i) and (ii) total and mean intensities of actin (CHD) and myosin (Rlc1) as a function of the diameter. The values are normalized by the value at 3.1 µm. The total intensity of actin is decreasing throughout closure and its mean intensity stays about constant and decreases for small rings. Until a diameter of 1.8 µm the total intensity of myosin is about constant and is decreasing as closure continues, as indicated by the guide for the eyes (dashed line). (iii) Myosin arms appear during closure. They appear for diameters smaller than 1.6 µm and on average at a diameter of 0.96 µm. The vertical dashed line indicates the arm appearance. The frequency of arm appearance was measured by Raghavan Thiagarajan, PhD student in the Riveline Lab.. n = 241 for intensity measurements in (i) and (ii), and n = 44 for arm analysis (iii), error bars indicate the standard deviation.

5.2.1 Modeling of the cytokinesis in fission yeast

The following model was developed by François Nédélec (EMBL) and Ester Lakatos (bachelor student in the Nédélec Lab.).

The speckle speed is of the same order of magnitude than the speed of nodes during condensation [167], but slower than the characteristic speed of actin (dis-)assembly and motors [55]. Additionally the speed of rotation is more than one order of magnitude larger than the closure speed, which is about 0.1 µm/min. Speckles move only by a small fraction radially of the distance they move on the perimeter.

The relatively slow motion of motors could be explained, if motors would by heavily loaded. This could indicate that the nodes are connected to larger entities, which impede motion. We propose that the nodes are connected to the wall building machinery, namely the β-glucan sythase proteins Bgs. Bgs are transmembraneous proteins which synthesize β-glucan, an essential building block of the fission yeast cell wall. Such a connection of actin to Bgs, would also link the cytokinetic ring to the cell wall.

We wondered if such a mechanism could divide the cell into two. Since fission yeast cells stand under a tugor pressure, Proctor *et al.* [124] suggested that myosin can not

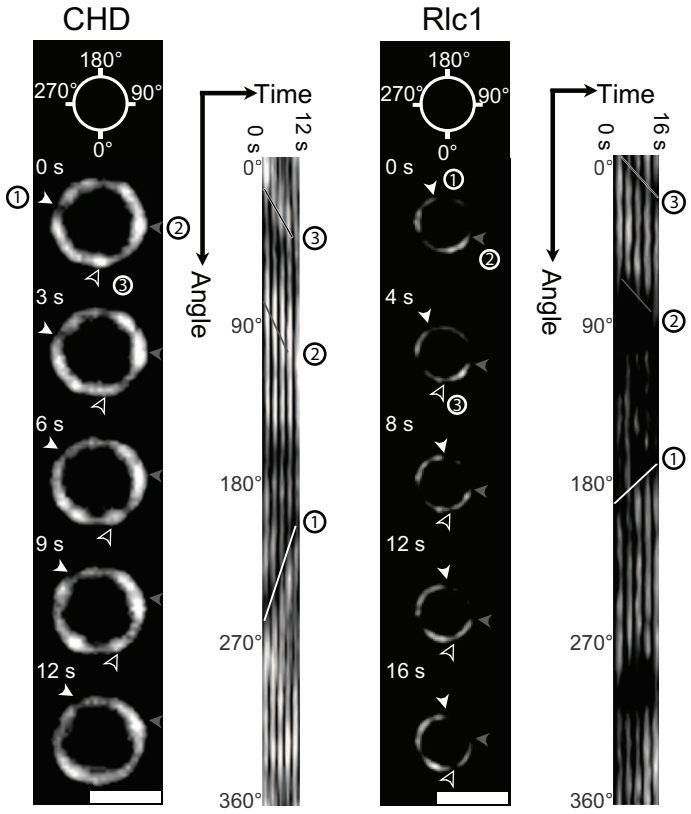

FIGURE 5.6: During ring closure, speckles of CHD and Rlc1 rotate on the ring clockwise and counterclockwise. The analysis is based on a kymograph representation of the ring after polar transformation. Different arrowheads highlight the motion of speckles on the ring and in the kymographs. Scale bars 2 µm.

apply enough force to close the ring. More specifically, summing up the maximal force of all myosin motors in the ring gives a value of about 10 nN. This value is about two orders of magnitude below the force needed to move the septum of a thickness w = 0.1 µm and an initial radius of $R_0 = 1.6$ µm against the pressure of P = 1 MPa. However, this reasoning implies a closure mechanism, which might not be correct. In particular it neglects, that the ring and membrane are supported by the cell wall. We propose that myosin is mainly applying a tangential force, which is visible as rotation. In this image myosin is pulling the wall building machinery mainly tangentially. Myosin would just lift the wall by the size of one β-glucan unit. If we estimate the size δ of one glucan unit to be few nanometers [111], the force associated to lifting the membrane for one unit is in

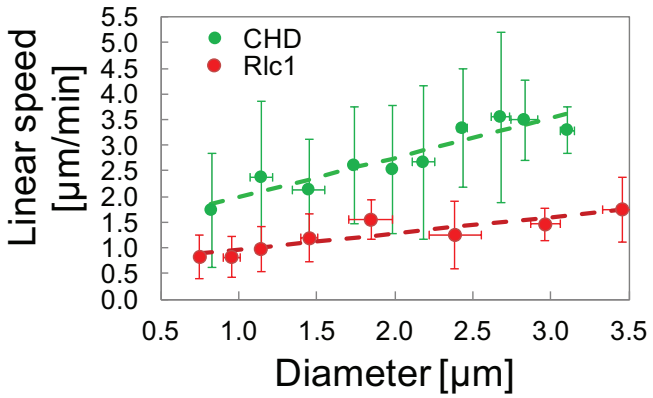

FIGURE 5.7: The analysis of speckle motion reveals a decrease in CHD and Rlc1 speed during closure. Error bars indicate the standard deviation, n = 202 for CHD and n = 77 for Rlc1, where n denotes the number of speckles.

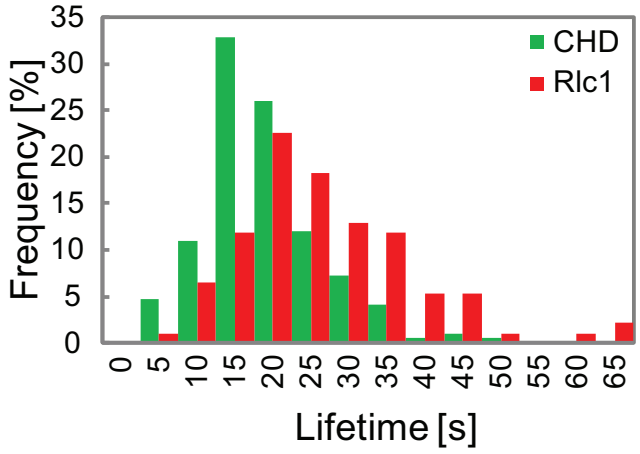

FIGURE 5.8: Histogram for the lifetime of speckles. The mean lifetime is 16.4 s±7.8 s (n = 192) for CHD and 24.1 s±11.6 s (n = 93) for Rlc1, where n denotes the number of speckles.

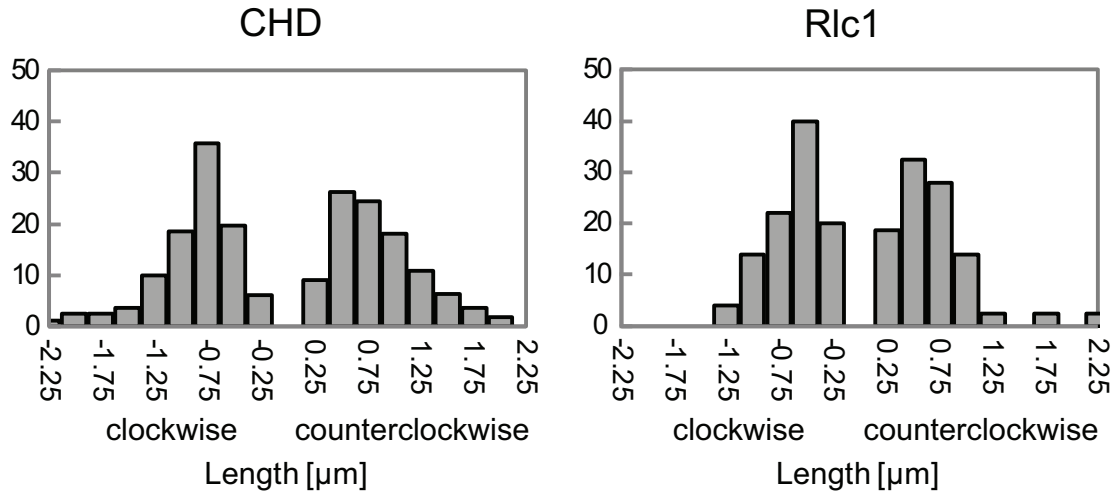

FIGURE 5.9: Distance of speckle movement for speckles rotating clockwise or counterclockwise. The mean distance for all CHD speckles is 0.72 µm ± 0.41 µm (n = 192) and 0.52 µm ± 0.34 µm (n = 93) for Rlc1 speckles, where n denotes the number of speckles.

the order of pN, which is in the order of magnitude of the force of single myosin [40]. In this framework, it is needed to compare energies – and not forces – to estimate if myosin activity could close the ring: The work W to build the wall against the pressure is given by: $W = \int_0^{R_0} F_{pressure} dR = \pi R_0^2 \mathrm{wP} \approx 10^6$ pNµm. To do this work during a typical closure time of 30 min requires a power of nearly 500 pNµm/s. The power of all N_{myo} together is given by $P_{myo} = F_{myo} v N_{myo}$ and amounts to more than 500 pNµm/s for F = 4 pN [40], speckle speed v = 2 µm/min and the number of myosin being $N_{myo} = 4000$ [178]. This calculation demonstrates, that myosin can do the work required for closure within the typical time of closure.

This model implies that Bgs also undergoes rotation. We tested this hypothesis as described in the following section.

5.2.2 Rotating wall machinery

To check the hypothesis, we visualized the wall building machinery by the fluorescence tagging of the two subunits of Bgs: Bgs1 and Bgs4. Indeed we find that both Bgs units rotate. Their speeds are a bit faster than the speed of actin and myosin speckles (Fig. 5.10).

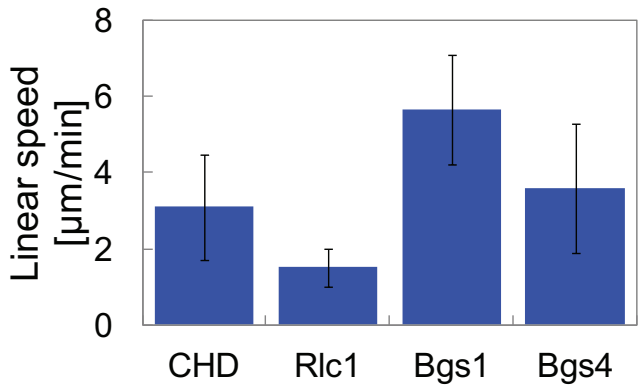

FIGURE 5.10: Comparison of speckle speeds for different proteins. For this measurement, rings with diameters of more than 2 µm were used. Error bars indicate the standard deviation, each mean value contains 15 to 112 measurements, in total 180 measurements.

To probe the relation between the rotation of the Bgs and the actomyosin cytoskeleton, we inhibited both factors separately. We first examined a Cps1: a temperature sensitive mutant defective in the cell wall synthesis [83]. At the restrictive temperature of 36°C the cell wall synthesis was blocked. However, we still observed rotation of Rlc1 with the same speed as in control cells at 36°C (Fig. 5.11). We conclude that myosin rotation is independent of cell closure and glucan synthesis.

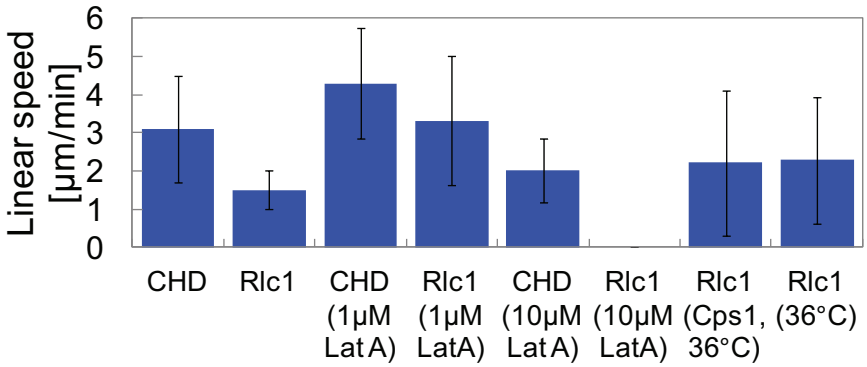

FIGURE 5.11: Comparison of speckle speeds in different conditions For this measurement, rings with diameters of more than 2 µm were used. Error bars indicate the standard deviation, each mean value contains 13 to 112 measurements, in total 324 measurements.

We also tested if the speckle rotations were affected by actin polymerization. We added 1 µM, 2 µM and 10 µM of Latrunculin A to dividing cells. We observed two behaviors: the ring was disrupted and immobile myosin speckles appeared, while actin was still rotating. The ring was not closing in these cases. We observed this systematically for 10 µM of Latrunculin A and occasionally for lower doses of Latrunculin A. Or the the ring seemed

intact and continued closure with a slower speed. Actin and myosin speckles rotated with an increased speed (Fig. 5.11). We speculate, that low doses of Latrunculin A might largely disconnect the ring from the cell wall, which leads to higher rotation speed due to reduced load and to a slowed closure. Large doses of Latrunculin A probably disrupt the ring and reduce speckle motion. Figure 5.12 shows an overlay in time of myosin and actin speckle of a cell incubated with 10 µM of Latrunculin A. Myosin speckles are still, but rotation of actin speckle is still observable. However, the overlay reveals that their location is restricted to the environment of Rlc1 speckles. We speculate that the myosin signal represents the position of the nodes. They are immobile, probably because the ring is disrupted. However, few actin polymerization is still visible in actin rotations. Actin localizes around the nodes, since they nucleate actin due to formins.

FIGURE 5.12: Overlay of 225 frames (dt = 3 s) of CHD and Rlc1 signal of cells incubated with 10 µM of Latrunculin A. Rlc1 speckles are static. Actin speckles are still moving, but their location is restricted to the environment of Rlc1 speckles. Scale bar 1 µm.

Altogether, this demonstrates that myosin rotation does not depend on an intact wall building machinery. The rotations seem to be a built-in property of this active gel. However, if the actomyosin ring is disturbed, the cell division is slowed down or totally inhibited.

We wanted to push our model further and see if the Bgs rotations would fit quantitatively to the closure speed. If one assumes that a number of G glucan synthases rotate with a speed v, the amount of new wall material deposited per unit time will be δ^2Gv. If D(t) is the diameter of the ring and w its width, the change in volume is given by $\dot{V} = \frac{\pi}{2} w D \frac{dD}{dt}$. Since the volume is reduced by the deposition of wall material, we obtain $\frac{\pi}{2} w D \frac{dD}{dt} = -\delta^2 G v$, from which one predicts (details in Appendix Section A.4.2):

$$D(t) = \sqrt{D_0^2 - 4t\frac{\delta^2 G v}{w\pi}} \tag{5.1}$$

where D_0 denotes the initial diameter D(0).

Figure 5.13 represents the fit of the diameter as a function of time with the above derived expression. The fit yields a value for δ^2G of 3700 nm^2 to 5850 nm^2 (for speckle velocities between 3.59 µm/min and 5.65 µm/min (see Fig. 5.10)). Assuming δ^2 to be around 1 nm^2, the ring would contain around 3700 to 5850 glucan sythesis units. A refined model taking into account the change in Bgs intensity and speckle speed can be

found in the appendix (Section A.4.2).

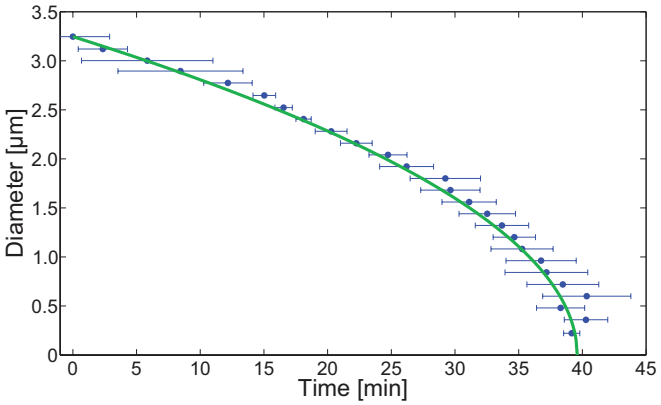

FIGURE 5.13: Measured diameter as a function of time (data from Fig.5.3) and the fit according to equation 5.1. This fit uses v = 5.65 µm/min and δ^2G = 3700 nm^2. (The corresponding fit, taking the mean speed of Bgs4, yields the same result, since the fit is given by the product of δ^2Gv, which is the same in both cases.)

We propose that myosin-driven rotation of Bgs leads to closure. In the previous section, we showed that this is energetically possible. We demonstrate also that Bgs is indeed rotating and that this rotation can quantitatively account for the closure speed. We predict the number of Bgs units to be in the order of 10^3. For a more precise prediction, we would need better knowledge of the glucan density in the wall and take into account other proteins involved in the building of the wall.

5.3 Simulation of the cytokinetic ring

The following simulation was developed by François Nédélec (EMBL) and Ester Lakatos (bachelor student in the Nédélec Lab.). The cytokinetic ring in fission yeast forms from nodes which contain formin [178]. Our model therefore consists of nodes which nucleate actin filaments and myosin (oligomers) which can crosslink filaments and slide them with respect to each other. This system is simulated with the program CytoSim [106]. The proteins are simulated in a circular geometry. The parameters of the simulation were varied and for most parameter sets the ring broke and collapsed. However, stable rings exhibited rotation of actin and myosin in both directions. This is in agreement with our observation that Rlc1 speckles also rotate without the septum closure. Solitary waves propagating in filament bundles were also reported in a theoretical study by Kruse *et al.* [73].

To simulate our hypothesis that the closure is driven by the tangential movement of the wall building machinery, glucan sythase units are added to the nodes. They add a portion of cell wall locally, when being moved for more than a threshold distance. Additionally, crosslinker symbolizing for example α-actinin are simulated in the ring (Fig. 5.14). This simulation is reproducing ring formation (Fig. A.20), as well as ring closure (Fig. 5.15). Ring condensation is faster than in experiments [123]. The closure time matches reasonably well with the measured values (Fig. 5.16). A list of important parameters for the

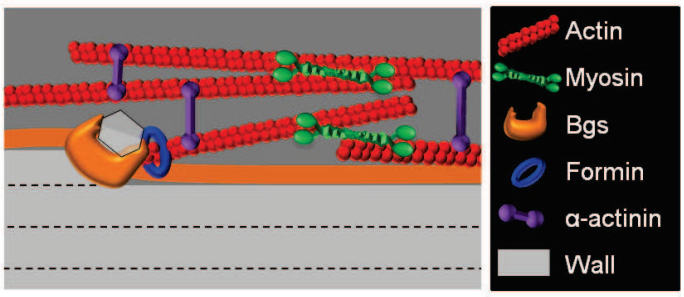

(A)

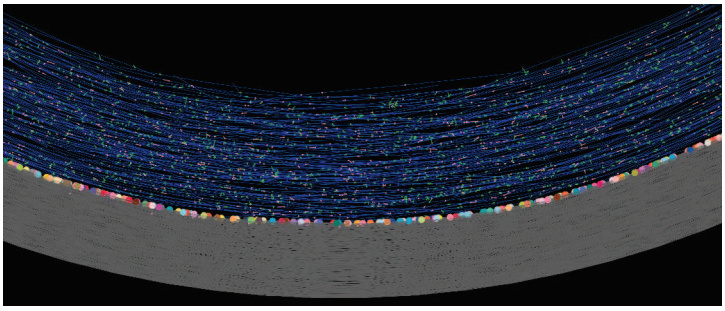

(B)

FIGURE 5.14: (A) Scheme of the simulated model. The ring is composed of actin, myosin and α-actinin. The wall synthesis machinery (Bgs) is connected to actin nucleators (formin). (B) Representation of the CytoSim simulation. Nodes (various colors) are attached to the membrane and build the wall (grey) after being displaced. They are attached to filaments (blue), which interact with crosslinkers (pink) and motors (green).

simulation is given in the Appendix (Tab. A.14)

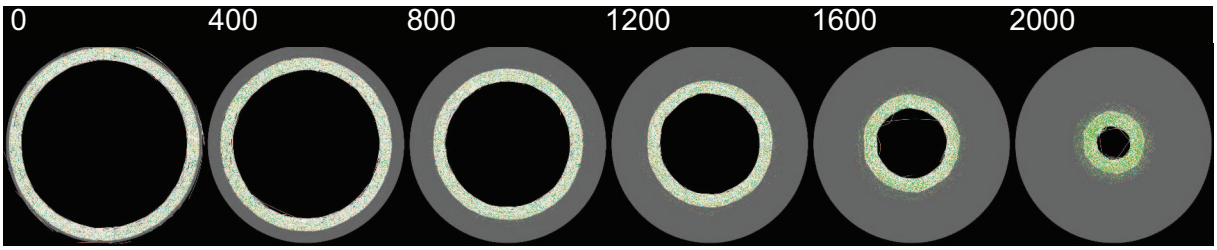

FIGURE 5.15: Simulation of the closure of the ring and septum. Actin and myosin rotation pulls nodes, which build the cell wall. White: actin filaments, green: myosin, pink: α-actinin, various colors: nodes, cell diameter 3.2 µm, time in s.

From the simulated data, we generated fake microscope images with a calculated point spread function (PSF). These images reveal speckle motion in actin, myosin and nodes. We transformed the images into kymographs and measured the speckle speed as described before (Fig. 5.17). We obtain similar speckle speeds in experiments and simulation within a factor of two (Fig. 5.18). Actin and myosin move faster than in the experiments, whereas nodes move slower than the experimentally measured speckle speed of Bgs1 and Bgs4. Actin and myosin speckles have about the same lifetime as in the experiments, but rotate over longer distances (Fig. A.21 and Fig. A.22).

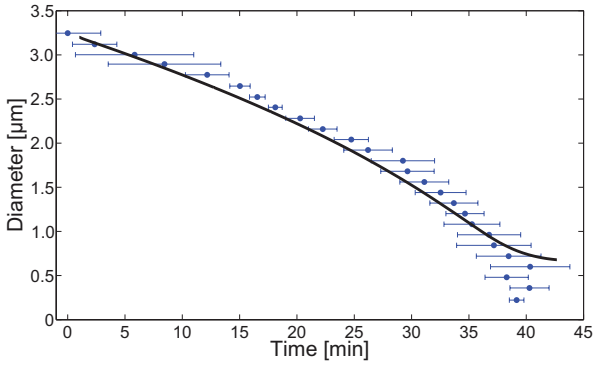

FIGURE 5.16: Comparison of the measured (blue) and simulated (black) diameter as a function of time. Until small diameters the simulation reproduces well the measured closure. Error bars indicate the standard deviation (data from Fig.5.3).

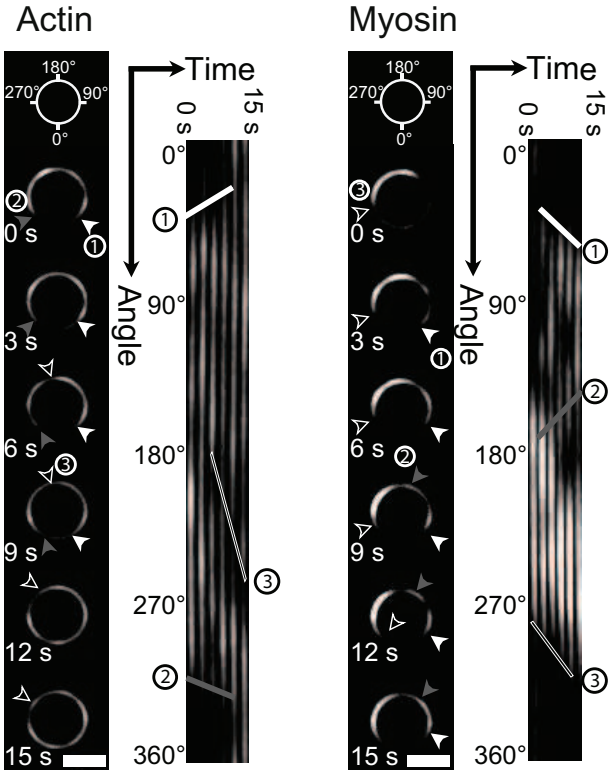

FIGURE 5.17: We generated fake microscope images of simulated objects, to directly compare with the experimental movies. Actin and myosin speckles visibly move on rings. Images are analyzed in the same way as the experimental images. Speckles are highlighted with arrowheads on the resulting kymographs. Scale bars 2 µm.

5.4 Healing of the ring

Daniel Riveline had observed healing of the cytokinetic ring after fraction. We speculate that another function of rotation might be the homogenization of material around the ring. This would stabilize the ring towards breakage due to local depletion of material. We therefore introduced damage in the ring by laser ablation of the ring. This experiment may be challenging, since damage of the cell wall leads to immediate shrinkage of the cell, since the pressure difference is set to zero. We therefore concentrated on rings, which had closed about one third or more, so that the ring would be not too close to the cell wall.

Figure 5.19 shows an example for a laser ablation in the cytokinetic ring in fission yeast. As indicated by the black circle, there is an opening of the ring. This allows us to be sure that the ring got really damaged, and exclude that the reduction of actin intensity is not only due to photobleaching. The ring is probably not opening more dramatically,

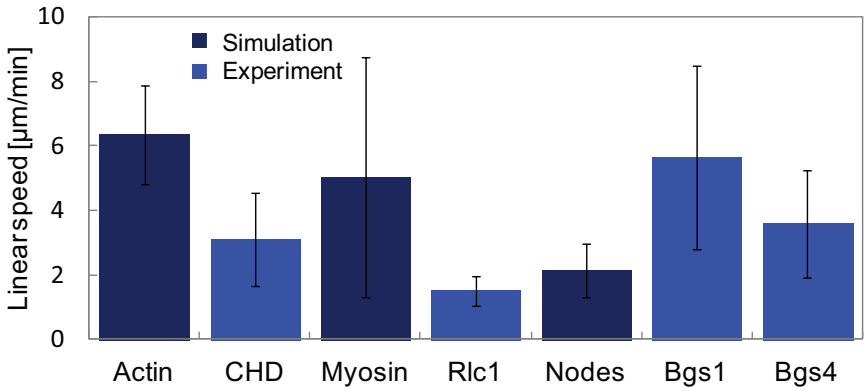

FIGURE 5.18: Comparison of the speckle speed for different proteins in experiments and simulation. The simulated speckles reveal motion of similar speeds as the experimentally found speckles within a factor of about two. We used rings with a diameter larger than 2 µm. Error bars indicate standard deviation, for the simulated data: each mean value contains 242 to 287 measurements, in total 794 measurements, measured data see Figure 5.7.

since the septum is supporting it. Already after about 6 s the ring is repaired, which suggests that this is due to speckle rotation. Also this shows that the ring is robust to local depletion of proteins. An interesting experiment would be the destruction of the ring with Latrunculin A and observation of actin and myosin dynamics after wash out.

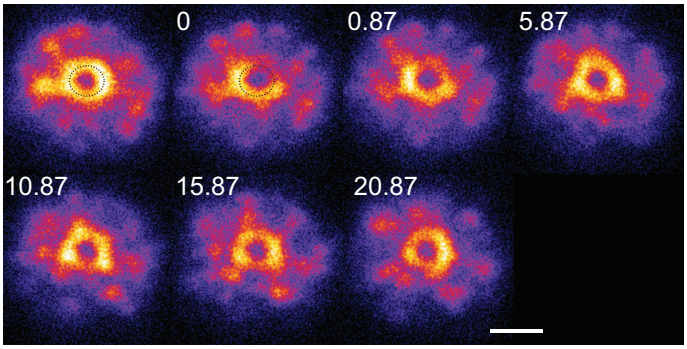

FIGURE 5.19: The cytokinetic ring, visualized for CHD, was laser ablated. The black circles on the first and second frame have the same size. They indicate that the ring is opening upon ablation. The introduced defect is repaired within few seconds at 27°C. Time in s, scale bar 2 µm.

6 Discussion

We wanted to gain a better understanding of mechanisms of organization of active gels in biological relevant context. The cytokinetic ring is a particularly interesting object of study. Not only it is an ubiquitous, well conserved process to divide cells. It is a relatively simple active gel *in vivo*.

In usual observation techniques, the ring is seen from the side. To access concentration distributions and dynamics, we visualized the entire cytokinetic ring in a sinlge plane of focus. We oriented cells in microcavities to impose an orientation of cell division in the plane of observation. The corresponding setup for fission yeast was developed by Daniel Riveline [130, 129]. Fission yeast shape variations are essentially restricted to elongation, due to the cell wall of fission yeast [128]. "*Egg cups*" seem the ideal setup to orient these cells. In contrast mammalian cells can take a multitude of cell shapes due to their active cortex and their polarization is not predefined. We pursued the development of three setups, taking advantage of the adaptability of cells.

We imposed cell orientation by different geometries of attachment sides. Cells in confinement were not dividing in our hands or escaped the imposed geometry. In the *vertical setup*, cells adapted to adhesive lines. They were additionally oriented by physically turning the substrate. The combination of both methods left only one axis of division left. The same principle worked for the *microcavity* setup. Though we choose a cavity size which did not impose a geometry *per se*, during the characteristic shape transformation during division, the cell had only one dimension to elongate.

We validated both setup and found the same dynamics in the newly developed setups and for cells on glass coverslips. Additionally we optimized the method by synchronizing cells. Attempts to measure closure speed and time as a function of the cell size (*scalability*) failed, since giant cells showed more than one axis of furrow ingression.

We also see actomyosin rings forming at the bottom surface of microcavity wells. We suggest that elastic microcavities might be an interesting setup to study contractility in actomyosin rings. We propose a technical realization of the setup, but we have only preliminary results about its implementation.

Before comparing the measurements and models for mammalian cells and fission yeast, I want to resume and discuss the results for each part. I will also discuss future lines of thought and experiments for each cell type. Finally, I will discuss similarities and the intriguing differences in both systems and models.

6.1 The cytokinetic ring in mammalian cells

We observed the cytokinetic ring in a single plane of focus and visualized different proteins known to be crucial in cytokinesis. We revealed a striking feature in the organization of the ring: we observed regular clusters in myosin and formin along the ring perimeter. In many cases we saw fusion and less often separation events. The ring exhibits also collective rotation of neighboring clusters. But what can we learn from these observations and measurements? How far is this organization connected to cytokinesis and the properties of the cytokinetic ring?

Proteins distributions in the cytokinetic rings Let us first take a look at the ingredients, i.e. at the distributions of the involved proteins. We find that though formin clusters colocalized with myosin clusters, we do not see a similar pattern in actin. The corresponding density distribution is rather flat. Though we see occasionally high density spots. This is astonishing, since formin is an actin nucleator. Probably formin bound actin shows a similar pattern as myosin. But it is more difficult to resolve, since actin is a filament. Even if the (+)-ends are regularly organized, the corresponding maxima in the intensity profile would be very broad in actin and probably merge with neighboring maxima. This idea is in agreement with estimates about the length of actin filaments, which might have a length of up to 1 µm [144]. Consequently, the filaments can probably span the interdistance of neighboring nodes. This would render the resolution of actin inhomogeneities difficult, because its distributions would exhibit broad maxima and a small contrast between minima and maxima. Better optical resolution techniques could provide some clarity on this question. Additionally we could try to obtain a better contrast by labeling actin with phalloidin in fixed cells. This would exclusively stain actin filaments. Excess of free fluorophores – be it free LifeAct, actin-GFP monomers or phalloidin – could be washed out. However, the pattern in myosin is clearly visible and formin colocalized with myosin, we therefore focused our analysis on the myosin pattern.

We wondered if these nodes could correspond to the contractile units as they were proposed by Carvalho *et al.* [20]. In their model, contractile units include septin and anillin, which might serve as membrane anchoring complexes. Our staining for both proteins revealed an inhomogeneous distribution of both proteins. However, we only saw partial colocalization between myosin clusters and septin and anillin high density regions. It is still interesting that anillin and septin exhibit a "patchy" distribution. Potentially they form functional units. It would be interesting to stain for septin and anillin simultaneously. A colocalization would reinforce the idea that they build mesoscopic complexes. Carvalho *et al.* made their observations in *C.elegans* embryos at early stages in development. It is not clear if their findings about intensity changes during closure and turnover rates hold true for mammalian cells. Our setup is suited to investigate these questions for other cell types. If we could follow septin and anillin in live cell experiments, we could potentially also reveal dynamics in their density distributions. In a simple model, contractile units would undergo rotation only, if neighboring units contract faster on one side than on the other. However, if these variations are moderate, their trajectories would rather show a radial movement. Since myosin and formin nodes move rather radially, I

would not expect a very different behavior for anillin and septin.

Myosin and formin colocalize in regular nodes. We suggest that they build functional units. For actin we cannot claim with great certainty the same distribution, although we see occasionally high density spot. This limitation in observation might be due to the filamentous nature of these proteins. Anillin and septin localize in the ring and exhibit also a "patchy" structure, but they show only partial colocalization with myosin motifs.

Characterization and probing of the pattern We characterized the pattern during closure and found that its organization is essentially preserved. Our main read-outs are the intensity ratio between minima and maxima (pattern coefficient), the node size and the node density. This gives a full characterization of the pattern. The analysis was carried out manually. This seemed to us to be the most precise way of characterizing the pattern. Ideally the characterization would be fully automatized. In an extremely regular pattern, auto-correlation and Fourier transformation would give the node sizes and interdistances as well as their frequencies. However, these means of analysis were not always suitable to characterize the pattern: due to large scale intensity inhomogeneities and natural irregularities in size and intensities, these methods did not deliver a clear read-out. However, though a manual analysis is potentially connected to errors, it allowed us to characterize fully the pattern with the described read-outs. Interestingly we find that the intensity ratio between minima and maxima and the size of the nodes does nearly not change during closure. The node density is increasing, but much less than what would be expected if the number of nodes would stay constant. This is remarkable, because it suggests that the pattern structure is somehow controlled during closure.

We evaluated the myosin turnover for myosin and found a recovery half-time of tens of seconds after photobleaching the entire ring. This lays in the same order of magnitude than the turnover of actin, but is slower than the turnover of other cortex proteins [138]. It also corresponds to measurements of Carvalho *et al.* on the cytokinetic ring. Bleaching part of the ring or alternativly the entire ring except a small part, did not reveal flows of myosin along the ring. We did these experiments on a setup with which we cannot resolve the myosin pattern. Ideally we would bleach single myosin clusters and estimate the recovery for these units. In a system with a very high turnover, I would expect myosin to distribute according to the distribution of binding partners, in particular of actin. With a higher turnover, myosin dynamics and density distribution are set by the interactions with other molecular partners. For example, we can explain the colocalization of formin and myosin in two ways: we can imagine that formin and myosin build a protein complex. We could also explain their colocalization, by assuming that myosin (or myosin minifilaments) are accumulating on the filament (+)-end, because they are (+)-end-directed motors. The latter explanation is only valid, if the turnover time is higher than the time of myosin filaments to move to the (+)-end.

Bleaching experiments are also an interesting tool to measure cortical flows. Alternatively, We could use a photoactivatable dye, and measure the speed of an exited region in the ring or the cortex.

We probed what would happen to the pattern if we would alter the activity of actin and myosin. Treatment with myosin inhibitor Blebbistatin and Latrunculin A, which is sequestering monomeric actin, rendered the pattern less regular. We can still see accumulations, but their sizes are increased and more broadly distributed. We saw the same for the interdistances between nodes. Probably the activity of myosin and actin is involved in the regulation of the pattern. Interestingly the drugs have two different effects on cell closure. Blebbistatin is stalling closure. Though the diameter does not change anymore, the pattern is becoming less regular. For Latrunculin A we see the opposite: the closure speed is transiently increased. However, we see that the effect of the drug to the pattern is the same. It would be interesting to follow the dynamics of the pattern upon addition of the respective drugs. We acquired the dynamics of cell closure with a setup which does not allow us to resolve the myosin motifs. We were still able to see that the ring seems to disassemble minutes after the addition of Blebbistatin, pointing in the direction that myosin serves also as crosslinker. The addition of Latrunculin A and Cytochalasin D lead to visible clusters of actin and myosin. It would be interesting to follow the transition of the pattern. Does the pattern in the case of Blebbistatin reach a new steady state? And on which timescale? What happens after inhibiting actin polymerization? Is the opening due to breaking of the ring? Can we relate a faster closure speed to a change in the pattern? We also see that different concentrations of Blebbistatin lead to different closure speeds, potentially due to changed stress generation. Characterizing the pattern as a function of the Blebbistatin concentration might therefore allow testing hypothesis about the relation of myosin activity, pattern characteristic and stress generation. The connection between the density distributions and the stress generation will be further discussed below, in the context of the model.

Stress generation related to pattern To relate the pattern with stress generation is also motivated by our observations of forming rings. We acquired cells before, during and after ring formation. Before closure, we see that myosin is distributed unevenly in the cortex. The pattern forms quite suddenly and simultaneously in all parts of the perimeter. The ring only closes as the pattern appears, indicating, that the pattern is associated to a higher stress generation. Simultaneously we see an increase in myosin intensity, which might initiate the pattern formation. It probably also contributes to a higher stress generation. We cannot completely disentangle both contributions. However, since the increase in myosin concentration is moderate, we believe that the pattern formation initiates the closure.

We tested if the ring would still close if it is disrupted by laser ablation experiments. Indeed the bundle (cut ring) is still constricting, which leads to a closing of the furrow. Strikingly, this closure is even faster than the closure in intact cells in the first seconds after ablation. Probably the breakage of the cortex is facilitating closure. For the time that we can follow the ring constriction, we observe that the motifs are maintained and that they move rather radially. We see neither that myosin is accumulating at the side opposite to the cut, which would be expected for a bundle, nor do we observe that motifs undergo strong tangential movement, as one might expect if the local contractility is

unbalanced. However, since we can follow the ring only for some tens of seconds, we might also miss these events, if they take place on longer time scales.

We speculate that rotation of the ring and the fact that the center of the ring moves during closure might be due to asymmetric stress distribution in the cortex or on the ring. It should be possible not to cut, but only to weaken the ring or the cortex with a well-chosen laser power. Such an experiment would need a very stable laser ablation setup to come to quantitative statements. However, one should be able to deduce qualitative statements from these experiments. We could probe if we could accelerate closure by weakening the cortex or induce rotation by locally damaging myosin clusters. Alternatively, we could locally apply a drug, like it was performed by Sedzinski *et al.* [145].

We developed a model to describe the stress generation in the cytokinetic ring. The model reduces the process of cell division to one dimension and describes the ring as a bundle of actin filaments, nucleators and myosin motors. We assume that this is a reasonable description of the contractile ring for the following reasons. Electron microscopy pictures and optical methods reveal that actin filaments are oriented parallel and circumferentially [143, 140, 94, 42]. Reymann *et al.* [126] and Mishra *et al.* [99] showed in their *in vitro* experiments, that the minimal set of ingredients for constricting actomyosin rings are actin, myosin, crosslinkers and nucleators (see Section 2.5.3). These rings were closing with a similar speed than the cytokinetic ring. In our model, crosslinkers are implicitly implemented in the viscosity. We do not need crosslinkers to maintain the integrity of the ring, since we reduce the ring to one dimension. We chose myosin and formin to form a complex. In fission yeast the ring is formed from nodes, including on average two formins and several myosins [178]. We also see experimentally that myosin and formin colocalize. They do not need to build a complex necessarily, but myosin might also accumulate at the filaments' (+)-ends. Additionally, Luo *et al.* [88] reported nodes of formin and myosin near the plasma membrane in spread cells. We want to check if DAAM1 is also in the cytokinetic ring in future experiments.

The model predicts a dynamic instability above a critical motor activity. A periodic pattern of high and low concentrations of motors, nucleators and filaments forms. This result is in qualitative agreement with our findings: as myosin concentration increases myosin and formin form a regular pattern of accumulations. The model reveals that the pattern is associated with an overlinear increase in stress generation with increasing motor activity. As discussed before, we have experimental indications connecting the pattern with stress generation. The model demonstrates that one can explain with simple ingredients the observed pattern formation and the increased stress generation associated with the order of filaments and motors. This result shows that it is sufficient to only consider myosin activity when discussing stress generation, but also the mesoscopic order of the system. I want to point out, that the increase in stress generation is not due to a sarcomeric order of the system as it is in muscle or in the *in vitro* ring of Reymann *et al.* [126]. In these systems, constriction is efficient because the amount of antiparallel filaments is increased. In our system this is also the case, but this does not lead to a stress generation, since we do not explicitly consider free myosins. Myosin is always in the center of bipolar filaments, and does therefore not mediate the interaction of antiparallel filaments. The stress contribution of filaments is largest if they are pulled on their ends,

and not in the middle. The higher stress generation might stem from the fact that filaments in an ordered system motors pull rather at the outer part of the filament than in the center.

In future versions of the model, we want to compare the pattern characteristics quantitatively to our measurements. Additionally we will implement a dynamic system size, which will allow us to simulate the closure. We also want to probe, if we can explain the effect of cytoskeletal drugs on the ring with our theoretical approach.

We saw experimentally that the inhibition of myosin dynamics and actin polymerization is decreasing the regularity of the pattern. The node density was decreasing and the node size increasing. Can the model give an explanation for these observations? Increasing myosin activity is indeed generating more and more pronounced patterns. However, a nearly absolute inhibition of myosin activity should drive the system back to a homogenous state. We fixed cells after 15 min of incubation with 100 µM Blebbistatin and evaluated the pattern. We still saw myosin clusters. However, we cannot say, if the pattern has reached a steady state. Possibly we would find no motifs anymore at later time-points. It is also possible, that Blebbistatin is not totally inhibiting myosin crosslinking. Indeed, most myosin is kept in state with weak actin affinity [70]. However, some myosin can be trapped in a actin binding state [158]. Additionally, we see that the ring is stalled and not opening like in the case of inhibition of myosin light chain kinase with ML-7. Inhibition of the MLCK is also inhibiting myosin mini-filament assembly. However, in the case of blebbistatin inhibition, mini-filaments should be maintained [183]. We speculate that overall absence of cortical contractility together with little crosslinking could lead to the stalling of the ring. Little crosslinking could also explain, why we still see a myosin pattern though myosin activity is inhibited.

We measured also that we can tune the speed of closure with low Blebbistatin concentration. We could further confirm the relation between closure speed and the myosin pattern, by characterizing it as a function of the closure speed. I expect to see a gradual decay of the pattern regularity after incubation with increasing Blebbistatin concentrations.

Latrunculin A is inhibiting actin polymerization, which leads to filament shorting. In the model, the period of the pattern is related to the filament length distribution and shorter filaments should lead to a reduction of the period of the pattern. This is not what we observe. Additionally the shorter filaments should rather reduce the stress in the system. But we measure an increased closure speed after the addition of the drug. The model might not accurately capture the effect of Latrunculin A. To check this, we should on the one hand capture the dynamic of the pattern after the addition of Latrunculin A. Addionally, we should check the dependence on the concentration of the drug. In the case of fission yeast, we saw two behaviors depending on the concentration. And on the other hand simulate a sudden reduction of the polymerization speed after the pattern has formed. To explain the increase in closure speed we should also keep in mind, that cytoskeletal drugs affect also the cortex. Latrunculin A is probably also reducing the contractility of the cortex, which might facilitate closure.

Conclusion We see a pattern of myosin and formin in the cytokinetic ring. The appearance of the pattern coincides with the onset of the ring closure. This indicates that the pattern is associated with stress generation. The pattern characteristics are essentially maintained during closure, which alludes to an active regulation of the pattern. Cytoskeletal drugs render the pattern less regular, suggesting that the pattern characteristics are regulated by actin and myosin activities. These interpretations find confirmation in the model, which relates the pattern characteristic to actin and myosin parameters. The model also demonstrates that the ordering of the actin bundle leads to an increase in stress generation which exceed strongly the stress generation in a homogeneous ring, with the same myosin activity. We show that a proper description of the ring needs to take into account not only the changes in myosin activity but also the order of actin filaments and motors.

6.2 The cytokinetic ring in fission yeasts

We oriented fission yeast cells in microcavities, which allowed us to see the entire cytokinetic ring in a single plane of focus. This perspective revealed different features such as myosin arms and rotations of inhomogeneities (speckles). We were also able to measure precisely the intensity of actin and myosin for rings of different diameters. We find that the total amount of myosin stays first roughly constant and is then decreasing, whereas the amount of actin is decreasing, as measured by the signal of CHD, a domain of an actin binding protein. Because of the ring closure, this results in an increase of myosin concentration and actin concentration stays nearly constant. Both do not behave the same way, since the decease in the total amount of actin is stronger than for myosin. These finding are in agreement with previously reported measurements [178]. Interestingly both proteins do not behave the same way. Possibly because myosin is not only bound to actin, but also to nodes, a protein complex that forms during formation of the ring [123]. There is also no apparent relation between the closure speed and the respective concentrations. We speculate that the loss of myosin proteins is associated to the appearance of myosin arms, since the appearance of arms coincides with the decrease of total myosin activity. Constant decrease in the amount of actin might be related to actin patches, which appear throughout closure near the membrane.

The most striking feature are rotating speckles of actin, myosin and β-glucan synthase (Bgs). They move with a velocity in the range of µm/min. Bgs1 and Bgs4 moves the fastest and myosin the slowest. Actin and myosin speckles rotate on average a bit less than 1/4 of the ring perimeter. We assume the speed of single proteins to be of the same order as the speckle motion. If so, it is worth noting that the speed of speckle motion is slower than the characteristic speed of motors and filaments as measured in motility assays. One source for slowing the motion could be crosslinking. Indeed, Reymann *et al.* [125] reported rotating accumulations of myosin in *in vitro* crosslinked actomyosin rings (see also Section 2.5.3). I estimate these speckles to rotate with speed of about 0.1 µm/min, and therefore about one order of magnitude below our speckles and also below the speed of filaments in sliding filament assays. A more detailed discussion of the *in vitro* rings

and our *in vivo* rings will be carried out in the next section. The speckle motion could be also impeded, if the cytoskeleton would be connected to other proteins. We propose that Bgs1 and Bgs4 rotations are indeed driven by actomyosin.

We suggest that the rotations of Bgs1 and Bgs4 are related to the closure mechanism in fission yeast. Our model suggests that Bgs1 and Bgs4 and possibly other proteins involved in the building of the wall move mainly tangentially along the ring. As they move, they add glucan units to the cell wall and build thereby little by little the septum. Since the closure mechanism has to work against a high turgor pressure, the ring could probably not close by constricting the cell membrane as it is probably the case in mammalian cells. Even if myosin would work with a maximal efficiency, they would be too weak to move the membrane and septum inward against the turgor pressure [124]. Instead, we propose that the ring and membrane are supported by the septum at each time-point. Myosin activity drives the closure, but by energizing the insertion of small portions of cell wall. We do not know, how Bgs works at a molecular level, but we can show by simple calculations that the maximal force of a single myosin motor is sufficient to allow the lifting of the membrane against the turgor pressure by one glucan unit. Few myosin could possibly displace Bgs sufficiently to insert one or few glucan units. This implies, that such a mechanism does not need a mesoscopic order to close the cytokinetic ring, *i.e.* myosin does not need to work in concert on large scales. It should also be pointed out that the rotation of speckles seems to be a property of the ring and thus due to the collective effect of actomyosin interactions. However, even uncoordinated, tangential movement would lead to closure. We see this movement by rotating speckles. This can be compared to the helicopter view of a marathon. Although each runner runs basically independent of other participants, it appears as local high density spots. Dependent on the spread of the distribution of the speed of individual runners, these high density spots are more or less persistent. However, if single myosins are moving with respect to their attachment sites, myosin does not work at stall force. Taking this into account, it is problematic to argue with the maximal force, which means that there must be some cooperation to pull Bgs units. Alternatively their movement could be due to the movement of their attachment sites, actin filaments and nodes.

We supported the model by deriving an expression for the closure speed as a function of the Bgs speckle speed. The analytic expression explains the shape of the diameter as a function of time. Basically the closure becomes faster and faster, because less and less material has to be added to obtain a reduction of the diameter ΔD. Our only fitting parameter δ^2G yields a prediction for the number of Bgs1 proteins in the ring of about 1000 to 5000. This is in the same order of magnitude as the absolute number of myosin proteins in the ring [178]. It is important to point out, that there are also other proteins involved in the septum formation, in particular the α-glucan syntheses Ags1 [29]. A complete description would therefore require the measurements of all proteins. In our description the diameter as a function of time depends also on the speed of the Bgs speckle. Slower speckle would lead to slower closure. We could test this hypothesis quantitatively by measuring the speckle speed of Bgs for different temperatures. Yeasts can grow at different temperatures. Their closure speed is slowed down for smaller temperature. Assuming that the number of Bgs units in the ring is independent of the temperature, our

fitting parameter δ^2G should be also temperature independent. Daniel Riveline showed that myosin speckle motion is slowed down with decreasing temperature (unpublished data). We therefore expect also a slower rotation of Bgs.

We tested our hypothesis further by probing the relation between actomyosin rotation and Bgs rotation. On the one hand, we inhibited septum formation by using a temperature sensitive mutant, defective in the cell wall synthesis [83]. Although the septum is not growing, we observe rotation of myosin speckle. These speckles move with the same speed as in cells without this mutation. This shows that speckle motion is independent of wall synthesis. The rotation of speckles in this active gel seems to be a built-in property. On the other hand we see, that with inhibit with Latrunculin A, myosin rotations are stopped. At the same time, the cell wall is not built anymore, suggesting that myosin rotation is needed for wall growth. To check that rotation of actin and myosin speckles are related to Bgs rotation on the one hand and that Bgs rotation are involved wall growth on the other hand, we should measure the speckle speed of Bgs in the presence of high doses of Latrunculin A. I suspect that we would see no Bgs rotation. Possibly Bgs would colocalize with the pronounced myosin accumulations.

Finally we implemented the proposed closure mechanism in CytoSim [106]. We simulated the interplay of actin filaments and myosin in a circular geometry. We see speckle rotation for both proteins. To reproduce our proposed closure mechanism, we added crosslinker and wall building units (nodes) to the network. Actin filaments are attached to these nodes. Indeed these nodes are pulled by the actomyosin network and they also reveal speckle motions. The simulation reproduces the experimentally measured closure speed, except for small diameter, where the closure is nearly stalled. In the simulation, actin filaments span the interior part of small rings, when their length is larger than the diameter. This leads to less rotation of nodes and slower closure. This might be simply an artifact from the simulation, since we did not observe this in cells. However, I speculate that since in cells microtubules occupy the inner part of the septum for small diameters, this might prevent that filaments cross the ring.

We can calculate fake microscope images from the simulations. We see clear speckle motions in these images. This representation of the simulation allowed us to analyze the simulated protein dynamics in the same way as for experimental data. We measured the speckle motion to be in the same order of magnitude as in cells. Based on our proposed closure mechanism, we implemented a simple system with only four kinds of proteins. With this approach, we can reconstitute *in silico* the closure dynamics and the speckle motion.

We suspect that another function of rotation could be homogenization of material along the ring. Indeed, when we laser ablate the ring, it is repaired within seconds. However, we cannot proove that this would not happen without actomyosin rotations. Ablation might also break filaments and lead to more polymerization sites. Another way of probing the healing capacities of the ring would be to destroy the ring with Latrunculin A and observe if the ring would reform after the washout of the drug. A signature for a healing due to speckle motion, in contrast to local nucleation and polymerization, would be if we could

observe that the depleted regions are essentially filled by the tangential movement of actin and myosin.

Mishra *et al.* [99] showed in system derived from spheroplast that the (see also Section 2.5.3) cytokinetic ring is also closing when detached from the cell wall and membrane. The closure is about two orders of magnitude faster than in fission yeast cells. That shows that the ring is contractile and does not only guide the wall building machinery. Unfortunately Mishra *et al.* did not document the concentration distribution along the perimeter and from the published movies we can neither conclude for nor against speckle motion in this system. It would be interesting to compare our *in silico* ring to their measurements. In simulations without the implementation of the wall building machinery, we have seen that the ring is contractile and exhibits protein rotations.

We saw that our new setup for observing fission yeast cell division in a sinlge plane of focus revealed an unreported dynamic of actin and myosin: we see rotating speckles. These rotation are independent of the closure and seem to be an inherent property of this active gel. We suggest that the rotation drives the rotation of the Bgs and that this tangential movement allows wall building machinery to build the cell wall against the turgor pressure. From this model we derived an analytic expression which fits the diameter as a function of time. Additionally, we simulated the ring with four basic ingredients: filaments, motors, crosslinkers and wall building units. With this reduced system we can show speckle motion and reproduce closure speed until small diameters.

6.3 Comparison of both systems

I presented our experimental and theoretical results on the cytokinetic ring in mammalian cells and in fission yeasts. Although these are two circular actomyosin gels, they exhibit different dynamics and patterns. How can we explain these differences? How does this relate to other studies on this field? Could we possibly reproduce the observations in one system in the other system?

Both rings show inhomogeneities in the distribution of ring components, in particular of myosin. The cytokinetic ring in mammalian cells exhibited a regular pattern of myosin clusters, whereas actin and myosin accumulations were rotating in fission yeast in both directions. The cytokinetic ring in mammalian cells has an initial diameter of about 20 µm and closes in about 5 min, fission yeast cells need about 30 min to close the ring of about 3 µm in diameter.

The different closure speeds are not only due to the differences in the actomyosin ring but also to the physical constraints. Mammalian cells do not have a rigid cell wall, but a viscoelastic cortex. Although the cortical contractility is increased prior to cell division, the pressure difference between the cell's inside and outside is few hundred Pa [151], this difference is not as high as in fission yeast, where the pressure difference is rather in the order of MPa [97]. Additionally the cell wall is not measurably deformed during closure but grows simultaneously with ring closure.

We therefore propose that the cytokinetic ring in mammalian cells is generating stress and this leads to contractility, which is sufficient to drive the closure. In particular we suggest that upon increased myosin activity the ring exhibits an instability, which leads to the organization of actin, myosin and nucleators in periodic clusters. Our theoretical analysis shows that such an order leads to an overlinear increase in stress with respect to the motor activity. This implies that prior to furrow ingression the cortex is not far from this threshold of pattern appearance. Possibly due to the overall increased contractility [151]. The order makes the division not only more efficient but renders the system also more sensitive to changes in myosin activity: relatively little changes in activity have an relatively strong impact on the stress generation.

In fission yeast the requirements to the ring seem to be different. The ring is too weak to close the ring with a mechanism as described for mammalian cells [124]. However, few myosins are strong enough to drive the insertion of glucan molecules. We propose that actin and myosin energize the closure by moving tangentially the wall building machinery. In this model the ring and the membrane are at any time supported by the septum. We estimate that in this model myosin alone can do the required work to close the ring against the turgor pressure with the typical time of closure.

We can associate a function to the organization of the ring in both cases. Since both systems have different requirements for closure, it seems to "to make sense" that the gel organizes in different ways. But can we also explain *why* we see different patterns?

In mammalian cells we see a nearly symmetric, regular pattern. In yeast cells, the speckle move in an apparently uncorrelated manner, except, that they move equally far clockwise and counterclockwise. This suggests that the fission yeast ring is prone to spontaneous symmetry breaking. The ring in fission yeast is a somehow small system: it forms of on average about 65 nodes, which consist of on average about 2 formins and 25 myosin and other proteins of similar quantities [178, 81] and probably not much more than 2000 filaments in total [62]. That means that in a cross-section there are only about 100 filaments – in mammalian cells the number of filaments per cross-section amounts rather to 5000 [144]. This suggests that the fission yeast ring is more sensitive to fluctuations. Unbalanced drag on a filament left and right leads to rotation. The same for motors: if the resistance of filaments that they crosslink, is unbalanced they will move.

We use two kinds of theoretical approaches: We describe the cytokinetic ring in mammalian cells with a mean field description and the ring in fission yeasts by an agent-based simulation. A mean field description can describe the behavior of large systems. Large systems allow averaging the ingredients, similar to a drop of water, which is better described by viscosity than by the properties of single water molecules. The simplification of the system permits to derive analytic expressions: we can give expressions for the stress generation and define for which parameter sets the system becomes unstable. In the simulation, individual proteins are simulated. To describe the system generally, the parameter space has to be probed. On the other hand a simulation can incorporate variability of processes, which might lead to fluctuations; bipolar filaments might have different lengths on both sides for example.

But the different dynamics might not only be due to the number of proteins, but also

to their respective concentrations. Reymann *et al.* [125] presented contractile actomyosin rings *in vitro* (see also Section 2.5.3). When they imposed a dotted or homogeneous pattern, the pattern was conserved in contracting rings, that is to say, that a homogeneous/dotted patterned maintained homogeneous/dotted, respectively. This looks very similar to our pattern in mammalian cells. However, we propose that the pattern forms by auto-organization from a homogeneous distribution. In the case of the *in vitro* ring, the pattern was imposed. In the study of Reymann *et al.* , rings crosslinked with α-actinin were weakly contractile. But myosin accumulated in clusters which were rotating. These myosin clusters were disassembling actin. They did not observe clusters in actin. We should carefully check if we find evidence that myosin would disassemble actin in fission yeast cells. This might contribute to the measured decrease in the amount of actin.

6.4 Conclusion

We present a new setup which allows us orienting fission yeasts and mammalian cells. This gives us a new perspective on the cytokinetic ring, which permits us to describe the ring, to reveal variation of concentrations along the perimeter and to perform methods, which would otherwise be difficult to use, such as FRAP and laser ablation. We can also reveal structures in the vicinity of the ring such as the cortex in mammalian cells and arms and patches withing the septum plane in fission yeast. This study is therefore an illustration, that the perspective on the cellular system matters. This might be relevant also for *C. elegans* embryos and budding yeasts, which also fit our setup [176].

We have two circular active gels and two behaviors. In fission yeast rings we find rotating actin and myosin speckles, in mammalian cells we see that the system goes from an homogeneous state to an ordered state of regular clusters. This order is preserved during closure. We suggest a function to both organizations: actin and myosin rotations guide the wall building machinery and allow closure against the turgor pressure. In mammalian cells the order leads to a superlinear increase in stress generation, which drives closure. We are not sure why the two systems exhibit different dynamics. It might be simply due to the low number of proteins involved in the system, which might renders it more sensitive to fluctuations. It might be also related to the parameters of the gel. Other studies show that rotations appear in strongly crosslinked systems [125]. We modeled both rings with two different approaches: a mean field description and an agent-based simulation. Both approaches were able to reproduce the respective features. In this case the difference in dynamics seems to be related to the kind of approach. Simulations can account for fluctuations, whereas a mean field approach is suited for large systems, since it averages over interactions between individual components.

We presented two models to explain the closure of the cytokinetic ring in mammalian cells and in fission yeasts. As discussed, some open questions are left and we proposed experiments to shed light on unclear aspects. Studies on other biological systems like *C. elegans* and budding yeast could complement our understanding of cytokinesis and reveal

other unexpected dynamics. Additionally *in vitro* experiments can help to answer questions, that we cannot answer in living cells, due to the crosstalk of different cell structures. In particular, such experiments might explain the transition between rotating and still speckles. Finally our models are restricted to few different proteins and flat geometries. In particular, we neglect the cortex in mammalian cells, which should be considered in a more complete model.

We see in both studies that the closure may not only be explained by extraction of actomyosin concentrations, simple addition of forces associated with single molecules as well as the reduction of the gel activity to a mesoscopic parameter. Only the observed dynamics and structure gave evidence for the models that we proposed and tested. We suggest that also in other systems, like actin rings in wound healing or dorsal closure in drosophila, but also in cell migration or the cell cortex the mesoscopic order might play a role in the understanding of stress generation and evolution of the system.

The transition from an homogeneous to a dotted pattern is controlled by myosin activity. Above a critical activity the stress generation is increasing superlinearly with myosin activity. Apart from the fact that stress generation becomes more efficient in this regime, the system is also more sensitive to changes in myosin activity. Another system where striated and homogeneous distributions occur are stress fibers. Potentially the pattern is also linked to myosin activity. On the other hand, we see that rings can also exhibit rotations of speckles. We propose that depending on the parameters of the gel, such as crosslinkers, the system can show one or the other behavior. In conclusion, we propose that depending on the ratio, and not only the types of proteins, the active gel can exhibit qualitatively different behaviors, which could be the basis for regulatory mechanisms of cytoskeleton structures. This demonstrates again the importance of understanding collective effects in active gel networks.

Bibliography

[1] Abercrombie, M., Heaysman, J. E., and Pegrum, S. M. Locomotion of fibroblasts in culture: I. Movements of the leading edge. *Experimental Cell Research 59*, 3 (1970), 393–8.

[2] Abercrombie, M., Heaysman, J. E., and Pegrum, S. M. Locomotion of fibroblasts in culture: II. Movements of particles on the dorsal surface of the leading lamella. *Experimental Cell Research 62* (1970), 389–98.

[3] Abercrombie, M., Heaysman, J. E., and Pegrum, S. M. Locomotion of fibroblasts in culture: II. "Ruffling". *Experimental Cell Research 60* (1970), 437–44.

[4] Abercrombie, M., Heaysman, J. E., and Pegrum, S. M. Locomotion of fibroblasts in culture: IV. Electron microscopy of the leading lamella. *Experimental Cell Research 67* (1971), 359–67.

[5] Abercrombie, M., Heaysman, J. E., and Pegrum, S. M. Locomotion of fibroblasts in culture: V. Surface marking with concanavalin A. *Experimental Cell Research 73* (1972), 536–9.

[6] Addinall, S. G., and Holland, B. The tubulin ancestor, FtsZ, draughtsman, designer and driving force for bacterial cytokinesis. *Journal of Molecular Biology 318*, 2 (2002), 219–36.

[7] Alberts, A. S. Identification of a carboxyl-terminal diaphanous-related formin homology protein autoregulatory domain. *The Journal of Biological Chemistry 276*, 4 (2001), 2824–30.

[8] Alberts, B., Johnson, A., Lewis, J., Raff, M., Roberts, K., and Walter, P. *Molecular Biology of the Cell*, 4 ed. Garland Science, 2002.

[9] Ananthakrishnan, R., and Ehrlicher, A. The forces behind cell movement. *International Journal of Biological Sciences 3*, 5 (2007), 303–17.

[10] Ang, S.-F., Zhao, Z.-s., Lim, L., and Manser, E. DAAM1 is a formin required for centrosome re-orientation during cell migration. *PloS ONE 5*, 9 (2010), 1–10.

[11] Arellano, M., Durán, A., and Pérez, P. Rho 1 GTPase activates the (1-3)beta-D-glucan synthase and is involved in Schizosaccharomyces pombe morphogenesis. *The EMBO Journal 15*, 17 (Sept. 1996), 4584–91.

[12] Backouche, F., Haviv, L., Groswasser, D., and Bernheim-Groswasser, A. Active gels: dynamics of patterning and self-organization. *Physical Biology 3*, 4 (2006), 264–73.

[13] Balaban, N. Q., Schwarz, U. S., Riveline, D., Goichberg, P., Tzur, G., Sabanay, I., Mahalu, D., Safran, S., Bershadsky, A., Addadi, L., and Geiger, B. Force and focal adhesion assembly: a close relationship studied using elastic micropatterned substrates. *Nature Cell Biology 3*, 5 (2001), 466–72.

[14] Bartolini, F., Moseley, J. B., Schmoranzer, J., Cassimeris, L., Goode, B. L., and Gundersen, G. G. The formin mDia2 stabilizes microtubules independently of its actin nucleation activity. *The Journal of Cell Biology 181*, 3 (2008), 523–36.

[15] Bement, W. M., Benink, H. a., and von Dassow, G. A microtubule-dependent zone of active RhoA during cleavage plane specification. *The Journal of Cell Biology 170*, 1 (2005), 91–101.

[16] Bement, W. M., Forscher, P., and Mooseker, M. S. A novel cytoskeletal structure involved in purse string wound closure and cell polarity maintenance. *The Journal of Cell Biology 121*, 3 (1993), 565–78.

[17] Bertin, A., McMurray, M. a., Thai, L., Garcia, G., Votin, V., Grob, P., Allyn, T., Thorner, J., and Nogales, E. Phosphatidylinositol-4,5-bisphosphate promotes budding yeast septin filament assembly and organization. *Journal of Molecular Biology 404*, 4 (2010), 711–31.

[18] Bornens, M., Paintrand, M., and Celati, C. The cortical microfilament system of lymphoblasts displays a periodic oscillatory activity in the absence of microtubules: implications for cell polarity. *The Journal of Cell Biology 109*, 3 (1989), 1071–83.

[19] Cameron, L. A., Footer, M. J., van Oudenaarden, A., and Theriot, J. A. Motility of ActA protein-coated microspheres driven by actin polymerization. *Proceedings of the National Academy of Sciences 96*, 9 (1999), 4908–13.

[20] Carvalho, A., Desai, A., and Oegema, K. Structural memory in the contractile ring makes the duration of cytokinesis independent of cell size. *Cell 137*, 5 (2009), 926–37.

[21] Caspi, A., Yeger, O., Grosheva, I., Bershadsky, A. D., and Elbaum, M. A new dimension in retrograde flow: centripetal movement of engulfed particles. *Biophysical Journal 81*, 4 (2001), 1990–2000.

[22] Castrillon, D. H., and Wasserman, S. A. Diaphanous is required for cytokinesis in Drosophila and shares domains of similarity with the products of the limb deformity gene. *Development 120*, 12 (1994), 3367–77.

[23] Chang, F., Drubin, D., and Nurse, P. Cdc12p, a protein required for cytokinesis in fission yeast, is a component of the cell division ring and interacts with profilin. *The Journal of Cell Biology 137*, 1 (1997), 169–82.

[24] Charras, G., Hu, C.-K., Coughlin, M., and Mitchison, T. J. Reassembly of contractile actin cortex in cell blebs. *The Journal of Cell Biology 175*, 3 (2006), 477–90.

[25] Coffman, V. C., Nile, A. H., Lee, I.-J., Liu, H., and Wu, J.-Q. Roles of Formin Nodes and Myosin Motor Activity in Mid1p-dependent Contractile-Ring Assembly during Fission Yeast Cytokinesis. *Molecular Biology of the Cell 20*, 24 (2009), 5195–210.

[26] Conti, M. A., and Adelstein, R. S. Nonmuscle myosin II moves in new directions. *Journal of Cell Science 121*, 404 (2008), 11–8.

[27] Cortés, J. C. G., Carnero, E., Ishiguro, J., Sánchez, Y., Durán, A., and Ribas, J. C. The novel fission yeast (1,3)beta-D-glucan synthase catalytic subunit Bgs4p is essential during both cytokinesis and polarized growth. *Journal of Cell Science 118* (2005), 157–74.

[28] Cortés, J. C. G., Ishiguro, J., Duran, A., and Ribas, J. C. Localization of the (1,3)beta-D-glucan synthase catalytic subunit homologue Bgs1p/Cps1p from fission yeast suggests that it is involved in septation, polarized growth, mating, spore wall formation and spore germination. *Journal of Cell Science 115*, 21 (2002), 4081–96.

[29] Cortés, J. C. G., Sato, M., Muñoz, J., Moreno, M. B., Clemente-Ramos, J. A., Ramos, M., Okada, H., Osumi, M., Durán, A., and Ribas, J. C. Fission yeast Ags1 confers the essential septum strength needed for safe gradual cell abscission. *The Journal of Cell Biology 198*, 4 (2012), 637–56.

[30] Cramer, L. P. Role of actin-filament disassembly in lamellipodium protrusion in motile cells revealed using the drug jasplakinolide. *Current Biology 9*, 19 (1999), 1095–105.

[31] Dembo, M., and Wang, Y.-l. Stresses at the Cell-to-Substrate Interface during Locomotion of Fibroblasts. *Biophysical Journal 76*, 4 (1999), 2307–16.

[32] Doubrovinski, K., and Kruse, K. Cytoskeletal waves in the absence of molecular motors. *EPL 83*, 18003 (2008), 18003–p1–6.

[33] Drechsel, D. N., Hyman, A. A., Hall, A., and Glotzer, M. A requirement for Rho and Cdc42 during cytokinesis in Xenopus embryos. *Current Biology 7*, 1 (1997), 12–23.

[34] Eisenmann, K. M., Harris, E. S., Kitchen, S. M., Holman, H. a., Higgs, H. N., and Alberts, A. S. Dia-interacting protein modulates formin-mediated actin assembly at the cell cortex. *Current Biology 17*, 7 (2007), 579–91.

[35] Engler, A. J., Sen, S., Sweeney, H. L., and Discher, D. E. Matrix elasticity directs stem cell lineage specification. *Cell 126*, 4 (2006), 677–89.

[36] Estey, M. P., Di Ciano-Oliveira, C., Froese, C. D., Bejide, M. T., and Trimble, W. S. Distinct roles of septins in cytokinesis: SEPT9 mediates midbody abscission. *The Journal of Cell Biology 191*, 4 (2010), 741–9.

[37] Fehon, R. G., McClatchey, A. I., and Bretscher, A. Organizing the cell cortex: the role of ERM proteins. *Nature Reviews. Molecular Cell Biology 11*, 4 (2010), 276–87.

[38] Field, C. M., Al-Awar, O., Rosenblatt, J., Wong, M. L., Alberts, B., and Mitchison, T. J. A purified Drosophila septin complex forms filaments and exhibits GTPase activity. *Journal of Cell Biology 133*, 3 (1996), 605–16.

[39] Field, C. M., Coughlin, M., Doberstein, S., Marty, T., and Sullivan, W. Characterization of anillin mutants reveals essential roles in septin localization and plasma membrane integrity. *Development 132*, 12 (2005), 2849–60.

[40] Finer, J. T., Simmons, R. M., and Spudich, J. A. Single myosin molecule mechanics: piconewton forces and nanometre steps. *Nature 368* (1994), 113–119.

[41] Fischer-Friedrich, E., Van Yen, R. N., and Kruse, K. Surface waves of Min-proteins. *Physical Biology 4*, 1 (2007), 38–47.

[42] Fishkind, D. J., and Wang, Y. L. Orientation and three-dimensional organization of actin filaments in dividing cultured cells. *The Journal of Cell Biology 123*, 4 (1993), 837–48.

[43] Flanagan, M. D., and Lin, S. Cytochalasins block actin filament elongation by binding to high affinity sites associated with F-actin. *Journal of Biological Chemistry 255*, 3 (1980), 835–8.

[44] Foe, V. E., and von Dassow, G. Stable and dynamic microtubules coordinately shape the myosin activation zone during cytokinetic furrow formation. *The Journal of Cell Biology 183*, 3 (2008), 457–70.

[45] Foethke, D., Makushok, T., Brunner, D., and Nédélec, F. Force- and length-dependent catastrophe activities explain interphase microtubule organization in fission yeast. *Molecular Systems Biology 5*, 241 (2009), 1–6.

[46] Gachet, Y., and Hyams, J. S. Endocytosis in fission yeast is spatially associated with the actin cytoskeleton during polarised cell growth and cytokinesis. *Journal of Cell Science 118*, 18 (2005), 4231–42.

[47] Gittes, F., Mickey, B., Nettleton, J., and Howard, J. Flexural rigidity of microtubules and actin filaments measured from thermal fluctuations in shape. *The Journal of Cell Biology 120*, 4 (1993), 923–34.

[48] Glotzer, M. The molecular requirements for cytokinesis. *Science 307*, 5716 (2005), 1735–9.

[49] Goley, E. D., and Welch, M. D. The ARP2/3 complex: an actin nucleator comes of age. *Nature Reviews. Molecular Cell Biology 7*, 10 (2006), 713–26.

[50] Green, R. A., Paluch, E., and Oegema, K. Cytokinesis in Animal Cells. *Annual Review of Cell and Developmental Biology 28*, June (2012), 29–58.

[51] Haraguchi, T., Kaneda, T., and Hiraoka, Y. Dynamics of chromosomes and microtubules visualized by multiple-wavelength fluorescence imaging in living mammalian cells: effects of mitotic inhibitors on cell cycle progression. *Genes to Cells 2*, 6 (1997), 369–80.

[52] Harris, E. S., and Higgs, H. N. Biochemical analysis of mammalian formin effects on actin dynamics. *Methods in Enzymology 406*, 1998 (2006), 190–214.

[53] Heese, M., Mayer, U., and Jürgens, G. Cytokinesis in flowering plants: cellular process and developmental integration. *Current Opinion in Plant Biology 1*, 6 (1998), 486–91.

[54] Hove, J. R., Köster, R. W., Forouhar, A. S., Acevedo-Bolton, G., Fraser, S. E., and Gharib, M. Intracardiac fluid forces are an essential epigenetic factor for embryonic cardiogenesis. *Nature 421* (2003), 172–7.

[55] Howard, J. *Mechanics of Motor Proteins and the Cytoskeleton*, 1 ed. Sinauer, Sunderland, 2001.

[56] Howard, J., Hudspeth, A., and Vale, R. Movement of microtubules by single kinesin molecules. *Nature 342* (1989), 154–8.

[57] Janmey, P. A., Hvidt, S., Käs, J., Lerche, D., Maggs, A., Sackmann, E., Schliwa, M., and Stossel, T. P. The mechanical properties of actin gels. *The Journal of Biological Chemestry 269*, 51 (1994), 32503–13.

[58] Joanny, J.-F., and Prost, J. Active gels as a description of the actin-myosin cytoskeleton. *HFSP journal 3*, 2 (Jan. 2009), 94–104.

[59] Joo, E., Surka, M. C., and Trimble, W. S. Mammalian SEPT2 is required for scaffolding nonmuscle myosin II and its kinases. *Developmental Cell 13*, 5 (2007), 677–90.

[60] Jülicher, F., Kruse, K., Prost, J., and Joanny, J.-F. Active behavior of the Cytoskeleton. *Physics Reports 449*, 1-3 (2007), 3–28.

[61] Jülicher, F., and Prost, J. Cooperative molecular motors. *Physical Review Letters 75*, 13 (1995), 2618–21.

[62] Kamasaki, T., Osumi, M., and Mabuchi, I. Three-dimensional arrangement of F-actin in the contractile ring of fission yeast. *The Journal of Cell Biology 178*, 5 (2007), 765–71.

[63] Kinoshita, M. Assembly of Mammalian Septins. *Journal of Biochemistry 134*, 4 (2003), 491–6.

[64] Kinoshita, M., Field, C. M., Coughlin, M. L., Straight, A. F., and Mitchison, T. J. Self- and actin-templated assembly of Mammalian septins. *Developmental Cell 3*, 6 (2002), 791–802.

[65] Kishi, K., Sasaki, T., Kuroda, S., Itoh, T., and Takai, Y. Regulation of cytoplasmic division of Xenopus embryo by rho p21 and its inhibitory GDP/GTP exchange protein (rho GDI). *The Journal of Cell Biology 120*, 5 (1993), 1187–95.

[66] Kishino, A., and Yanagida, T. Force measurements by micromanipulation of a single actin filament by glass needles. *Nature 334* (1988), 74–6.

[67] Koenderink, G. H., Dogic, Z., Nakamura, F., Bendix, P. M., MacKintosh, F. C., Hartwig, J. H., Stossel, T. P., and Weitz, D. A. An active biopolymer network controlled by molecular motors. *Proceedings of the National Academy 106*, 36 (2009), 15192–7.

[68] Kolega, J. Phototoxicity and photoinactivation of blebbistatin in UV and visible light. *Biochemical and Biophysical Research Communications 320*, 3 (2004), 1020–5.

[69] Koonce, M. P., Strahs, K. R., and Berns, M. W. Repair of laser-severed stress fibers in myocardial non-muscle cells. *Experimental Cell Research 141* (1982), 375–84.

[70] Kovács, M., Tóth, J., Hetényi, C., Málnási-Csizmadia, A., and Sellers, J. R. Mechanism of blebbistatin inhibition of myosin II. *The Journal of Biological Chemistry 279*, 34 (2004), 35557–63.

[71] Kovar, D. R., Kuhn, J. R., Tichy, A. L., and Pollard, T. D. The fission yeast cytokinesis formin Cdc12p is a barbed end actin filament capping protein gated by profilin. *The Journal of Cell Biology 161*, 5 (2003), 875–87.

[72] Kron, S. J., and Spudich, J. a. Fluorescent actin filaments move on myosin fixed to a glass surface. *Proceedings of the National Academy of Sciences 83*, 17 (1986), 6272–6.

[73] Kruse, K., Camalet, S., and Jülicher, F. Self-Propagating Patterns in Active Filament Bundles. *Physical Review Letters 87*, 13 (2001), 138101.

[74] Kruse, K., Joanny, J.-F., Jülicher, F., Prost, J., and Sekimoto, K. Generic theory of active polar gels: a paradigm for cytoskeletal dynamics. *The European Physical Journal. E 16*, 1 (2005), 5–16.

[75] Kruse, K., and Jülicher, F. Actively contracting bundles of polar filaments. *Physical Review Letters 85*, 8 (2000), 1778–81.

[76] Kruse, K., and Jülicher, F. Self-organization and mechanical properties of active filament bundles. *Physical Review E 67*, 5 (2003), 1–16.

[77] Kruse, K., and Jülicher, F. Oscillations in cell biology. *Current Opinion in Cell Biology 17*, 1 (2005), 20–6.

[78] Kruse, K., and Riveline, D. *Spontaneous mechanical oscillations: implications for developing organisms.*, 1 ed., vol. 95. Elsevier Inc., 2011.

[79] Kumar, S., Maxwell, I. Z., Heisterkamp, A., Polte, T. R., Lele, T. P., Salanga, M., Mazur, E., and Ingber, D. E. Viscoelastic retraction of single living stress fibers and its impact on cell shape, cytoskeletal organization, and extracellular matrix mechanics. *Biophysical Journal 90*, 10 (2006), 3762–73.

[80] Lancaster, O. M., Le Berre, M., Dimitracopoulos, A., Bonazzi, D., Zlotek-Zlotkiewicz, E., Picone, R., Duke, T., Piel, M., and Baum, B. Mitotic rounding alters cell geometry to ensure efficient bipolar spindle formation. *Developmental Cell 25*, 3 (2013), 270–83.

[81] Laporte, D., Coffman, V. C., Lee, I.-J., and Wu, J.-Q. Assembly and architecture of precursor nodes during fission yeast cytokinesis. *The Journal of Cell Biology 192*, 6 (2011), 1005–21.

[82] Laporte, D., Ojkic, N., Vavylonis, D., and Wu, J.-Q. α-Actinin and fimbrin cooperate with myosin II to organize actomyosin bundles during contractile-ring assembly. *Molecular Biology of the Cell 23*, 16 (2012), 3094–110.

[83] Liu, J., Wang, H., McCollum, D., and Balasubramanian, M. K. Drc1p/Cps1p, a 1,3-beta-glucan synthase subunit, is essential for division septum assembly in Schizosaccharomyces pombe. *Genetics 153*, 3 (1999), 1193–203.

[84] Loisel, T. P., Boujemaa, R., Pantaloni, D., and Carlier, M. F. Reconstitution of actin-based motility of Listeria and Shigella using pure proteins. *Nature 401*, 6753 (1999), 613–6.

[85] Loose, M., Fischer-Friedrich, E., Ries, J., Kruse, K., and Schwille, P. Spatial regulators for bacterial cell division self-organize into surface waves in vitro. *Science 320*, 5877 (2008), 789–92.

[86] Loughlin, R., Heald, R., and Nédélec, F. A computational model predicts Xenopus meiotic spindle organization. *The Journal of Cell Biology 191*, 7 (2010), 1239–49.

[87] Loughlin, R., Wilbur, J. D., McNally, F. J., Nédélec, F., and Heald, R. Katanin contributes to interspecies spindle length scaling in Xenopus. *Cell 147*, 6 (2011), 1397–407.

[88] Luo, W., Yu, C.-H., Lieu, Z. Z., Allard, J., Mogilner, A., Sheetz, M. P., and Bershadsky, A. D. Analysis of the local organization and dynamics of cellular actin networks. *The Journal of Cell Biology 202*, 7 (2013), 1057–73.

[89] Lyass, L. A., Bershadsky, A. D., Gelfand, V. I., Serpinskaya, A. S., Stavrovskaya, A. A., Vasiliev, J. M., and Gelfand, I. M. Multinucleation-induced improvement of the spreading of transformed cells on the substratum. *Proceedings of the National Academy of Sciences 81*, 10 (1984), 3098–102.

[90] Martin, A. C. Pulsation and stabilization: contractile forces that underlie morphogenesis. *Developmental Biology 341*, 1 (2010), 114–25.

[91] Martin, P., and Lewis, J. Actin cables and epidermal movement in embryonic wound healing. *Nature 360* (1992), 179–83.

[92] Martin, S. G., and Berthelot-Grosjean, M. Polar gradients of the DYRK-family kinase Pom1 couple cell length with the cell cycle. *Nature 459*, 7248 (2009), 852–6.

[93] Mattila, P. K., and Lappalainen, P. Filopodia: molecular architecture and cellular functions. *Nature Reviews. Molecular Cell Biology 9*, 6 (2008), 446–54.

[94] Maupin, P., and Pollard, T. D. Arrangement of actin filaments and myosin-like filaments in the contractile ring and of actin-like filaments in the mitotic spindle of dividing HeLa cells. *Journal of Ultrastructure and Molecular Structure Research 94*, 1 (1986), 92–103.

[95] Mavrakis, M., Azou-Gros, Y., Tsai, F.-C., Alvarado, J., Bertin, A., Iv, F., Kress, A., Brasselet, S., Koenderink, G. H., and Lecuit, T. Septins promote F-actin ring formation by crosslinking actin filaments into curved bundles. *Nature Cell Biology 16*, 4 (2014), 322–34.

[96] Mendes Pinto, I., Rubinstein, B., Kucharavy, A., Unruh, J. R., and Li, R. Actin Depolymerization Drives Actomyosin Ring Contraction during Budding Yeast Cytokinesis. *Developmental Cell 22*, 6 (2012), 1247–60.

[97] Minc, N., Boudaoud, A., and Chang, F. Mechanical forces of fission yeast growth. *Current Biology 19*, 13 (2009), 1096–101.

[98] Minc, N., Burgess, D., and Chang, F. Influence of cell geometry on division-plane positioning. *Cell 144*, 3 (2011), 414–26.

[99] Mishra, M., Kashiwazaki, J., Takagi, T., Srinivasan, R., Huang, Y., Balasubramanian, M. K., and Mabuchi, I. In vitro contraction of cytokinetic ring depends on myosin II but not on actin dynamics. *Nature Cell Biology 15*, 7 (2013), 853–9.

[100] Morone, N., Fujiwara, T., Murase, K., Kasai, R. S., Ike, H., Yuasa, S., Usukura, J., and Kusumi, A. Three-dimensional reconstruction of the membrane skeleton at the plasma membrane interface by electron tomography. *The Journal of Cell Biology 174*, 6 (2006), 851–62.

[101] Moseley, J. B., Mayeux, A., Paoletti, A., and Nurse, P. A spatial gradient coordinates cell size and mitotic entry in fission yeast. *Nature 459*, 7248 (2009), 857–60.

[102] Muñoz, J., Cortés, J. C. G., Sipiczki, M., Ramos, M., Clemente-Ramos, J. A., Moreno, M. B., Martins, I. M., Pérez, P., and Ribas, J. C. Extracellular cell wall β(1,3)glucan is required to couple septation to actomyosin ring contraction. *The Journal of Cell Biology 203*, 2 (2013), 265–82.

[103] Mukhina, S., Wang, Y.-L., and Murata-Hori, M. Alpha-actinin is required for tightly regulated remodeling of the actin cortical network during cytokinesis. *Developmental Cell 13*, 4 (2007), 554–65.

[104] Murphy, C. T., Rock, R. S., and Spudich, J. a. A myosin II mutation uncouples ATPase activity from motility and shortens step size. *Nature Cell Biology 3*, 3 (2001), 311–5.

[105] Naumanen, P., Lappalainen, P., and Hotulainen, P. Mechanisms of actin stress fibre assembly. *Journal of Microscopy 231*, 3 (2008), 446–54.

[106] Nédélec, F., and Foethke, D. Collective Langevin dynamics of flexible cytoskeletal fibers. *New Journal of Physics 9*, 11 (2007), 427.

[107] Nishimura, Y., and Yonemura, S. Centralspindlin regulates ECT2 and RhoA accumulation at the equatorial cortex during cytokinesis. *Journal of Cell Science 119*, 1 (2006), 104–14.

[108] Nolen, B. J., Tomasevic, N., Russell, A., Pierce, D. W., Jia, Z., McCormick, C. D., Hartman, J., Sakowicz, R., and Pollard, T. D. Characterization of two classes of small molecule inhibitors of Arp2/3 complex. *Nature 460*, 7258 (2009), 1031–4.

[109] O'Connell, C. B., Wheatley, S. P., Ahmed, S., and Wang, Y. L. The small GTP-binding protein rho regulates cortical activities in cultured cells during division. *The Journal of Cell Biology 144*, 2 (1999), 305–13.

[110] Oegema, K., Savoian, M. S., Mitchison, T. J., and Field, C. M. Functional analysis of a human homologue of the Drosophila actin binding protein anillin suggests a role in cytokinesis. *The Journal of Cell Biology 150*, 3 (2000), 539–52.

[111] Osumi, M. The ultrastructure of yeast: cell wall structure and formation. *Micron 29*, 2/3 (1998), 207–33.

[112] Paluch, E., Piel, M., Prost, J., Bornens, M., and Sykes, C. Cortical actomyosin breakage triggers shape oscillations in cells and cell fragments. *Biophysical Journal 89*, 1 (2005), 724–33.

[113] Pantaloni, D., Boujemaa, R., Didry, D., Gounon, P., and Carlier, M.-F. The Arp2/3 complex branches filament barbed ends: functional antagonism with capping proteins. *Nature Cell Biology 2*, 7 (2000), 385–91.

[114] Paoletti, A., and Chang, F. Analysis of mid1p, a protein required for placement of the cell division site, reveals a link between the nucleus and the cell surface in fission yeast. *Molecular Biology of the Cell 11*, 8 (2000), 2757–73.

[115] Pelham, R. J., and Chang, F. Actin dynamics in the contractile ring during cytokinesis in fission yeast. *Nature 419*, 6902 (2002), 82–6.

[116] Pelham, R. J., and Wang, Y.-l. Cell locomotion and focal adhesions are regulated by substrate flexibility. *Proceedings of the National Academy of Sciences 94* (1998), 13661–5.

[117] Pérez, P., and Ribas, J. C. Cell wall analysis. *Methods 33*, 3 (2004), 245–51.

[118] Piekny, A. J., and Glotzer, M. Anillin is a scaffold protein that links RhoA, actin, and myosin during cytokinesis. *Current Biology 18*, 1 (2008), 30–6.

[119] Piekny, A. J., and Maddox, A. S. The myriad roles of Anillin during cytokinesis. *Seminars in Cell & Developmental Biology 21*, 9 (2010), 881–91.

[120] Plaçais, P.-Y., Balland, M., Guérin, T., Joanny, J.-F., and Martin, P. Spontaneous Oscillations of a Minimal Actomyosin System under Elastic Loading. *Physical Review Letters 103*, 15 (2009), 158102.

[121] Plotnikov, S. V., Pasapera, A. M., Sabass, B., and Waterman, C. M. Force fluctuations within focal adhesions mediate ECM-rigidity sensing to guide directed cell migration. *Cell 151*, 7 (2012), 1513–27.

[122] Pollard, T. D. Mechanics of cytokinesis in eukaryotes. *Curr Opin Cell Biol 22*, 1 (2010), 50–6.

[123] Pollard, T. D., and Wu, J.-Q. Understanding cytokinesis: lessons from fission yeast. *Nat. Rev. Mol. Cell Biol. 11*, 2 (2010), 149–55.

[124] Proctor, S. A., Minc, N., Boudaoud, A., and Chang, F. Contributions of turgor pressure, the contractile ring, and septum assembly to forces in cytokinesis in fission yeast. *Current Biology 22*, 17 (2012), 1601–8.

[125] Reymann, A.-C., Boujemaa-Paterski, R., Martiel, J.-L., Guérin, C., Cao, W., Chin, H. F., De La Cruz, E. M., Théry, M., and Blanchoin, L. Actin network architecture can determine myosin motor activity. *Science 336*, 6086 (2012), 1310–4.

[126] Reymann, A.-C., Martiel, J.-L., Cambier, T., Blanchoin, L., Boujemaa-Paterski, R., and Théry, M. Nucleation geometry governs ordered actin networks structures. *Nature Materials 9*, 10 (2010), 827–32.

[127] Riedl, J., Crevenna, A. H., Kessenbrock, K., Yu, J. H., Neukirchen, D., Bradke, F., Jenne, D., Holak, T. A., Werb, Z., Sixt, M., and Wedlich-Soldner, R. Lifeact : a versatile marker to visualize F-actin. *Nature Methods 5*, 7 (2008), 605–607.

[128] Riveline, D. Explaining lengths and shapes of yeast by scaling arguments. *PLoS ONE 4*, 7 (2009), 1–5.

[129] Riveline, D. Methods for observing cells with cell wall or invertebrate embryos with oblong eggshell. WO 201314430. *Patent* (2013).

[130] Riveline, D., and Buguin, A. Devices and methods for observing the cell division. WO/2010/092116. *Patent* (2010).

[131] Riveline, D., Ott, A., Jülicher, F., Winkelmann, D. a., Cardoso, O., Lacapère, J. J., Magnúsdóttir, S., Viovy, J. L., Gorre-Talini, L., and Prost, J. Acting on actin: the electric motility assay. *European Biophysics Journal 27*, 4 (1998), 403–8.

[132] Riveline, D., and Wollrab, V. Devices and methods for observing eukaryotic cells without cell wall. WO/2013/135809. *Patent* (2013).

[133] Riveline, D., Zamir, E., Balaban, N. Q., Schwarz, U. S., Ishizaki, T., Narumiya, S., Kam, Z., Geiger, B., and Bershadsky, a. D. Focal contacts as mechanosensors: externally applied local mechanical force induces growth of focal contacts by an mDia1-dependent and ROCK-independent mechanism. *The Journal of Cell Biology 153*, 6 (2001), 1175–86.

[134] Rizvi, S. A., Neidt, E. M., Cui, J., Feiger, Z., Skau, C. T., Gardel, M. L., Kozmin, S. A., and Kovar, D. R. Identification and characterization of a small molecule inhibitor of formin-mediated actin assembly. *Chemistry & Biology 16*, 11 (2009), 1158–68.

[135] Robbins, E., and Marcus, P. I. Mitotically Synchronized Mammalian Cells: a Simple Method for Obtaining Large Populations. *Science 144*, 3622 (1964), 1152–3.

[136] Saarikangas, J., and Barral, Y. The emerging functions of septins in metazoans. *EMBO Reports 12*, 11 (2011), 1118–26.

[137] Saitoh, M., Ishikawa, T., Matsushima, S., Naka, M., and Hidaka, H. Selective Inhibition of Catalytic Activity of Smooth Muscle Myosin. *Journal of Biological Chemistry 262*, 16 (1987), 7796–801.

[138] Salbreux, G., Charras, G., and Paluch, E. Actin cortex mechanics and cellular morphogenesis. *Trends in Cell Biology 22*, 11 (2012), 536–545.

[139] Salbreux, G., Prost, J., and Joanny, J.-F. Hydrodynamics of Cellular Cortical Flows and the Formation of Contractile Rings. *Physical Review Letters 103*, 5 (2009), 1–4.

[140] Sanger, J. M., and Sanger, J. W. Banding and polarity of actin filaments in interphase and cleaving cells. *The Journal of Cell Biology 86*, 2 (1980), 568–75.

[141] Schaller, V., Weber, C., Semmrich, C., Frey, E., and Bausch, A. R. Polar patterns of driven filaments. *Nature 467*, 7311 (2010), 73–77.

[142] Schroeder, T. E. The contractile ring. *Zeitschrift für Zellforschung und Mikroskopische Anatomie 109*, 4 (1970), 431–449.

[143] Schroeder, T. E. Actin in dividing cells: contractile ring filaments bind heavy meromyosin. *Proceedings of the National Academy of Sciences of the United States of America 70*, 6 (1973), 1688–92.

[144] Schroeder, T. E. The contractile ring and furrowing in dividing cells. *Annals of the New York Academy of Sciences 582* (1990), 78–87.

[145] Sedzinski, J., Biro, M., Oswald, A., Tinevez, J.-Y., Salbreux, G., and Paluch, E. Polar actomyosin contractility destabilizes the position of the cytokinetic furrow. *Nature 476* (2011), 462–6.

[146] Severson, A. F., Baillie, D. L., and Bowerman, B. A Formin Homology protein and a profilin are required for cytokinesis and Arp2/3-independent assembly of cortical microfilaments in C. elegans. *Current Biology 12*, 24 (2002), 2066–75.

[147] Sirotkin, V., Berro, J., Macmillan, K., Zhao, L., and Pollard, T. D. Quantitative Analysis of the Mechanism of Endocytic Actin Patch Assembly and Disassembly in Fission Yeast. *Molecular Biology of the Cell 21* (2010), 2894–904.

[148] Small, J. V., Stradal, T., Vignal, E., and Rottner, K. The lamellipodium: where motility begins. *Trends in Cell Biology 12*, 3 (2002), 112–20.

[149] Spector, I., Shochet, N., Kashman, Y., and Groweiss, A. Latrunculins: novel marine toxins that disrupt microfilament organization in cultured cells. *Science 219*, 4584 (1983), 493–5.

[150] Spudich, J. The myosin swinging cross-bridge model. *Nature Reviews. Molecular Cell Biology 2* (2001), 387–92.

[151] Stewart, M. P., Helenius, J., Toyoda, Y., Ramanathan, S. P., Muller, D. J., and Hyman, A. A. Hydrostatic pressure and the actomyosin cortex drive mitotic cell rounding. *Nature 469*, 7329 (2011), 226–30.

[152] Storm, C., Pastore, J., MacKintosh, F., Lubensky, T., and Janmey, P. A. Nonlinear elasticity in biological gels. *Nature 435* (2005), 191–5.

[153] Straight, A. F., Cheung, A., Limouze, J., Chen, I., Westwood, N. J., Sellers, J. R., and Mitchison, T. J. Dissecting temporal and spatial control of cytokinesis with a myosin II Inhibitor. *Science 299*, 5613 (2003), 1743–7.

[154] Stricker, J., Falzone, T., and Gardel, M. L. Mechanics of the F-actin cytoskeleton. *Journal of Biomechanics 43*, 1 (2010), 9–14.

[155] Su, K.-C., Takaki, T., and Petronczki, M. Targeting of the RhoGEF Ect2 to the equatorial membrane controls cleavage furrow formation during cytokinesis. *Developmental Cell 21*, 6 (2011), 1104–15.

[156] Surrey, T., Nédélec, F., Leibler, S., and Karsenti, E. Physical properties determining self-organization of motors and microtubules. *Science 292*, 5519 (2001), 1167–71.

[157] Svitkina, T. M., and Borisy, G. G. Organization and Treadmilling of Actin Filament Array in Lamellipodia. *Journal of Cell Biology 145*, 5 (1999), 1009–26.

[158] Takács, B., Billington, N., Gyimesi, M., Kintses, B., Málnási-Csizmadia, A., Knight, P. J., and Kovács, M. Myosin complexed with ADP and blebbistatin reversibly adopts a conformation resembling the start point of the working stroke. *Proceedings of the National Academy of Sciences 107*, 15 (2010), 6799–804.

[159] Takiguchi, K. Heavy meromyosin induces sliding movements between antiparallel actin filaments. *Journal of Biochemistry 109*, 4 (1991), 520–7.

[160] Tang, J., Erikson, R. L., and Liu, X. Checkpoint kinase 1 (Chk1) is required for mitotic polo-like kinase 1 (Plk1). *Proceedings of the National Academy of Sciences 103*, 32 (2006), 11964–9.

[161] Théry, M., Jiménez-Dalmaroni, A., Racine, V., Bornens, M., and Jülicher, F. Experimental and theoretical study of mitotic spindle orientation. *Nature 447*, 7143 (2007), 493–6.

[162] Tilney, L. G., DeRosier, D. J., and Tilney, M. S. How Listeria exploits host cell actin to form its own cytoskeleton. I. Formation of a tail and how that tail might be involved in movement. *The Journal of Cell Biology 118*, 1 (1992), 71–81.

[163] Tinevez, J.-Y., Schulze, U., Salbreux, G., Roensch, J., Joanny, J.-F., and Paluch, E. Role of cortical tension in bleb growth. *Proceedings of the National Academy of Sciences 106*, 44 (2009), 18581–6.

[164] Trepat, X., Wasserman, M. R., Angelini, T. E., Millet, E., Weitz, D. A., Butler, J. P., and Fredberg, J. J. Physical forces during collective cell migration. *Nature Physics 5*, 6 (2009), 426–30.

[165] Tse, J. R., and Engler, A. J. Preparation of hydrogel substrates with tunable mechanical properties. *Current Protocols in Cell Biology Chapter 10*, June (2010), Unit 10.16.1–10.

[166] Turlier, H., Audoly, B., Prost, J., and Joanny, J.-F. Furrow constriction in animal cell cytokinesis. *Biophysical Journal 106*, 1 (2014), 114–23.

[167] Vavylonis, D., Wu, J.-Q., Hao, S., O'Shaughnessy, B., and Pollard, T. D. Assembly mechanism of the contractile ring for cytokinesis by fission yeast. *Science 319*, 5859 (2008), 97–100.

[168] Vavylonis, D., Wu, J.-Q., Hao, S., O'Shaughnessy, B., and Pollard, T. D. Assembly mechanism of the contractile ring for cytokinesis by fission yeast. *Science 319*, 5859 (2008), 97–100.

[169] von Dassow, G., Verbrugghe, K. J. C., Miller, A. L., Sider, J. R., and Bement, W. M. Action at a distance during cytokinesis. *The Journal of Cell Biology 187*, 6 (2009), 831–45.

[170] Wachsstock, D., Schwarz, W., and Pollard, T. D. Cross-linker dynamics determine the mechanical properties of actin gels. *Biophysical Journal 66*, 3 (1994), 801–9.

[171] Wachsstock, D. H., Schwartz, W. H., and Pollard, T. D. Affinity of alpha-actinin for actin determines the structure and mechanical properties of actin filament gels. *Biophysical Journal 65*, 1 (1993), 205–14.

[172] Wald, A. *Dynamik und mechanische Eigenschaften kontraktiler Ringe unter Berücksichtigung bipolarer Filamente*. Saarland University, Master Thesis, 2013.

[173] Watanabe, S., Ando, Y., Yasuda, S., Hosoya, H., Watanabe, N., Ishizaki, T., and Narumiya, S. mDia2 induces the actin scaffold for the contractile ring and stabilizes its position during cytokinesis in NIH 3T3 cells. *Molecular Biology of the Cell 19*, 5 (2008), 2328–38.

[174] Watanabe, S., Okawa, K., Miki, T., Sakamoto, S., Morinaga, T., Segawa, K., Arakawa, T., Kinoshita, M., Ishizaki, T., and Narumiya, S. Rho and anillin-dependent control of mDia2 localization and function in cytokinesis. *Molecular Biology of the Cell 21*, 9 (2010), 3193–204.

[175] Whitfield, M. L., Zheng, L. X., Baldwin, A., Ohta, T., Hurt, M. M., and Marzluff, W. F. Stem-loop binding protein, the protein that binds the 3' end of histone mRNA, is cell cycle regulated by both translational and posttranslational mechanisms. *Molecular and Cellular Biology 20*, 12 (2000), 4188–98.

[176] Wollrab, V., Caballero, D., Thiagarajan, R., and Riveline, D. Ordering single cells and single embryos in 3D confinement. *JoVE (in press)*.

[177] Woolf, V. The waves. *1 ed. Urban Romantics London* (2012), Original work published in 1931.

[178] Wu, J.-Q., and Pollard, T. D. Counting cytokinesis proteins globally and locally in fission yeast. *Science 310*, 5746 (2005), 310–4.

[179] Yang, J., and Shen, M. H. Polyethylene glycol-mediated cell fusion. *Methods in Molecular Biology 325*, 7 (2006), 59–66.

[180] Yoshizaki, H., Ohba, Y., Kurokawa, K., Itoh, R. E., Nakamura, T., Mochizuki, N., Nagashima, K., and Matsuda, M. Activity of Rho-family GTPases during cell division as visualized with FRET-based probes. *The Journal of Cell Biology 162*, 2 (2003), 223–32.

[181] Yüce, O., Piekny, A. J., and Glotzer, M. An ECT2-centralspindlin complex regulates the localization and function of RhoA. *The Journal of Cell Biology 170*, 4 (2005), 571–82.

[182] Zhang, J., Kong, C., Xie, H., McPherson, P. S., Grinstein, S., and Trimble, W. S. Phosphatidylinositol polyphosphate binding to the mammalian septin H5 is modulated by GTP. *Current Biology 9*, 24 (1999), 1458–67.

[183] Zhao, F.-Q., Padrón, R., and Craig, R. Blebbistatin stabilizes the helical order of myosin filaments by promoting the switch 2 closed state. *Biophysical Journal 95*, 7 (2008), 3322–9.

[184] Zigmond, S. H., Evangelista, M., Boone, C., Yang, C., Dar, A. C., Sicheri, F., Forkey, J., Pring, M., and Kl, O. Formin Leaky Cap Allows Elongation in the Presence of Tight Capping Proteins. *Current Biology 13*, 20 (2003), 1820–3.

[185] Zumdieck, A., Kruse, K., Bringmann, H., Hyman, A. A., and Jülicher, F. Stress generation and filament turnover during actin ring constriction. *PloS ONE 2*, 1 (2007), e696.

[186] Zumdieck, A., Lagomarsino, M., Tanase, C., Kruse, K., Mulder, B., Dogterom, M., and Jülicher, F. Continuum Description of the Cytoskeleton: Ring Formation in the Cell Cortex. *Physical Review Letters 95*, 25 (2005), 1–4.

A Appendix

A.1 Abbreviations

Table A.1: Tabel of Abbrivations

Abbrivation	Full name
ActA	Actin assembly-inducing protein
ADP	Adenosine diphosphate
Ags	α-glucan sythase
APS	Ammonium persulfate
Arp	Actin-related protein
ATP	Adenosine triphosphate
Bgs	β-glucan sythase
BSA	Bovine serum albumin
CCD	Charge-coupled device
CHD	Calponin homology domain
DAAM1	Disheveled-associated activator of morphogenesis
DAPI	4',6-Diamidino-2-phenylindole dihydrochloride
DIC	Differential interference contrast
DMEM	Dulbecco's modified eagle's medium
DMSO	Dimethyl sulfoxide
DNA	Deoxyribonucleic acid
DPBS	Dulbecco's phosphate-buffered saline
ECM	Extracellular matrix
EDTA	Ethylenediaminetetraacetic acid
EM	Electron microscopy
EMM	Edinburgh minimal medium
ERM	Ezrin-radixin-moesin
FRAP	Fluorescence recovery after photobleaching
GDP	guanosine diphosphate
GFP	Green fluorescent protein
GTP	guanosine triphosphate
HyD	Hybrid detectors

Continued on next page

Table A.1 – continued from previous page

Abbrivation	Full name
L-15	Leibovitz-15
LB medium	Lysogeny broth medium
mDia	Mammalian homolog of diaphanous
MeOh	Methanol
MYH9	Myosin heavy chain 9
MLCK	Myosin light chain kinase
NHS	Acrylic acid N-hydroxysuccinimide ester
OD	Optical density
PBS	Phosphate buffered saline
PC	Pattern coefficient
PDMS	Polydimethylsiloxane
PFA	Paraformaldehyde
PLL-g-PEG	Poly(l-lysine)-graft-poly(ethylene glycol)
PMT	Photomultiplier tube
Rlc1	Regulatory light chain
RNA	Ribonucleic acid
ROCK	Rho kinase
SMIFH2	Small molecule inhibitor of formin homology 2 domains
StDev	Standard deviation
TBS	Trisbuffered saline
TE buffer	Tris-EDTH buffer
TEMED	tetramethylethylenediamine
TMCS	Chlorotrimethylsilane
TCA	Trichloroacetic acid
UV	Ultraviolet
WASP	Wiskott-Aldrich syndrom protein
YES	Yeast extract

A.2 Supplementary information about materials and methods

A.2.1 Microfabrication

The following Tables contain information about products and materials related to microfabrication protocols.

Table A.2: Microfabrication products

Product	Brand (Supplier)	Reference	Comment
Silicon wafer	Si-Mat		3", P/Boron, <100>
SU-8 photoresist	MicroChem		
Developer SU-8	Chimie Tech Services	DevSU8/4	
PDMS, Sylgard 184	Dow Corning (Neyco, Ellsworth)	DC184-1.1 , 0002-01-000032	
Hydrogen peroxide	Acros Organic	202460010	35 wt % solution in water
Sulforic acid	Sigma Aldrich	30743	95 - 97 %
Silane (3-(Mercapto) propyltrimethoxysilane)	Fluorochem	S10475	
Fibronectin (Rhodamin)	Cytoskeleton (tebu-bio)	027FNR01-A	
PLL-g-PEG	SuSoS AG		0.1 mg/ml working dilution
Chlorotrimethylsilane	Sigma Aldrich	C72854	$\geq$ 97%
Polystyrene, film	Good fellow	ST311025	25 µm

Table A.3: Microfabrication equipment

Product	Company	Reference	Comment
Spin coater	Laurell Technologies corporation	WS-400B-6NPP/Lite	
Mask aligner	SUSS MicroTec	MJB3	
Photolithography mask, acetate	Selba		50800 dpi
Oxygen plasma cleaner	Diener Electronic	Zepto B	Usual settings: 30 s, O_2, flow 5,5, power 2,5

A.2.2 Materials and methods for mammalian cells

The following section gathers all supplementary information about products and protocols related to the treatment and setups related to experiments with mammalian cells.

Table A.4: Products and references used for culturing mammalian cells

Product	Brand (Supplier)	Reference	Comment
BCS (Bovine Calf Serum)	Sigma Aldrich	C8056	
FBS (Fetal Bovine Serum)	Thermo Scientific HyClone (Thermo Fisher Scientific)	10309433	
L-Glutamine	Sigma Aldrich	G7513	Added to medium at a final concentration of 2 mM
DMEM (Dulbecco's Modified Eagle Medium)	Invitrogen Gibco (Thermo Fisher Scientific)	12007559	high glucose
Geneticin	Invitrogen (Thermo Fisher Scientific)	11548616	Added after replating at a 0.5 mg/ml concentration
Puromycin	Invitrogen Gibco (Thermo Fisher Scientific)	12122530	Added after replating at a 1 μg/ml concentration
Penicillin streptomycin	Invitrogen Gibco (Thermo Fisher Scientific)	11548876	Dilution in culture medium 1 %
Trypsin-EDTA	Invitrogen Gibco (Thermo Fisher Scientific)	11570626	
Leibovitz L-15 medium	Invitrogen Gibco (Thermo Fisher Scientific)	11540556	
DMSO (Dimethyl sulfoxide)	Sigma Aldrich	D8418	

Table A.5: Cytoskeleton and cell cycle drugs

Product	Brand (Supplier)	Reference	Comment
(–) Blebbistatin	Sigma Aldrich	B0560	stored at –20°C, light sensitive
CK-666	Sigma Aldrich	SML0006	stored at 4°C
Cytochalasin D	Sigma Aldrich	C8273	stored at –20°C
Latrunculin A	Sigma Aldrich	L5163	stored at –20°C
ML-7	Sigma Aldrich	I2764	stored at –20°C
Monastrol	Sigma Aldrich	M8518	stored at –20°C
Nocodazole	Sigma Aldrich	M1404	stored at 4°C
SMIFH2	Sigma Aldrich	S4826	stored at 4°C
Thymidine	Sigma Aldrich	T1895	stored at 4°C
DMSO (Dimethyl sulfoxide)	Sigma Aldrich	D8418	stored at RT

Table A.6: Products used for the different experimental setups

Product	Brand (Supplier)	Reference	Comment
Fibronectin	Sigma Aldrich	F1141	Stock 1 mg/ml, for experiments usually used at a 20 μg/ml dilution in PBS
Mineral oil	Sigma Aldrich	M8410	

Table A.7: Products used for DNA amplification and transfection

Product	Brand (Supplier)	Reference
Competent bacteria (One Shot TOP10)	Invitrogen Gibco (Thermo Fisher Scientific)	1066-6493
LB medium and agar plates	IGBMC media facility	
EndoFree® Plasmid Maxi Kit	Qiagen	12362
Lipofectamine 2000®	Invitrogen Gibco (Thermo Fisher Scientific)	11668
Opti-MEM®	Invitrogen Gibco	11058-021

Things to do before starting

- Add the provided RNase A solution to Buffer P1 before use. Use one vial of RNase A (centrifuge briefly before use) per bottle of Buffer P1, to give a final concentration of 100 µg/ml.
- To prepare endotoxin-free 70% ethanol, add 40 ml of 96–100% ethanol to the endotoxin-free water supplied with the kit.
- Check Buffer P2 for SDS precipitation due to low storage temperatures. If necessary, dissolve the SDS by warming to 37°C.
- Pre-chill Buffer P3 at 4°C.
- Optional: Add the provided LyseBlue reagent to Buffer P1 and mix before use. Use one vial LyseBlue (centrifuge briefly before use) per bottle of Buffer P1 to achieve a 1:1000 dilution. LyseBlue provides visual identification of optimum buffer mixing thereby preventing the common handling errors that lead to inefficient cell lysis and incomplete precipitation of SDS, genomic DNA, and cell debris. For more details see "Using LyseBlue reagent" on page 15.

Procedure

1. **Pick a single colony from a freshly streaked selective plate and inoculate a starter culture of 2–5 ml LB medium containing the appropriate selective antibiotic. Incubate for approx. 8 h at 37°C with vigorous shaking (approx. 300 rpm).**
   Use a tube or flask with a volume of at least 4 times the volume of the culture.
2. **Dilute the starter culture 1/500 to 1/1000 into selective LB medium. For high-copy plasmids, inoculate 100 ml medium with 100–200 µl of starter culture. For low-copy plasmids, inoculate 250 ml medium with 250–500 µl of starter culture. Grow at 37°C for 12–16 h with vigorous shaking (approx. 300 rpm).**
   Use a flask or vessel with a volume of at least 4 times the volume of the culture. The culture should reach a cell density of approximately 3–4 x 10^9 cells per milliliter, which typically corresponds to a pellet wet weight of approximately 3 g/liter medium (see page 12).
3. **Harvest the bacterial cells by centrifugation at 6000 x *g* for 15 min at 4°C.**
   ⊛ If you wish to stop the protocol and continue later, freeze the cell pellets at –20°C.
4. **Resuspend the bacterial pellet in 10 ml Buffer P1.**
   For efficient lysis it is important to use a vessel that is large enough to allow complete mixing of the lysis buffers. Ensure that RNase A has been added to Buffer P1.
   If LyseBlue reagent has been added to Buffer P1, vigorously shake the buffer bottle before use to ensure LyseBlue particles are completely resuspended.
   The bacteria should be resuspended completely by vortexing or pipetting up and down until no cell clumps remain.
5. **Add 10 ml Buffer P2, mix thoroughly by vigorously inverting the sealed tube 4–6 times, and incubate at room temperature (15–25°C) for 5 min.**
   Do not vortex, as this will result in shearing of genomic DNA. The lysate should appear viscous. Do not allow the lysis reaction to proceed for more than 5 min. After use, the bottle containing Buffer P2 should be closed immediately to avoid acidification from CO_2 in the air.
   If LyseBlue has been added to Buffer P1 the cell suspension will turn blue after addition of Buffer P2. Mixing should result in a homogeneously colored suspension. If the suspension contains localized colorless regions or if brownish cell clumps are still visible, continue mixing the solution until a homogeneously colored suspension is achieved.
   During the incubation prepare the QIAfilter Cartridge:
   Screw the cap onto the outlet nozzle of the QIAfilter Maxi Cartridge.
   Place the QIAfilter Cartridge in a convenient tube.
6. **Add 10 ml chilled Buffer P3 to the lysate, and mix immediately and thoroughly by vigorously inverting 4–6 times. Proceed directly to step 7. Do not incubate the lysate on ice.**
   Precipitation is enhanced by using chilled Buffer P3. After addition of Buffer P3, a fluffy white material forms and the lysate becomes less viscous. The precipitated material contains genomic DNA, proteins, cell debris, and KDS. The lysate should be mixed thoroughly to ensure even potassium dodecyl sulfate precipitation. If the mixture still appears viscous, more mixing is required to completely neutralize the solution. It is important to transfer the lysate into the QIAfilter Cartridge immediately in order to prevent later disruption of the precipitate layer.
   If LyseBlue reagent has been used, the suspension should be mixed until all trace of blue has gone and the suspension is colorless. A homogeneous colorless suspension indicates that the SDS has been effectively precipitated.
7. **Pour the lysate into the barrel of the QIAfilter Cartridge. Incubate at room temperature (15–25°C) for 10 min. Do not insert the plunger!**
   Important: This 10 min incubation at room temperature is essential for optimal performance of the QIAfilter Maxi Cartridge. Do not agitate the QIAfilter Cartridge during this time. A precipitate containing proteins, genomic DNA, and detergent will float and form a layer on top of the solution. This ensures convenient filtration without clogging. If, after the 10 min incubation, the precipitate has not floated to the top of the solution, carefully run a sterile pipet tip around the walls of the cartridge to dislodge it.
8. **Remove the cap from the QIAfilter Cartridge outlet nozzle. Gently insert the plunger into the QIAfilter Maxi Cartridge and filter the cell lysate into a 50 ml tube.**
   Filter until all of the lysate has passed through the QIAfilter Cartridge, but do not apply extreme force. Approximately 25 ml of the lysate is generally recovered after filtration.
   ☞ Remove a 120 µl sample of the filtered lysate and save for an analytical gel (sample 1) in order to determine whether growth and lysis conditions were optimal.
9. **Add 2.5 ml Buffer ER to the filtered lysate, mix by inverting the tube approximately 10 times, and incubate on ice for 30 min.**
   After the addition of Buffer ER the lysate appears turbid, but will become clear again during the incubation on ice.
10. **Equilibrate a QIAGEN-tip 500 by applying 10 ml Buffer QBT, and allow the column to empty by gravity flow.**
    Flow of buffer will begin automatically by reduction in surface tension due to the presence of detergent in the equilibration buffer. Allow the QIAGEN-tip to drain completely. QIAGEN-tips can be left unattended, since the flow of buffer will stop when the meniscus reaches the upper frit in the column.
11. **Apply the filtered lysate from step 9 to the QIAGEN-tip and allow it to enter the resin by gravity flow.**
    The presence of Buffer ER may cause the lysate to become turbid again. However, this does not affect the performance of the procedure.
    ☞ Remove a 120 µl sample of the flow-through and save for an analytical gel (sample 2) in order to determine the efficiency of DNA binding to the QIAGEN Resin.
12. **Wash the QIAGEN-tip with 2 x 30 ml Buffer QC.**
    Allow Buffer QC to move through the QIAGEN-tip by gravity flow. The first wash is sufficient to remove all contaminants in the majority of plasmid preparations. The second wash is particularly necessary when large culture volumes or bacterial strains containing large amounts of carbohydrates are used.
    ☞ Remove a 240 µl sample from the combined wash fractions and save for an analytical gel (sample 3).
    Important: For all subsequent steps use endotoxin-free plasticware (e.g., new polypropylene centrifuge tubes) or pretreated glassware.
13. **Elute DNA with 15 ml Buffer QN.**
    Collect the eluate in a 30 ml endotoxin-free or pyrogen-free tube. Use of polycarbonate centrifuge tubes for collection is not recommended as polycarbonate is not resistant to the alcohol used in subsequent steps.
    Note: For constructs larger than 45–50 kb, prewarming the elution buffer to 65°C may help to increase yield.
    ☞ Remove a 60 µl sample of the eluate and save for an analytical gel (sample 4).
    ⊛ If you wish to stop the protocol and continue later, store the eluate at 4°C. Storage periods longer than overnight are not recommended.
14. **Precipitate DNA by adding 10.5 ml (0.7 volumes) room-temperature isopropanol to the eluted DNA. Mix and centrifuge immediately at ≥15,000 x *g* for 30 min at 4°C. Carefully decant the supernatant.**
    All solutions should be at room temperature in order to minimize salt precipitation, although centrifugation is carried out at 4°C to prevent overheating of the sample. Alternatively, disposable conical bottom centrifuge tubes can be used for centrifugation at 5000 x *g* for 60 min at 4°C. Isopropanol pellets have a glassy appearance and may be more difficult to see than the fluffy, salt-containing pellets that result from ethanol precipitation. Marking the outside of the tube before centrifugation allows the pellet to be more easily located. Isopropanol pellets are also more loosely attached to the side of the tube, and care should be taken when removing the supernatant.
15. **Wash DNA pellet with 5 ml of endotoxin-free room-temperature 70% ethanol (add 40 ml of 96–100% ethanol to the endotoxin-free water supplied with the kit) and centrifuge at ≥15,000 x *g* for 10 min. Carefully decant the supernatant without disturbing the pellet.**
    Alternatively, disposable conical-bottom centrifuge tubes can be used for centrifugation at 5000 x *g* for 60 min at 4°C. The 70% ethanol removes precipitated salt and replaces isopropanol with the more volatile ethanol, making the DNA easier to redissolve.
16. **Air-dry the pellet for 5–10 min, and redissolve the DNA in a suitable volume of endotoxin-free Buffer TE.**
    Redissolve DNA pellet by rinsing the walls to recover all the DNA, especially if glass tubes have been used. Pipetting the DNA up and down to promote resuspension may cause shearing and should be avoided. Overdrying the pellet will make the DNA difficult to redissolve. DNA dissolves best under alkaline conditions; it does not easily dissolve in acidic buffers.

Determination of yield

To determine the yield, DNA concentration should be determined by both UV spectrophotometry at 260 nm and quantitative analysis on an agarose gel. For reliable spectrophotometric DNA quantification, A_{260} readings should lie between 0.1 and 1.0.

Agarose gel analysis

We recommend removing and saving aliquots during the purification procedure (samples 1–4). If the plasmid DNA is of low yield or quality, the samples can be analyzed by agarose gel electrophoresis to determine at what stage of the purification procedure the problem occurred (see page 36).

FIGURE A.1: Protocol for DNA purification copied from the Quiagen Endofree® Plasmid Purification Handbook

A.2.2.1 Alternative staining protocols

To stain for formin mDia2 we tried different fixing and staining protocols. In addition to the protocol in the main text, we used the following procedure.

i) Cells incubated for 15 min on ice in 10 %TCA (trichloroacetic acid). The 10 % TCA (w/v in distilled water) dilution is prepared freshly before the experiment.

ii) Fixed cells are washed three times in PBS containing 30 mM glycine (G-PBS).

iii) They are incubated with 0.2 % triton in G-PBS for 5 min on ice.

iv) Cells are incubated with 3 % BSA (bovine serum albumin) in PBS for 1 h.

v) Cells are incubated for 2 h with the primary antibody.

vi) Cells are three times washed with trisbuffered saline (TBS) containing 0.1 % Tween-20 (TBST)

vii) Cells are incubated with the secondary antibody for 45 min.

Alternatively, cells were fixed by incubation for 5 min in pre-cooled methanol at -20 Â°C. This protocol was used for staining for mDia2 and control staining experiments. The staining protocol was published in [173, 174].

Table A.8: Product information for fixation and staining protocols

Product	Brand (Supplier)	Reference	Comment
PFA (Paraformaldehyde)	Sigma Aldrich	P6148	PFA solution is prepared in a 3 % dilution in PBS
DPBS (Dulbecco's Phosphate-Buffered Saline)	Invitrogen Gibco (Thermo Fisher Scientific)	11530486	
Triton	Sigma Aldrich	93443	
Glycerol	Sigma Aldrich	G2025	
Glycerin	Sigma Aldrich	50046	
BSA (Bovine Serum Albumin)	Sigma Aldrich	A2153	
TWEEN® 20	Sigma Aldrich	P1379	
TBS (Tris Buffered Saline)	Sigma Aldrich	94158	

Table A.9: List of antibodies and dyes for staining

Antibody	Brand/Source	Reference
Anti-anillin (anti-rabbit)	Glotzer Lab	Piekny *et al.* [118]
Anti-mDia2 (antirabbit)	Narumiya Lab	Watanabe *et al.* [174]
Phalloidin AlexaFluro 488	Invitrogen (Thermo Fisher Scientific)	A12379
Phalloidin AlexaFluro 546	Invitrogen (Thermo Fisher Scientific)	A22283
Anti-paxillin (anti-mouse)	Transduction Laboratories	610051
Anti-phosphotyrosine (anti-rabbit)	Transduction Laboratories	610009
Anti-septin7 (anti-rabbit)	Proteintech	13818-1-ap
AlexaFluro 350 (anti-rabbit)	Molecular Probes (Thermo Fisher Scientific)	A-11046
AlexaFluro 488 (anti-rabbit)	Molecular Probes (Thermo Fisher Scientific)	A-11034
AlexaFluro 647 (anti-rabbit)	Molecular Probes (Thermo Fisher Scientific)	A-21245
Cy3 (anti-rabbit)	Jackson ImmunoResearch	111-166-047
Cy3 (anti-mouse)	Jackson ImmunoResearch	115-165-146
DAPI (4',6-Diamidino-2-phenylindole dihydrochloride)	Sigma Aldrich	32670
Hoechst 33342	Thermo Fisher Scientific	10150888

Table A.10: Product information for polyacrylamide protocols

Product	Brand (Supplier)	Reference	Comment
Acetic acid	Sigma Aldrich	33209	$\geq$ 99.8 %
3-(trimethoxysilyl)propylmethacrylate	Sigma Aldrich	M6514	$\geq$ 98.0 %
Acrylamide solution	Sigma Aldrich	A4058	40 %
N,N'-Methylenebisacrylamide solution	Sigma Aldrich	M1533	2 % in H_2O
Ammonium persulfate	Sigma Aldrich	A9164	$\geq$ 98.0 %
Acrylic acid N-hydroxysuccinimide ester (NHS)	Sigma Aldrich	A8060	$\geq$ 90 %
TEMED (Tetramethylethylenediamine)	Roth	2367.3	$\geq$ 99.0 %
Latex beads, carboxylate-modified polystyrene, fluorescent red	Sigma Aldrich	L3030	size 2.0 μm
Latex beads, amine-modified polystyrene, fluorescent blue	Sigma Aldrich	L0780	size 0.05 μm
Latex beads, carboxylate-modified polystyrene, fluorescent red	Sigma Aldrich	L3280	size 0.5 μm

Table A.11: Product information for giant cells protocol

Product	Brand (Supplier)	Reference	Comment
Cytochalasin D	Sigma Aldrich	C8273	
PEG (Polyethylene glycol solution)	Sigma Aldrich	73034	molecular weight 1400 - 1600

A.2.3 Materials and methods for fission yeast

The media and agar plates A.12 were prepared by the IGBMC media facility.

Table A.12: Product information for fission yeast culture

Product	Brand (Supplier)	Reference
EMM (powder)	MP Biomedicals	114110012
YES (powder)	MP Biomedicals	114101522
EMM agar (powder)	MP Biomedicals	114110232
YES agar (powder)	MP Biomedicals	114101732
SP supplemements (powder)	MP Biomedicals	114104012
Glycerol	Sigma Aldrich	G2025

A.3 The cytokinetic ring in mammalian cells – Supplementary Information

In the following section, I will present some supplementary results about the cytokinetic ring in mammalian cells.

A.3.1 Different setups and protocols

We developed different setups to visualize the cytokinetic ring in one plane of focus. We also experimented with different protocols to synchronize cells or to produce giant cells.

A.3.1.1 Sandwich setup

In order to influence the plane of division, we confined cells between two glass coverslips. We hoped, that this geometry of attachment sites would bring cells to divide in a plane parallel to the coverslips. However, cells were detaching from one of the glass coverslips before we could see a cell division (Fig. A.2).

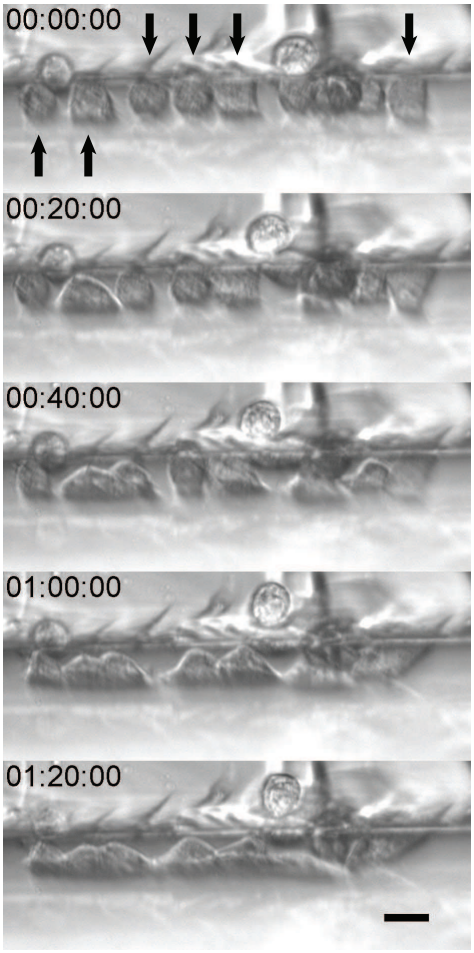

FIGURE A.2: NIH3T3 cells confined between two parallel glass coverslips. The coverslips are held together with two binder clips. Aluminum foil in between the plates serves as spacer. At the beginning, cells are attached on both sides (arrows), but detach after some time and spread on one of the coverslips. Time in hh:mm:ss, scale bar 20 µm.

A.3.1.2 Vertical setup

To see the cytokinetic ring in one plane of focus, we were tilting the substrate to which cells adhered. Additionally we patterned the substrate with elongated fibronectin motifs. Cells elongate along the fibronectin pattern and divide in a plane perpendicular to the lines. To maximize the number of cells per experiment, we stacked sheets of polystyrene foils. We used polystyrene to easy the handling. However, the quality of the images that we obtained with this setup were not satisfying (Fig. A.3). This is probably due to diffraction in and reflection on polystyrene.

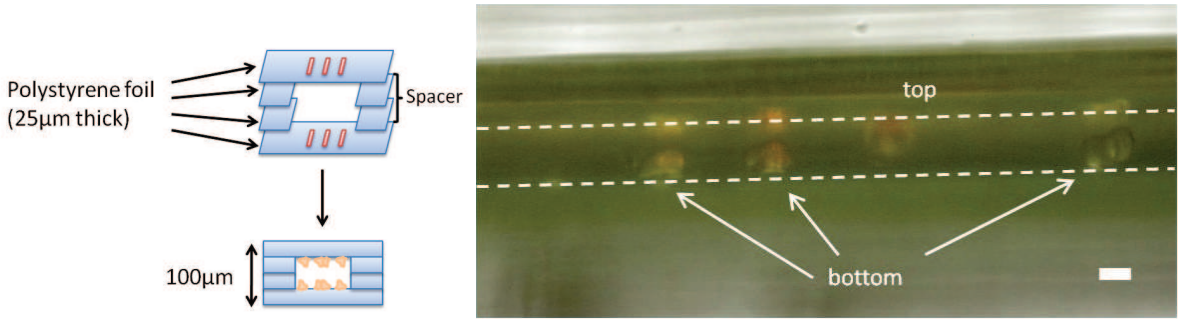

(A) (B)

FIGURE A.3: (A) To multiply the lines of cells, polystyrene foils were stacked. (B) Image of HeLa cells in this configuration. Cells are reflected on the other side of the foil. (red: LifeAct, green: myosin, scale bar 20 µm).

A.3.1.3 Synchronization protocol

We wanted to check, if trypzinisation of synchronized cells would change the cell cycle. We therefore fixed cell synchronized cells after replating and compared to synchronized cells, which were not replated (Fig. A.4).

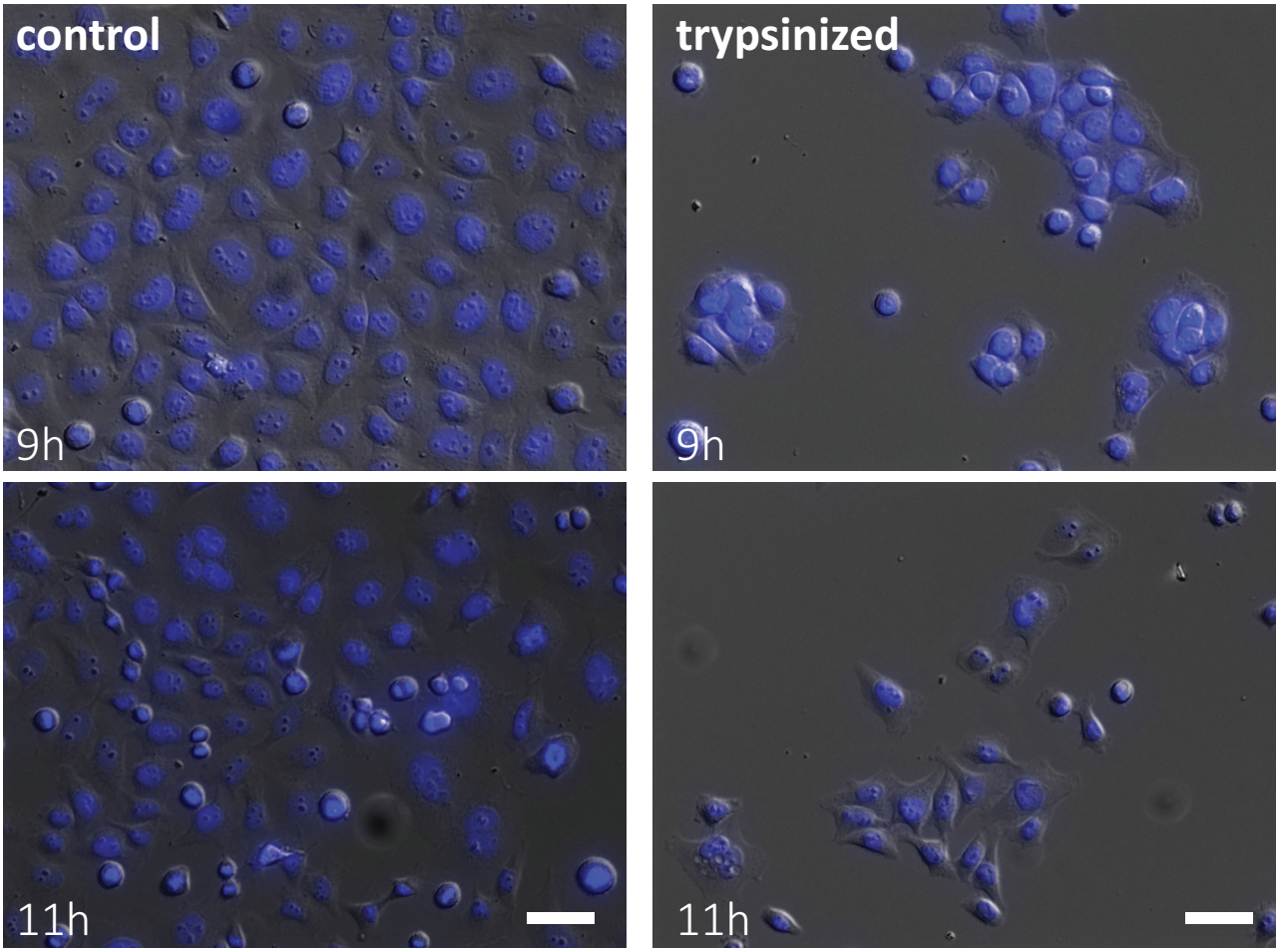

FIGURE A.4: HeLa cells synchronized with the double thymidine block. Cells on the right were replated by trypsinization after the release from the block. Cells were fixed and stained with DAPI at the indicated time after release. Scale bar 50 µm.

The mitotic shake-off, is not synchronizing cells by manipulating the cell cycle, but rather separating mitotic cells from non-mitotic cells. We wanted to know for how long we could observe mitotic cells with this protocol A.5.

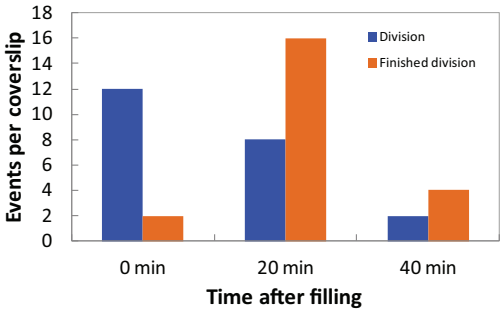

FIGURE A.5: Microcavity coverslips are filled with cells shaken off from a flask. Cells were fixed right after, 20 min and 40 min after filling. The events of closing rings and rings, which finished constriction (diameter around 1 µm), were counted. Most rings constrict in the first 20 min after shake-off.

A.3.1.4 Giant cells

We wanted to measure the closure speed as a function of the cell size. To generate giant cells, we incubated cells with PEG, which is fusing membranes. The result is depicted in Figure A.6, where large cells are visible.

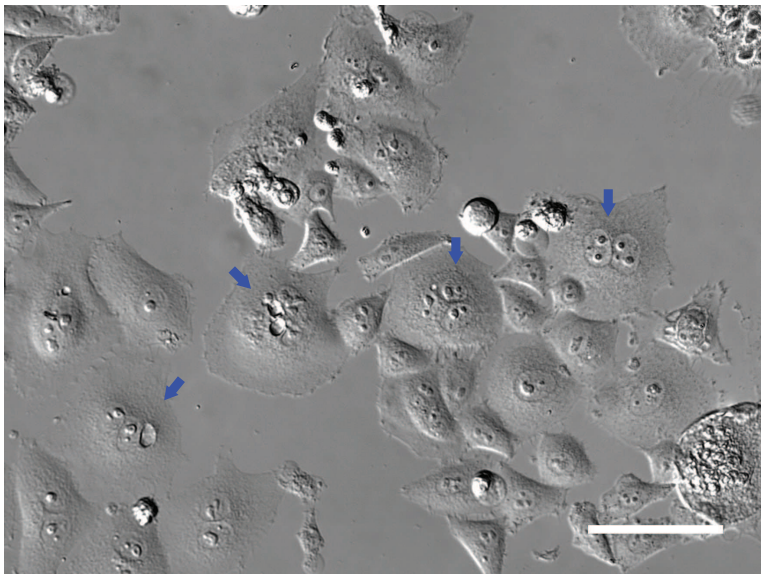

FIGURE A.6: Cells were incubated with PEG and then washed with medium. Fused cells have several nuclei and are larger (examples are emphasized by arrows). Scale bar 100 µm.

A.3.2 The cytokinetic ring in mammalian cells

A.3.2.1 Pattern in the cytokinetic ring

Not all microscopes allowed us to see a pattern in the cytokinetic ring. We did not reveal it with the inverted epifluorescent and confocal microscopes (Fig. A.7).

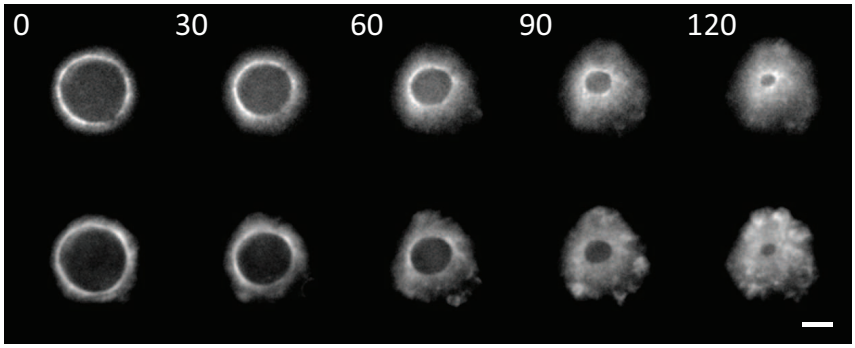

(A) Epifluorescence microscope, inverted

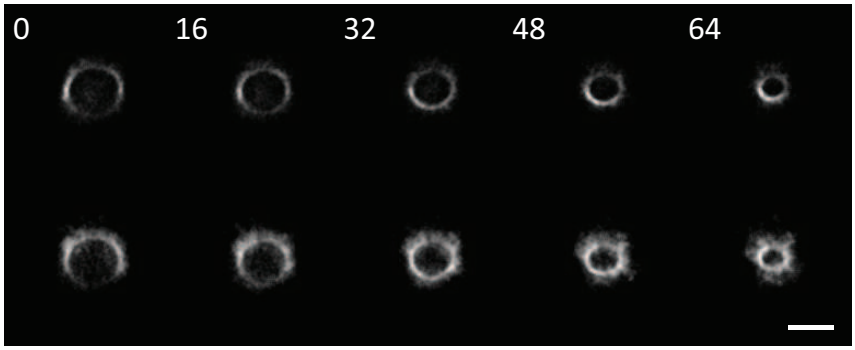

(B) Spinning disk microscope, inverted

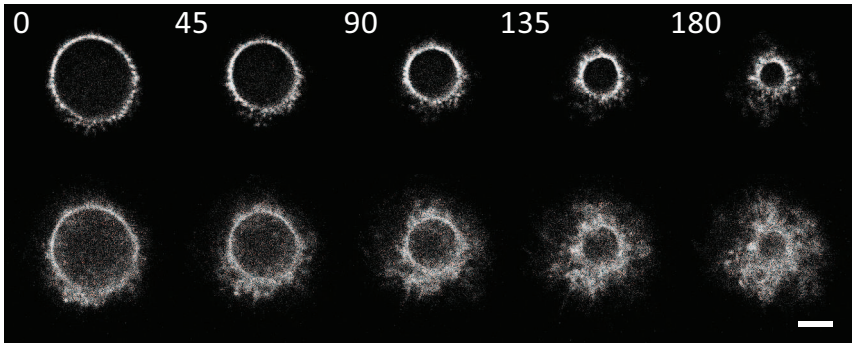

(C) Confocal microscope, upright

FIGURE A.7: Comparison of the image quality of the cytokinetic ring for different microscopes. (A) Epifluorescence microscope, inverted, 60x, oil, 1.4 NA. (B) Spinning disk microscope, inverted, 63x oil, 1.4 NA. (C) Confocal microscope, upright, 60x water, 0.95 NA. Top: myosin, bottom: actin. Time in s, scale bars 5 µm.

Some rings underwent striking rotations. Figure A.8 shows two examples of these rotations in addition to the main text.

We were not able to stain successfully for formin with the antibodies that we had at

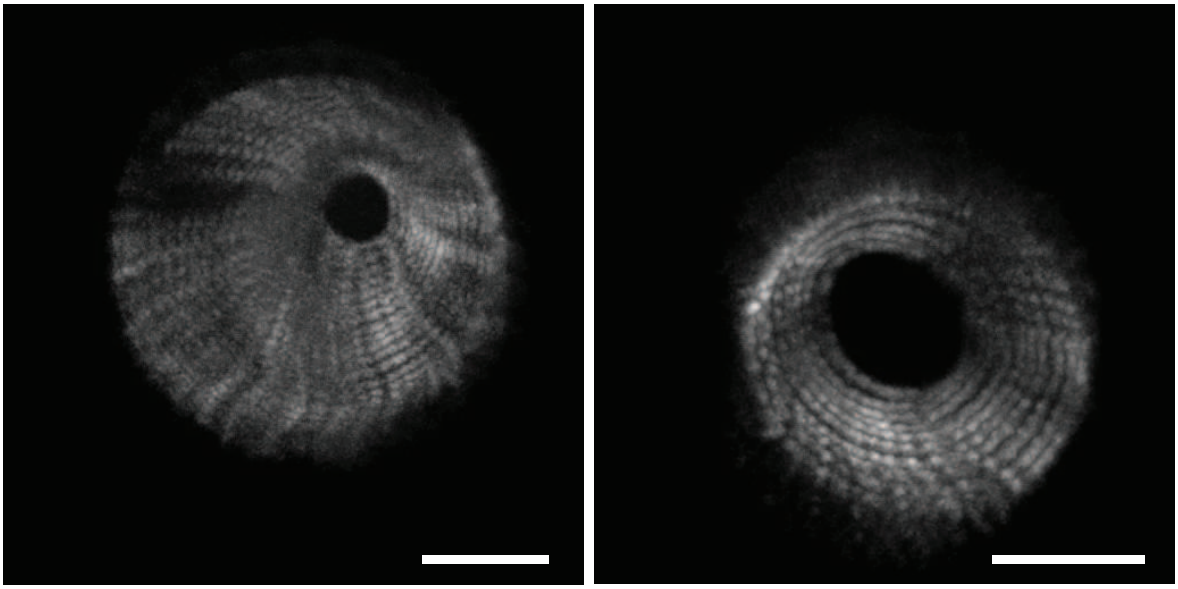

(A) (B)

FIGURE A.8: Two examples of cells, which show rotation of myosin accumulations during closure. Overlay of 23 (A) and 10 (B) subsequent images with times between images of 15 s (A) and 16.8 s (B). Scale bars 5 µm.

hand A.9. We suspect that the antibodies were not suited for the staining. Possibly they got damaged during the transport.

We stained HeLa cells for anillin and septin 7. Figure A.10 and A.11 show examples of these stainings in addition to the examples in the maintext.

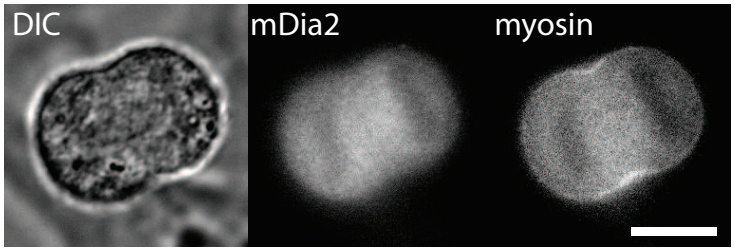

(A)

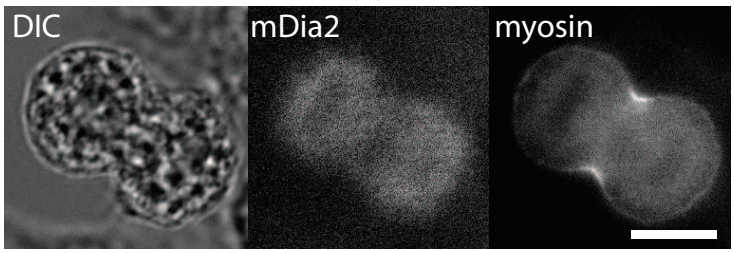

(B)

FIGURE A.9: HeLa cells stably transfected with GFP labeled myosin and stained for mDia2. Cells were fixed with (A) TCA or (B) MeOH as described in A.8. The staining does not reveal accumulations of mDia2 in the cleavage furrow. Probalby because the antibodies were damaged. Scale bars 10 µm.

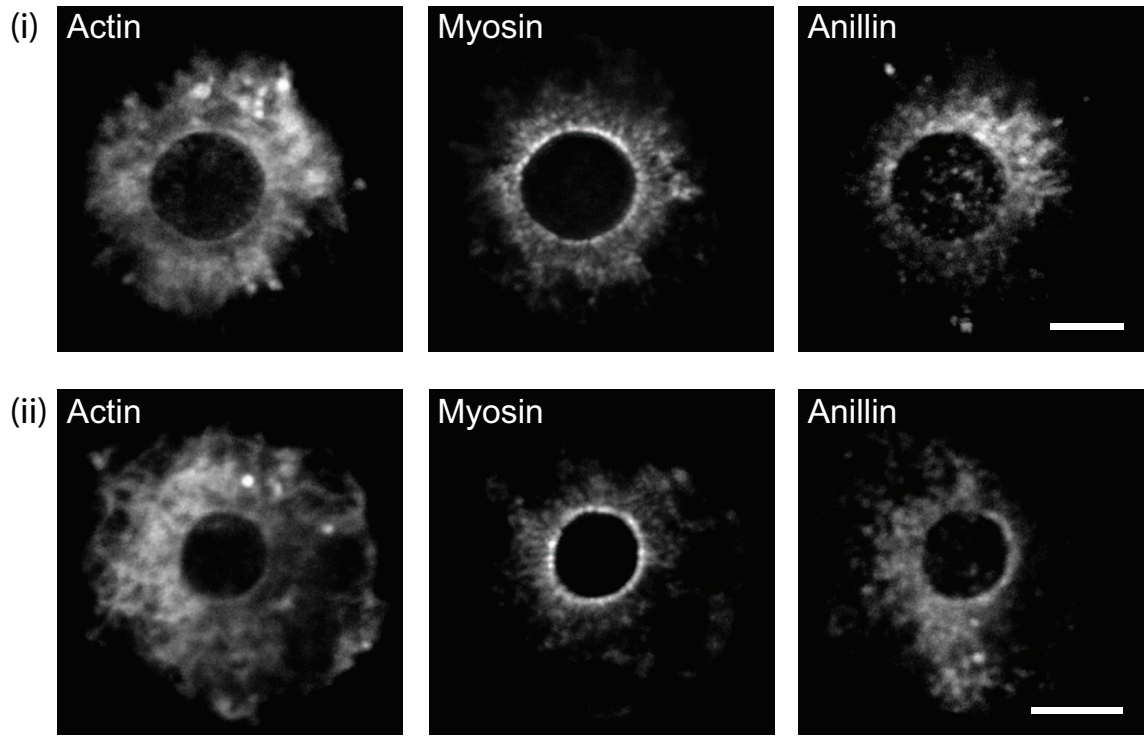

FIGURE A.10: HeLa cells expressing LifeAct-mCherry and myosin-GFP stained for anillin. Overlay of (i) 16 z-planes, distance (dz = 0.3 µm) and (ii) 9 z-planes (dz = 0.3 µm). Scale bars 5 µm.

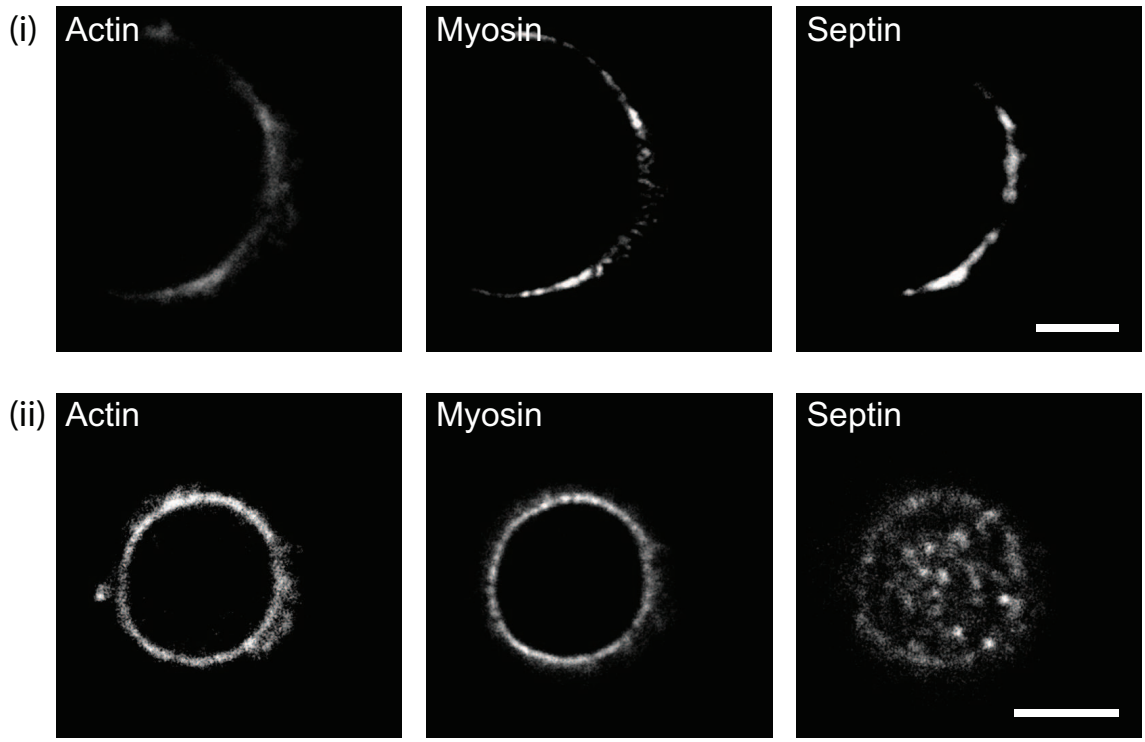

FIGURE A.11: HeLa cells expressing LifeAct-mCherry and myosin-GFP stained for septin7. Scale bars 5 µm.

A.3.2.2 Theoretical description

Anne Wald and Karsten Kruse developed a model to describe the cytokinetic ring [172]. In this model myosin is attached to formin and both are in the center of bipolar filaments. Myosin activity induces filament currents. Their analytical expression is :

$$\begin{aligned} j^{bp}(x,l,t) =& \alpha \int_0^L dl' \Big\{ \int_0^{l'} d\xi \Big(c^+(x+\xi,l',t) - c^-(x-\xi,l',t) \Big) c^{bp}(x,l,t) \\ &+ \Big(2 \int_0^{min(l,l')} d\xi \Big(c^{bp}(x+\xi,l',t) - c^{bp}(x-\xi,l',t) \Big) c^{bp}(x,l,t) \\ &\int_{min(l,l')}^{max(l,l')} d\xi \Big(c^{bp}(x+\xi,l',t) - c^{bp}(x-\xi,l',t) \Big) c^{bp}(x,l,t) \Big) \Big\} \end{aligned} \tag{A.1}$$

$$j^+(x,l,t) = 2\alpha \int_0^L dl' \int_0^{l'} d\xi c^{bp}(x+\xi,l',t) c^+(x,l,t) \tag{A.2}$$

$$j^-(x,l,t) = -2\alpha \int_0^L dl' \int_0^{l'} d\xi c^{bp}(x-\xi,l',t) c^-(x,l,t) \tag{A.3}$$

where j^{bp} and $j^{\pm}$ denote the currents of bipolar and (+)- and (–)-filaments.

Filaments can interact, when they overlap with the center of a bipolar filament. Accordingly a bipolar filament can interact with other bipolar filaments and monopolar filaments. Monopolar filaments can only interact with bipolar filaments. The integrals evaluate the overlap between filaments. The sign gives the direction of the flow. Bipolar filaments can be dragged in both directions depending on the position of the bipolar filaments they interact with. The flows scale with the myosin activity α.

The density of the nucleators is given by:

$$\partial_t n(x,t) = D_n \partial_x^2 n(x,t) - \mu n + \nu_d \int dl \; c^{bp}(x,l,t) \tag{A.4}$$

The first term describes the diffusion. Nucleators become bipolar filaments, when they nucleate filaments, as described by μn. Nucleators are set free with the rate ν_d by dissociation of bipolar filaments of any length l.

A.3.2.3 Probing material parameters

We probed the influence of myosin activity and actin (de-)polymerization by using different cytoskeleton drugs. Upon the addition of ML-7, which is inhibiting the myosin light chain kinase, the ring opened immediately (Fig. A.12).

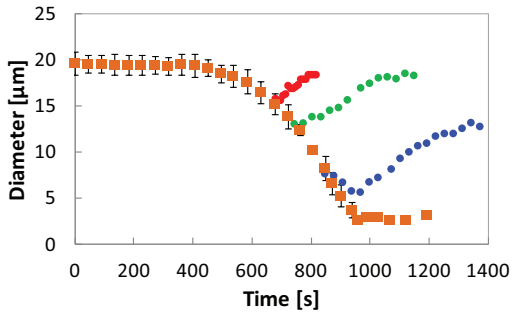

FIGURE A.12: Three examples of closure after addition of ML-7 (various colors, control in orange). Rings open after addition of the drug.

We also used different actin related drugs. Cytochalasin D is capping the (+)-end and inhibiting polymerization. After Cytochalasin D (1 µM) addition the ring continues to close and opens in some cases. The actin and myosin accumulate to clusters, which might include material from the cortex (see Fig. A.13).

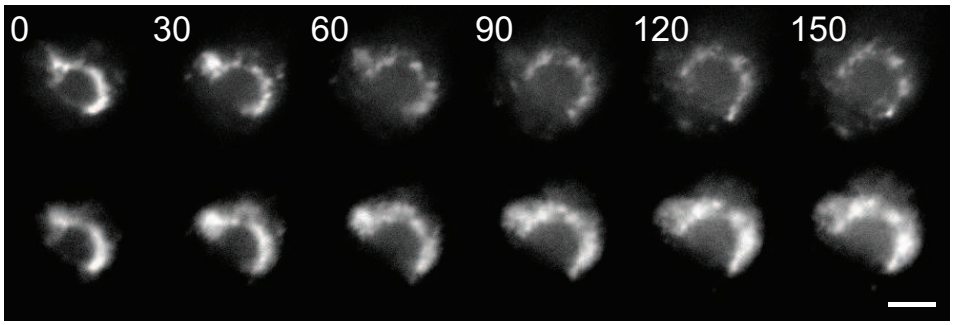

FIGURE A.13: Time lapse of a ring after addition of Cytochalasin D (top: myosin, bottom: actin). Myosin reveals patches around the ring. The time lapse was acquired with an inverted epifluorescence microscope. Time in s, scale bar 5 µm.

Jasplakinolide, which is stabilizing actin filaments did not have an effect on the closure speed (Fig. A.14), neither directly after closure, neither up to 50 min after addition. We did not see an effect of the formin SMIFH2 on dividing cells (Fig. A.15). However, ring formation seemed to be inhibited after addition of the drug.

To evaluate the effect of Blebbistatin and Latrunculin A on the ring pattern, we fixed cells after the addition of either of the drugs. Figure A.16 shows additional examples of fixed cytokinetic rings.

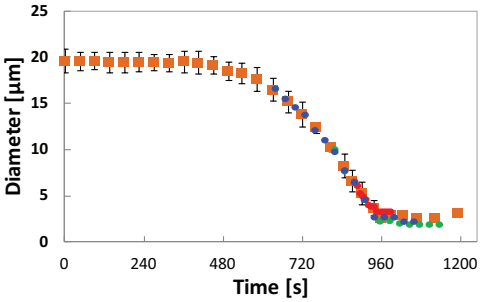

FIGURE A.14: Three examples of closure after addition of Jasplakinolide (various colors, control in orange). The cell closure is unaffected.

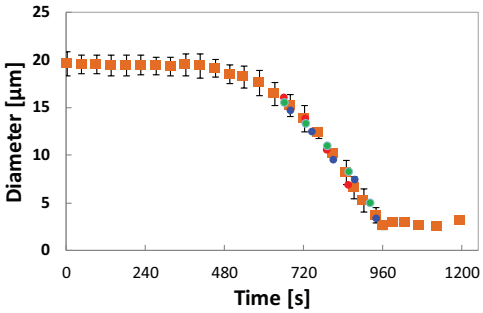

FIGURE A.15: Three examples of closure after addition of SMIFH2 (various colors, control in orange). The cell closure is unaffected.

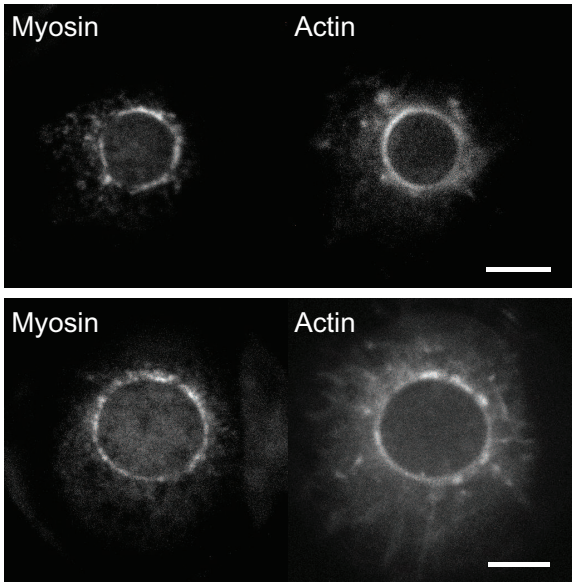

(A) Blebbistatin

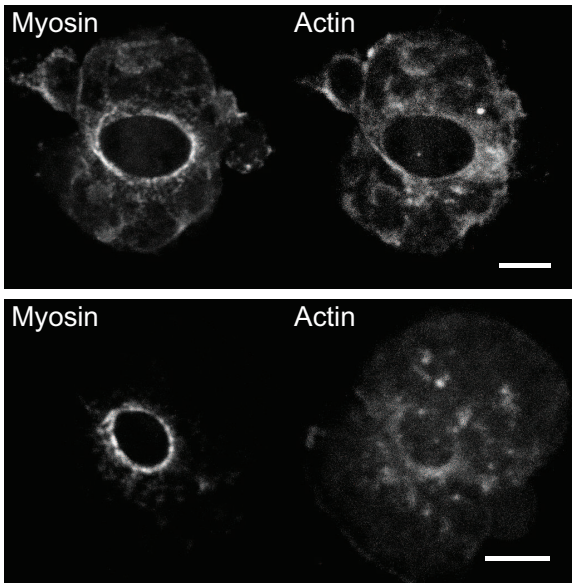

(B) Latrunculin A

FIGURE A.16: Other examples of cytokinetic rings after the addition of cytoskeleton drugs. (A) Ring in myosin and actin 15 min after the addition of 100 µM Blebbistatin. Overlay of 16 and 17 z-planes (dz = 0.3 µm). (B) Ring in myosin and actin 1.5 min after the addition of 1.5 µM Latrunculin A. Overlay of 26 and 16 z-planes (dz = 0.3 µm). Scale bars 5 µm.

A.3.2.4 Myosin mobility and turnover

To determine flows or turnover of myosin, we used different bleaching patterns. We bleached a region of the ring and traced the recovery (Fig. A.17). No striking fluxes are observable.

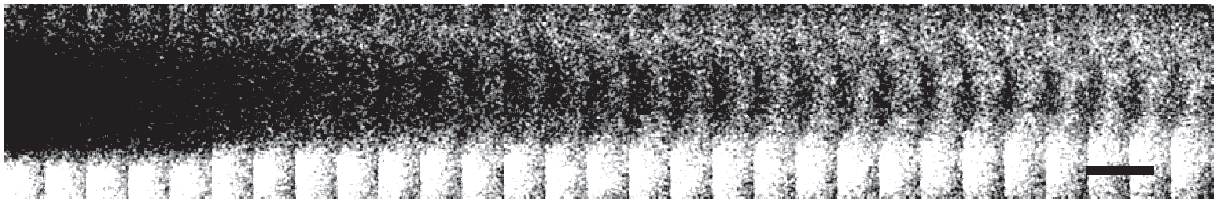

FIGURE A.17: Time lapse of a part of the cytokinetic ring after bleaching of GFP-myosin. Time between images 1.5 s, scale bar 2 µm.

A.4 The cytokinetic ring in fission yeast – Supplementary Information

A.4.1 Intensity measurements

In Figure 5.5 we show the total and mean intensities of actin and myosin in the ring. In the following I present, how we deduce the fit for the mean intensities from the linear guide for the eyes of the total intensity.

If the total intensities, so the total amounts of proteins N, depend linearly on the diameter D. The mean intensities, so the protein concentrations C, depend on the diameter as follows: $C = \frac{N(D)}{A(D)}$, with A: projected area of the ring. The area is given by: $A = \frac{\pi}{4}(D^2 - D_i^2)$, D and D_i denote the outer and inner diameter of the ring. Since the ring thickness ΔR is constant, we can write $A = \pi(\Delta R D - \Delta R^2)$. This gives for the concentrations $C(D) = \frac{mD+N_0}{\pi(\Delta R D - \Delta R^2)}$, with $N = mD + N_0$ describing the linear fit of the total intensity. We measured ΔR to be 3 pixel = 0.24 µm.

A.4.2 Analytical prediction of the rate of closure

According to our model the closure is driven by the rotation of wall building proteins. The wall has the geometry of a hollow cylinder and its volume is:

$$V(t) = \frac{\pi}{4} w (D_0^2 - D(t)^2) \tag{A.5}$$

where D_0=D(0) is the outer diameter and D(t) the inner one. So the change in volume is:

$$\frac{dV}{dt} = -\frac{\pi}{2} w D \frac{dD}{dt} \tag{A.6}$$

The increase in wall volume depends on the speed v and number G of wall building proteins:

$$\frac{dV}{dt} = \delta^2 G v \tag{A.7}$$

from which one derives:

$$\frac{\pi}{2} w D \frac{dD}{dt} = -\delta^2 G v \tag{A.8}$$

The solution when v and G are constants is simply:

$$D(t) = \sqrt{D_0^2 - 4t \frac{\delta^2 G v}{w\pi}} \tag{A.9}$$

For the fit in Figure 5.13 we used the following parameters: a typical cell diameter before closure is $D_0 = 3.2$ µm and the wall thickness w is about 100 nm. For the speed we used the measured speckle speed of Bgs1 and Bgs4 (v = 5.65 µm/min and v = 3.59 µm/min, see Figure 5.10). The only free parameter is δ^2G where δ^2 correspond to the added area and G to the number of Bgs proteins. We fitted δ^2G = 3700 nm^2 for Bgs1 and δ^2G = 5850 nm^2 for Bgs4.

Refined model In a more general model we take into account the fact that the number of wall building proteins and their rotation speed are not constant, but instead depend approximately linearly on the diameter D of the ring:

$$G = G_0(aD + b) \tag{A.10}$$

and

$$v = cD + d \tag{A.11}$$

The parameters a, b are derived from a linear fit of the relative intensity measurements and c, d are derived from the linear fit of the speckle speed of Bgs1 (Figure A.18).

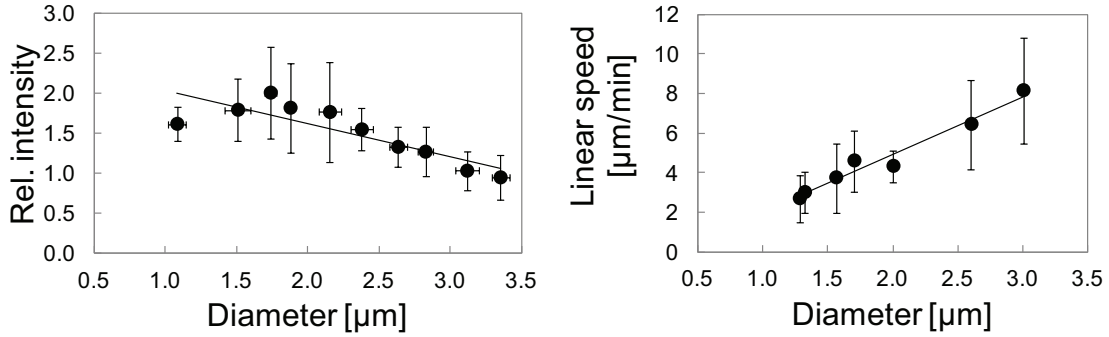

FIGURE A.18: Intensities and speckles velocities for Bgs1. Intensity of Bgs1 on the ring and septum increases with closing rings (left); the linear velocity of Bgs1 speckles decreases (right). Temperature 27°C. n_{int}=142 and n_{speed}=7, where n denotes the number of cells, error bars indicate the standard deviation.

The rate of added volume V is now:

$$\frac{dV}{dt} = \delta^2 G_0 \underbrace{(aD + b)}_{\substack{\text{change in} \\ \text{rel. intensity}}} \underbrace{(cD + d)}_{\substack{\text{change in} \\ \text{speckle speed} \\ [\mu m/min]}} \tag{A.12}$$

Combining equations A.6 and A.12 together yields:

$$\delta^2 G_0(aD + b)(cD + d) = -\frac{\pi}{2} w D \frac{dD}{dt} \tag{A.13}$$

$$\int_0^t dt' = -\frac{\pi w}{2\delta^2 G_0} \int_{D_0}^{D} \frac{x}{(ax + b)(cx + d)} dx \tag{A.14}$$

$$t = \frac{-\pi w}{2\delta^2 G_0(bc - ad)} [\frac{b}{a} ln(\frac{aD + b}{aD_0 + b}) - \frac{d}{c} ln(\frac{cD + d}{cD_0 + d})] \tag{A.15}$$

The following parameters were used to fit the experimentally measured closure speed:

The experimentally measured diameter is plotted together with the simulated diameter and the predictions from the two models (Fig. A.19). In both models the only fitted parameter is δ^2G.

TABLE A.13: Parameters to fit the experimentally measured closure speed

Experimentally determined values		
w	Septum thickness	0.1 µm
D_0	Initial diameter	3.2 µm
a	Change of rel. intensity	$-0.49\,\mu m^{-1}$
b		2.67
c	Change of speckle speed	$2.84\,min^{-1}$
d		0.82 µm/min
Fitted value		
$\delta^2 G_0$		$1950\,nm^2$

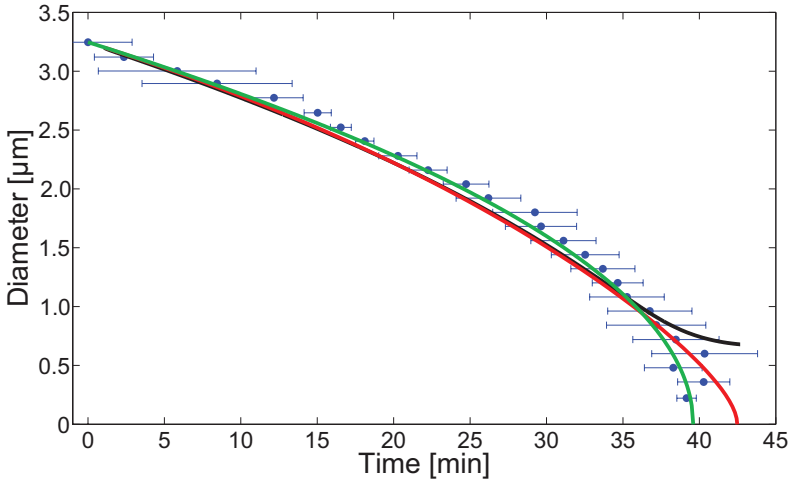

FIGURE A.19: Experimentally measured diameter (blue) is plotted together with the simulated diameter (black) and the predictions from the two models (green: simple model, red: refined model).

A.4.3 Simulation of the cytokinetic ring

The ring was implemented in CytoSim and simulated. The model reproduces ring formation from a band of nodes (Fig. A.20).

We measured the characteristics of the speckle motion as before in the experimentally acquired movies. Figure A.21 and A.22 show the speckle lifetime and rotation length. We obtain similar values as in the experiments within the range of a factor of two.

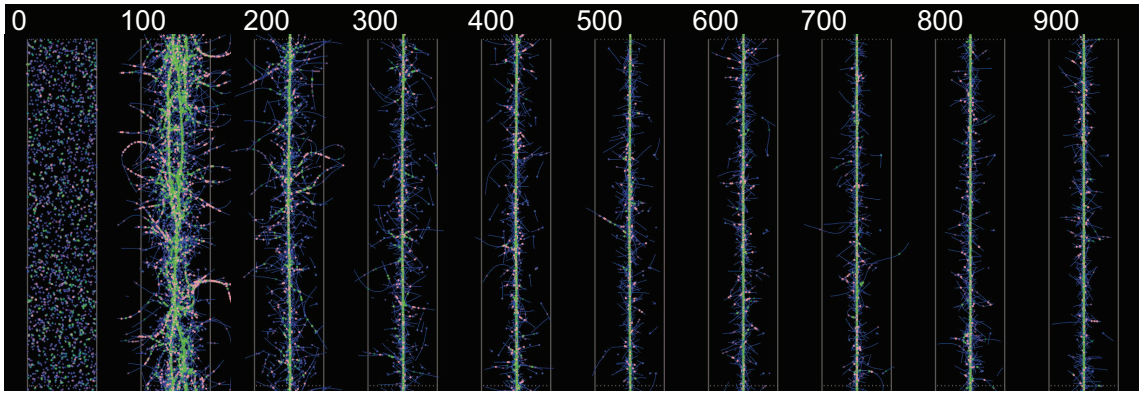

FIGURE A.20: Simulation of the condensation of the ring. The ring condenses essentially in less than 200 s. Blue: actin filaments, green: myosin, pink: α-actinin, time in s, the dimensions of the simulation are 1 µm x 5 µm.

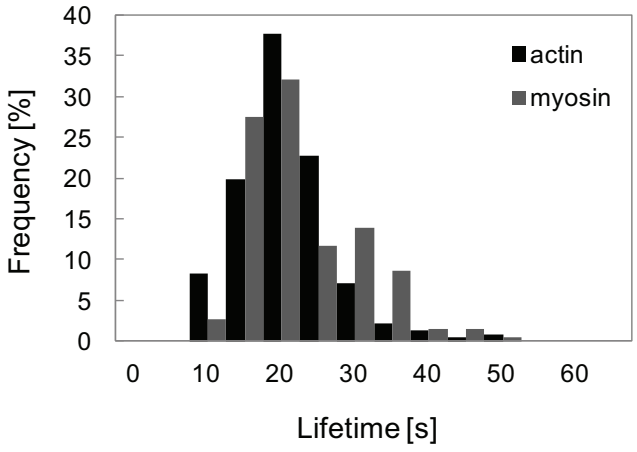

FIGURE A.21: The average lifetime of actin speckles is 18.3±6.4 s (mean and standard deviation, n = 242) and 19.9±7.5 s (mean and standard deviation, n = 265) for myosin speckles.

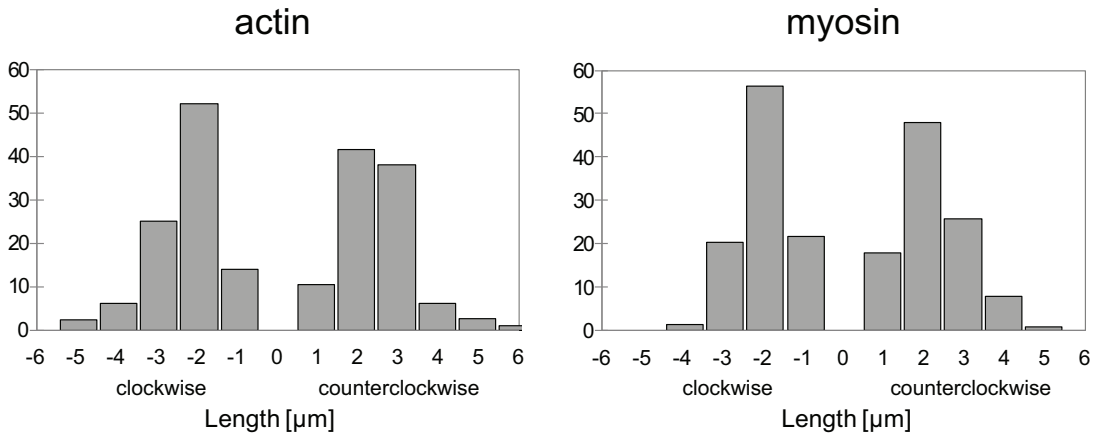

FIGURE A.22: Analysis of the rotation of actin and myosin speckles shows that motion is similar in both directions. Actin speckles move on average by 2.1±0.8 µm (mean and standard deviation, n = 242), while myosin speckles move by 1.8±0.8 µm (mean and standard deviation, n = 265).

Table A.14: Important simulation parameters

Parameter	Value
Global	
Radius	1.6 µm
Viscosity	1 Ns/m^2
Actin	
Stiffness	10 pN/µm
(+)-end assembly	0.1 µm/s
(+)-end disassembly (after release from node)	0.5 µm/s
(–)-end disassembly	0.03 µm/s
Node	
Number	2000
Nucleation rate	1.0 s^{-1}
Detachment rate	0.1 s^{-1}
Myosin	
Number	5000
Binding rate	10 s^{-1}
Binding range	25 nm
Unbinding rate	0.25 s^{-1}
Unloaded speed	0.6 µm/s
Stall force	4 pN
α-actinin	
Number	3000
Binding rate	10 s^{-1}
Binding range	10 nm
Unbinding rate	0.5 s^{-1}
Unbinding force	10 pN

Viktoria WOLLRAB

Active gels *in vivo*: Patterns and dynamics in cytokinetic rings and their functions in cell division

Résumé

Les structures d'acto-myosine sont impliquées dans de nombreuses fonctions cellulaires. Comprendre leur organisation et leur comportement collectif est toujours difficile. Nous avons étudié l'anneau cytokinétique dans les cellules de mammifères et dans les levures de fission, en orientant les cellules dans les microcavités, ce qui permet de voir l'anneau dans un seul plan focal. Avec cette configuration, nous révélons de nouvelles structures et des dynamiques distinctes pour les deux systèmes cellulaires. Dans les cellules de mammifères, nous trouvons des motifs réguliers de la myosine et la formine. Les caractéristiques de ces motifs sont stables tout au long de sa fermeture et leur apparition coïncide avec la constriction. Nous proposons que ce phénomène est une propriété inhérente du réseau d'acto-myosine et que la formation de ces motifs entraîne une augmentation du stress. Ces hypothèses sont confirmées par notre modèle en champ moyen. Par contraste, l'anneau de levure de fission montre des inhomogénéités tournantes de l'actine, de la myosine, des protéines de la construction de la paroi (Bgs) et d'autres protéines. La dynamique des inhomogénéités de myosine est inchangée, si la croissance de la paroi est inhibée. Cependant, l'inhibition du mouvement des inhomogénéités conduit à l'arrêt de la fermeture. Nous proposons que la fermeture de l'anneau est entraînée par la rotation de l'actine et de la myosine qui tirent des protéines Bgs, lesquelles construisent ainsi le septum. Cette hypothèse est confirmée par nos calculs et par des simulations numériques. Nous suggérons que la transition entre les états de différents ordres et dynamiques pourrait être une façon de réguler *in vivo* les systèmes d'acto-myosine.

Mots-clés : Anneau cytokinétique, actine, myosine, gel actif, effet collectif, physique cellulaire, cellules de mammifères, levures de fission, microfabrication, théorie, champ moyen, simulation

Résumé en anglais

Actomyosin structures are involved in many cell functions. Understanding their organization and collective behavior is still challenging. We study the cytokinetic ring in mammalian cells and in fission yeasts, by orienting cells in microcavities. This allows seeing the ring in a single plane of focus. With this setup, we reveal new structures and distinct dynamics for both cellular systems. In mammalian cells we find a pattern of regular clusters of myosin and formin. The characteristics of this pattern are stable throughout closure and its formation coincides with the onset of constriction. We propose that its characteristic is an inherent property of the actomyosin network and that its formation leads to an increase in stress generation. These hypotheses are supported by our theoretical mean field model. In contrast, fission yeast rings show rotating inhomogeneities (*speckles*), *i.e.* rotations of actin, myosin, cell wall building proteins (Bgs) and other proteins. Myosin speckles dynamic is unchanged, if wall growth is inhibited. However, the inhibition of speckle motion leads to stalled closure. We propose that the ring closure is driven by the rotation of actin and myosin, which pull Bgs thereby building the septum. This model is supported by our calculations and by numerical simulations. We suggest that the transition between states of different orders and dynamics might be a way to regulate actomyosin systems *in vivo*.

Key words: Cytokinetic ring, actin, myosin, active gel, collective effect, cell physics, mammalian cells, fission yeasts, microfabrication, theory, mean field, simulation